IMPERIAL COLLEGE LONDON
UNIVERSITY OF LONDON

ULTRASONIC WAVEGUIDE SENSORS FOR FLUID CHARACTERISATION AND REMOTE SENSING

by

Frédéric Bert Cegla

A thesis submitted to the University of London for the degree of
Doctor of Philosophy

Department of Mechanical Engineering
Imperial College London
London SW7 2BX

January 2006

Abstract

This thesis addresses two physical problems which both benefit from a new approach using guided ultrasonic waves.

The first application relates to fluid characterisation. Conventional equipment for fluid characterization has drawbacks due to the need of a straight, unobstructed path across the fluid specimen, a perfectly parallel reflector, diffraction effects and penetration problems in highly attenuating fluids. The use of ultrasonic waveguides can alleviate these problems by separating the transducer from the measurement area and by guiding the ultrasonic energy along a flexible waveguide of fixed geometry. The theoretical modelling, design and construction of a wave guide sensor for fluid characterization of hot or radioactive fluids and liquids in general is presented. The sensor makes use of a guided interface wave. This wave was named the quasi-Scholte wave because of its similarity to the Scholte wave that is widely known in geophysics. It is a non-leaky guided wave that travels in a plate immersed in a fluid. A substantial fraction of its energy travels in the fluid and is trapped at the interface. It thus does not radiate energy away from the waveguide. This makes this mode very sensitive to the fluid properties. It is shown that the fluid bulk velocity and attenuation can be retrieved accurately using this method. Furthermore it is shown that the use of other guided wave modes can be used to extract further fluid properties so as to completely characterize the fluid acoustically.

The second application relates to non-destructive testing in harsh environments. Conventional ultrasonic non-destructive testing uses a piezoelectric transducer close to the area to be inspected. This becomes impossible above temperatures of about 300-400 C when conventional piezo-electric materials reach their Curie point and become depolarized, which removes their ability to send or receive ultrasonic signals. A remedy to this problem was found in using waveguides for remotely monitoring thickness and defects within a structure under extreme conditions. The waveguide separates the hot structure from the transducer which is located in a cool and safe place. Essentially, this represents an acoustic cable along which ultrasound is sent. The two main issues that had to be investigated are the wave propagation along waveguides of different candidate geometries and the geometry and method of

attachment of the waveguide to the sample that is to be tested. The problems are that the acoustic pulse has to remain strong and as undistorted as possible while propagating along the waveguide, and when transmitting from the waveguide into the sample. A system was designed and tested successfully at temperatures over 550 C.

Acknowledgements

The support from many people has considerably influenced the writing of this thesis. I am most thankful to Prof. Peter Cawley and Dr. Mike Lowe for their excellent guidance, stimulation and support as well as for giving me the opportunity to join the NDT-Laboratory.

The help and discussions with several of my colleagues was also always helpful. In a friendly environment I have learned plenty from every single member of the NDT-group but most influential were Dr. Francesco Simonetti and Mr. Daniel Hesse. I am also very grateful to Dr. Mark Evans and Dr. Thomas Vogt for their help and advise with experimental equipment.

My gratitude to Prof. Richard Challis and Dr. Andrew Holmes from the University of Nottingham should also be expressed. They carried out validation measurements for results presented in this thesis. I am also very glad to have had the opportunity to discuss some of the work presented here with Prof. Peter Nagy from the University of Cinncinati who visited the Laboratory for a while.

Finally, I would also like to acknowledge the continued encouragement and support from my family and my fiancé Jaimini, without them the work would have been a great deal harder.

Contents

List of Figures

List of Tables

Nomenclature

A, a	Arbitrary constants
$[A]$	Global matrix
$A(x, y)$	Two dimensional wave field amplitude modelled using Huygen's principle
b	Unit vector parallel to the imaginary part of k
B	Arbitrary constant
c	Bulk velocity
$c_{scholte}$	Scholte wave velocity
c_{liquid}	Liquid bulk wave velocity
c_{ph}	Phase velocity
C_{entry}	Reflection coefficient for an entry reflection
C_{order}	Circumferential order of a FE analysis
C_{QS}	Quasi-Scholte wave velocity
C_B	Bulk wave velocity
C_g	Group velocity
C_{gA0}	Group velocity of the $A0$ mode
D	Distance
$D(x, y)$	Distance from a point on a transducer as a function position
E	Young's modulus
f	Frequency
ΔF	Difference in frequency
g	Ratio of two shear moduli $\frac{G_2}{G_1}$
$G_{1,2}$	Shear modulus of material 1 or 2
h	Plate thickness
hc	Heat transfer coefficient
H	Vector potential
$H_0^{(2)}(x)$	Hankel function of the second kind
i	$\sqrt{-1}$
k	Wavenumber

continued on next page

continued from previous page

k_r	Real part of wavenumber
k_i	Imaginary part of wavenumber
k	Thermal conductivity
K	Bulk modulus
$L_{1,2}$	Longitudinal partial wave and identifier
M	Measurand property
n	Unit vector parallel to the real part of k
ΔN	Difference in index of minima
P	Fluid property
P	Force
P_{area}	Average power flow through the waveguide cross section
QS	Quasi-Scholte mode
R	Radius
r, θ, z	cylindrical coordinates
S	Sensitivity, Signal amplitude
S_{Bvel}	Sensitivity to bulk wave velocity
S_{visc}	Sensitivity viscosity
$S_{\alpha b}$	Sensitivity to bulk wave attenuation
$T_{1,2}$	Transverse partial wave and identifier
ΔT	Time difference
t	Time
u	Displacement
u_1, u_2, u_3	Displacement components in Cartesian coordinates
u_R	Displacements due to compressional waves
u_θ	Displacements due to shear waves
$\ddot{u}$	Acceleration
V	Wave velocity
x, y, z	Cartesian coordinates
x_2, x_1	Immersion depth 2 and 1 in the QS mode experiment
x_i	Cartesian coordinates in Einstein notation

continued on next page

continued from previous page

α	Attenuation per unit length (np/m)
$\alpha_{Scholte}$	Quasi-Scholte wave attenuation
α_1, α_2	$\sqrt{1-\frac{c_{ph}}{c_l}}$ identity used in the global matrix
β_1, β_2	$\sqrt{1-\frac{c_{ph}}{c_s}}$ identity used in the global matrix
γ	Wavenumber projection on the y direction
δ_{ij}	Kronecker delta
$\epsilon_{i,j}$	Strain tensor
η	Dynamic viscosity
η_F	Fluid dynamic viscosity
η_{eff}	Effective dynamic viscosity
ν	Kinematic viscosity, Poisson's ratio
λ, μ	Lamé moduli
λ', μ'	imaginary part of complex Lamé moduli
λ_f	Fluid bulk modulus
λ	Wavelength
μ	Shear modulus
κ	Wave attenuation per wavelength (np/wl)
ξ	Wavenumber projection on the x direction
ρ	Density
σ_{ij}	Stress tensor
$\tau(x)$	Shear stress as a function of x
ϕ	Scalar potential
ω	Angular frequency
$\times$	Vector product
$\cdot$	Scalar product
∇	Three-dimensional differential operator
im	Subscript, denotes the imaginary part
re	Subscript, denotes the real part
s	Subscript, refers to shear type waves
s	Subscript, refers to solid material

continued on next page

continued from previous page

F	Subscript, refers to fluid material
T	Subscript, refers to shear type waves
L	Subscript, refers to longitudinal type waves
+	Subscript, refers to wave travelling in the positive y direction
-	Subscript, refers to wave travelling in the negative y direction
$*$	Indicates a Fourier transformed variable

Chapter 1

Introduction

1.1 Motivation

Millions of litres of complex fluids are produced by industry daily. Products range from food and beverages to petro chemicals and paints. During the manufacturing process measurements and monitoring of fluid properties are important for process and quality control. Ultrasonic test equipment measuring bulk velocity and attenuation of a fluid can be used to measure concentration levels of substances in liquids, phase transitions, particle sizes and many other properties [1], [2], [3].

Conventional ultrasonic test cells require a straight and unobstructed path between transmitting and receiving transducers. This is difficult to achieve if the system needs to be integrated into a reaction vessel that contains stirring mechanisms. In highly attenuative materials the separation between transducers has to be very small in order to transmit enough energy across the gap. Therefore flow rates of highly attenuative fluids through a test cell are limited. Other disadvantages of test cells are the need for corrections for geometrical effects like beam spreading or diffraction. Furthermore standard piezo electric transducers depolarise at high temperatures and since the transducer has to be in contact with the fluid it is not possible to measure fluids at elevated temperatures ($> 250°C$).

An attractive alternative to test cell based approaches could be the use of a guided ultrasonic interface wave to measure the fluid properties. In this thesis the use of the quasi-Scholte mode for fluid property measurements was investigated. The quasi-Scholte mode is an ultrasonic interface wave trapped at the surfaces of a plate that is immersed in a liquid. It resembles the Scholte wave on a single boundary between a solid and a liquid. A large proportion of the energy of the interface wave is travelling in the liquid which makes it very sensitive to the fluid properties. The energy contained within the wave decays with distance from the interface so that the energy is localised at the interface between solid and liquid or plate and liquid for the quasi-Scholte mode. The waveguide therefore determines the geometry of the problem completely which removes diffraction or beam spreading issues. It is also possible to separate the transducer location from the sensing area which potentially enables measurements at high temperatures and in harsh environments. A sketch illustrating the principle of the 'dipstick' interface wave measurement and the conventional test cell based measurement of fluid properties is shown in figure 1.1.

The dipstick separates the transducer from the test region and so allows measurements to be taken in conditions that the transducer itself cannot tolerate. This concept has other applications and one of them is thickness gauging at high temperatures which is addressed in the second part of this thesis.

Whilst thickness monitoring is a routine task at room temperature, standard equipment fails at elevated temperatures ($> 300°C$) and when exposed to high radiation levels. This is mainly due to depolarisation of the piezo-electric transducer materials at temperatures above the Curie point and under the influence of radiation. Current research is being carried out to find more robust transducer materials that work at extreme conditions [4], [5], however the development and production of these materials is expensive which makes them currently comparable to expensive alternative techniques such as laser ultrasonics. Therefore the use of a buffer waveguide system for structural monitoring in harsh environments is very attractive. It allows the use of standard ultrasonic equipment to excite and receive ultrasonic signals at a waveguide end that is located in a safe environment while the testing is carried out

at the other waveguide end under extreme conditions.

Potential applications of the buffer waveguide in power plants, petro chemical plants or general processing plants with the benefit of reducing shut down times can be envisaged. An 'acoustic cable' would be installed after subcritical wall thinning due to erosion or corrosion has been found in a plant component during a routine non-destructive testing check up. Instead of prolonging the shut down of the plant to wait for replacement components, the plant could be restarted immediately and the condition of the feature of concern can be monitored. In case the component reaches a critical condition an emergency shut down could be carried out, however it is more likely that the critical part would survive until the next scheduled shut down for which an effective replacement can be planned. The monitoring of erosion or corrosion of pipe walls, boiler components or elbow sections is thus possible.

The development of a robust waveguide and the optimisation of the wave propagation therein was carried out. The geometry of the waveguide and the polarisation of the wave in the waveguide were also investigated in order to find a waveguide that can simultaneously act as source and receiver of bulk waves on a test piece. A sketch of the principle of the waveguide monitoring system is shown in figure 1.2.

1.2 Thesis outline

Following this outline, in chapter 2 a brief review of basic wave propagation in bulk media is presented. The main principles and mathematical expressions for bulk waves are given. Then guided waves, which result from a superposition of reflections of bulk waves at boundaries, are introduced. A section in the chapter also summarises existing guided wave material property measurement techniques before the chapter closes with a brief overview of ultrasonic spectrometry.

The theoretical modelling of the quasi-Scholte mode is the subject of chapter 3.

Modelling is developed from the simple Scholte interface wave on a half space to a plate immersed in an ideal, Newtonian or Non-Newtonian fluid. The main characteristics such as mode shapes and velocity dispersion curves as well as the quasi-Scholte mode sensitivity to fluid bulk properties are reported.

An experimental apparatus was devised to validate the theoretical predictions with actual measurements of the quasi-Scholte mode behaviour. The excitation method of the quasi-Scholte mode, the measurement setup as well as results on Newtonian and Non-Newtonian liquids are presented in chapter 4.

Experimental observations showed the need to change from a plate geometry to a strip in order to reduce potential errors and make the method more practical. Whilst an A0 (flexural) like strip mode that can mode convert into a quasi-Scholte type strip mode was found and could also successfully be tested, a non-dispersive shear horizontal (SH) mode of the strip was also found. The great potential of this non-dispersive SH strip mode for non destructive testing in harsh environments was realised and further research was focused on the development of an 'acoustic cable' for this purpose. Chapter 5 investigates wave propagation in strips of rectangular cross section with special focus on the non-dispersive, lowest order, shear horizontal strip mode.

Chapter 6 considers the characteristics of waveguide sources on an object. In the analysis the waveguide and the object were uncoupled by considering a half space with surface loading. The half space represented by the test piece is much larger than the waveguide. The stress mode shapes transmitted through the waveguide were used to represent surface loads on the test piece. Different polarisations and geometries of surface loads were considered to represent different waveguide modes and geometries.

The knowledge acquired in chapters 5 and 6 was employed to build a waveguide system for thickness gauging and monitoring in chapter 7. The waveguide-structure

joint is the most critical part of the assembly and several joining methods from manual coupling with shear couplant via clamping to permanent attachment by means of welding or soldering were investigated. A prototype was built and thickness measurements on a calibration block at room temperature as well as thickness monitoring at 500°C for long periods (> 1 month) were carried out.

Chapter 8 summarises the main findings of this thesis and indicates future work and improvements for both techniques. Some of the work on the quasi-Scholte mode has been published. A list of these publications is given at the end of the thesis after the references section.

1.3 Figures

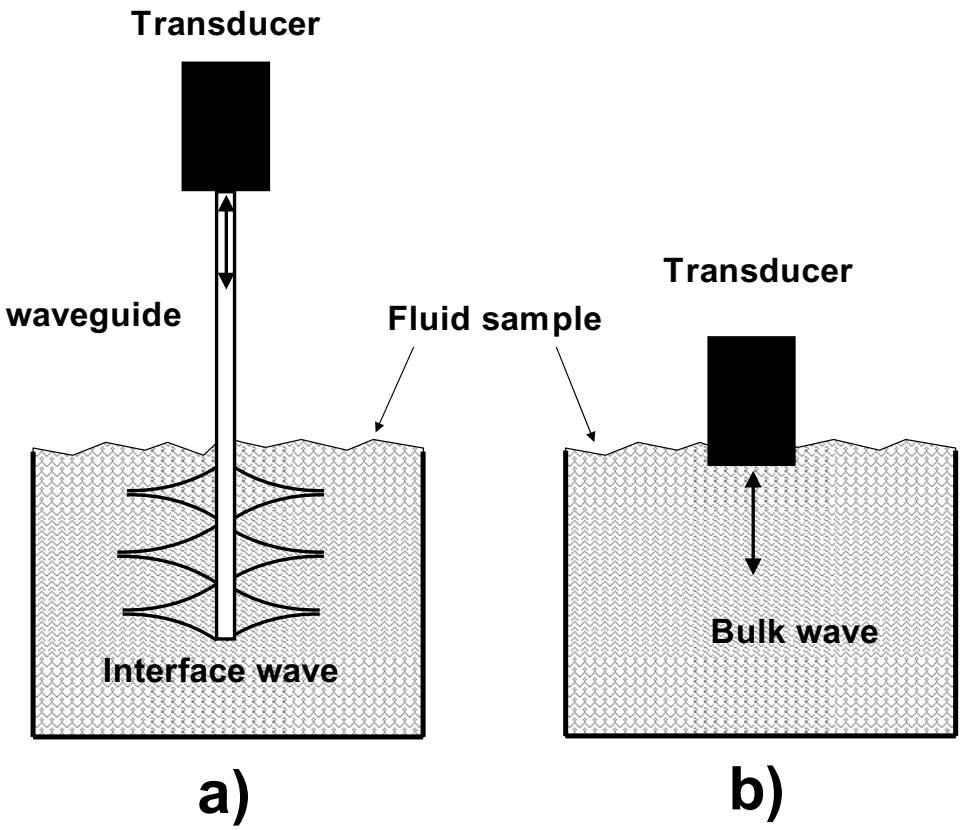

Figure 1.1: Sketch of the of the principle of a) a 'dipstick' interface wave measurement of fluid properties and b) a fluid property measurement using a conventional test cell setup.

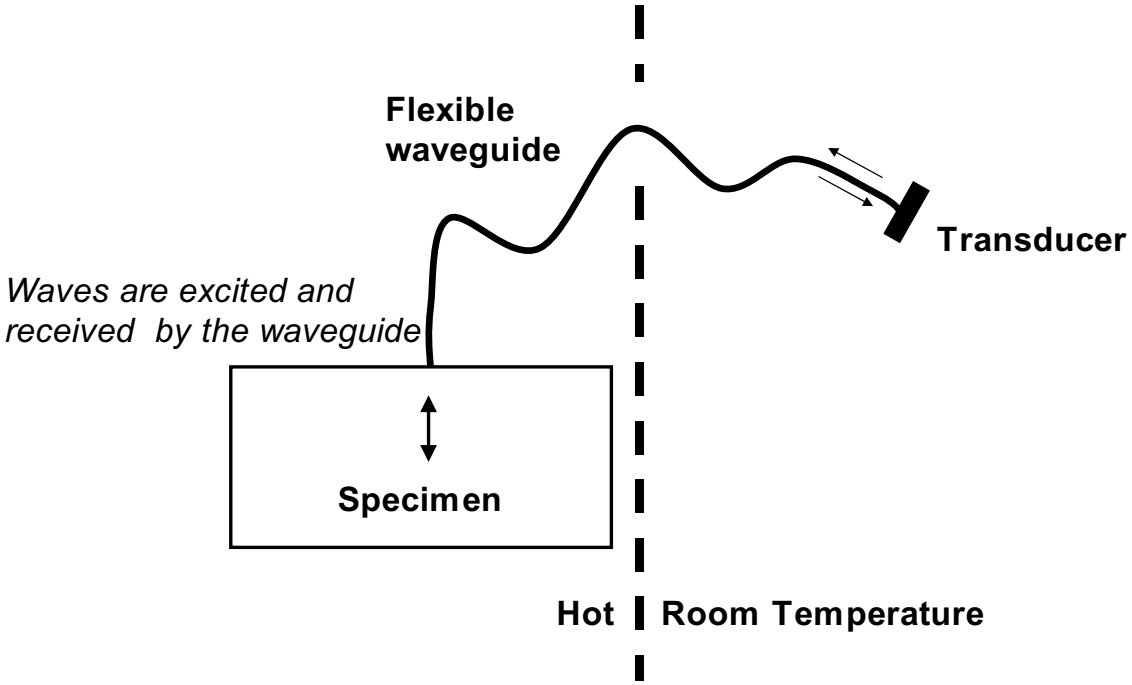

Figure 1.2: Sketch of the principle of the 'acoustic cable' waveguide remote monitoring system.

Chapter 2

Basic principles of bulk and guided waves

2.1 Wave propagation in bulk media

The propagation of elastic waves in infinite isotropic media has gained a lot of attention in the literature. There are many texts that describe the underlying principles [6], [7], [8], [9]. Therefore here only a short introduction to the underlying equations will be given. Starting in a Cartesian coordinate system the general equation of motion is given by:

$$\rho \frac{\partial^2 u}{\partial t^2} = \nabla \sigma \tag{2.1}$$

where ρ is the density of the medium, u is the displacement and σ the stress field tensor in the medium. ∇ is the differential operator. It is convenient to introduce Hooke's law to relate stresses to strains and displacements.

$$\sigma_{ij} = \lambda \delta_{ij} \epsilon_{kk} + 2\mu \epsilon_{ij} \tag{2.2}$$

$$\epsilon_{ij} = \frac{1}{2}\left(\frac{\partial u_i}{\partial x_j} + \frac{\partial u_j}{\partial x_i}\right) \tag{2.3}$$

By substituting equations 2.2 and 2.3 into equation 2.1 the Navier equation is obtained.

$$\rho\frac{\partial^2 u}{\partial t^2} = (\lambda+\mu)\frac{\partial}{\partial x_i}\frac{\partial u_j}{\partial x_j} + \mu\frac{\partial^2 u_i}{\partial x_j^2} \tag{2.4}$$

which may be expressed in vector form:

$$\rho\ddot{u} = (\lambda+\mu)\nabla(\nabla.u) + \mu\nabla^2 u \tag{2.5}$$

By means of the Helmholtz decomposition the displacement field can be separated into a scalar (ϕ) and vector (H) potential [10].

$$u = \nabla\phi + \nabla\times H \tag{2.6}$$

In combination with equation 2.5 after some algebra the following expression is obtained:

$$\nabla[\rho\frac{\partial^2\phi}{\partial t^2} - (\lambda+2\mu)\nabla\phi^2] + \nabla\times[\rho\frac{\partial^2\phi}{\partial t^2} - \mu\nabla^2 H] = 0 \tag{2.7}$$

Thus equation 2.7 can be split into two independent equations; one for the dilatational or equivoluminable (ϕ) motion and one for rotational (H) motion.

$$\frac{\partial^2\phi}{\partial t^2} = c_l^2\nabla^2\phi \tag{2.8}$$

$$\frac{\partial^2 H}{\partial t^2} = c_s^2\nabla^2 H \tag{2.9}$$

where

$$c_l = \sqrt{\frac{\lambda+2\mu}{\rho}} \tag{2.10}$$

$$c_s = \sqrt{\frac{\mu}{\rho}} \tag{2.11}$$

c_l and c_s are the velocities of dilatational (longitudinal) and rotational (shear) waves in the infinite isotropic medium. A general solution to 2.8 and 2.9 can be found by:

$$\phi, H = Ae^{i(k_{l,s}x-\omega t)} \tag{2.12}$$

with the secular equation

$$k_{l,s}^2 = \frac{\omega^2}{c_{l,s}^2} \tag{2.13}$$

where x is the spatial coordinate of the wave, t is the time variable, A is an arbitrary wave amplitude, ω is the angular frequency, c_l and c_s are the longitudinal and shear wave velocities respectively and k_l and k_s are the corresponding wavenumbers. The secular equation links the wavenumber of the wave to the velocity of the wave. In general the wavenumber is a complex vector:

$$k = n \cdot k_{re} + ib \cdot k_{im} \tag{2.14}$$

where n and b are the unit vectors defining the directions of k_{re} and k_{im} respectively. Substituting this into 2.12 yields the following description of a wave:

$$\phi = Ae^{i(n\cdot k_{re}x+ib\cdot k_{im}x-\omega t)} = Ae^{i(n\cdot k_{re}x-\omega t)}e^{-b\cdot k_{im}x} \tag{2.15}$$

This clearly shows that the harmonic oscillatory term in time and space remains with k_{re} as characteristic wavenumber, while the imaginary component of the wavenumber k_{im} simply adds an exponential decay. Thus the phase velocity of a wave is defined by the real part of the wavenumber

$$c_{ph} = \frac{\omega}{k_{re}} \tag{2.16}$$

and the attenuation is described by the imaginary component of the wavenumber k_{im}.

The secular equation for a complex wavenumber is the following:

$$\frac{\omega^2}{c^2} = k_{re}^2 - k_{im}^2 + i2k_{re}k_{im}(n \cdot b) \tag{2.17}$$

For an elastic wave the phase velocity is purely real. This results two conditions for the complex secular equation 2.17. Either $k_{im} = 0$ which describes the propagation of homogeneous plane waves, or $k_{im} \neq 0$ but $(n \cdot b) = 0$ which describes an inhomogeneous wave whose attenuation vector k_{im} is normal to the propagation direction. Both waves travel unattenuated in the direction of their phase. Examples of inhomogeneous waves in liquids are Scholte and Rayleigh waves, while leaky Lamb waves are an example of inhomogeneous waves with attenuation in the direction of travel [11], [12].

The above analysis can be extended to viscoelastic materials. The approach is well described in the literature ([13], [14], [15]) and hence only the results will be mentioned here. As for elastic waves the governing equations in the viscoelastic case can be split up into shear and longitudinal waves with their respective velocities:

$$c_l = \sqrt{\frac{\lambda + 2\mu}{\rho} + i\frac{\lambda' + 2\mu'}{\rho}} \tag{2.18}$$

$$c_s = \sqrt{\frac{\mu}{\rho} + i\frac{\mu'}{\rho}} \tag{2.19}$$

where c_l, c_s are the complex longitudinal and shear bulk velocities respectively, ρ is the density, λ and μ are the real Lamé constants and λ' and μ' are the imaginary Lamé constants. This time the complex secular equation 2.17 will result in real and imaginary wavenumber vectors that are non zero and in general n and b are neither parallel nor perpendicular. In experiments the wave velocity and attenuation of a material are measured on a parallel propagation path. This measures the phase velocity along the propagation path and the attenuation (projection of imaginary wavenumber) in the direction of propagation.

2.2 Guided Waves

Guided waves are waves that, like light in an optical fibre, are guided along the structure in which they propagate. Here 'guided wave' refers to an elasto-dynamic guided wave rather than any other type of wave. Elasto-dynamic guided waves have been known since the last century and perhaps the simplest type of guided wave is the Rayleigh wave [16] that is guided along the interface of an infinite elastic half space and a vacuum. In contrast to bulk waves that were introduced in section 2.1 a condition for guided waves to develop is the existence of an interface between two materials. The basic principles of elastic guided waves are very well known and several textbooks [8], [17], [18] discuss the topic, thus here an extensive treatment is omitted and only the main characteristics are revised.

In a plate, guided waves are often also called 'Lamb waves' [19] and can be thought of as a superposition of shear and longitudinal waves that propagate in the plate material and get reflected back and forth between the two surfaces of the plate. The feature that defines a guided wave is, as for waves in general, the complex wavenumber which is expressed in the plane of the structure along the propagation direction. The complex wavenumber is generally a function of frequency; its calculation results from the boundary conditions that are imposed at the surfaces of a waveguide. There are infinitely many solutions to the governing equations which makes it possible for many guided wave modes to coexist. Each mode has its own phase velocity-frequency relation and a corresponding mode shape.

A typical dispersion curve for a 1 mm thick steel plate is displayed in figure 2.1. The curve shows the phase velocity of different modes as a function of frequency. The phenomenon of a changing phase velocity with frequency is called dispersion, it results in the distortion of the shape of a multi frequency wave packet that propagates for long distances. This is a very important effect that has to be taken care of when working with long range guide wave applications [20], [21] (see also section 2.2.1).

Figure 2.1 also shows different lines; these are the different propagating modes (non propagating modes are omitted here) which are labelled in the conventional style, with S and A representing symmetric and antisymmetric modes respectively and the numbers indicating their harmonic order. The higher the frequency the shorter is the wavelength of ultrasonic waves and more and more mode solutions exist at higher frequencies.

In figure 2.1 the phase velocity is plotted against the product of frequency times thickness. Guided waves are strongly geometry dependent; however for the simple plate case the dispersion curves can be normalized with respect to thickness by plotting them against the frequency thickness product. For example a 2mm thick plate at 0.5MHz has the same phase velocity as a 5mm thick plate at 200 kHz.

The dispersion curve in figure 2.1 was obtained using a software tool (DISPERSE [22]) especially developed for the tracing of dispersion curves in multilayered plate systems [23] and multilayered cylindrical structures [24]. The software uses the partial wave technique and represents the waves in each layer by partial longitudinal and shear waves that leave and enter a layer boundary. On each boundary the boundary conditions (continuity or fixed values for stresses and displacements) have to be fulfilled. At each frequency this allows the assembly of a global matrix [25]. The problem results in an eigenvector-eigenvalue problem which can be solved. The eigenvalues correspond to the wavenumber of a mode while the eigenvectors represent the mode shape of this particular mode. A solution of the displacement takes the below form:

$$U(t) = U(x_2)e^{i(kx_1-\omega t)} \tag{2.20}$$

where $U(x_2)$ is a displacement distribution function (mode shape), k is the wavenumber of the guided wave mode, x_1 the propagation direction, x_2 the direction normal to the propagation direction, ω the angular frequency and t the time variable.

The complex wavenumber and mode shape describe a guided wave mode completely.

However the solutions only describe the modes that can propagate in a free system. To excite a mode a transducer will have to be attached to the waveguide system. This modifies the system and supports the excitation of selected modes only. The excitability function [26] can be used to evaluate the likely mode excitation efficiency of a transducer for a certain mode at a certain position on the waveguide.

2.2.1 Dispersion

An ultrasonic signal pulse is made up of several frequency components. If the frequency components travel with the same velocity the pulse shape will be conserved over the whole propagation path. However if the frequency components travel at different velocities, they will disperse out with propagation distance from the source. This makes the original signal shape longer and less strong in amplitude. Figure 2.2 shows a 5 cycle 500 kHz Hanning windowed A0 mode (steel plate 1mm) signal at excitation and after a propagation path of 0.5 m. The dispersion in form of a change in signal shape is clearly noticeable. The major frequency components that are contained within the excitation signal range from 350 to 650 kHz. The A0 mode is considerably dispersive in this region. The effects of diminished signal amplitude and increased signal length are both detrimental to ultrasonic techniques and especially for the purposes of thickness gauging and defect monitoring. The increased signal length reduces the resolution of the device while the reduced signal amplitude reduces the propagation range and the signal to noise ratio.

Dispersion however can be corrected for by methods such as described by Wilcox et al. [27]. Another means of overcoming dispersion effects is the use of time reversal [28]. A signal is sent along the waveguide, it propagates dispersively along the waveguide and a distorted signal returns to the transducer. The signal is recorded and then time reversed, i.e. the signal is sent back to front so that the slower travelling parts that arrive later are sent first and faster parts are sent later. The faster signals catch up with the slower ones so that the received signal is undistorted at the receiver position. The time reversed signal can either be simulated or measured. Therefore apart from being another complication, dispersion can be overcome as

long as a single mode propagates in the waveguide.

2.2.2 Mode shapes

The mode shapes of a mode are the displacement, stress or other related property variations across the cross section of the waveguide. Figure 2.1 shows that three propagating modes exist at low frequencies. Theses are the fundamental three plate waves of compressional, flexural and shear horizontal nature. Figure 2.3 displays the plate geometry that is considered here, the polarisation directions and sketches of the three fundamental modes. In the limit of low frequency thickness products the displacement mode shape of each of the fundamental modes is uniform across the cross section and in the direction of polarisation (for flexural modes there is a linear variation of the less strong in-plane displacement across the thickness). At higher frequency thickness products the mode shape will start to vary across the cross section (thickness) of the plate. Usually mode shapes are displayed in a plot displaying the position against the amplitude of displacement or stress component of the mode. The mode shapes are of arbitrary absolute amplitude but show the correct relative amplitude compared to another displacement or stress component.

Figure 2.4 shows the mode shapes of the three fundamental modes at a low frequency thickness product (0.1 MHz mm). Figure 2.5 shows the mode shape of the same fundamental modes at higher frequency thickness products. The displacements deviate considerably from the almost uniform profiles observed at low frequency thicknesses, except for the SH0 for which the mode shape does not change with frequency.

2.2.3 Wave propagation in rods and wires

Dispersion curves for a rod/wire of 1 mm radius have been traced using the DISPERSE software and are shown in figure 2.6. The naming convention that is shown in the figure has been adopted after Silk and Bainton [29]. The first letter L,T,F

stands for longitudinal, torsional and flexural wave. The first number in the bracket corresponds to the circumferential order of the mode. The circumferential order of a mode specifies the variation of the mode shape around the circumference of the structure. For example a circumferential order of 1 indicates that the mode shape varies sinusoidally around the circumference with one complete sinusoidal cycle. Circumferential order 2 would vary with 2 complete cycles, order 3 with 3 sinusoidal cycles and so on. Since torsional and longitudinal waves always are axisymmetric their first number in the bracket is always zero. The second integer in the bracket indicates the mode number and differentiates the modes of the same family. There are an infinite number of circumferential orders and an infinite number of modes for each of these circumferential orders. Figure 2.6 only displays the axisymmetric (order 0) and the first circumferential order of flexural waves to avoid crowding the figure with excessive amounts of data.

The phase velocity dispersion curves of a rod or wire overall show similar characteristics to those of a plate. The fundamental modes originate from the same velocities as in the plate case at the low frequency limit (L-Bar velocity, T- shear velocity, F-0) and asymptote to the same velocities as in the plate case at high frequencies (L,F-Rayleigh velocity, T-shear velocity). The transition from the low frequency behaviour to the high frequency behaviour occurs earlier for rods than in the plate case.

2.3 Existing techniques for material property measurements using waveguides

Guided wave testing has found applications in long range pipe testing [20]. During application in the field it was noted that embedded and coated pipes adversely affected guided wave propagation. This considerably reduced propagation range of the waves in the waveguide. The undesirable effect on the wave propagation characteristics led researchers to investigate whether the embedding material properties could be investigated by the use of guided ultrasonic waves.

Nagy and co-workers [30], [31] investigated the effect of fluid loading on thin wires. Kim and Bau [32] and Shepard and Friesel [33] investigated the possibility of density measurement using guided waves. Vogt et al. [34], [35], [36] thoroughly described the theory of embedding material property measurements using guided waves. They measured fluid viscosity using a torsional wave in a wire, they repeated the same exercise using a longitudinal wave and also evaluated the bulk velocity of the surrounding medium this way. The effect of leakage was used to measure the embedding material properties. Leakage of energy is caused due to excitation of bulk waves in the surrounding medium. These bulk waves are set up due to surface displacements of the waveguide and then radiate away from the waveguide. A torsional wave in a waveguide (or a shear horziontal wave in a plate see section 3.5) is ideal for viscosity measurements since it only exhibits rotational/shear displacements at the surface of the waveguide. This entrains more or less liquid and thus causes more or less wave attenuation depending on the liquid viscosity. The same effect can be used with the lowest order compressional L$(0, 1)$ mode of a wire. At higher frequencies this mode has the additional advantage of mainly exhibiting out-of-plane surface displacements due to the Poisson effect. At these operational frequencies leakage is mainly due to leakage of longitudinal waves from the waveguide surface, which enables the determination of the longitudinal bulk velocity of the fluid.

When the embedding medium is attenuating the guided wave very strongly another method can also be used. Under these conditions a strong entry reflection of the guided wave can be noted. Analysis of this entry reflection can also be used to determine the material properties [36].

However all of the above methods effectively measure the influence of the impedance of the embedding medium at the surface of the waveguide. None of the energy that returns to the transducer has actually travelled in the embedding medium. Since the bulk attenuation of a fluid does not influence its impedance significantly it is almost impossible to determine the bulk attenuation of an embedding fluid from those measurements. This issue has been addressed in this thesis. The use of an

interface wave whose energy travels in the waveguide as well as in the embedding fluid makes the guided wave measurement sensitive to both velocity and attenuation of the embedding medium. The guided wave that was used was called the quasi-Scholte wave due to its similarity to the Scholte wave between two half-spaces that is commonly seen in geophysics. The Scholte and quasi-Scholte wave theory will be thoroughly discussed in chapter 3.

2.4 Ultrasonic spectrometry

In ultrasonic spectrometry the velocity and attenuation spectrum of a material are measured. As in any other spectrometry certain features in the ultrasonic velocity and attenuation spectrum can be utilised to identify properties of the investigated material. The simplest example to illustrate this is the determination of density or modulus from a measured ultrasonic velocity. For ideal fluids the identity $c_L = \sqrt{\frac{K}{\rho}}$ can be used to either deduce the bulk modulus (K) or density (ρ) of the investigated material once the other is known. In reality materials are not ideal and more specific data has to be extracted from a sample. The differences in velocity and attenuation spectra help to monitor phase transitions, chrystallisation, melting, freezing, curing, addition of ingredients and other processes [37]. Ultrasonic spectroscopy is an important measurement technique especially in the food industry. An important industrial application of ultrasonic spectrometry is particle sizing [2], [38]. Here the attenuation caused by scattering from the particles in suspensions or emulsions is measured and through mathematical models related to particle size [39], [40], [41]. The main advantage of ultrasonic spectrometry is the possibility to examine opaque samples where standard optical techniques fail. Measurements are also fast and no prior treatment of the material to be investigated is needed. The principle of the technique is described below.

The properties of the material to be measured are the ultrasonic velocity and the attenuation over a wide range of frequencies (typically $0.1 - 20$ MHz). The velocity is the distance that an acoustic signal travels per unit time and the attenuation is the decrease in amplitude of this signal per unit distance. There are several ways to

measure these quantities, the most common techniques being through-transmission, pulse echo and interferometry. Schematics of the three techniques are shown in figure 2.7. In every technique a transducer (E) excites an ultrasonic signal and either the same transducer receives the signal (pulse echo, interferometry) or another transducer (R) is used to pick up the signal (through-transmission). In pulse echo and through transmission the transducers are accurately mounted and aligned in a test cell so that the distance between the transducer faces or the transducer and the back wall is precisely known. Then a sample is placed into the test cell in between the transducers and a signal is excited at the transducer. From the time between excitation and reception of the signal the ultrasonic velocity in the sample can be determined. The attenuation is determined either by comparison of the decrease in amplitude of the signal in the test sample to the decrease in amplitude of a sample with known attenuation or by the decrease in amplitude between successive reverberations of the signal (pulse echo). However for accurate measurements the reflection coefficient of the walls has to be taken into account. Also beam spreading and misalignment can lead to errors. To ensure that the velocity and attenuation are determined at each frequency, either a narrow band toneburst (consisting of many cycles) is excited at one frequency and the experiment is repeated for each frequency within the region of interest or a broad band pulse is excited and Fourier transform techniques are used to extract the velocity and attenuation at each frequency contained within the excitation pulse.

In the interferometer technique, standing waves are produced between a movable reflector and the fixed transducer in the test cell. When the reflector moves towards or away from the transducer a series of maxima and minima in received signal amplitude are detected by the transducer. These maxima and minima are due to constructive and destructive interference of the standing waves. The distance between two maxima is equal to half a wavelength and by the identity $c = f\lambda$ the velocity of the wave can be deduced. The attenuation is determined by the decrease in amplitude of successive maxima as the reflector moves further and further away from the transducer. The main disadvantage of this method is that it has to be carried out at a single frequency and that it will take a long time to construct a complete spectrum.

A disadvantage of all test cell based techniques is the inherent need for a test cell. Transducers have to be accurately aligned and a test cell is very difficult to integrate into a reaction vessel. The environment might be very hostile, high temperatures would disable standard commercially available transducers and stirring devices make it impossible to install a bulky test cell within a reaction vessel. The overall measured attenuation in a test cell has to be of the order of 0.5 np/m in order to avoid large error magnification [42]. This limits the sample size of the test cell and if highly attenuating materials flow through a test cell this imposes very slow flow rates.

2.4.1 Particle size determination

Particle size determination in emulsions and suspensions is based on comparison of experimental ultrasonic velocity and attenuation spectra with theoretically predicted spectra from mathematical models. McClements [37] and Challis et al. [3] summarise the most important aspects.

Waves propagating in emulsions and suspensions are altered in several ways: a) waves are scattered and change direction b) waves are attenuated due to different energy absorbtion mechanisms c) waves that travel through the suspended particles and scattered waves interfere with the waves that propagated unaltered through the medium.

The scattering of an ultrasonic wave depends on the wavelength to particle radius ratio. There are three regimes identified. The long wavelength radius regime ($\lambda > R$), the intermediate wavelength radius regime ($\lambda \sim R$) and the short wavelength radius regime ($\lambda < R$). The long wavelength radius regime is the most important as most ultrasonic measurements fall into this category, here particle sizes are of the order of 10 micro metres and less. The mechanisms that scatter waves at the particles are mainly due to differences in thermophysical properties of the embedding material and the particle. Under the local pressure and temperature oscillations caused by the passing ultrasonic wave the particles contract or expand and start pulsating. This scatters wave energy into all different directions (monopole scattering). Differences in density of the particle and the surrounding fluid will cause oscillatory motion of the particle (dipole scattering) as the ultrasonic wave passes. All these processes

are not ideal and absorb energy, thus causing an excess attenuation compared to the pure fluid. Mathematically there are also different models for highly concentrated (multiple scattering) and less concentrated (single scattering) emulsions and suspensions.

Different theoretical models for wave propagation in fluids containing particles exist [39], [40], [41] and [43]. In all these models the thermophysical constants of the contained materials are entered. Since in real life the the size of particles varies (polydispersity) a distribution function can be entered. The models then predict a velocity and attenuation frequency spectrum. This spectrum is compared to the measured data and the parameters for the particle size distribution that best fit to the mathematical model are determined. Using these methods particle sizes in the range from 0.01 to 30 micro meters can be analysed. If the intermediate wavelength radius regime is also used the whole particle size range can be covered [37]. Particle sizing is a very well developed specialist field in which very advanced models and accurate measurements setups are used. Several commercial ultrasonic particle anlaysers exist currently (Opus [Sympatec GmbH, Germany],Ultrasizer [Malvern Instruments Ltd.,UK] and DT-1200 [Dispersion Technology,USA]).

2.5 Summary

In this background chapter the basics of ultrasonic wave propagation in unbounded media were presented. Then the basic characteristics of guided waves were recalled and references to modelling techniques including the global matrix method were given. Existing guided wave material property measurements rely on the attenuation due to leakage or the analysis of an entry reflection to characterise the material. Both leakage and the entry reflection are insensitive to the bulk attenuation of an embedding fluid. However for fluid characterisation the bulk wave attenuation can be very important as for example for the application of particle size determination. The bulk velocity and attenuation measurement of a sample as usually determined in ultrasonic spectrometry is a very powerful tool to monitor industrial processes. Ultrasonic measurement technology is well developed in the form of test cells, which however possess inherent short comings. In the following chapters the development

of a guided wave "dipstick" sensor is described. The sensor is measuring the same ultrasonic velocity and attenuation spectra as the conventional test cell based techniques (see section 2.4), however it removes the need of a test cell with its short comings and consists solely of a waveguide that is immersed in the sample fluid.

2.6 Figures

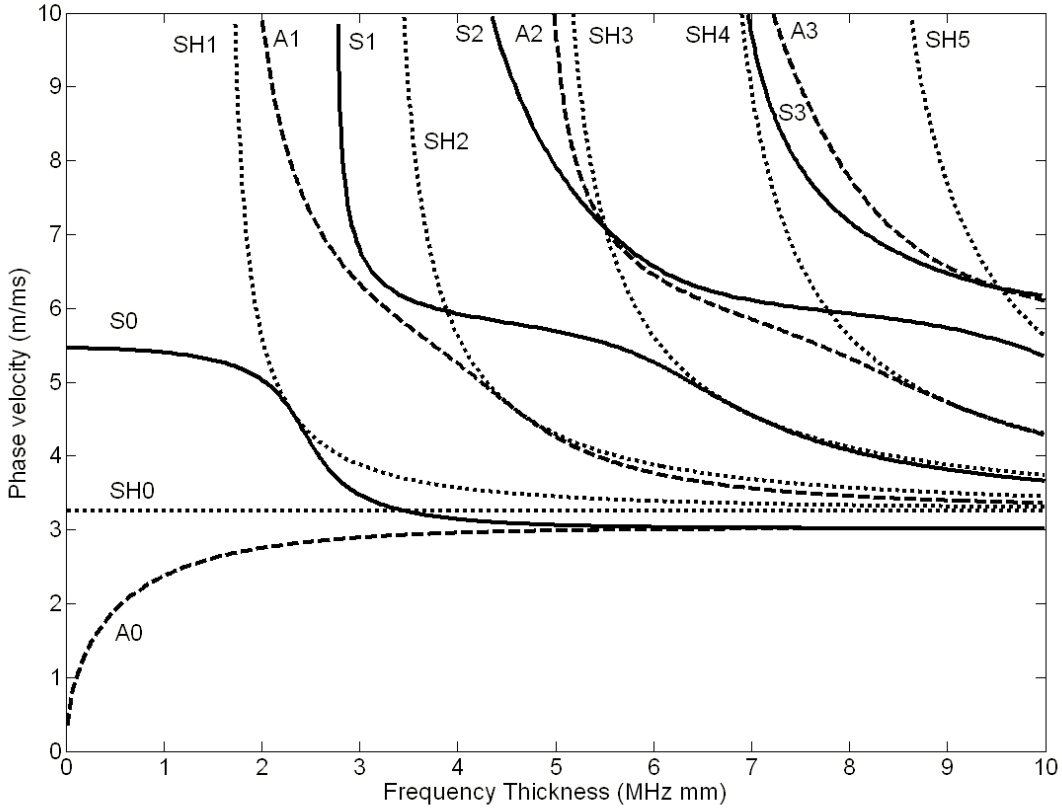

Figure 2.1: Phase velocity dispersion curves for a steel plate: Compressional modes (—), Flexural modes (- - -) and Shear Horizontal modes (· · ·)

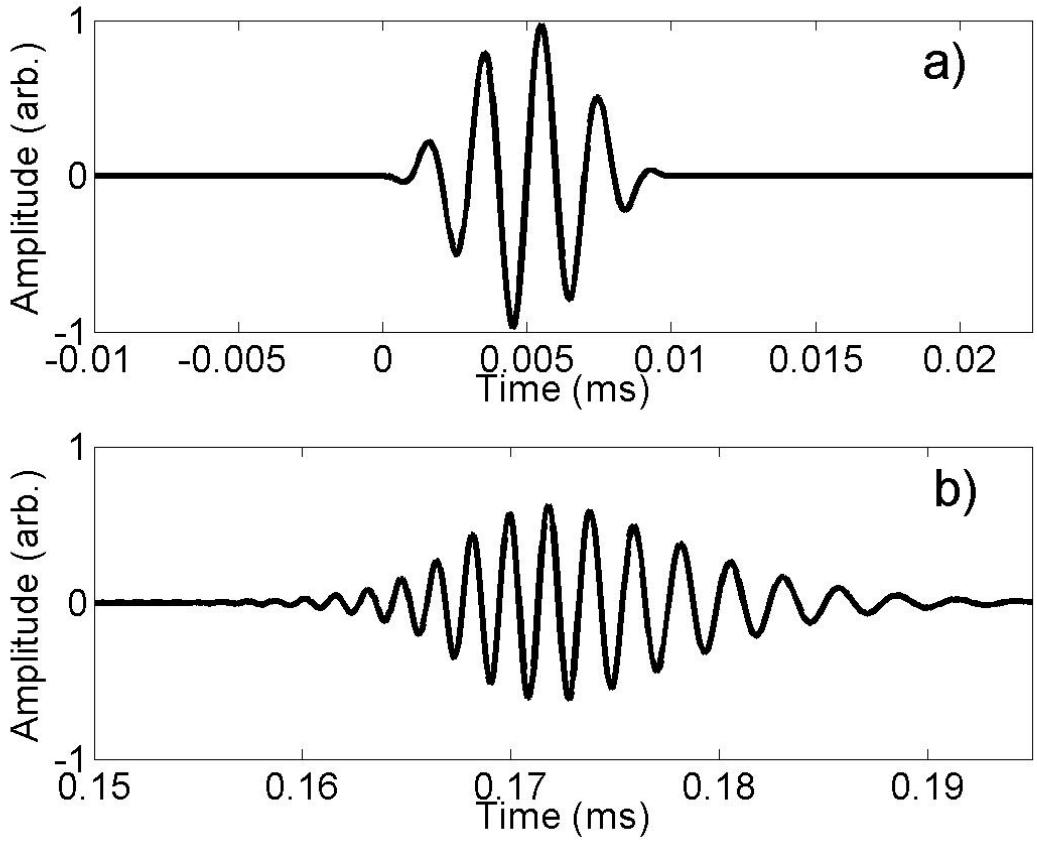

Figure 2.2: 5 cycle Hanning windowed excitation signal (a) and a prediction by the DISPERSE [22] software of the signal after 0.5m propagation distance as A0 mode on a 1mm thick steel plate (b)

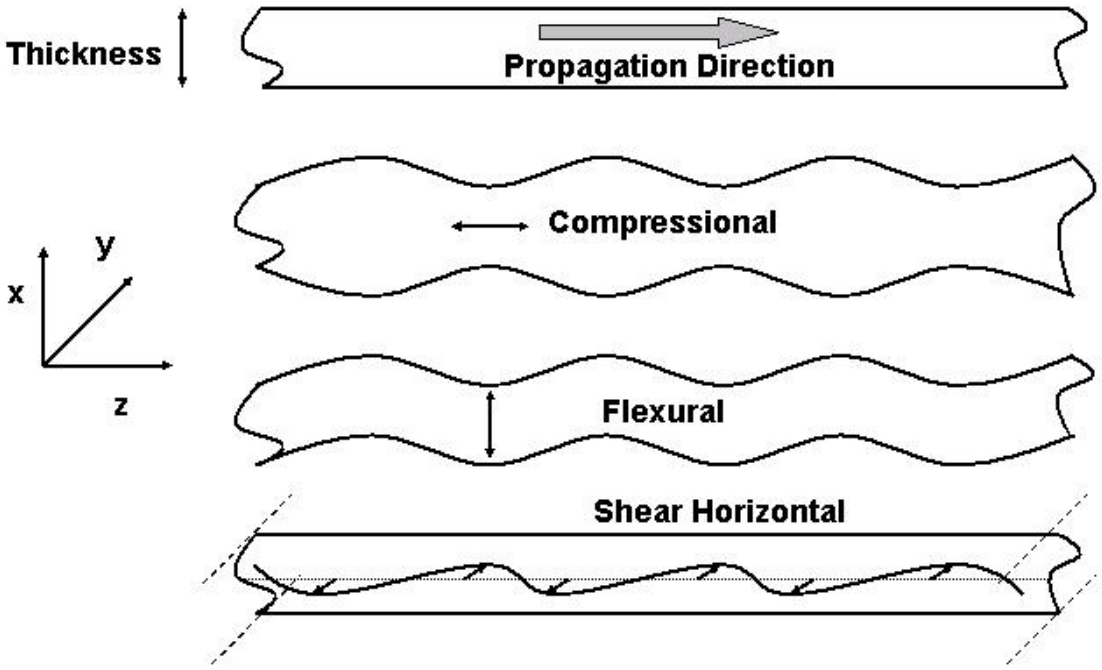

Figure 2.3: Schematic of an infinite plate, its cross section and the polarisation of the three fundamental plate wave modes.

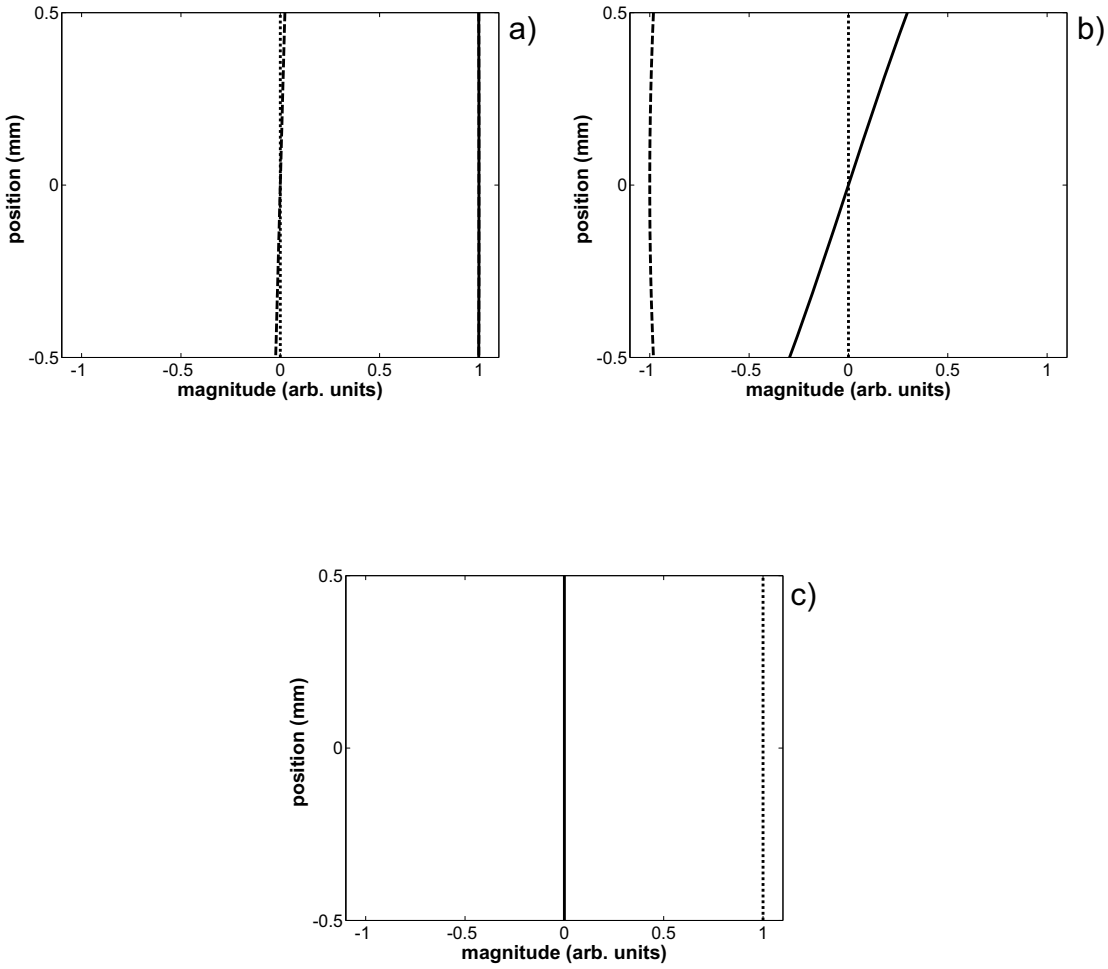

Figure 2.4: Mode shapes of the (a) $S0$ mode, (b) $A0$ mode and (c) $SH0$ mode at frequency thickness 0.1 MHz mm of a steel plate. (—) in-plane (z direction) displacement, (- - -) out-of-plane (x direction) displacement, ($\cdots$) in-plane (y direction) displacement

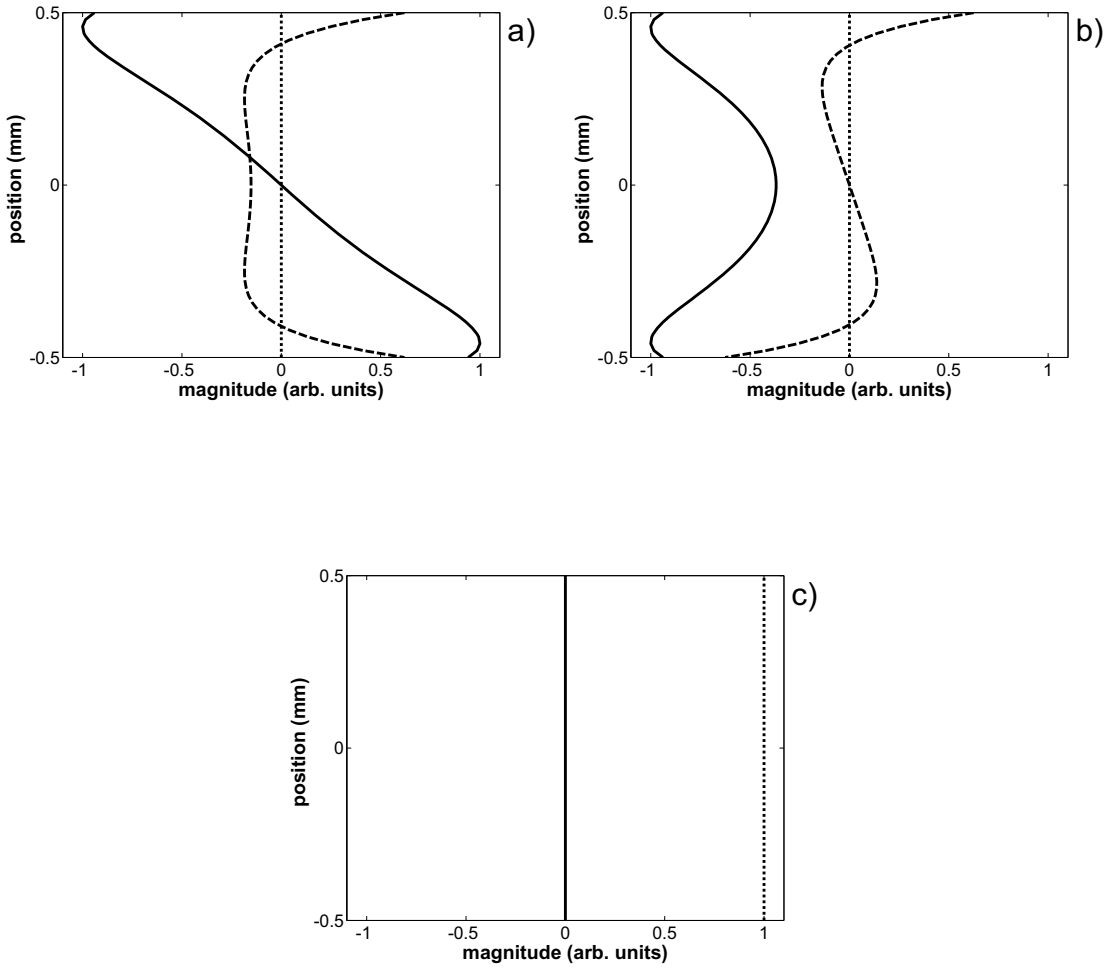

Figure 2.5: Mode shapes of the (a) $S0$ mode, (b) $A0$ mode and (c) $SH0$ mode at frequency thickness 6 MHz mm of a steel plate. (—) in-plane (z direction) displacement, (- - -) out-of-plane (x direction) displacement, ($\cdots$) in-plane (y direction) displacement

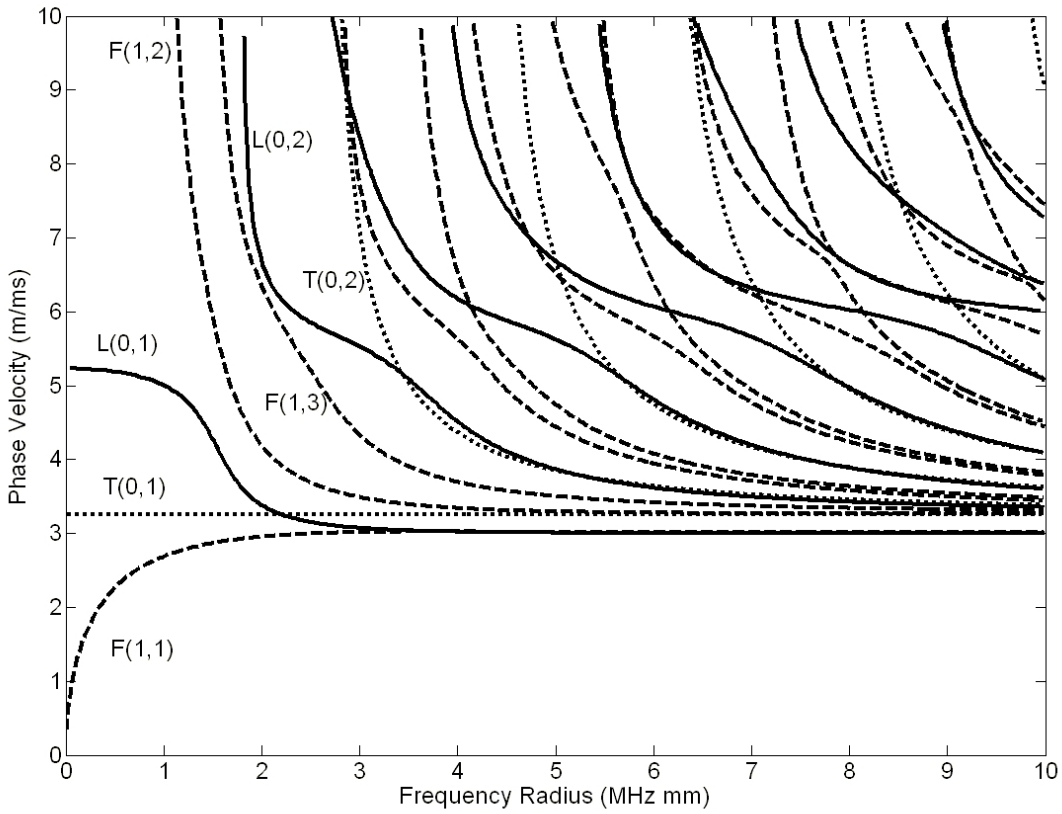

Figure 2.6: Phase velocity dispersion curves for a steel rod: Longitudinal modes (—), Flexural modes (- - -) and Torsional modes (· · ·) [only order 0 and order 1 modes are shown].

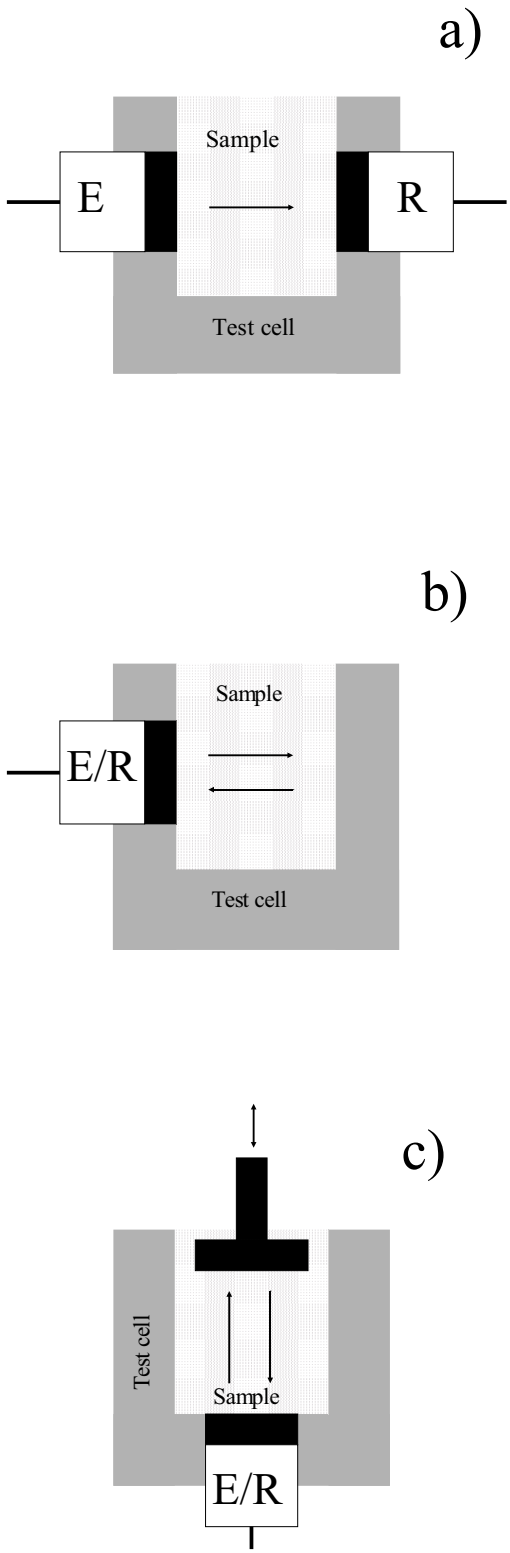

Figure 2.7: Schematics of the different measurement methods in ultrasonic spectrometry: (a) through transmission (b) pulse echo (c) interferometer

Chapter 3

Scholte mode and Quasi-Scholte mode Theory

3.1 The Scholte wave

At the interface of a liquid and solid there exist two propagating solutions to the governing equation: the leaky Rayleigh wave and the Stoneley-Scholte wave [44]. This thesis focuses on the latter and will for the sake of clarity refer to it as the Scholte wave. The Scholte wave is a special case of a Stoneley wave (on a solid/liquid interface) which was first pointed out by Scholte [45]. Subsequently the wave gained a lot of interest and work on it was extended and revised by many other authors; Pilant [46], Volkenstein and Levin [47], Padilla *et al.* [48], Glorieux *et al.* [44] and Meegan *et al.* [49] have extensively modelled the Scholte interface wave on a boundary between two half-spaces.

For the Scholte wave to exist an interface system of an elastic solid half-space coupled to a liquid half-space is required. A sketch of such a system can be seen in figure 3.1. The interface wave will propagate energy along the path described by the interface, as long as any curvature effects of the interface are large compared to the wavelength of the wave. The wave energy of the Scholte wave is distributed over both materials, the solid and the liquid, depending on the material properties of both half-spaces. For the purposes of fluid characterisation which is discussed in this thesis a high

energy content in the fluid is desirable; while in geophysics for the characterisation of marine sediment a high energy content in the solid is more desirable. The mode shape of the Scholte wave on a Steel/Water interface is shown in figure 3.2.

Figure 3.2 illustrates that the displacements amplitudes for the Steel/Water interface are extremely large in the liquid compared to the solid. The polarisation of the displacement is also mostly parallel to the interface with a small component of out-of-plane displacement. The wave amplitude decays in an exponential manner with distance from the interface and is unnoticeable at distances far from the interface. The extent to which the wave penetrates into the fluid depends on the frequency; at low frequencies the wave penetrates further into the liquid than at high frequencies. The Scholte wave in this special case can thus roughly be approximated by a longitudinal bulk wave that travels along the interface but decays away from the interface. It is therefore ideal for fluid property measurements.

3.2 Theoretical modelling of the Scholte wave

The properties of an interface wave can be theoretically modelled using the partial wave technique as described in references [8] and [23]. Recall the sketch of the interface wave system shown in figure 3.1. The displacements and stresses in the system are determined by combining the general solution of the displacements and stresses in each material with the system boundary conditions (continuity of stresses and displacements across the interface and no incoming partial waves). After some algebra the system of equations can be expressed in matrix form as follows:

$$\begin{bmatrix} -(1+\beta_1^2) & -2\beta_1 & (1+\beta_2^2)g & -2\beta_2 g \\ 2\alpha_1 & (1+\beta_1^2) & 2\alpha_2 g & -(1+\beta_2^2)g \\ 1 & \beta_1 & -1 & \beta_2 \\ -\alpha_1 & -1 & -\alpha_2 & 1 \end{bmatrix} \cdot \begin{pmatrix} L_1 \\ T_1 \\ L_2 \\ T_2 \end{pmatrix} = 0 \tag{3.1}$$

where L_1 and L_2 are the amplitudes of the longitudinal partial waves in materials 1 and 2 respectively; T_1 and T_2 are the corresponding shear partial waves. The remaining parameters in the equation are defined by:

$$\alpha_n^2 = 1 - \frac{c^2}{C_{ln}^2} \tag{3.2}$$

$$\beta_n^2 = 1 - \frac{c^2}{C_{tn}^2} \tag{3.3}$$

$$g = \frac{G_2}{G_1} \tag{3.4}$$

where n = 1, 2 represent the materials; C_l represents the longitudinal velocity and C_t the transverse velocity; G_1 and G_2 are the shear moduli of the materials.

In order for a non trivial solution to exist, the determinant of the term in square brackets in equation 3.1 has to equal zero. In the case of an interface between an ideal fluid ($G_1 = 0$) and an elastic solid the matrix equation reduces to:

$$\begin{bmatrix} i\rho_f c_l^2 & (1+\beta_2^2)G_2 & -2\beta_2 G_2 \\ 0 & 2\alpha_2 G_2 & -(1+\beta_2^2)G_2 \\ \alpha_1 & i\alpha_2 & -i \end{bmatrix} \cdot \begin{pmatrix} L_1 \\ L_2 \\ T_2 \end{pmatrix} = 0 \tag{3.5}$$

After some algebra this results in the characteristic equation for a Scholte wave [8]:

$$\left[2 - \left(\frac{c}{c_{t2}}\right)^2\right]^2 - 4\sqrt{1 - \left(\frac{c}{c_{t2}}\right)^2}\sqrt{1 - \left(\frac{c}{c_{l2}}\right)^2} - i\frac{\rho_l}{\rho_s}\left[\frac{c_l}{c_{l2}}\frac{\sqrt{c_{l2}^2 - c^2}}{\sqrt{c^2 - c_l^2 c_{t2}^4}}\right] = 0 \tag{3.6}$$

where c_l is the liquid bulk velocity, ρ_l is the liquid density, c_{l2} is the solid longitudinal bulk velocity, c_{t2} is the solid transverse bulk velocity, ρ_s is the solid density and c is the Scholte wave velocity. This expression yields the phase velocity (or wavenumber) - frequency relationship that describes the mode. In this special case of a wave propagating along the interface of an elastic solid and an ideal fluid the mode is non dispersive, i.e. the phase velocity does not change with frequency.

By substituting the calculated phase velocity into equation 1 and fixing the amplitude of one partial wave at unity the mode shape of the Scholte wave can be evaluated [23]. Figure 3.2 shows the mode shape of a Scholte wave on a steel-water interface.

3.2.1 Influence of material properties on the Scholte wave

The theoretical description of the Scholte wave has been thoroughly investigated by many researchers ([44],[47],[50]). It can be shown that the phase velocity of the Scholte wave is limited by the lower of the fluid or the transverse bulk velocity of the elastic medium ($c_{scholte} < c_{liquid}, c_{t,solid}$). The dependence of the Scholte wave velocity on the density and longitudinal velocity ratio of the neighbouring materials can be displayed on a contour map as shown in figure 3.3. The Scholte wave velocity is close to the fluid velocity when the solid material is very stiff and dense. As the stiffness of the solid compared to the fluid reduces, which is indicated by moving upward on the ordinate in figure 3.3, the Scholte velocity decreases. Also by reducing the solid density the Scholte velocity is reduced (movement to the right on the abscissa).

The distribution of the fraction of energy flowing in the fluid and solid also depends on the density ratio of the two materials. A similar contour map to that of figure 3.3 has been created to visualise the distribution of energy flow in the two materials. Figure 3.4 shows the fraction of the total energy flow that is located in the liquid for different density and longitudinal velocity ratios of the two media.

The contour maps of the Scholte wave velocity and energy distribution in figure 3.3 and 3.4 have been plotted for a fixed value of Poisson's ratio, which in this case was 0.2865 and corresponds to a material like steel. The analysis can be carried out for other Poisson's ratios which will slightly alter the contour maps. The availability and affordability of steel made it the material of choice and hence its Poisson's ratio was chosen for the contour maps.

3.2.2 Modelling a viscous fluid

The derivation of the properties of the Scholte mode for an ideal fluid has been dealt with above. The derivation for a viscous fluid uses a similar approach. Here the fluid is assumed to be Newtonian. The viscous medium is modelled as a solid with appropriate parameters. More theoretical details on this approach are described in [22], [30]. The following equations representing the viscous fluid can be deduced:

$$C_l = \left(\frac{\lambda_f}{\rho}\right)^{1/2} \tag{3.7}$$

$$\kappa_l = \left(\frac{4\pi\omega\nu}{3C_l^2}\right) \tag{3.8}$$

$$C_s = (2\omega\nu)^{1/2} \tag{3.9}$$

$$\kappa_s = 2\pi \tag{3.10}$$

where C_l is the longitudinal bulk wave velocity, λ_f is the fluid bulk modulus. κ_l is the longitudinal bulk wave attenuation (nepers per wavelength), ω the angular frequency and ν the kinematic viscosity of the fluid. C_s stands for the shear bulk wave velocity and κ_s for the shear bulk wave attenuation (nepers per wavelength). Equations 3.7-3.10 assume low viscosities which introduces some simplifications in their derivations [22].

In order to solve for the viscous Scholte equation the complex bulk velocities and moduli have to be entered into equations 3.2-3.4. These are found from equations 3.7-3.10 by the following expression:

$$c_{ln} = \frac{C_l}{1 + i\frac{\kappa_l C_l}{\omega}} \tag{3.11}$$

$$c_{tn} = \frac{C_s}{1 + i\frac{\kappa_s C_s}{\omega}} \tag{3.12}$$

$$g = \frac{G_2}{-i\omega\rho_l\nu} \tag{3.13}$$

where c_{ln} is the complex longitudinal bulk velocity of material n and c_{tn} is the complex transverse bulk velocity of material n.

By substituting the above equations into equations 3.2-3.4 where applicable, a new characteristic equation and mode shape can be found. The Scholte wave in this system becomes dispersive and attenuated. However the dispersion effect is relatively weak and for small viscosities the map in figure 3.3 still accurately represents the velocity and density dependence. The model can also easily be extended to non-viscous fluids as long as the quantities c_{ln} and c_{tn} of equations 3.11 to 3.13 can be determined, for example by means of another model or direct measurement.

3.3 Properties of the quasi-Scholte plate mode

In real life it is impossible to find a semi-infinite half-space; a very thick piece of solid material would have to be used which would be inconvenient to handle. Therefore another boundary was introduced to the system. This creates a plate that is immersed in an infinite (in practice large) space of liquid. In this new fluid-plate system a mode that is very similar to the Scholte wave exists. The mode was termed quasi-Scholte (QS) mode, because it asymptotically approaches the Scholte wave velocity at high frequencies. In the following section the quasi-Scholte mode will be examined in more detail. A software package called DISPERSE [22] was used to trace the dispersion curves. DISPERSE is a multi purpose package to trace dispersion curves in multiple material layer stacks of solid materials and viscous fluids. Also a routine solely for the purpose of tracing the quasi-Scholte mode dispersion curves was written in Matlab and the basic equations behind the routine are outlined in Appendix A. It was verified that both programs yield the same results.

Here the DISPERSE solutions for an embedded plate mode are shown and discussed. First an inviscid fluid is used as the embedding medium and then a viscous liquid.

The velocity dispersion characteristics are virtually unchanged by the introduction of viscosity but the attenuation is noticeably affected. A steel plate ($c_l = 5959.5m/s$, $c_s = 3260m/s$, $\rho_{steel} = 7932kg/m^3$, thickness=1 mm) is embedded in an infinite space of water ($c_l = 1500m/s$, $\rho_{water} = 1000kg/m^3$). Figure 3.5 shows the phase velocity dispersion curve of the plate Scholte mode. The phase velocity of the quasi-Scholte plate mode rises with frequency from zero and gradually asymptotes to the non-dispersive Scholte wave velocity of two elastic half spaces. A physical explanation of the asymptotic behaviour is the decrease of mode wavelength with increasing frequency. At a certain point the wavelength will be small compared to the thickness of the plate. Since the Scholte wave displacements decay in an exponential manner away from the interface the mode resembles a mode on an infinite halfspace at high frequencies, whereas at lower frequencies the two interfaces of the plate interact. The phenomenon is also well known in plate waves where the A0 and S0 modes are asymptotic to the Rayleigh wave solution [51]. In the remainder of this thesis the plate Scholte mode will be referred to as the quasi-Scholte (QS) mode, the terminology being similar to that of a quasi-Rayleigh wave on a finite plate.

The similarities of the quasi-Scholte mode and the A0 mode in a free plate are highlighted by their mode shapes. Figure 3.6(a) shows that the out of plane displacement component at 100kHzmm is almost constant across the section of the plate and the strain energy density indicates that most of the energy is propagating in the plate. At higher frequencies most of the energy is travelling in the fluid as shown in figure 3.6(b). Figure 3.6(c) shows the mode shape in the plate only at 2MHzmm. Displacements decay away from the surfaces and are a minimum at the centre of the plate. This illustrates the effect of the quasi-Scholte mode becoming asymptotic to an interface wave (Scholte wave) at high frequencies as discussed above.

An important property of the quasi-Scholte mode is its change in energy partition between fluid and solid with frequency. Figure 3.7 shows the fraction of energy flow that is situated in the plate and fluid at different frequencies. At low frequencies ($< 500kHzmm$) the energy travels predominantly in the plate while at high frequencies ($> 1MHzmm$) most of the energy travels in the fluid. The cross over point

of the two curves occurs at about $400kHzmm$ for a steel plate embedded in water. This means that the mode can be made more or less sensitive to the embedding medium properties. If highly attenuating materials are surrounding the wave guide, careful frequency selection will allow an appropriate fraction of energy to travel in the plate so that a reasonable propagation range can be obtained.

The sensitivity of the QS-mode to bulk fluid properties is demonstrated best by graphs that plot QS-mode dispersion curves for different properties of the embedding fluid. Figure 3.8 shows the quasi-Scholte mode group velocity as a function of frequency for different longitudinal velocities of the embedding fluid. Figure 3.9 displays the theoretical attenuation of the quasi-Scholte mode as a function of frequency for different viscosities at a fixed longitudinal bulk velocity of the embedding medium. A more detailed treatment of the QS-mode sensitivity to fluid properties can be found in section 3.4.

There are two attenuation mechanisms for the quasi-Scholte and Scholte modes. The first is the leakage of shear waves from the plate surface into the embedding viscous fluid and the second is the attenuation of a longitudinal bulk wave in the viscous fluid. Energy that is guided along the interface in the form of an evanescent longitudinal wave will be attenuated by longitudinal attenuation. In the case of a purely Newtonian viscous fluid this attenuation is due to viscosity and can be modelled by equation 3.8 (assuming low viscosities [31]). Also for Newtonian fluids both attenuation mechanisms depend on the viscosity only (see equations 3.8,3.9,3.10). At low frequencies the shear leakage is dominant while at higher frequencies the evanescent longitudinal wave attenuation contributes significantly to the quasi-Scholte mode attenuation. Figure 3.10 shows the total attenuation of the quasi-Scholte mode on an aluminium plate ($c_l = 6320.0m/s$, $c_s = 3130m/s$, $\rho_{al} = 2700kg/m^3$, thickness=1 mm) immersed in glycerol ($c_l = 1860m/s$, $\rho_{glycerol} = 1258kg/m^3$ $\eta_{glycerol} = 1Pas$). A line showing the attenuation due to shear leakage only is also shown (the lines are traced in DISPERSE; for the shear leakage only case the longitudinal attenuation is set to $\kappa_l = 0$ in equation 3.8) . The difference between the two curves is linked to the longitudinal bulk attenuation of the fluid. Thus if the longitudinal bulk velocity and

the shear properties of the fluid are known, it is possible to measure the longitudinal bulk attenuation of the fluid surrounding the waveguide.

Figure 3.10 considers a viscous liquid. The shear properties of the liquid are described by equations 3.9, 3.10. Therefore the longitudinal attenuation and the shear velocity of the embedding medium are both functions of viscosity and frequency. This has the effect that the quasi-Scholte mode attenuation is almost entirely dependent on the viscosity of the fluid. The phrase "almost entirely dependent" is used here since the longitudinal bulk velocity of the fluid has a small effect on the QS-mode attenuation and the viscosity has a small effect on the group velocity of the QS-mode. The group velocity of the QS-mode changes by about 10 m/s ($\sim 0.5\%$ of C_l) when the viscosity changes from 0 to 1 Pas for a glycerol-like fluid ($c_l = 1860m/s$, $\rho_{glycerol} = 1258kg/m^3$ $\eta_{glycerol} = 1Pas$). For a Newtonian viscous fluid the quasi-Scholte mode group velocity is almost entirely dependent on the fluid bulk velocity and its attenuation is almost entirely dependent on the fluid viscosity. It can therefore be concluded that a measurement of the QS mode group velocity and its attenuation can be used to determine the fluid bulk velocity and viscosity.

The assumption of a Newtonian viscous fluid links the bulk shear velocity and bulk longitudinal attenuation of the fluid to the viscosity; they therefore are not independent properties. However for a more complex non-Newtonian fluid, the attenuation and viscosity become two independent fluid properties. Therefore for a non-Newtonian fluid the quasi-Scholte mode attenuation will also not solely depend on viscosity but also on the fluid bulk attenuation. This is illustrated in figure 3.11, where the QS-mode attenuation is plotted for a liquid of the same viscosity but with different longitudinal bulk wave attenuation. In order to extract the fluid bulk attenuation using the QS-mode it is therefore necessary to know the fluid shear properties or in other words its complex shear velocity. This can be done using a method such as that described by Vogt [36]. He used a torsional wave in a rod that is immersed in a viscous fluid. By evaluating the attenuation of the wave, the shear leakage and thus shear properties of the fluid were determined. The use of a torsional wave in a rod is physically analogous to a SH-wave in a plate. The latter was used for the work presented in this thesis since the quasi-Scholte mode also

propagates in a plate geometry and therefore the same plate can be used to carry out a different measurement. Section 3.5 describes the use of the fundamental SH0 mode in a plate to extract the fluid shear properties.

3.4 Quasi-Scholte mode sensitivity to fluid properties

This section investigates the sensitivity of the quasi-Scholte mode to the fluid bulk properties. The sensitivity indicates the change in measured property due to a change in the actual fluid bulk property. Here the sensitivity is defined as:

$$S = \frac{\partial M}{\partial P} \tag{3.14}$$

where S is the sensitivity, M the measured quantity and P the fluid property that is changing. It is important to know the sensitivity of a measurement technique in order to identify how accurate it can be and how different sources of error can influence the measurement. The quasi-Scholte mode is influenced by all the bulk properties of the fluid, namely bulk velocity, viscosity and bulk attenuation; while each of these properties simultaneously affect the quasi-Scholte mode, one property is isolated, this property is then changed and the effect on the measured quantity is predicted.

3.4.1 Sensitivity to the fluid bulk velocity

For bulk velocity measurements of fluids using the quasi-Scholte mode, the group velocity or phase velocity of the quasi-Scholte mode can be identified as the measured quantity and the bulk velocity as the measurand, the property to be measured. The sensitivity of the quasi-Scholte mode to the fluid bulk velocity thus can be defined as:

$$S_{Bvel} = \frac{\partial C_{QS}}{\partial C_B} \tag{3.15}$$

where S_{Bvel} is the sensitivity to the bulk velocity, C_{QS} is the quasi-Scholte mode velocity, either group or phase velocity and C_B is the fluid bulk velocity that surrounds the plate.

The DISPERSE software [22] was used to calculate the quasi-Scholte mode group and phase velocity dispersion curves for different bulk velocities. Results of the group and phase velocity sensitivity to the fluid bulk velocity are shown in figure 3.12 and 3.13 respectively.

The sensitivity depends on the properties of the fluid and the plate. Therefore plates of a different material than steel and fluids with higher or lower bulk velocities than water will have a different sensitivity of the quasi-Scholte mode velocity to the fluid bulk velocity. However in practice most liquids are water based and steel is a cheap and readily available material that is well suited to the application. Hence sensitivities close to those shown in figures 3.12 and 3.13 will most likely be encountered. Figures 3.12 and 3.13 also show that the quasi-Scholte mode is insensitive at frequencies below 0.2 MHz mm. The group velocity is always more sensitive than the phase velocity and in the frequency thickness range of $0.25 - 0.5$ MHz mm the quasi-Scholte mode group velocity is most sensitive to the fluid bulk velocity. At high frequencies a change in bulk velocity is reflected in a change of equal magnitude in the group velocity of the quasi-Scholte mode.

3.4.2 Sensitivity to the fluid shear viscosity

For fluid viscosity measurements the attenuation of the quasi-Scholte mode will have to be used. The definition of sensitivity now becomes the following:

$$S_{Visc} = \frac{\partial \alpha_{Scholte}}{\partial \eta_F} \tag{3.16}$$

where S_{Visc} is the sensitivity to fluid viscosity, $\alpha_{Scholte}$ is the attenuation of the quasi-Scholte mode and η_F is the fluid shear viscosity. The DISPERSE software [22] was used to calculate the quasi-Scholte mode attenuation dispersion curves for

different fluid shear viscosities. Results of the sensitivity to the fluid shear viscosity are shown in figure 3.14.

Figure 3.14 shows that the sensitivity to viscosity increases with frequency thickness. Below 0.2 MHz mm the sensitivity is less than 1 np/m/Pas; it rises to 5 np/m/Pas at about 0.5 MHz mm, and keeps on rising at higher frequencies.

3.4.3 Sensitivity to the fluid longitudinal bulk attenuation

The fluid longitudinal bulk attenuation influences the quasi-Scholte mode attenuation. Therefore the sensitivity of the quasi-Scholte mode attenuation measurement to the fluid bulk attenuation was also determined. The definition of sensitivity now becomes the following:

$$S_{\alpha b} = \frac{\partial \alpha_{Scholte}}{\partial \alpha_F} \tag{3.17}$$

where $S_{\alpha b}$ is the sensitivity to fluid bulk attenuation, $\alpha_{Scholte}$ is the attenuation of the quasi-Scholte mode in nepers per wavelength and α_F is the fluid bulk longitudinal attenuation in nepers per wavelength.

Figure 3.15 shows that the sensitivity never reaches unity. In the frequency-thickness product range from $0.2 - 0.5$ MHz mm the sensitivity rises from $0.2 - 0.7$. The sensitivity never reaches unity because at any frequency, less than the total wave energy travels in the fluid. However at high frequencies the sensitivity approaches unity, because almost all of the energy travels in the fluid. Then the quasi-Scholte mode resembles a longitudinal bulk wave that is trapped at and propagates along the plate surface.

3.5 Liquid shear property determination using the SH0 mode

The shear properties of the liquid are determined using a method that has been validated by Vogt *et al.* [52]. They used a torsional wave in a rod. Here the lowest

order Shear Horizontal (SH) mode is used which is the plate equivalent of a torsional wave in a rod. The SH mode exhibits displacement purely in the plane of the plate and does not show any out-of-plane displacements at the plate surface, see figure 3.16. At the plate surface the liquid is sheared and shear waves in the liquid will be set up. Due to the high attenuation of shear waves in liquids, the energy is dissipated rapidly and the shear waves do not penetrate far into the liquid. The SH mode propagating in the plate is attenuated along its propagation path due to energy lost in shearing the fluid. The attenuation is dependent on the viscosity of the fluid and can be approximated by

$$\alpha = \frac{1}{2h}\left(\frac{2\rho_f \omega \eta}{\rho_s G}\right)^{1/2} \tag{3.18}$$

where h is the plate thickness, ρ_f is the fluid density, ρ_s is the solid density, ω is the angular frequency, η is the fluid viscosity and G is the shear modulus of the plate. The derivation of equation 3.18 is shown in Appendix B.

The formula works very well for frequency-plate thickness products up to about 2MHz-mm, where the assumption of a constant mode shape across the plate starts to break down. (The mode shape of the SH-mode for a free plate is independent of frequency [8], however when a viscous fluid surrounds the plate the mode shape becomes frequency dependent). A comparison of equation 3.18 with the exact numerical solution of the equations obtained using the DISPERSE software [22] shows agreement to within 0.4% at 2MHz for a 1 mm thick steel plate immersed in glycerol. The difference at 1MHz for the same plate is 0.04%. The frequency-thickness products reported in this thesis are all below 1MHz-mm and therefore the simple approximate solution of equation 3.18 was used to model attenuation and to retrieve the viscosity from measured values of the SH mode attenuation. Strictly speaking the above analysis is only true for Newtonian fluids. However the effective viscosity of the liquid determined by equation 3.18 describes the influence of the shear behaviour of the liquid on the plate and can be evaluated at each frequency. This allows different effective viscosities to be determined at different shear rates which is in essence a non-Newtonian model. The effective viscosity is then used to evaluate a liquid shear velocity which can be entered into the model of the quasi-Scholte mode

([53], appendix A).

3.6 Summary

In this chapter the Scholte wave was introduced. Modelling techniques are well established in the literature and have been summarised for ideal and viscous fluids in contact with an elastic solid half space. Numerical results for Scholte wave phase velocities and energy distribution between the two materials were presented for a range of material property combinations. Then the quasi-Scholte mode plate mode was introduced. The change of geometry from a half space to a plate immersed in a fluid complicates the analysis slightly and mainly introduces a frequency dependence of the quasi-Scholte mode characteristics. At high frequencies the plate mode behaves like the Scholte wave on a half space. A physical explanation for this is that the wavelength of the wave becomes very small compared to the plate thickness and due to the evanescent nature of the Scholte wave only one interface is seen by the wave. Two different attenuation mechanisms of the Scholte and quasi-Scholte wave were identified: shear leakage and attenuation due to fluid bulk attenuation.

The sensitivity of the quasi-Scholte mode to several fluid bulk parameters has been analysed. It was found that the group velocity of the quasi-Scholte mode is very sensitive to the fluid bulk velocity. In the range of $0.25 - 0.5$ MHz mm the group velocity of the quasi-Scholte mode on a steel plate is most sensitive to the fluid bulk velocity. The phase velocity is not as sensitive as the group velocity and since it is more difficult to evaluate the phase velocity using a pulse echo measurement its use is not recommended. The analysis revealed that the sensitivity to fluid shear viscosity increases with increasing frequency. However it has to be kept in mind that at higher frequencies the overall attenuation will be higher and can introduce practical difficulties and sources of error. It was also found that the sensitivity to bulk longitudinal attenuation increases from zero to unity in an "S" shaped curve with frequency. The transition region lies in the frequency thickness product range of $0.25 - 0.5$ MHz mm which corresponds to the range of maximum sensitivity of the group velocity to the fluid bulk velocity. It is believed that this increase in sensitivity is due to the fact that a higher fraction of the quasi-Scholte mode energy

is travelling in the fluid and thus the effect of the fluid properties is more strongly reflected in the quasi-Scholte mode properties.

3.7 Figures

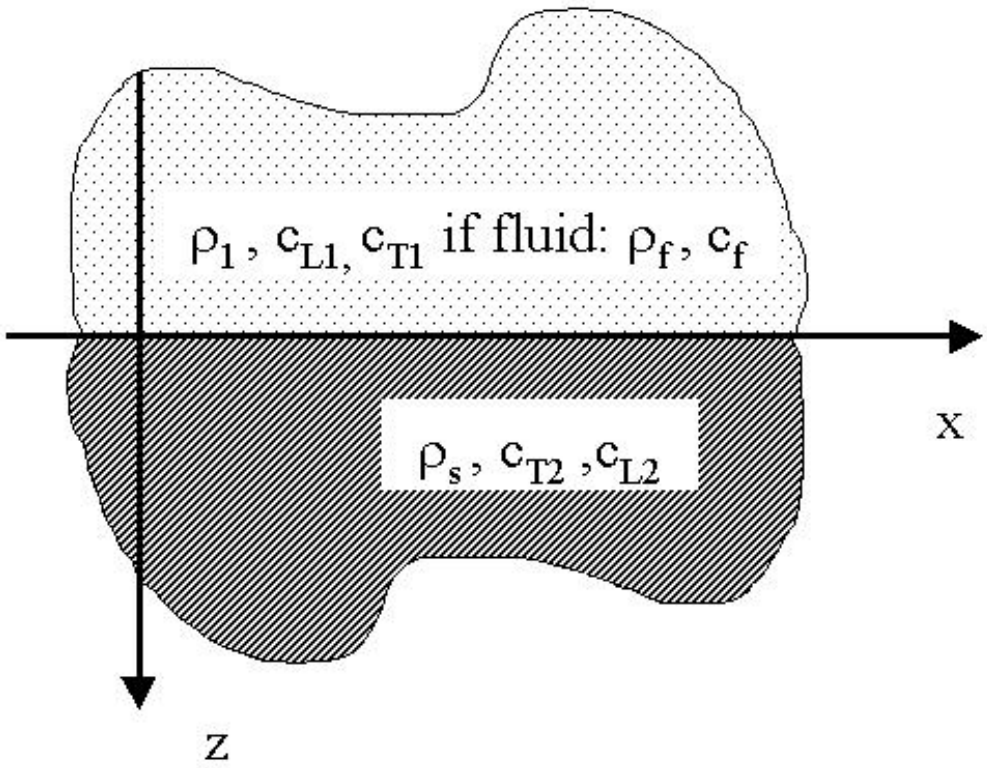

Figure 3.1: Sketch of the system used to study the Scholte wave

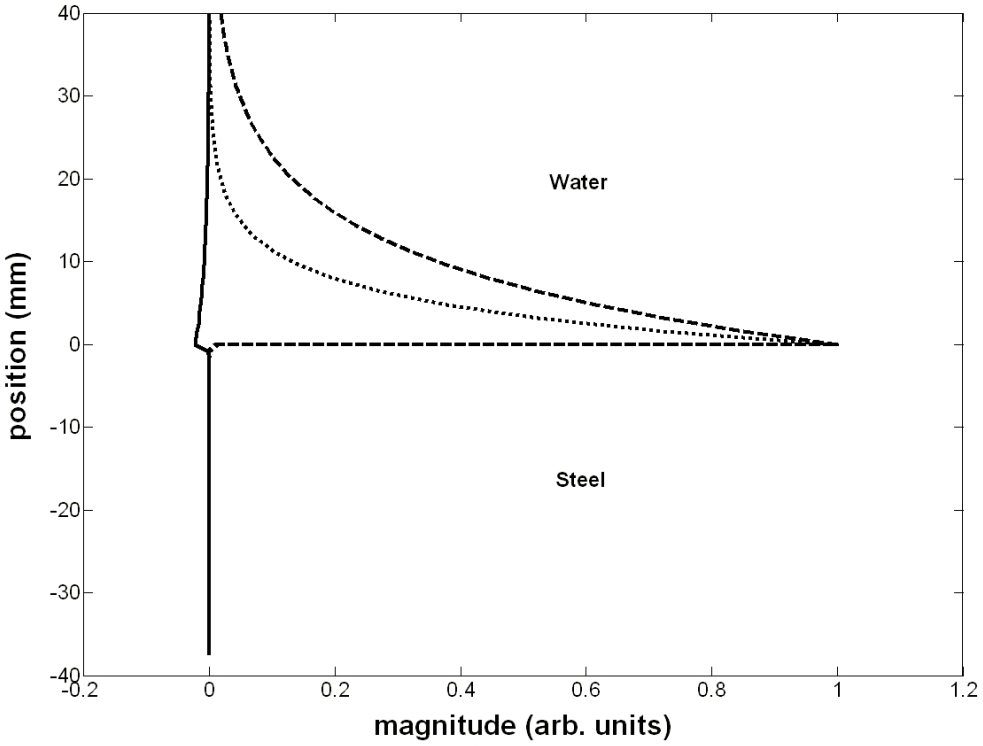

Figure 3.2: Mode shape of the Scholte wave on a Steel Water interface at 1 MHz [(—) out of plane displacement, (- - -) in plane displacement, (· · ·) strain energy density]

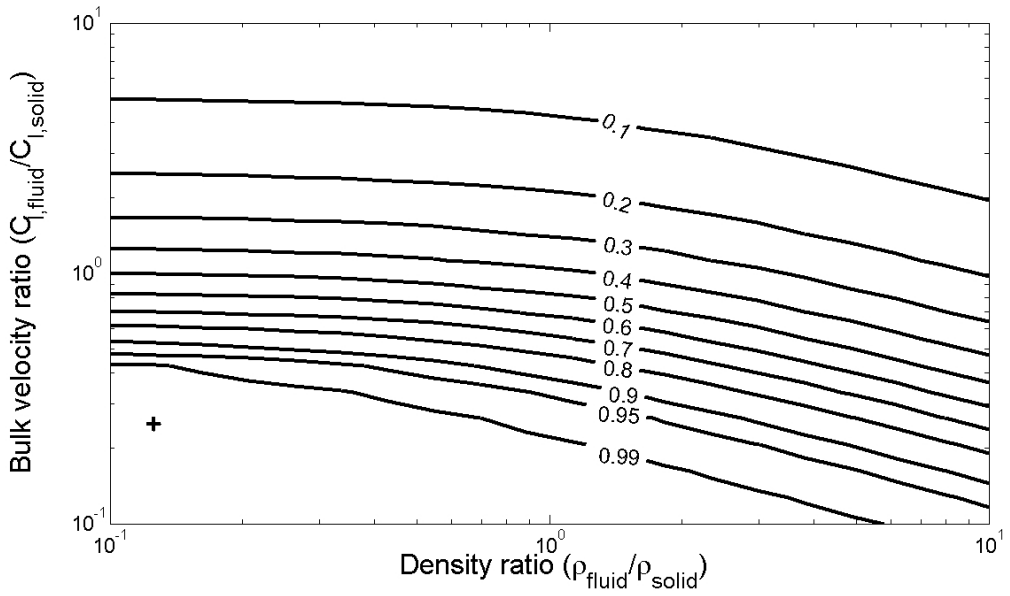

Figure 3.3: Contour map of the Scholte wave phase velocity to fluid bulk velocity ratio ($\frac{C_{scholte}}{C_{fluid}}$) as a function of density and longitudinal velocity ratios ($\frac{\rho_{fluid}}{\rho solid}, \frac{C_{l,fluid}}{C_{l,solid}}$) of the bulk materials (at fixed Poisson's ratio $\nu = 0.2865$). The (+) sign indicates a steel/water interface.

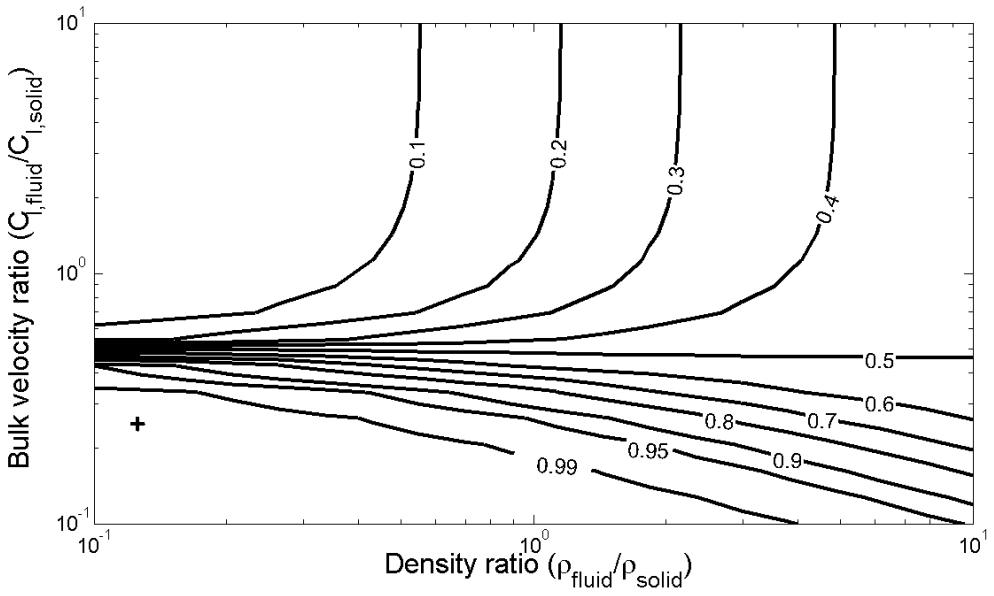

Figure 3.4: Contour map showing the fraction of Scholte wave energy that travels in the fluid ($\frac{E_{fluid}}{E_{total}}$) as a function of density and longitudinal velocity ratios ($\frac{\rho_{fluid}}{\rho solid}$, $\frac{C_{l,fluid}}{C_{l,solid}}$) of the bulk materials. (at fixed Poisson's ratio $\nu = 0.2865$). The (+) sign indicates a steel/water interface.

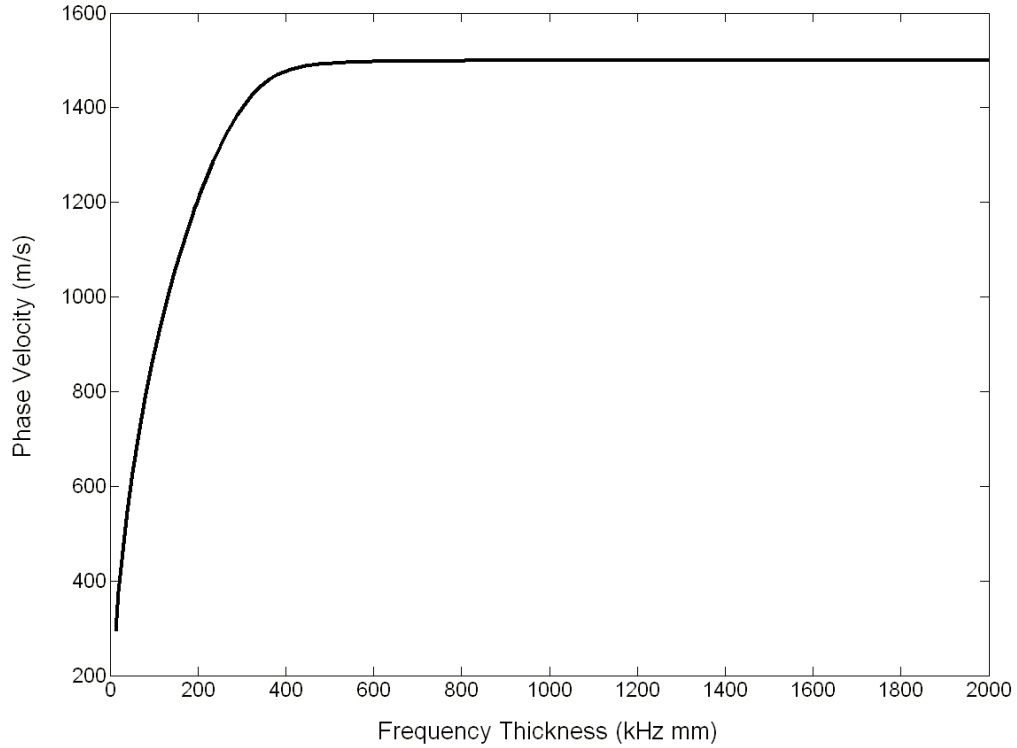

Figure 3.5: The phase velocity dispersion of the quasi-Scholte mode on a steel plate surrounded by water (see text for material properties).

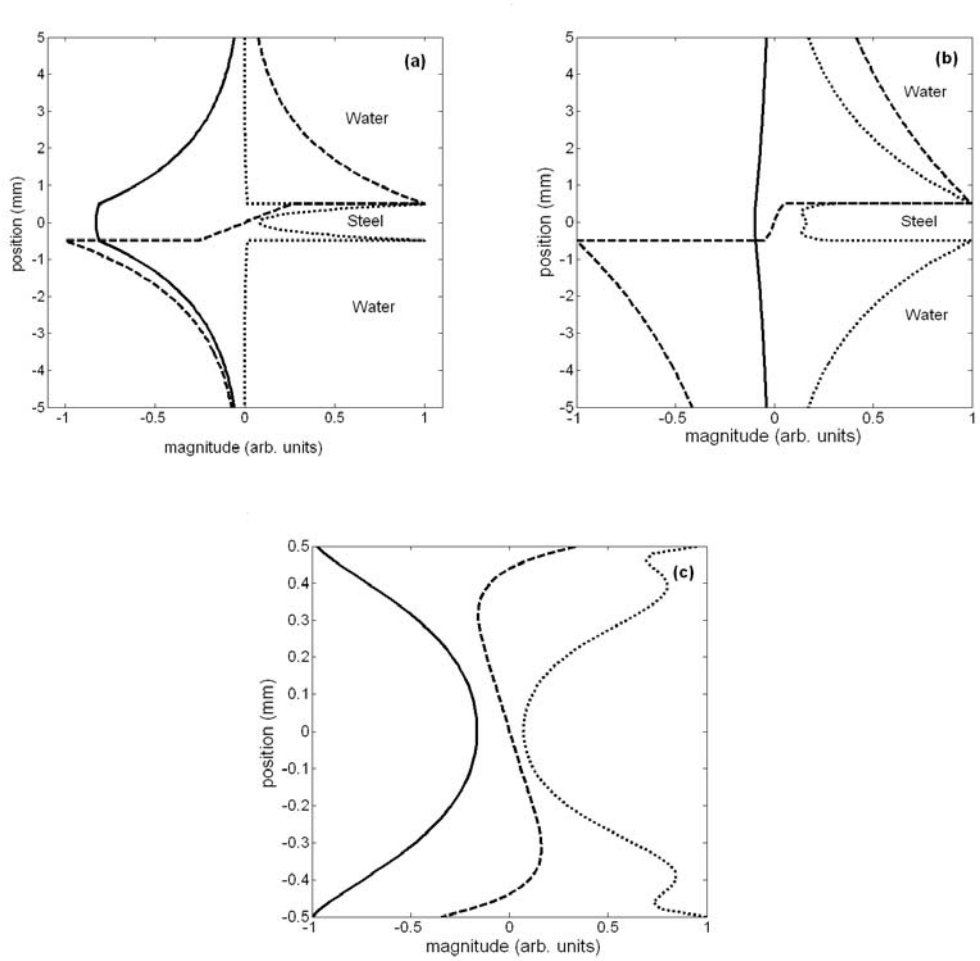

Figure 3.6: Mode shapes of the quasi-Scholte mode (water/steel) at frequency thicknesses (a) 0.1 MHz-mm (b) 0.5 MHz-mm (c) 2 MHz-mm (in plate only) for a 1 mm thick plate [(—) out of plane displacement, (- - -) in plane displacement, $(\cdots)$ strain energy density]

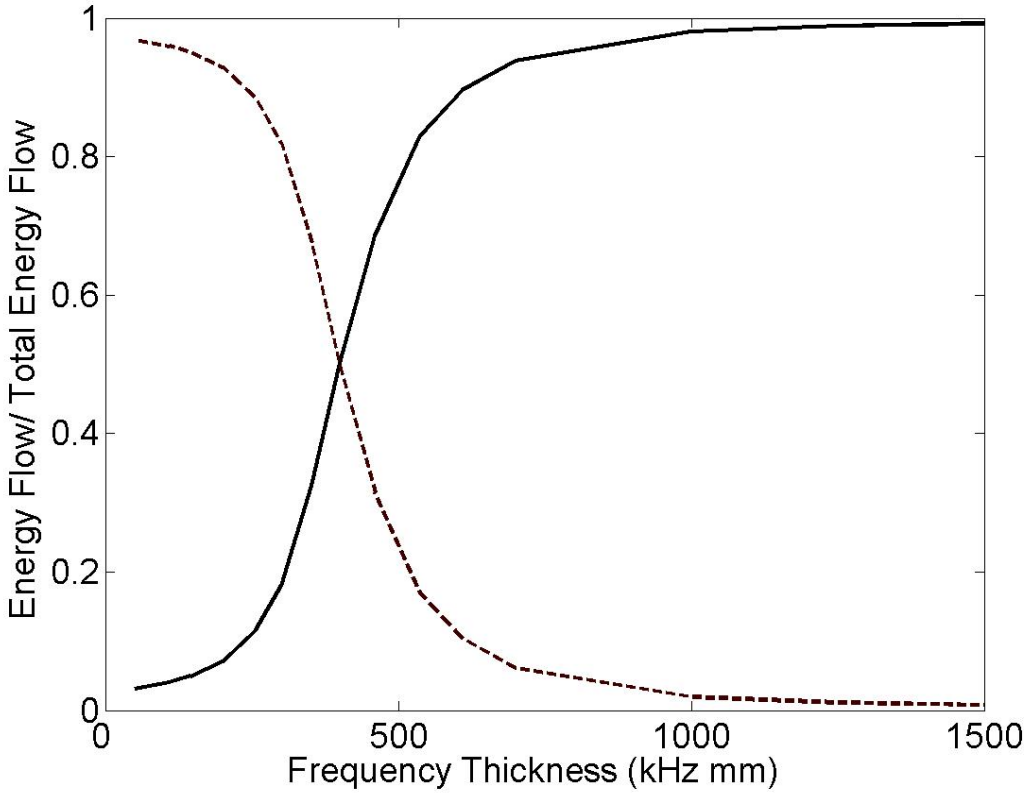

Figure 3.7: Quasi-Scholte energy flow localised in the fluid (water) and plate (steel) as a function of frequency [(—) Energy flow in fluid, (- - -) Energy flow in plate].

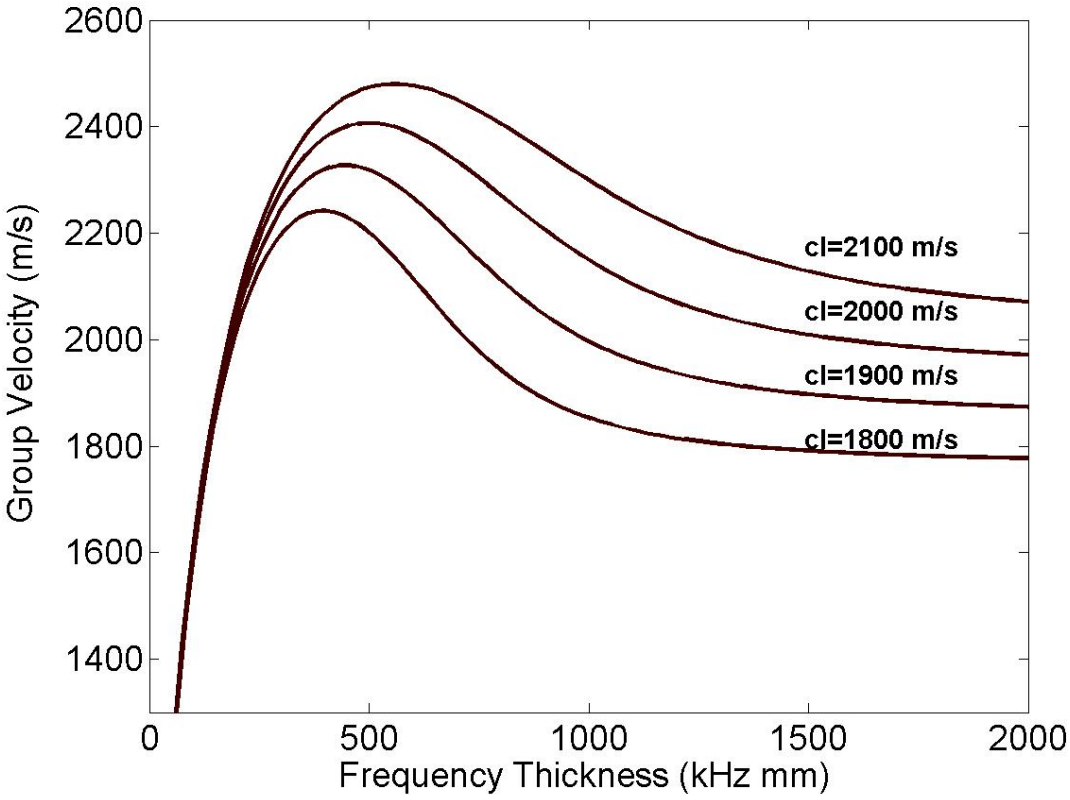

Figure 3.8: Quasi-Scholte mode group velocities as a function of frequency for different longitudinal bulk velocities (c_l) (The other properties are as in figure 3.10)

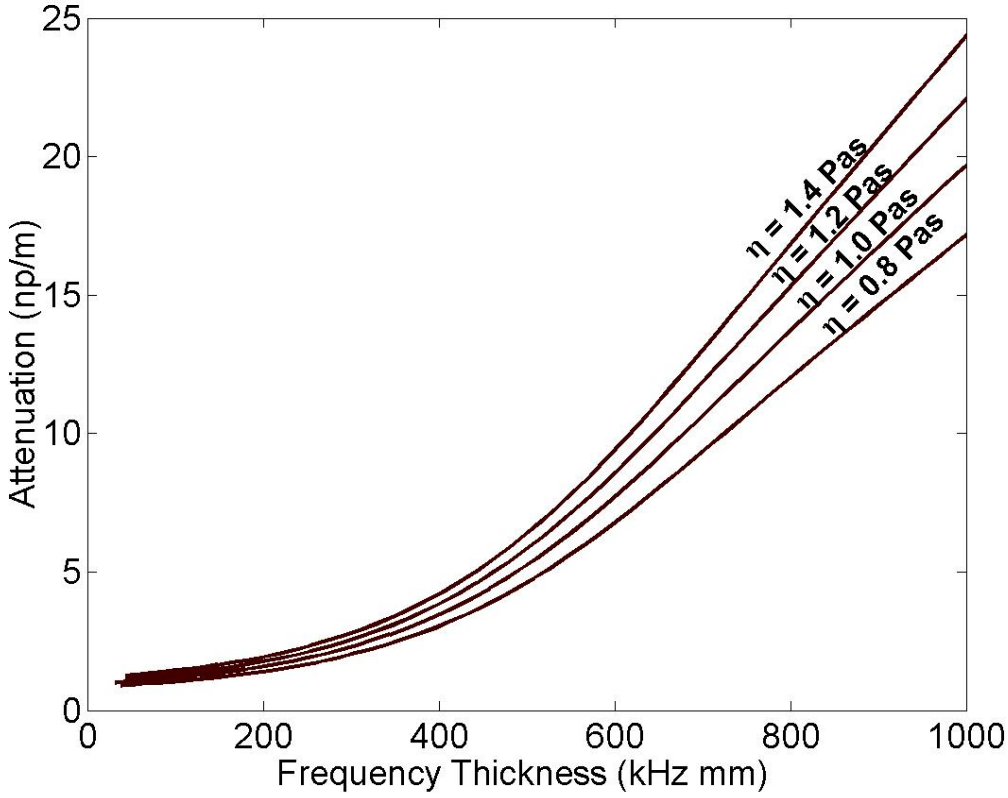

Figure 3.9: Quasi-Scholte mode attenuation as a function of frequency for different viscosities (η) at $c_l = 1800m/s$ (The other properties are as in figure 3.10)

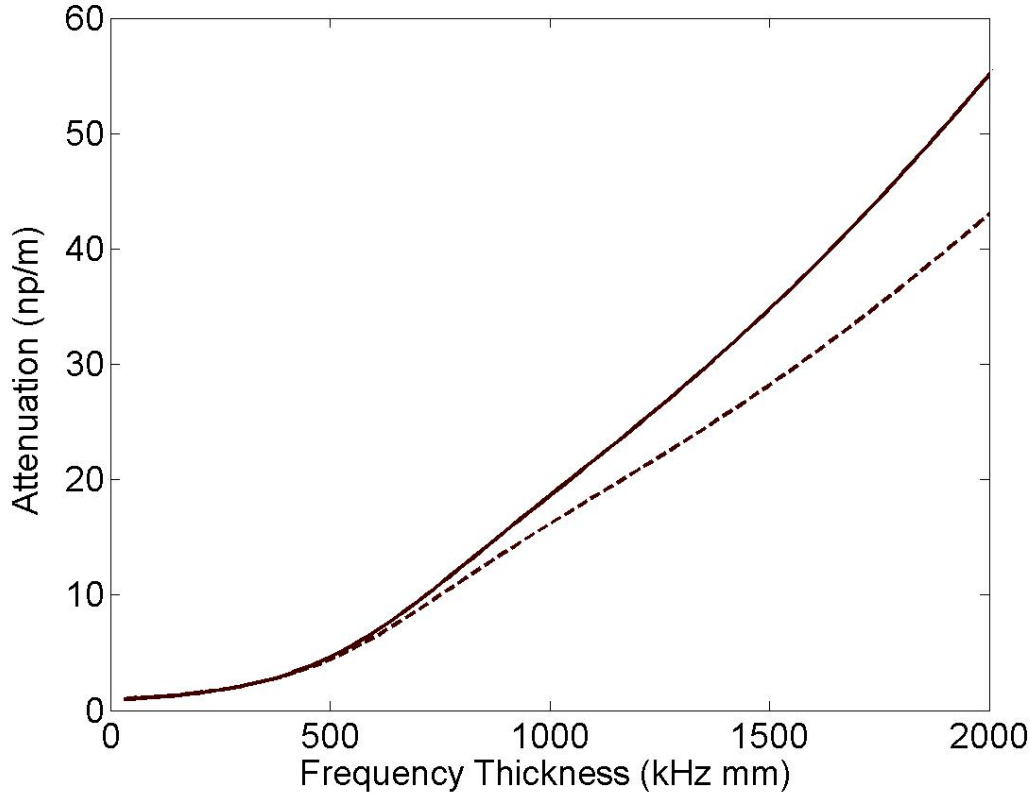

Figure 3.10: Total attenuation (—) of the quasi-Scholte mode and attenuation due to shear leakage only (- - -) as a function of frequency for an aluminium plate ($\rho = 2700kg/m^3$, $C_l = 6320m/s$, $C_s = 3130m/s$) immersed in glycerol ($\rho = 1258kg/m^3$, $C_l = 1900m/s$, $\eta = 1Pas$)

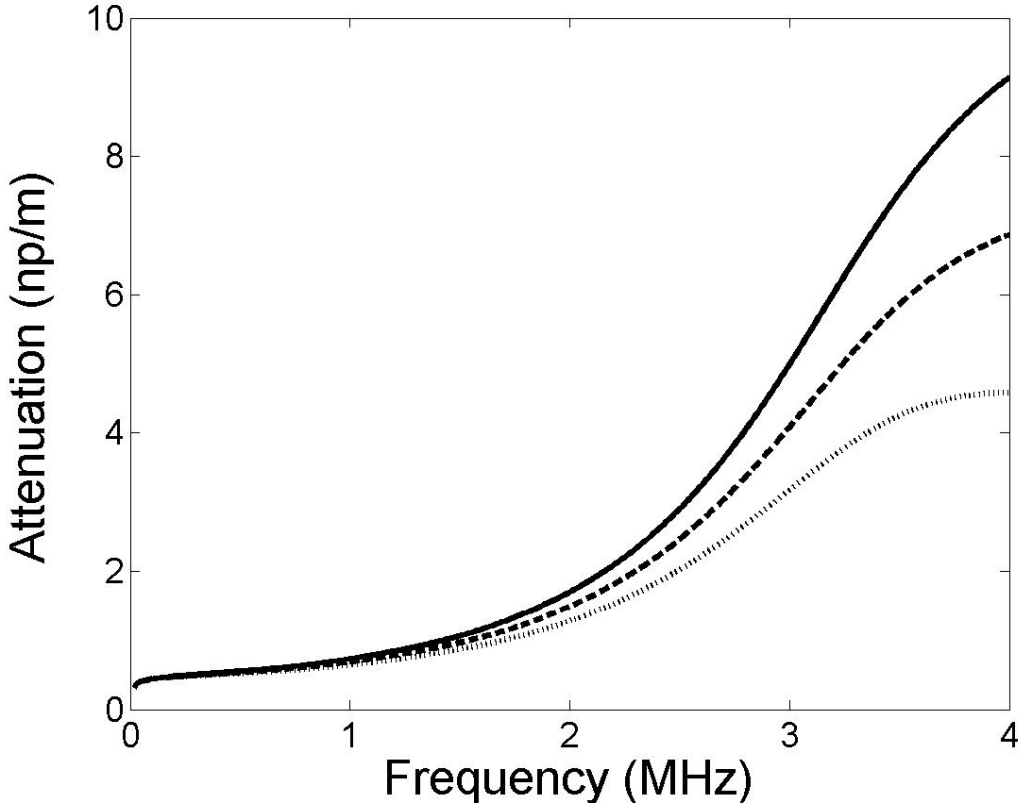

Figure 3.11: Attenuation dispersion curves of the quasi-Scholte mode for a 0.105 mm thick steel plate immersed in water of density 1000 kg/m^3, bulk velocity 1500 m/s and viscosity 1 mPas only ($\cdots$), viscosity 1 mPas and longitudinal attenuation 0.001 Np/wl (- - -) and viscosity 1 mPas and longitudinal attenuation 0.002 Np/wl (—). The attenuation unit Np/wl stands for Nepers per wavelength. The quasi-Scholte mode is attenuated by shear leakage due to viscosity and an additional attenuation due to fluid longitudinal bulk attenuation.

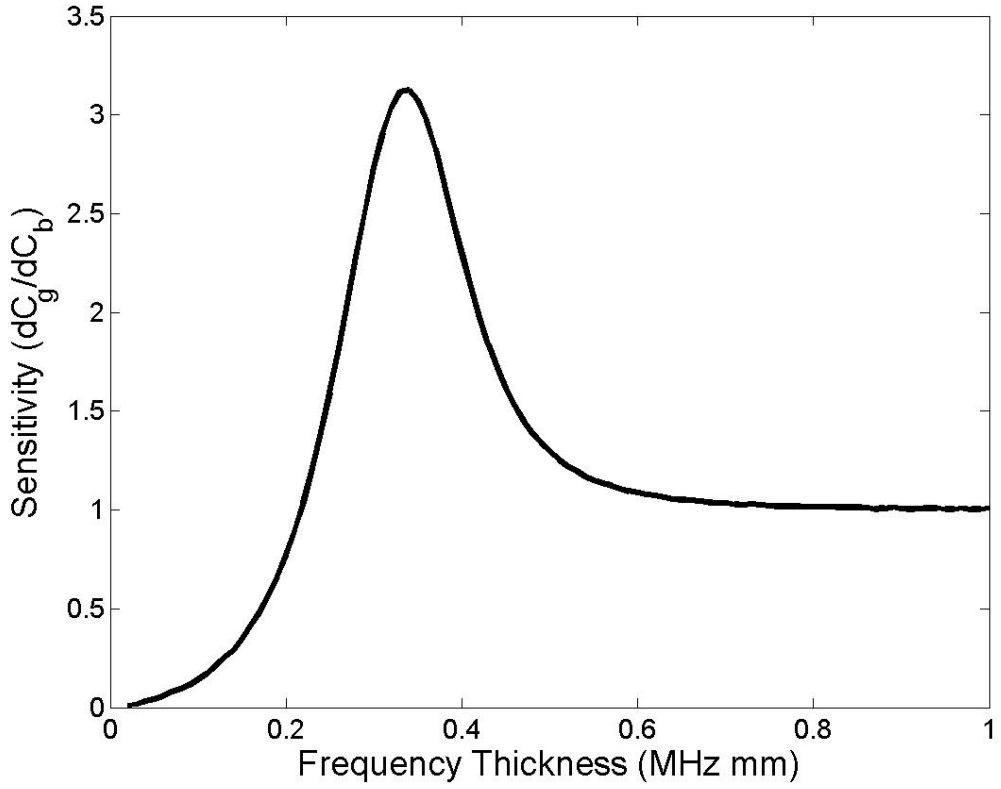

Figure 3.12: The group velocity sensitivity of the quasi-Scholte mode to a change in fluid bulk velocity for a 1mm steel plate surrounded by water ($\rho_{steel} = 7932kg/m^3$,$C_l = 5959.5m/s$, $C_s = 3260m/s$, $\rho_{water} = 1000kg/m^3$, $C_l = 1500m/s$).

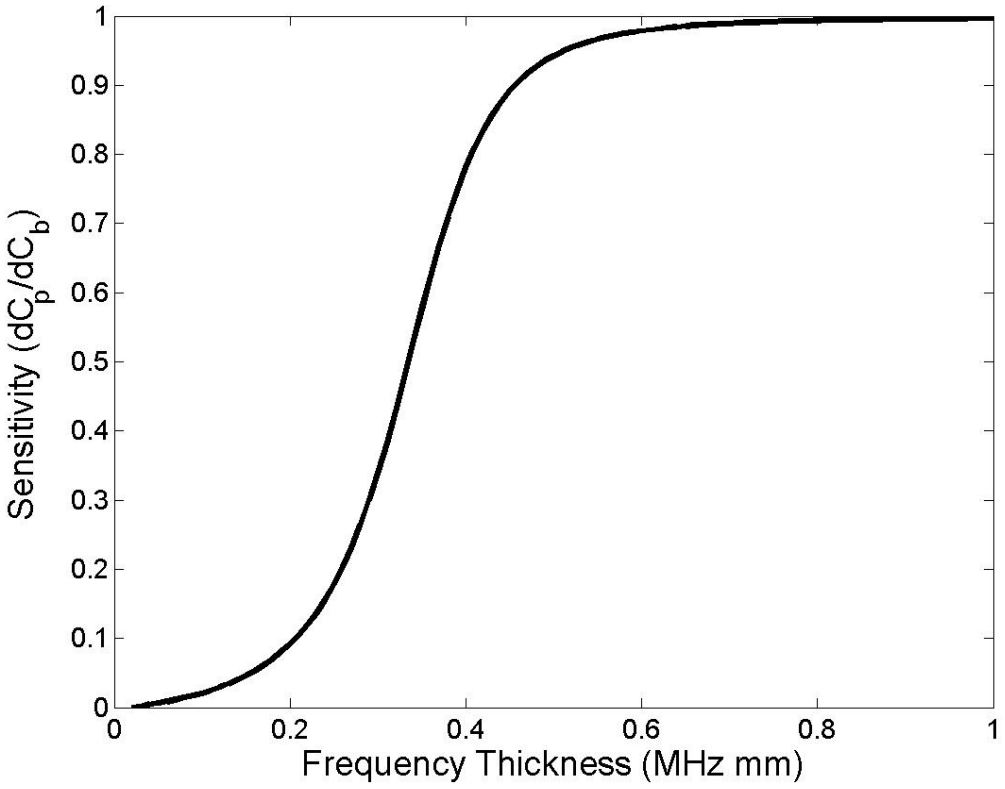

Figure 3.13: The phase velocity sensitivity of the quasi-Scholte mode to a change in fluid bulk velocity for a 1mm steel plate surrounded by water ($\rho_{steel} = 7932kg/m^3$, $C_l = 5959.5m/s$, $C_s = 3260m/s$, $\rho_{water} = 1000kg/m^3$, $C_l = 1500m/s$).

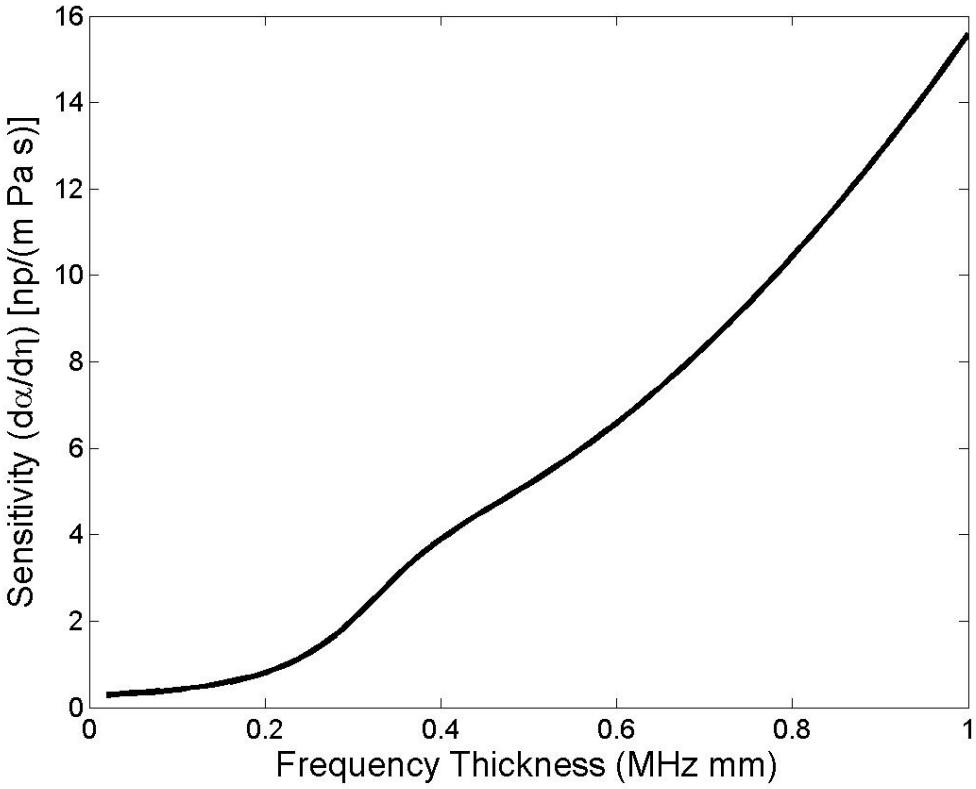

Figure 3.14: The attenuation sensitivity of the quasi-Scholte mode to a change in fluid shear viscosity for a 1mm steel plate surrounded by water with viscosity $\eta = 1$Pas ($\rho_{steel} = 7932kg/m^3$, $C_l = 5959.5m/s$, $C_s = 3260m/s$, $\rho_{water} = 1000kg/m^3$, $C_l = 1500m/s$).

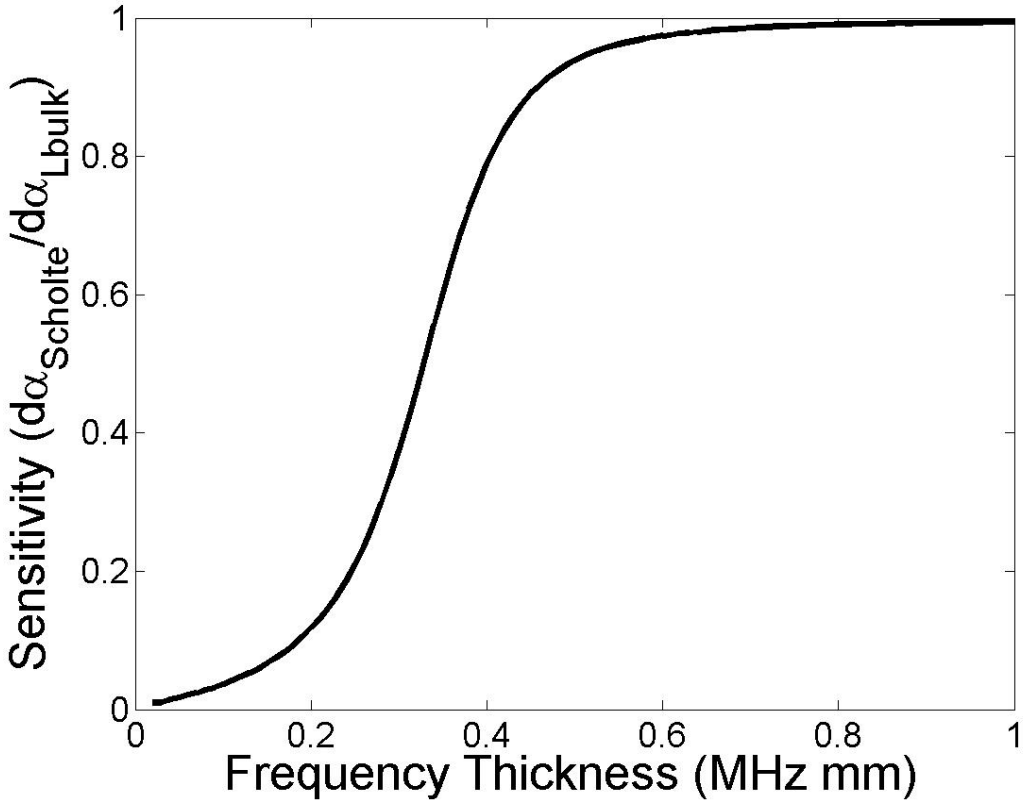

Figure 3.15: The attenuation sensitivity of the quasi-Scholte mode to a change in fluid longitudinal bulk attenuation for a 1mm steel plate surrounded by water with viscosity $\nu = 1$Pas and longitudinal bulk attenuation of $\alpha = 0.01$ np/wl ($\rho_{steel} = 7932kg/m^3$, $C_l = 5959.5m/s$, $C_s = 3260m/s$, $\rho_{water} = 1000kg/m^3$, $C_l = 1500m/s$).

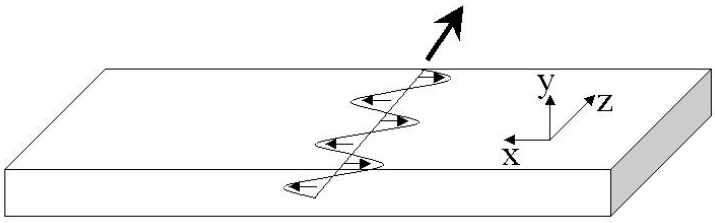

Figure 3.16: Schematic of the propagation of a Shear horizontal (SH) wave in a plate.

Chapter 4

Quasi-Scholte mode Experiments

4.1 Overview

A range of experiments was carried out to validate the results obtained by the theoretical model described in chapter 3. Experimental results from QS mode measurements were validated by measurements in a conventional ultrasonic test cell. In section 4.2 methods of excitation of the Scholte and quasi-Scholte wave that have been reported in the literature are discussed. One method of excitation was chosen and a measurement apparatus was built. The basic apparatus that was used is described in section 4.3. For the evaluation of fluid bulk attenuation an additional measurement of the fluid shear properties is needed. The transduction method could be altered to also excite a shear horizontal plate mode. The experimental arrangement for this is described in section 4.4. Section 4.5 briefly presents the ultrasonic test cell that was used for validation measurements. Then results are presented in section 4.6. Some discrepancies between the test cell measurements and the QS mode measurements were found. In section 4.7 possible error sources are considered. These considerations will be useful for the design of a future QS mode measurement apparatus. The experimental findings of this chapter are summarised in section 4.8.

4.2 Excitation of the Scholte and quasi-Scholte mode

Many ways of exciting Scholte waves have been reported in the literature (see e.g. [54],[55],[56],[57],[58]). Nasr et al. [54] and McLean et al. [55] used a comb-like transducer (PVDF or micro-machined) that preferentially excites a certain wavelength range at the interface of a solid and a liquid to excite Scholte waves. Desmet et al. [56] used laser excitation to create the Scholte wave at the interface. DeBilly et al. [57] and Matula et al. [58] used the concept of mode conversion from a Rayleigh (or $A0$ wave on a plate) to the Scholte wave. They generated a clean mode on an unimmersed section of the waveguide using conventional techniques, the wave then propagates into the liquid and part of its energy converts into the Scholte mode. This latter approach of mode conversion from an A0 plate wave was also chosen for the experiments reported in this thesis. The method is reliable, cheap and easily set up. It also separates the transducer from the embedding medium and thus does not require the transducer to be submerged in the liquid. This prevents bulk waves that travel parallel to the interface from being setup in the liquid at the same time as the Scholte wave. It also separates the transducer from harsh environments like high temperature, highly corrosive or radioactive fluids. Wedge like methods (excitation by means of angled incidence) were ruled out because a fluid of lower bulk velocity than the embedding fluid bulk velocity is needed. Attaching this wedge or angled fluid channel to the waveguide would become difficult and changes of incident angle as required for producing different wavenumbers would be technically challenging and make the device cumbersome.

The method of mode conversion that was chosen to excite the quasi-Scholte mode in a plate fluid system also has shortcomings. Mode conversion is not efficiently achieved at all frequencies. Notably, at high frequencies the efficiency of mode conversion from the A0 mode of a free plate to the quasi-Scholte mode of an immersed plate is low. An explanation for this can be found in the distribution of mode energy within the QS mode as shown in figure 3.7. At high frequencies, above 500 kHz-mm, almost all of the QS mode energy travels in the fluid, which means that

excitation from the plate will be difficult. However the energy of the incident A0 mode is entirely located in the plate. The mode shapes of the A0 mode of the free plate and the QS mode, while very similar at low frequencies, become more and more different at high frequencies. This trend is also illustrated in the wavenumber dispersion curves of the free plate A0 mode and the QS mode. Figure 4.1 shows that at low frequency thicknesses (< 500 kHz-mm) the wavenumbers of the A0 mode of a free plate and the QS mode of an immersed plate are similar while at higher frequency thicknesses they tend apart. The wavenumber of the leaky A0 mode of an immersed plate is also displayed. Tracing of this mode is very difficult and its behaviour is anomalous at low frequency thicknesses (see Dickey et al. [59]) therefore the mode has only been displayed from frequency thicknesses above 220 kHz-mm where it becomes supersonic with respect to the embedding fluid bulk velocity. For the purposes here this is sufficient to illustrate that the wavenumber of the leaky A0 mode tends away from the free plate A0 mode wavenumber at low frequency thicknesses. The mode shapes of all three modes in the plate are very similar at frequency thickness products below 0.6 MHz-mm. Mode conversion from the free plate A0 mode favours the QS mode at low frequency thicknesses and the leaky A0 mode at higher frequency thickness products.

Since the quasi-Scholte mode is more sensitive to fluid properties at higher frequencies there is an optimum frequency window in which the method of mode conversion from the A0 to QS mode works and at the same time information can be extracted from the fluid. It is important to excite the QS mode strongly in a frequency thickness window where it is sensitive to the fluid but also still excitable. This window was found to lie between 200 and 400 kHz-mm for a steel plate immersed in water. The window will shift slightly for different plate materials and liquids that are interrogated but no drastic changes are expected.

4.3 The setup

The experimental setup used was designed to excite the quasi-Scholte mode on a plate immersed in a fluid and to measure its group velocity and attenuation. Figure 4.2 shows a schematic of the apparatus. A shear transducer was attached

to the centre of an end of a plate. It was attached in such a way that it would produce out-of-plane movements uniformly across the thickness of the plate. This was known to excite the A0 mode of a free plate reliably. Figure 4.3 shows the configuration of transducer and plate. Plates of two different thicknesses were used to excite the quasi-Scholte mode within two different frequency thickness ranges. The first plate was made out of Aluminium ($\rho = 2700kg/m^3$, $C_l = 6320m/s$ and $C_s = 3130m/s$) and had a thickness of 0.94 mm, the second plate was made of stainless steel ($\rho = 7764kg/m^3$, $C_l = 6000m/s$ and $C_s = 2700m/s$) and was 0.105 mm thick. The material properties were determined by velocity measurements of the fundamental guided wave modes. The Aluminium plate was 100 mm wide and 200 mm long, while the stainless steel plate was 96 mm wide and 135 mm long.

A 500 kHz shear transducer (Panametrics Inc.) was used to excite the A0 mode in the Aluminium plate while a 5 MHz shear transducer (Panametrics Inc.) was used for the thinner stainless steel plate. Transducers were either coupled to the plate by clamping them onto the cross section using treacle as shear couplant or by bonding them with epoxy.

A vessel containing a fluid sample was placed beneath the plate on a table of variable height. By changing the height of the table the plate could conveniently be immersed in the fluid to different depths; the angle between the fluid surface and the plate was 90 degrees.

The fluid temperature was recorded using a thermocouple that was immersed in the liquid. The whole setup could also be placed in a temperature controlled environment as was done for measurements on suspensions. The signal was sent and received by a waveform generator (Macro Design Ltd.), a LeCroy 9400A Storage Oscilloscope was used to store the signal and the data was then transferred to a PC for processing. The transducer was excited with a Hanning windowed toneburst. The excited A0 wave travelled along the plate until it hit the fluid surface. Here part of the wave was reflected back as an entry reflection and the rest converted into modes in the fluid-plate system: a highly attenuated leaky A0 mode and the quasi-Scholte mode. After a short propagation distance only the quasi-Scholte mode remained. It was reflected by the end of the plate and converted back into an A0 mode at the point where the plate leaves the liquid (some energy was also reflected back into

the fluid). The wave then propagated along the plate structure until it reached the transducer again. A typical time trace is displayed in figure 4.4. The entry reflection, plate end reflection and a reverberation in the fluid are clearly visible. Data for tonebursts at different centre frequencies and two different immersion depths were collected for the aluminum plate setup. For later experiments on the thinner stainless steel plate the technique was further developed and only one broadband signal was sent and received.

The group velocity and attenuation of the quasi-Scholte mode were then extracted from the collected data using the following equations:

$$C_g = \frac{2(x_2 - x_1)}{\left(\Delta T + \frac{2(x_2 - x_1)}{C_{gA0}}\right)} \tag{4.1}$$

$$\alpha = -\frac{1}{2(x_2 - x_1)} ln \left(\frac{S_2(\omega)}{S_1(\omega)}\right) \tag{4.2}$$

where $x_1 < x_2$ are two different immersion depths, ΔT is the time difference between the arrival of the wave packages at the two immersion states, C_{gA0} is the group velocity of the A0 free plate mode and S_1 and S_2 are the signal amplitudes at the respective immersion depths.

In order to eliminate the effects of dispersion on the measured attenuation the magnitude of the Fourier transform at the centre frequency of each toneburst was used in equation 4.2. For the aluminium plate the difference in arrival time ΔT was evaluated by cross correlating the signals at the two immersion depths. The maximum of this function corresponds to the time shift between the two signals [58]. The cross correlation method could be used in this case because signals of a narrow bandwidth were used and propagation distances were short so that dispersion effects were negligible. In the setup of the stainless steel plate two other methods of evaluating the time shift between signal arrivals were used: the amplitude spectrum method (see Pialucha et al. [60]) and the method of zero phase slope, which is described in Appendix C.

The wavenumber in both systems (plate only, plate-fluid) is very similar so it is assumed that beam spreading effectively stays constant. It was verified that the plate was large enough and that reflections from the plate edges were not present in the recorded signal by a simple experiment: pressure was applied to the surfaces of the plate by squeezing it between the fingers. This has the effect of damping the wave propagating across the point where pressure is applied. When the plate was squeezed at the centre the signal was almost completely attenuated while pressing the sides, edges and corners did not have any identifiable effect on the signal amplitude.

4.4 SH wave attenuation measurements

At the end of section 3.3 the need for a determination of liquid shear properties in order to measure bulk longitudinal attenuation using the quasi-Scholte mode was expressed. It was found that the setup of the plate and transducer could easily be adjusted to excite SH waves simultaneously to the QS mode. This is possible due to the different velocities of the modes and the temporal separation that this causes between the signals. Figure 4.5 shows two time traces obtained using the stainless steel plate setup, in which the transducer polarisation and the plate were slightly misaligned. Arrivals of 3 signal packets can clearly be differentiated. They correspond to the three different lowest order propagating modes of the plate: S0, SH0 and A0 converted into QS mode in the immersed section. The excitation of the S0 and SH0 mode is caused by misalignment of the transducer polarisation direction with the plane of the plate. The arrival of the SH wave is indicated in figure 4.5 where the plate and transducer were slightly misaligned while it is not visible in figure 4.4 where better alignment between transducer polarisation direction and the plane of the plate were achieved. The attenuation of the signal is easily analysed as for the QS mode signal, see equation 4.2.

Equation 3.18 can be used to retrieve the viscosity of the liquid from the SH wave attenuation measurement. As mentioned in section 3.5 the analysis is strictly only true for Newtonian liquids. If however an effective viscosity is determined at each frequency, the shear behaviour of the liquid is adequately retrieved and accounted

for.

4.5 Ultrasonic Test cell

An alternative method of determining the fluid bulk properties was needed to validate the results from the quasi-Scholte mode measurements. An ultrasonic test cell that was developed at the University of Nottingham (UK) [61] was used to carry out these validation measurements of fluid bulk velocity and attenuation. This setup consisted of a transducer at one end of the cell which sent a wide bandwidth signal across the fluid sample to a receiver. The exciter and receiver were thick slabs of piezo-electric material. The time delay and amplitude loss were then used to obtain the velocity and attenuation in the sample. This technique is standard and the reader is referred to Challis *et al.* [61] for further details. Sample sizes were about 25 ml for the test cell and the fluid could be temperature controlled to within 0.1 degrees centigrade. Figure 4.6 shows a schematic of the test cell.

4.6 Results

4.6.1 Newtonian Fluids

The quasi-Scholte mode measurement method was first tried on Newtonian fluids. The parameters to be determined were the bulk velocity and viscosity of the fluid. Glycerol was chosen as the test fluid. The density of a glycerol sample was measured to be $1258 kg/m^3$ and the aluminium plate properties were evaluated experimentally as $\rho = 2700 kg/m^3$, $C_l = 6320 m/s$ and $C_s = 3130 m/s$. The temperature was determined to be 23°C. Results were extracted from the time traces as described in section 4.3. Figure 4.7(a) shows the measured group velocity of the quasi-Scholte mode as a function of frequency and a theoretically modelled curve (DISPERSE [22]) was fitted to the measured data. For the low viscosities of glycerol, the group velocity dispersion relation of the quasi-Scholte mode is essentially only dependent on the longitudinal velocity as described in section 3.3. Thus it is possible to extract

the longitudinal bulk velocity of the glycerol as 1930 m/s. Figure 4.7(b) shows the measured and theoretically predicted attenuation for the quasi-scholte mode. The measured attenuation fits best to a predicted viscosity of 0.82 Pas. An estimate of the error in the measured viscosity, based on repeatability, is about 8%.

To validate the above results a measurement of the bulk longitudinal velocity was carried out. This yielded a value of 1900 m/s. Also an alternative method of measuring viscosity was utilised; this method involved the measurement of the torsional T(0) mode attenuation of a rod immersed in glycerol as described by [36]. Using this approach the viscosity was determined to be 0.89 Pas. The measurement environment for this experiment, unlike later experiments, was not temperature controlled. The humidity was not controlled either but the two experiments were carried out almost simultaneously (less than 10 minutes apart). The measured results compared well to each other and literature data. Kaye and Laby [62] state the viscosity of 99% glycerol to be 0.9 Pas at 23°C.

The quasi-Scholte mode was also used to measure the properties of honey. Figure 4.8(a) shows the measured group velocity and figure 4.8(b) shows the measured attenuation of the quasi-Scholte mode of the 0.94mm aluminium plate immersed in honey (Gale's Clear Honey, Premier Ambient Products (UK) Ltd., Spalding PE12 9EQ). The average bulk velocity of the honey was determined to be 2140 $\pm$ 30 m/s and the average viscosity was evaluated at 19.2 $\pm$ 1.17 Pas, where the quoted uncertainty is based on repeatability of the measurement results.

The results for honey show that the method also works for very viscous fluids. Despite its many different constituents the behaviour of honey is described well by a Newtonian fluid [63]. As stated in section 3.2.2 low viscosities ($<$ 30 Pas) are currently assumed in the modelling of the quasi-Scholte mode and therefore errors will introduce if the same model is used for highly viscous liquids. Honey is still modelled well by assuming low viscosities, however high viscosity formulations for equations 3.7-3.10 can be implemented [22] for more viscous fluids. High viscosity fluids will also exhibit significant shear leakage that can partially be limited by al-

tering measurement frequency and propagation length. Highly viscous liquids will also affect the quasi-Scholte mode group velocity which complicates the extraction of bulk velocity and attenuation.

To facilitate the extraction of fluid bulk properties from the measured quasi-Scholte mode data an inversion technique was developed. An iterative routine was programmed that automatically traced the quasi-Scholte mode group velocity dispersion curves for a given embedding fluid bulk velocity and viscosity. The result was compared to the measured data points and the fluid bulk velocity was adjusted in the right direction to reduce the mismatch between prediction and measurement. Once a prediction point below and above the measured data was obtained a bi-section scheme reduced the step size of the iteration. A maximum limit of iterations was set and a result within a tolerance of 0.1 m/s or Np/m was accepted as a successful iteration.

The iteration and inversion technique was first tested on a sample of distilled water and a 5% ethanol-distilled water solution. To increase the range of bulk velocities that could be measured the sample solutions were measured at different temperatures between 10 and 30 degrees centigrade. The stainless steel plate was used to carry out the measurements. Results are displayed in figure 4.9. The marker of the bulk velocity indicates the mean velocity obtained from the inversion routine, while the error bars indicate the standard deviation of the set of values obtained at different frequencies from the mean value. Distilled water and the ethanol-water mixture are non-dispersive fluids so that the velocity should be the same at all frequencies. However due to noise in the group velocity measurement, and errors, slight differences in velocity at different frequencies are obtained. The mean value is also offset from the theoretically predicted curve. This is believed to be due to the positioning uncertainty of the plate (0.5%). Even with these errors in the data the measurement results compare very well to literature data that was obtained from Povey [1]. The trend of increased velocity at increased temperature is clearly reflected by the measurements in figure 4.9.

4.6.2 Non-Newtonian Fluids

Once it was established that the QS mode model could correctly yield the properties of Newtonian fluids, the evaluation of non-Newtonian fluids could be addressed. The non-Newtonian fluids that were chosen were aqueous suspensions of silicon dioxide. Four different aqueous suspensions of silica particles were obtained and prepared. Two commercial colloidal silica samples Syton-$HR50$ (Du Pont de Nemours & Co. Inc., USA) and Snowtex-ZL (Nissan Chemical Industries Ltd., Japan) were used as well as two custom made samples from SILMIKRON silica dust (*Quarzwerke* GmbH, Germany). Two different amounts of the silica dust ($50g$ and $150g$) were stirred into 400 ml of distilled water and then treated in an ultrasonic cleaning bath for 30 minutes to break up any agglomerations. The suspension was then left to settle for half a day before it was transferred into another flask. Any deposit at the bottom of the flask was discarded. The process was repeated until no more deposit was collecting after half a day. The suspension was then believed to be sufficiently stable to last for the duration of an experiment (less than half an hour). The four different suspensions had different volume fractions and particle sizes which are summarized in table 4.1.

Suspension	particle diameter (μm)	Volume fraction (%)	Density (kg/m^3)	Viscosity (mPas)
Snowtex-ZL	0.07	23	1294	1.9
Syton$-HR50$	0.05	30.4	1388	3.2
SILMIKRON-150	> 1	5.2	1065	1.1
SILMIKRON-50	> 1	1.7	1020	1.1

Table 4.1: Particle size (by manufacturer), volume fraction (either by manufacturer or calculated from the density), density (measured) and viscosity (SH-wave measurement at 3MHz) of the different investigated suspensions.

Experiments were carried out successively using a conventional test cell and the quasi-Scholte mode setup. In both cases the fluid was temperature controlled to 25 degrees centigrade. The experiments were carried out and the data was processed.

The measured quantities from the quasi-Scholte mode and ultrasonic test cell experiments do not yield comparable quantities, they have to be converted and can then be compared in two different ways: the forward model and the inverted model.

The forward problem consists of determining the dispersion curves for the quasi-Scholte mode from the measured bulk wave velocity and attenuation in the ultrasonic test cell. Group velocity as well as the attenuation of the quasi-Scholte mode are determined as functions of frequency for a given set of input parameters which are either known or determined from the ultrasonic test cell measurement. There are fixed input parameters (plate material density, plate material longitudinal and transverse bulk velocity) and variable input parameters (fluid density, fluid longitudinal and shear wave velocity, fluid longitudinal and shear wave attenuation). Now the dispersion curves obtained by modelling the plate surrounded by a fluid whose properties were determined by the ultrasonic test cell could be compared to the actually measured dispersion curves in the quasi-Scholte mode experiment.

In the inversion the measured properties (group velocity and attenuation) of the quasi-Scholte mode are inverted to obtain the properties of the fluid that an ultrasonic test cell would deliver (bulk wave velocity and bulk wave attenuation). The approach developed here used an iteration to evaluate the fluid bulk properties. An initial guess for the fluid properties is used to evaluate the quasi-Scholte mode properties in the forward model. The measured data and the predicted data are compared and the fluid properties are adjusted before they are re-entered into the global matrix (see appendix A). Two parameters are adjusted simultaneously: longitudinal bulk velocity and the part of the longitudinal attenuation which is in excess of the viscosity induced dissipation. The parameters are increased in constant steps. A bi-section scheme is used once two consecutively entered fluid property values yield a result either side of the measured quasi-Scholte data point. The procedure is repeated until the modelled solution agrees to within a tolerance value (0.1 m/s, 0.1 Np/m) with the measured quasi-Scholte mode data.

The forward model

Figure 4.10 displays the measured group velocity of the quasi-Scholte mode and the predicted group velocity obtained by modelling the fluid properties measured in the ultrasonic test cell. The results in figure 4.10 show a very good agreement of the predicted and measured values. The lines trace the same path and only small deviations from the predicted values are seen in the actual measurement. The errors in the measured velocity are surprisingly small; a positioning accuracy of 0.5% in the immersion depth of the plate explains the different offsets for the curves of the four samples.

Figure 4.11 displays the measured attenuation of the quasi-Scholte mode and the predicted attenuation obtained by forward modelling using the fluid properties measured in the ultrasonic test cell. The results show good agreement between measurements of the quasi-Scholte mode attenuation and the predicted quasi-Scholte mode attenuation obtained from the fluid property measurement (bulk velocity C_L and bulk attenuation α) in a test cell for the commercially obtained colloidal silica samples. The attenuation of the purpose made SILMIKRON samples still agreed well in trend but were offset by about 20% above the prediction from the bulk wave measurement. The attenuation measurement is more prone to the influence of errors, see section 4.7. In order to reduce the effects of noise in the measured attenuation data a quadratic curve was fitted to it. The error bars in figure 4.11 indicate the standard error ($< 0.5\%$) of the attenuation data and the curve fit. (The error bars in the attenuation graph of figure 4.11 appear smaller than the error bars of the velocity graph of figure 4.10. However this is simply due to the expanded scale of figure 4.10, the percentage velocity error is substantially smaller than the percentage attenuation error.)

The higher values of attenuation of the SILMIKRON suspension indicate the sensitivity of the quasi-Scholte mode to non-viscous dissipative mechanisms in fluids. The viscosities of the commercial samples Snowtex-ZL and Syton-HR50 are greater by a factor of 2 and 3 respectively (see Table 4.1), however the quasi-Scholte mode measurement reveals a lower attenuation than for the SILMIKRON samples. The

loss of energy into the embedding liquid due to shear coupling in the SILMIKRON samples must be less than that for the commercial samples. If viscosity was the only attenuation mechanism, SILMIKRON should exhibit a lower attenuation than the commercial samples, but the measured attenuation in the SILMIKRON samples was higher. This is due to scattering of the wave at particles in the suspension; it is well known that scattering increases attenuation in fluids [3].

However the total attenuation of the quasi-Scholte mode is not as high as the attenuation experienced by a bulk wave in the strongly scattering SIMLIKRON fluids. This is because only a fraction (20-40% depending on the frequency) of the energy of the quasi-Scholte mode travels in the embedding fluid see chapter 3. This is an attractive feature for the investigation of highly attenuative and scattering fluids.

Inversion

The inversion technique was then used on the silica suspension data. The results from the velocity inversion are summarised in figure 4.12. The agreement between the test cell measurements and the inverted quasi-Scholte mode measurements is good. The errors that were apparent in the forward model (section 4.6.2) are retained. The mean values of the lines are also offset by up to 0.5%, which is believed to be caused by the uncertainty with which the immersion depth of the plate is determined.

The results in figure 4.13 show the longitudinal bulk wave attenuation obtained from the inversion of the quasi-Scholte measurements. These results show worse agreement compared to the forward modelled data. Qualitatively the method correctly identifies the magnitude of the attenuation in the samples: SILMIKRON-150 exhibits the most attenuation, then SILMIKRON-50, while Snowtex-ZL and Syton-HR50 are least attenuating. However the quantitative values differ from those obtained using the ultrasonic test cell, sometimes by more than 25%. As in the forward approach the inverted quasi-Scholte mode data shows a consistently higher attenu-

ation than the test cell measurements. Error bars in figure 4.13 show the standard error introduced by using a quadratic curve fit to represent measured quasi-Scholte mode data.

At low frequencies the error in attenuation is greatest; this is believed to be partly due to the curve fit that seems to be less good at low frequencies but could also be due to the fact that less energy travels in the liquid at low frequencies. The sensitivity to the fluid properties is also not as high at low frequencies as it is at high frequencies see section 3.4.

4.7 Error considerations

In order to allow future refinement of the QS mode measurement technique, sources of error in the measurement had to be identified. The errors in the velocity measurement, the attenuation measurement and processing of data were considered separately.

The sources of error in the velocity measurements are the most obvious. The sampling frequency of the digitizer which records the signal introduces the most basic uncertainty in the velocity measurement by limiting the temporal resolution of the signal acquisition. Noise in the received signal represents another source of error. If processing is carried out in the time domain this can cause errors in the detection of the arrival of a peak amplitude for example. However since the signal to noise ratio and the sampling frequency were large in all measurements these errors were small. The main uncertainty that entered the velocity measurement was believed to be the uncertainty with which the immersion depth could be determined. The immersion depth was determined visually by means of a ruler. This was believed to be accurate to within $0.5 - 1.5\%$ depending on the care taken and the overall distance to be measured. Indeed the velocity measurements that were carried out agreed with validation measurements and literature data within this range of uncertainty.

In figure 4.12 and figure 4.10 step like variations about the expected smooth velocity curves can be seen. They are most visible in the curve for SIMIKRON-150. These variations are of the same order as the positioning inaccuracies (about 0.5%). They are believed to be due to the resolution limit of the amplitude spectrum method [60](also see Appendix C.4) which was used to determine the velocity at different frequencies from a broadband signal. In the amplitude spectrum method the Fourier transform of a signal that contains the originally sent signal and the received signal is calculated. Due to phase differences in both the sent and the received signal the spectrum of the combined signal will contain a number of maxima and minima. The velocity of the wave can then be calculated by the following equation

$$V = \frac{\Delta F}{\Delta N} D. \tag{4.3}$$

where ΔF is the frequency difference between two minima in the process signal, ΔN is the number of minima in between ΔF (in this case 1) and D is the distance separating the two points at which the signals were acquired.

Equation 4.3 is used to determine the velocity by means of the amplitude spectrum method. If the frequency resolution becomes an important fraction of the frequency difference between two minima, errors due to the frequency resolution of the spectrum can arise. In this case finite size steps in the velocity measurement are caused. A way to improve on this could be by increasing the frequency resolution in real terms or by means of zero padding. However it would be better to adjust the separation distance D between the signals to increase ΔF. If this is not possible a different method of velocity measurement should be chosen (see for example the method of zero phase slope in Appendix C).

Attenuation measurements are known to be more prone to error than velocity measurements. There are many factors that influence the signal amplitude: the output voltage of the signal generator, amplifier and cable connection quality, the consistency of coupling between the transducer and the waveguide, just to mention a few. Attenuation errors also arise due to geometrical faults within the setup. For exam-

ple refraction of the travelling wave at the position where the waveguide enters the fluid can occur. The quasi-Scholte mode velocity is considerably slower than the A0 velocity of the free plate. If the wave enters the liquid at an angle different from the normal, the beam will be refracted and on return to the transducer its position will be offset slightly. A considerable decrease in amplitude can be observed at the transducer; this effect was verified experimentally: a possible remedy is the change from the plate geometry to a rectangular cross section strip.

The uncertainty with which the immersion depth is determined also introduces an error in the attenuation measurement. On top of this, noise always enters the measurement and in order to avoid larger errors due to the noise in the signal the overall attenuation has to lie between 0.5 and 1 Np/m. This is an inherent problem with any attenuation measurement which has been pointed out by Kalashnikov and Challis [42].

Finally errors can also enter the final result due to errors in processing techniques. Several error sources within processing have been identified. When the group velocity and attenuation spectra of the measured signals were processed small oscillations about a general curve trend were observed. To smoothen out these oscillations a curve fit was used. The standard deviation of the curve fit from the actual data was very small ($< 0.5\%$). A quadratic curve was used as fit partly because the viscous part of the attenuation is expected to vary with the square of frequency and the velocity also has the shape of an inverted parabola.Figure 4.14 illustrates measurement data and the respective curve fit. The use of this curve fit can cause errors.

During processing the accumulation of errors from the individual required measurements also takes place. For example measurements of the plate material properties, fluid density and viscosity are needed together with the QS-mode measurement to process the final result. The A0 free plate mode group velocity is also required to calculate the QS-mode velocity, see equation 4.1. An error in this A0 group velocity measurement will directly enter the QS-mode group velocity result.

Another potential source of large error can be found in the processing of the longitudinal bulk attenuation from the measured QS-mode attenuation. A viscosity measurement using the SH-mode is necessary. In fluids where the contribution of the fluid longitudinal bulk attenuation to the QS-mode attenuation is small compared to the attenuation due to shear leakage, large errors in the processing of the longitudinal bulk attenuation from the QS-mode attenuation can be expected. This is because the inversion is ill posed and a small error in the SH-wave viscosity measurement will be disproportionately amplified to yield a very large error in the estimated fluid bulk longitudinal attenuation. An example for this is seen in the inversion method results of the Syton-HR50 suspension, whose viscosity is almost entirely responsible for the QS-mode attenuation. The forward modelled results for Syton-HR50 agree very well in this case.

For the future construction of an improved measurement apparatus it is recommended to address the largest sources of error first. Therefore a method of accurately determining the immersion depth should be implemented. This could be achieved by shielding the unimmersed parts of the waveguide from the liquid by a cover for example. The total immersion depth should also be chosen in such a way that the overall measured attenuation lies as close as possible to 0.5 np. This might impose the use of different immersion depth for the QS mode and the SH mode measurements. The material properties of the plate and the density of the fluid should be determined as precisely as possible. The geometry of the waveguide should be changed from a plate to a strip in order to eliminate refraction effects due to angled entry of the plate into the liquid. However it should be kept in mind that the inversion of QS mode attenuation measurements to yield the bulk longitudinal fluid attenuation will always be ill posed for viscous fluids whose bulk longitudinal attenuations are small.

4.8 Summary

In this chapter the experimental studies that were carried out with the quasi-Scholte mode are reported. The mode conversion from A0 mode of a free plate to the quasi-

Scholte mode of an embedded plate was chosen as excitation method. A setup was built and measurements on several fluids were carried out. By means of the QS-mode group velocity measurement the fluid bulk velocity could be determined to within 0.5 %. The main error was identified to be due to positioning inaccuracies of the plate.

The attenuation measurement of the quasi-Scholte mode was used to determine the viscosity of a Newtonian fluid. For Non-Newtonian fluids the QS-mode attenuation cannot be solely described by the viscosity. The QS-mode attenuation now depends on the viscosity and the longitudinal bulk attenuation of the liquid. By use of an additional measurement using the SH-mode of the plate the shear properties of the fluid were determined. This allowed the longitudinal bulk attenuation of the fluid to be retrieved from the QS-mode attenuation measurement.

The presence of the two different attenuation mechanisms of the QS mode (shear leakage and longitudinal bulk attenuation) was illustrated by showing that the QS mode attenuation of a low viscosity but high bulk attenuation fluid (SILMIKRON-150) is higher than the QS mode attenuation of a high viscosity and low bulk attenuation fluid (SYTON-HR50). Comparisons of the QS-mode measurements with results from an ultrasonic test cell showed good agreement for both methods in the forward model. Velocity measurements were achieved with good accuracy and attenuation measurements also agreed well.

In the inversion technique velocity measurements could still be carried out accurately however the error of the longitudinal bulk attenuation measurement was relatively large. This can be due to ill conditioning of the inversion technique. Several sources of error have been identified. Errors were due to general limitations in attenuation measurements, the need of an experimental determination of viscosity that is prone to error, an ill posed inversion problem and geometrical issues with the setup. Some errors could be eliminated by further refinement of the measurement setup, such as a geometry change from a plate to a strip, accurate determination of the immersion depth and a reduction of error in the determination of the effective viscosity.

4.9 Figures

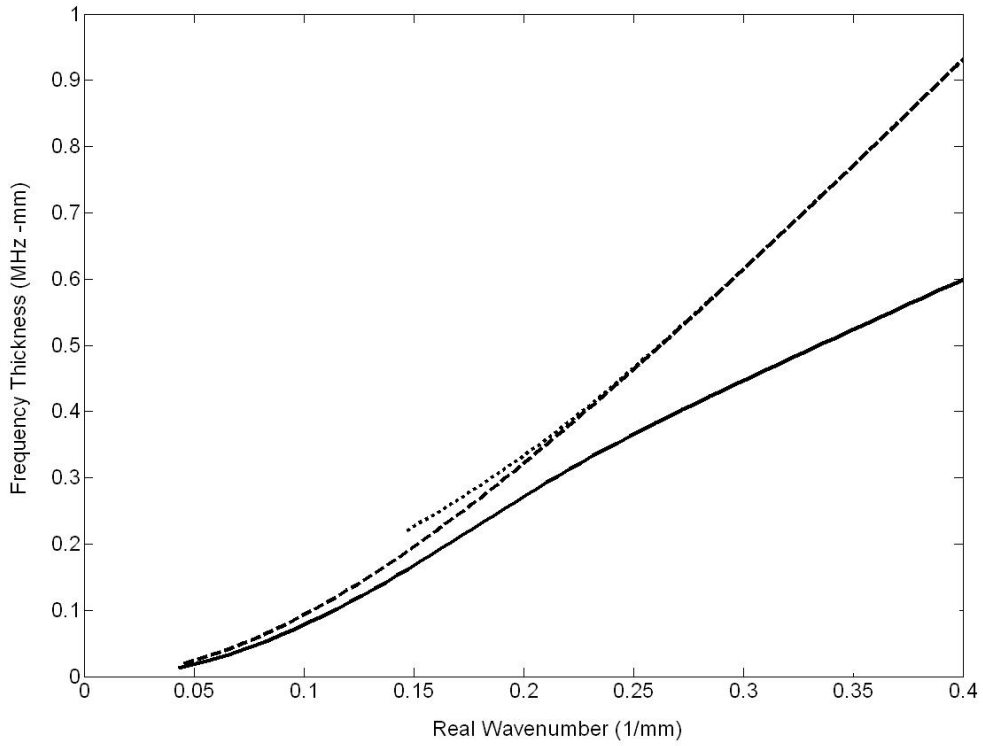

Figure 4.1: Frequency versus wavenumber plot for the QS mode (—), the A0 mode (- - -) of a free plate and the leaky A0 mode ($\cdots$) of a steel plate immersed in water (steel: $\rho = 7932kg/m^3$, $C_l = 6000m/s$, $C_s = 3260m/s$; water $\rho = 1000kg/m^3$, $C_l = 1500m/s$)

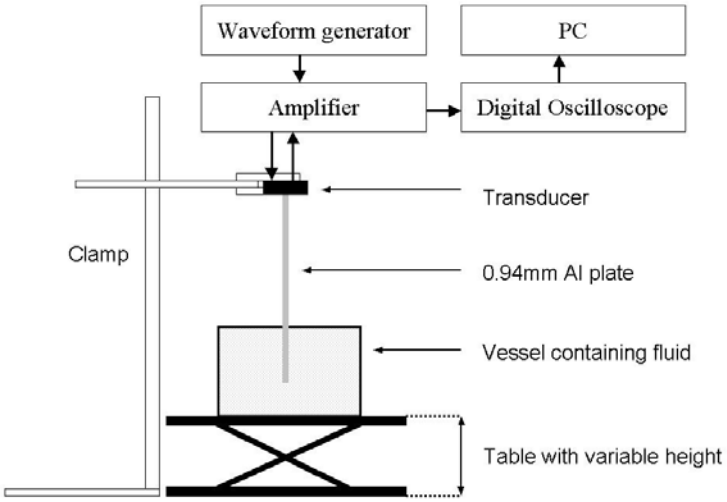

Figure 4.2: Experimental setup

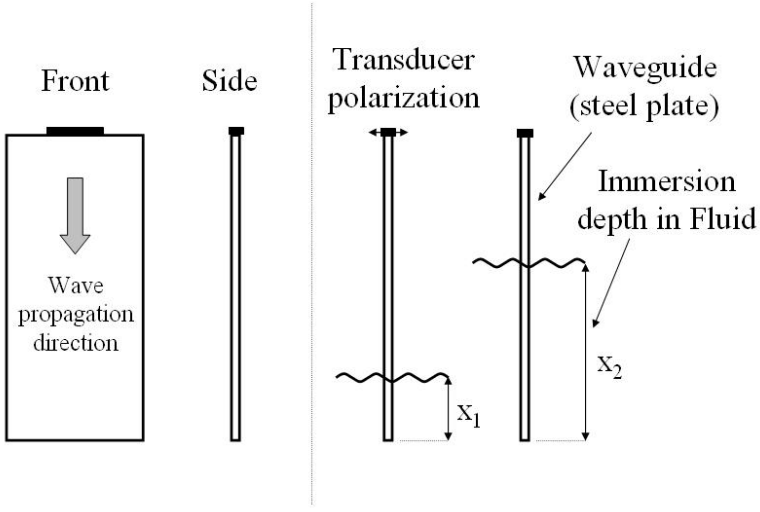

Figure 4.3: Schematic of the Transducer orientation and plate setup.

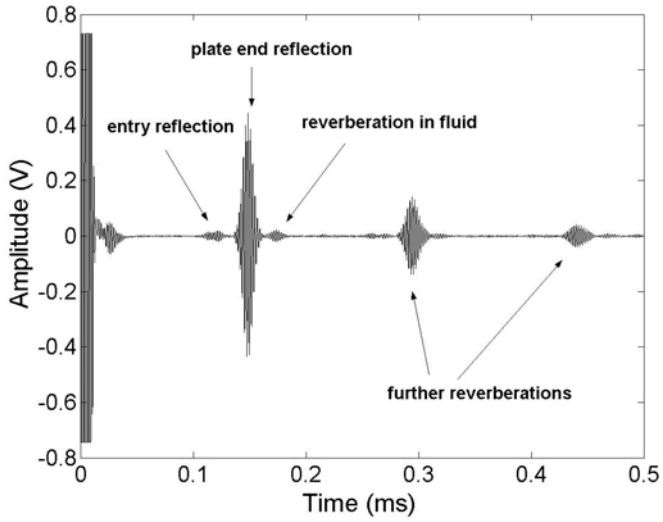

Figure 4.4: Time trace at 500 kHz with aluminium plate 30 mm immersed in Glycerol

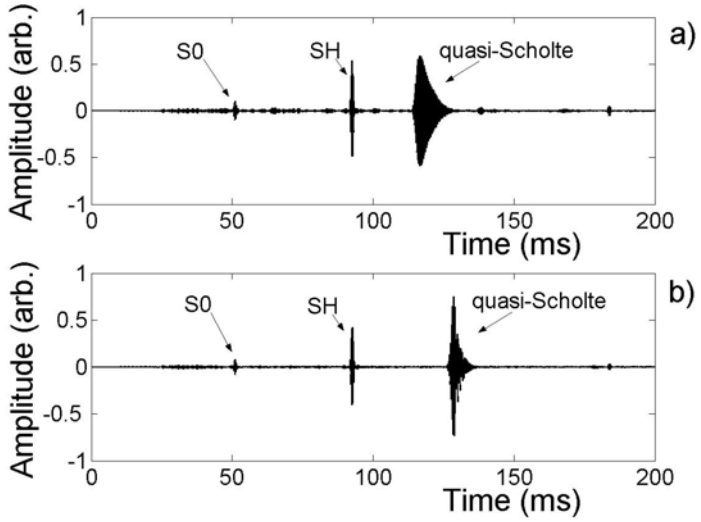

Figure 4.5: Time trace at 3 MHz with stainless steel plate immersed a) 20 mm and b) 80 mm in Water.

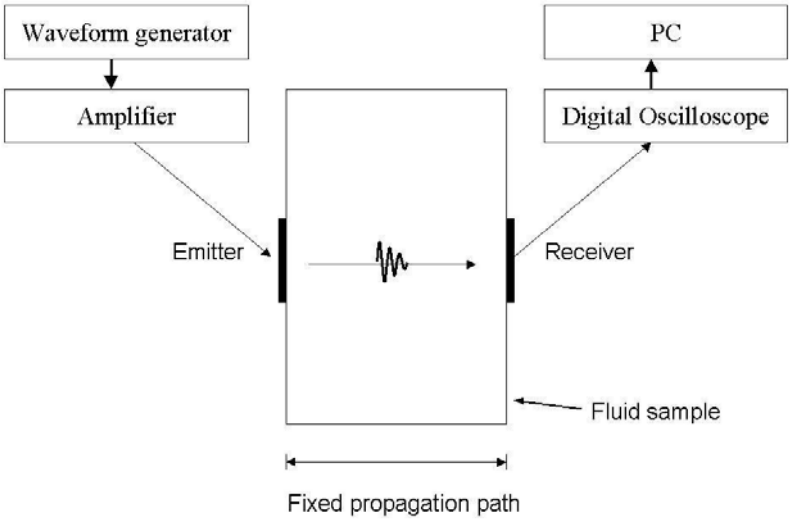

Figure 4.6: Schematic of a conventional test cell.

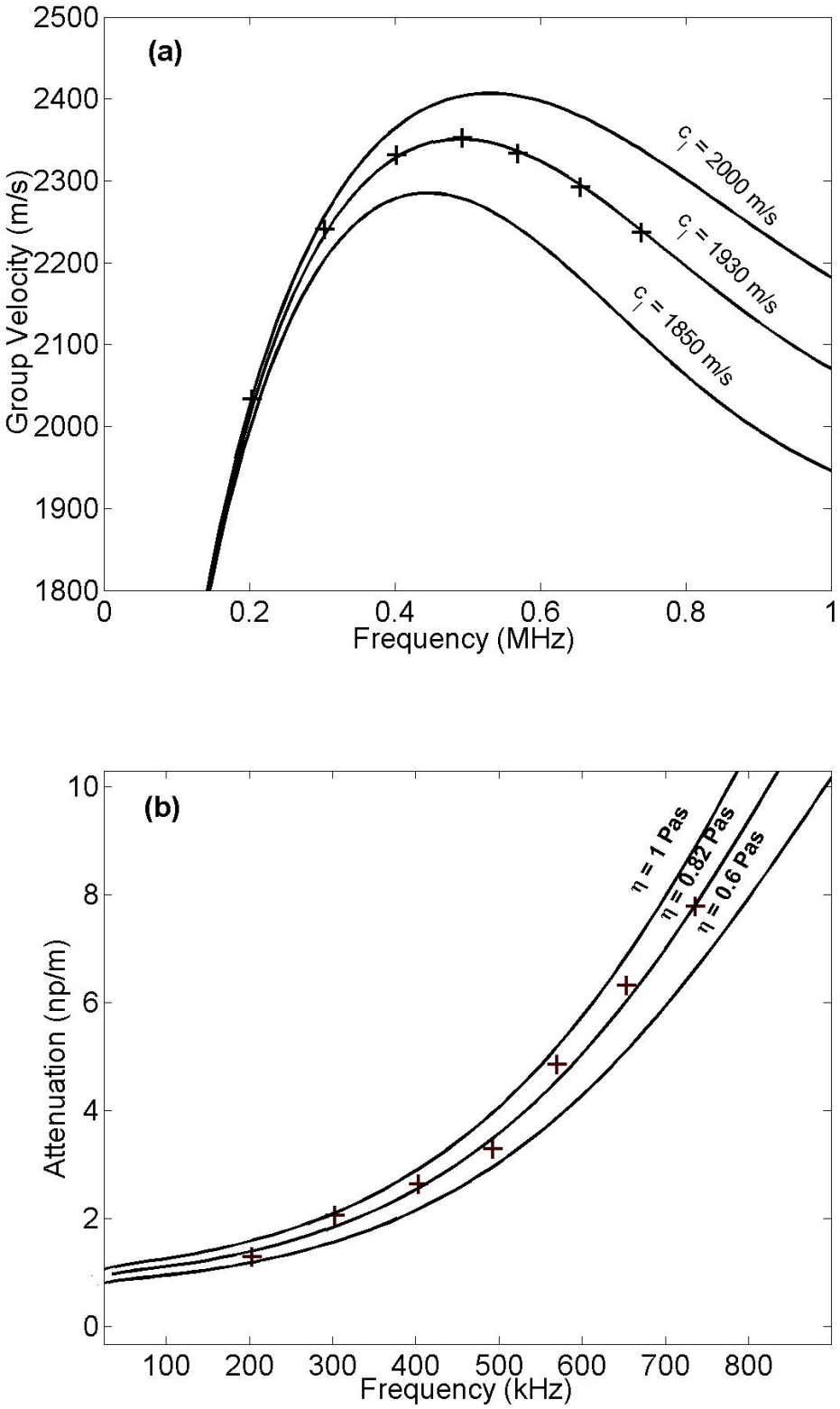

Figure 4.7: Measured (+) and theoretically predicted (—) (a) group velocity and (b) attenuation of the quasi-Scholte mode on a 0.94 mm thick aluminium plate immersed in glycerol ($\rho = 1258kg/m^3$, $C_l = 1930m/s$, $\eta = 0.82Pas$)

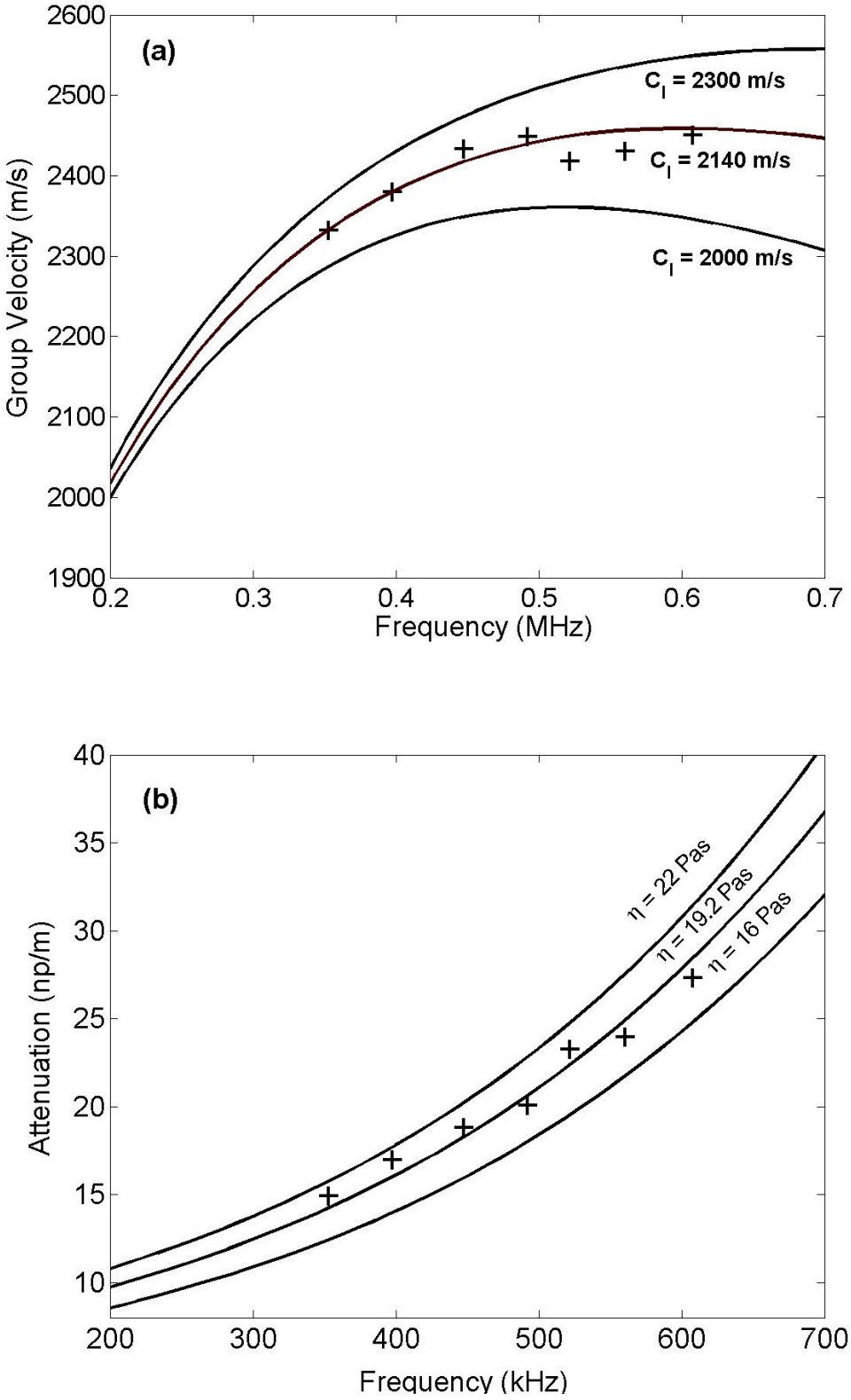

Figure 4.8: Measured (+) and theoretically predicted (—) (a) group velocity and (b) attenuation of the quasi-Scholte mode on a 0.94 mm thick aluminium plate immersed in honey ($\rho = 1400kg/m^3$, $C_l = 2140m/s$, $\eta = 19.2Pas$)

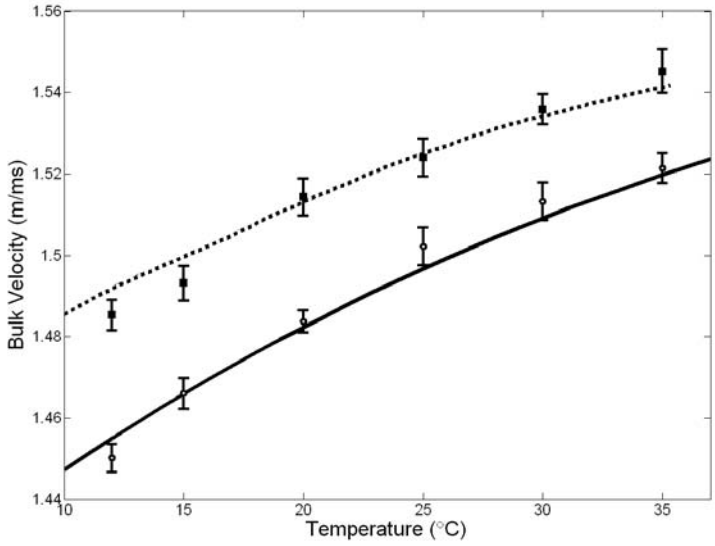

Figure 4.9: Literature data from Povey [1]for distilled water (—) and 5 % ethanol-distilled water mixture (- - -) for the bulk velocity and data from the inversion of the quasi-Scholte mode measurement (distilled water o, 5 % ethanol-distilled water ■)

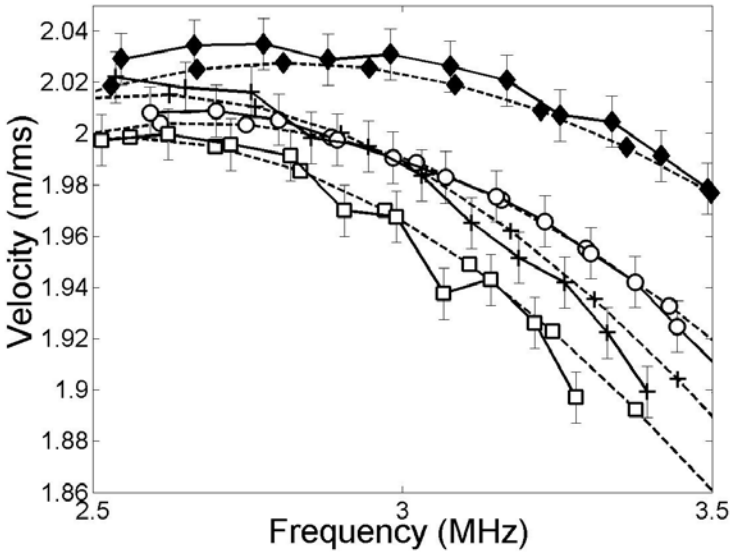

Figure 4.10: Quasi-Scholte mode group velocity obtained by forward modelling using the fluid bulk velocity and attenuation from the ultrasonic test cell measurement (- - -) and by direct measurement of the quasi-Scholte mode (—) [Snowtex-ZL (o), Syton-HR50 (♦), SILMIKRON-50 (+), SILMIKRON-150 (□)]. The errorbars indicate errors due to the 0.5 % uncertainty in evaluating the immersion depth.

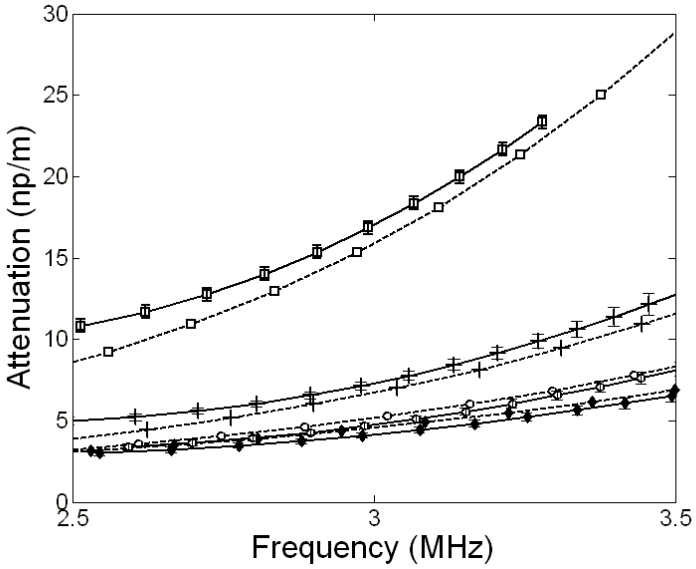

Figure 4.11: Quasi-Scholte mode attenuation obtained by forward modelling using the fluid bulk velocity and attenuation from the ultrasonic test cell measurement (- - -) and by direct measurement of the quasi-Scholte mode (—) [Snowtex-ZL (o), Syton-HR50 (♦), SILMIKRON-50 (+), SILMIKRON-150 (□)]. The error bars indicate the standard error of the signal and a curve fit (see text).

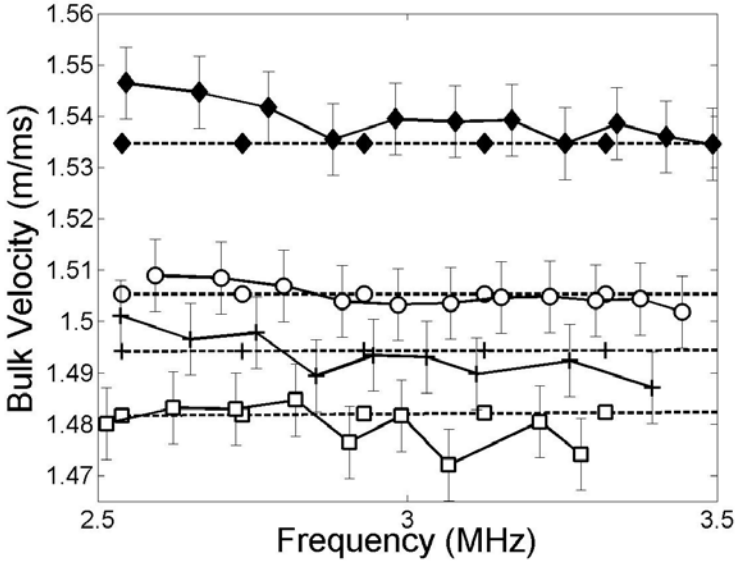

Figure 4.12: Fluid bulk velocity from the ultrasonic test cell measurement (- - -) and by inversion of the quasi-Scholte mode measurement (—). [Snowtex-ZL (o), Syton-HR50 (♦), SILMIKRON-50 (+), SILMIKRON-150 (□)] The errorbars indicate errors due to the 0.5 % uncertainty in evaluating the immersion depth.

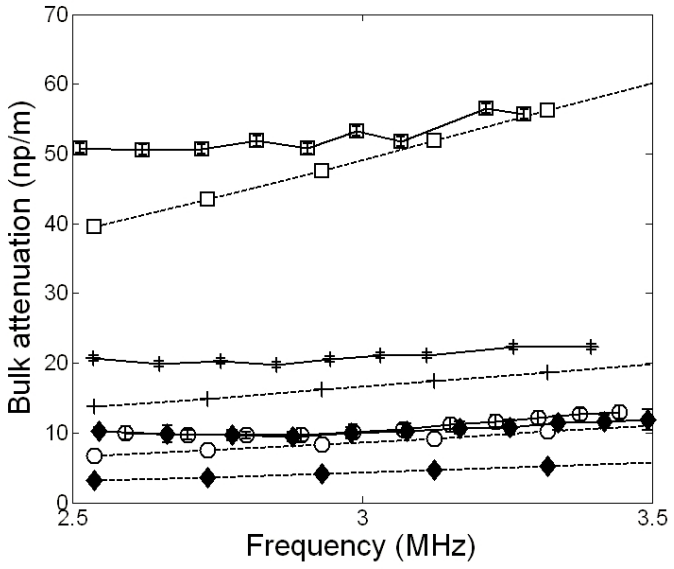

Figure 4.13: Fluid bulk attenuation from the ultrasonic test cell measurement (- - -) and by inversion of the quasi-Scholte mode measurement (—) [Snowtex-ZL (o), Syton-HR50 (♦), SILMIKRON−50 (+), SILMIKRON−150 (□)]. The error bars indicate the standard error of the signal and a curve fit (see text).

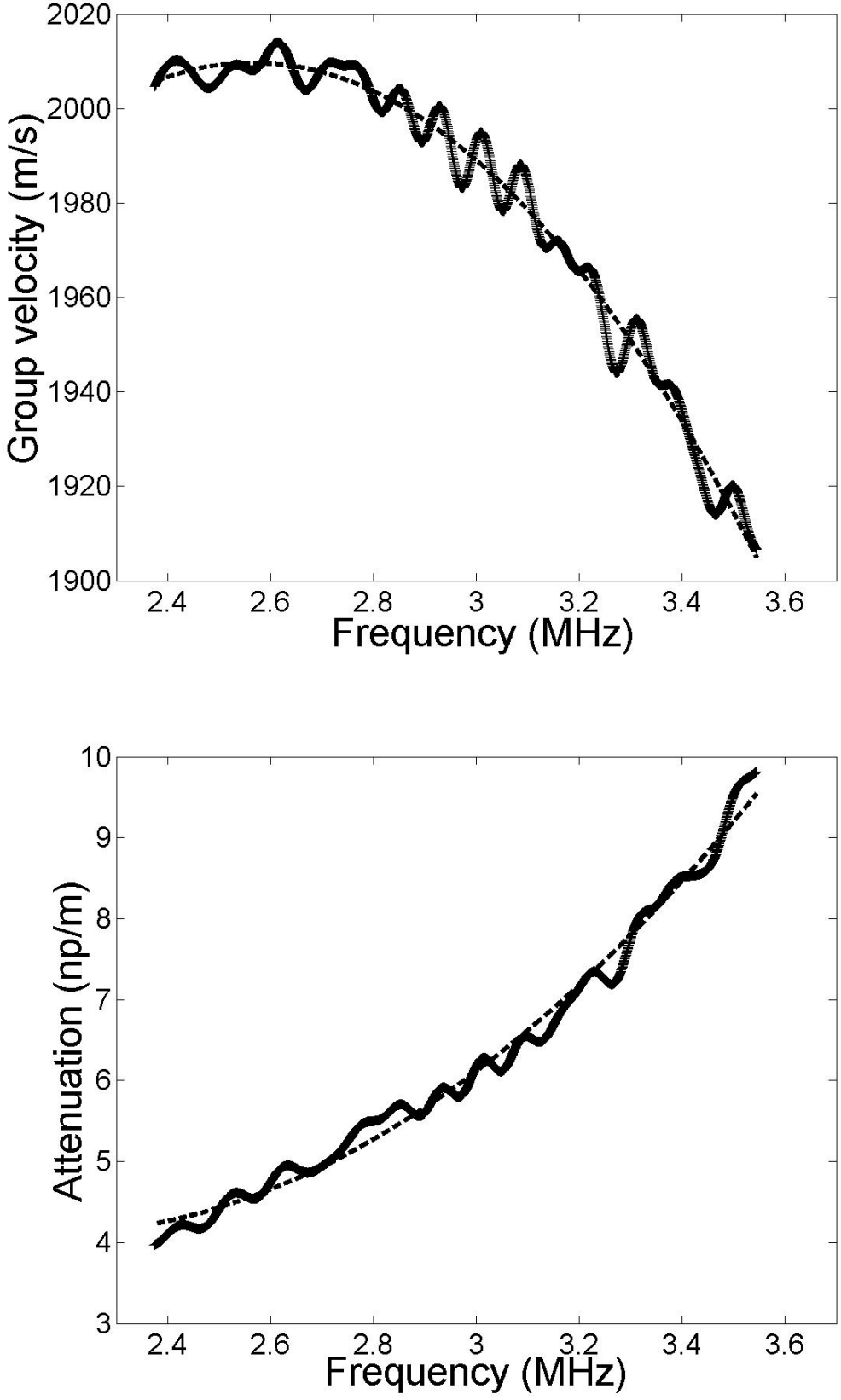

Figure 4.14: Raw measurement data (—) and the quadratic curve fit (- - -) for a Snowtex-ZL sample.

Chapter 5

Non-dispersive wave propagation in thin flexible waveguides

5.1 Shear horizontal mode

The work presented in chapters 3 and 4 suggested the investigation of propagating modes in a strip of rectangular cross section. The search for a strip mode similar to the A0 mode of an infinitely wide plate was started. It was hoped that this strip mode could be used to excite a strip QS-mode, which was needed to further develop the QS-mode measurement method and make it more practical.

During the investigation an A0-like mode was found and experimentally excited. However during the analysis it was also found that non-dispersive "shear horizontal" like strip modes could easily be excited in strips of rectangular cross section. It was realised that such a mode could be used to transmit ultrasonic energy from a transducer through the strip waveguide to a structure non-dispersively and over relatively long distances.

A non-dispersive waveguide has a high potential to be used in applications such as ultrasonic thickness gauging or monitoring of cracks in structures at elevated temperatures ($> 300°C$), in harsh environments or in places where access is limited.

These tasks are straight forward for ultrasonic inspection equipment at room temperatures or in safe environments. However in harsh environments such as the ones described above, standard ultrasonic NDT equipment fails due to a number of reasons, the most important being the loss of the transducer capabilities to send and receive signals due to depolarisation of piezo electric materials at high temperatures (Curie point of piezo-ceramics is typically about 250°C) or under the influence of high radiation levels.

Currently researchers are working on the development of transducer materials that can withstand extreme conditions [4], [5]. The development and the manufacture of these new materials is very expensive, therefore the alternative method of using a waveguide to transmit energy from a standard transducer in a safe environment into the structure at extreme conditions is very attractive. It was decided to focus further research onto this field. The remainder of the work reported in this thesis therefore concentrates on the development of an "acoustic cable" for non-destructive testing of a structure.

The main difficulties for the implementation of an "acoustic cable" are the need for an efficient excitation of a clean non- or marginally-dispersive signal and an attachment to the structure that optimises transmission of a clean and strong signal into the structure to be interrogated. These two tasks were separated. Wave propagation in waveguides is discussed in this chapter while the source characteristics of waveguides on half-spaces are considered in chapter 6.

Whilst currently there exist no NDT devices for structural interrogation using a flexible waveguide to separate the transducer from the test-piece, several publications on non-dispersive waveguides and buffer rods for high temperature applications can be found. These articles are mainly motivated by the field of fluid flow metering where a strong signal needs to be sent across a fluid conduit. The flow velocity is then evaluated by a change in transit time from a transducer on one side of the conduit to a receiver on the other side of the conduit. These embodiments of marginally dispersive waveguides and their working principle will be outlined in section 5.3 af-

ter a short section that highlights the desired wave propagation characteristics of 'acoustic cable' buffer waveguides. Then wave propagation in strips of rectangular cross section will be discussed. At the end of the chapter in section 5.5 experimental work that has been carried out on rods, bundles of wires, wires and rectangular strips is presented.

5.2 Desirable waveguide characteristics

There are several desirable characteristics that a waveguide should have for the successful transmission of ultrasonic pulses from a transducer through the waveguide into another structure. These characteristics will be discussed here. For this we recall some of the basics of guided wave propagation which were described in section 2.2.

Single mode excitation

When examining figure 2.1 one notices that the number of propagating modes that exist in a plate structure is large; indeed it is infinite, the higher the frequency of operation the more modes exist. At any chosen frequency there are several modes that can propagate. If two modes of similar velocity propagate in the plate their signals will interfere or if the propagation distance is long enough, two separate arrivals will be recorded. This will complicate the analysis of signals considerably if the signals are close together. If more than a couple of modes propagate in the plate it becomes nearly impossible to separate and differentiate the reflections and arrivals of one mode from the signal arrivals of another mode. Therefore it is important to limit the number of modes that propagate in a waveguide and ideally to use a single pure mode to carry out testing.

The closer the transducer induced displacements match the mode shape of a mode, the stronger this mode will be excited compared to other modes that do not match the motion induced by the transducer. In a plate at low frequency thicknesses ($<$ 1.7MHz mm) only three propagating modes exist. These fundamental modes have distinct polarisation directions and can therefore rather easily be excited by applying

a uniform displacement profile across the section of the plate in the direction of one of the axes of the coordinate system (see 2.3). At higher frequencies, where higher order modes are present and the mode shapes of the fundamental modes considerably differ from a uniform profile across the plate thickness, it becomes more difficult to excite a single mode. In these cases transduction methods using a wedge or comb like transducers can be employed, see for example Monkhouse et al. [64]. However for these reasons the traditional approach to single mode excitation is to operate at low frequency thickness products.

In practice perfect excitation is not possible due to imperfections of the waveguide or the transducer. However a single mode can be preferentially excited by certain transducer configurations. Other modes will be excited at much lower amplitudes and cause coherent noise. In general a good single mode excitation excites one mode about 40 dB above other modes which allows satisfactory measurements.

Non-dispersiveness

In figure 2.2 the effects of dispersion are illustrated. Distortion and elongation of the pulse shape decrease the spatial resolution with which an object could be monitored and the amplitude loss due to dispersion considerably reduces the range of the guided wave and therefore the length of a useable waveguide. Even though techniques to counter the effects of dispersion exist with time reversal [28] and dispersion compensation [27], these techniques complicate the method unnecessarily and require excitation of complicated temporal signals and arbitrary waveform generators. Therefore propagation in the waveguide should be non- or marginally-dispersive. The traditional way of achieving this is to operate at low frequency thicknesses; however if high spatial resolution and thus high frequencies are needed the waveguide dimensions become very small.

Flexibility and low thickness

Apart from the cost savings and practical advantages that the use of a flexible and thin waveguide entails, there is also a technical advantage due to the small dimen-

sions of the waveguide. A thin waveguide is much better at isolating a transducer from a hot environment than a larger cross section rod. This is illustrated in figure 5.1 where the temperature distribution along three different waveguides is plotted. One end of each waveguide is attached to a hot (600°C) structure while the other end protrudes freely into surrounding air at room temperature (25°C). The heat transfer in the waveguide is modelled as described by Mills [65] for steady state heat transfer along a fin. While the thin steel wave guides of characteristic dimension 1 mm ensure a temperature drop below 100°C within 100 mm of length of the waveguide, the thick rod of characteristic dimension 20mm only achieves a similar temperature drop over 500mm of length.

Half a metre is a considerable clearance that the rigid larger diameter rod device will need, while a thin, flexible waveguide can possibly be bent around corners to reach into inaccessible areas.

Low attenuation and high corrosion resistance

The waveguide merely acts as a channel to send/receive the signal to and from an area where it will interact with a structure to collect information. Ideally this should occur without losses along the path that the signal is sent, therefore losses in the waveguide should be minimised. In this respect longitudinal modes perform better since they are attenuated less at high temperatures. According to Papadakis et al. [66] there is no significant increase in the longitudinal or shear wave attenuation of steel at 2MHz up to temperatures of $\sim$ 700°C. Above 700°C the shear wave attenuation starts to increase considerably to about 0.5 Np/cm at 1100°C, while the longitudinal attenuation increases moderately and then reduces again to 0.1 Np/cm at 1100°C. However shear waves allow the use of lower frequencies for the same resolution due to their slower wave velocity. Attenuation due to the grain size of the material may also become important (see Reynolds and Smith [67]).

The waveguide material will also have to be robust enough to withstand an aggressive environment and should be highly corrosion and radiation resistant. Therefore stainless steel or ceramics are materials of choice for the waveguide.

5.3 Non-dispersive waveguides in the literature

The work reported in the literature has mainly been motivated by the application of flow monitoring of hot fluids in pipes. A substantial number of publications were found to be in the form of patents. Lynnworth and co-workers [68], [69], [70] have developed a series of wire bundle systems in order to produce marginally dispersive propagation of extensional waves along a waveguide system. They identified dispersion as the main problem. In order to minimise dispersion in the waveguide they excite the $L(0,1)$ mode in very thin wires. Due to the small diameter of the wires the waveguide operates at low frequency thickness products where the phase velocity is almost frequency independent and marginally dispersive, see section 2.6. In order to obtain a strong signal many wires were put together in a bundle. Winston and Brunk [71] have suggested a similar method using single or multiple wires, however they did not specify any further information about an implementation of the method.

Heijnsdijk and van Klooster [72] have proposed a coiled foil waveguide as an alternative to a bundle of rods. The thickness of the foil is arranged to be much smaller than the smallest wavelength to be propagated; this ensures that the frequency thickness product of the foil is very low and therefore compressional pulses will essentially propagate non-dispersively along the foil. The foil is coiled around an axis parallel to the propagation direction and so if unwrapped would be very long in the direction parallel to propagation. This mimics a plane wave propagating along the foil where interferences from edges are kept to a minimum.

Jen and co-workers [73], [74], [75], [76] have tried to limit the number of modes travelling in a thin bar by adding an attenuative cladding on the outside of the bar. The bar can be of a tapered shape. It is essentially an attempt to remove the effects of the waveguide boundaries mainly by damping and limiting the reflections of the surface. The number of trailing echoes is thus almost entirely removed; however the effects of dispersion are not entirely removed and the signal is slightly delayed, slightly distorted and strongly attenuated. This method is an improvement to even older solutions that utilise uniformly and non-uniformly threaded bars as waveg-

uides [77], [78]. Nevertheless Jen's method, like the threaded bars, suffers from high attenuation over relatively short propagation distances. The relatively high attenuation limits the propagation distance for this waveguide. At the same time a longer waveguide is needed to isolate the transducer from high temperatures due to the large diameter of the waveguide (see figure 5.1).

For the purpose of fluid flow metering Lynnworth [79] also patented a device that he called the "hockey stick". It carries a shear wave in a rectangular section bar to an angled section. The angle of the end of the "hockey stick" is coupled to a pipe wall in order to promote mode conversion from the shear wave to a compressional wave in the liquid. On the other side of the pipe the compressional wave converts back to a shear wave and is picked up in a similar device. A sketch of the "hockey stick" system for fluid flow metering is shown in figure 5.2.

5.4 Wave propagation in rectangular strips

The modelling of very wide plates is accurately achieved by the assumption of an infinitely wide plate. The shorter the width of the plate/strip becomes the more it starts influencing the wave propagation and it becomes necessary to model the rectangular strip as a one dimensional waveguide with a constant cross section; a family of modes can propagate along the waveguide. Mindlin and Fox [80] were the first to describe the propagating modes of a bar of rectangular cross section. Their solution was made up of a superposition of several flexural, longitudinal and shear modes that propagate in infinite plates of the width and thickness of the bar respectively. The solutions for the infinite plates were superposed in order to fulfil the boundary conditions of zero stress all around the perimeter of the cross section. This method enabled them to determine the dispersion characteristics of the bar at distinct frequencies and aspect ratios of the bar. A solution for all frequencies and aspect ratios was however not possible. More recently the continuous tracing of dispersion curves for wave propagation in structures of arbitrary cross section has become possible through the use of finite element (FE) eigensolvers. Wilcox et al.

[81], Mukdadi et al. [82], Hayashi et al. [83] and Gavric [84] have reported methods of tracing dispersion curves for L-shaped sections, rail heads and strips.

The method of Wilcox et al. has the advantage that it can be carried out with standard finite element programs. It has been employed here to analyse the modes propagating in 1mm thick steel strips of a much larger width (> 15mm was chosen). The method works by defining an axisymmetric model with a very large radius compared to the dimensions of the cross section. The section of the axisymmetric body represents the cross section of the wave guide, see figure 5.3. Due to the very large radius the structure approximates a straight waveguide. For the finite element eigensolver a specific cyclic order can be specified. This specifies the number of wavelengths that exist around the circumference of the axisymmetric body. For example a cyclic order of 1 corresponds to a wavelength equal to the circumference of the structure. For a cyclic order of 2 there are two wavelengths around the circumference and so on. Therefore the wavelength of the solution is determined by the following equation:

$$\lambda = \frac{2\pi R}{C_{order}} \tag{5.1}$$

where R is the radius of the model and C_{order} is the cyclic order of the FE eigensolver. At each cyclic order the FE-eigensolver routine will determine several resonant frequencies. These frequencies correspond to different modes. The wavenumber dispersion curves for the meshed cross section can now be determined by plotting the resonant frequencies against the wavenumber, which is determined using equation 5.2 and the identity

$$k = \frac{2\pi}{\lambda} \tag{5.2}$$

where k is the circular wavenumber and λ the wavelength. This method therefore yields a set of discrete frequency solutions at each wavenumber. A typical set of results is shown in figure 5.4. Wilcox et al. developed software that connects adjacent solution points to form a continous solution line in the wavenumber frequency

domain. This represents a mode. The joining up of adjacent points to a line is carried out by comparing the mode shapes of adjacent solutions and by using the slope of the curve of existing solutions to predict the continuation of the curve, which is similar to the method presented by Lowe [23]. A software coding of this had been developed by Wilcox and was merely used here to extract results for the desired geometries. The finite element software that determined the eigen solutions was the FINEL 77 code which was developed by Hitchings [85] at Imperial College.

Phase velocity dispersion curves can be obtained from the wavenumber frequency plot by converting them using the following identity:

$$C_{ph} = \frac{\omega}{k} \tag{5.3}$$

Once the phase velocity is determined the group velocity can be calculated using:

$$C_{gr} = \frac{\partial \omega}{\partial k} = C_{ph} + k\frac{\partial C_{ph}}{\partial k} \tag{5.4}$$

An interesting aspect to note about the technique is that the determined FE eigen solutions are confined to a rectangular domain in the frequency - wavenumber space. However when this is transformed into a phase velocity - frequency space the solutions will be bound in a space between the two lines $C_{ph} = (1/k_{min})\omega$ and $C_{ph} = (1/k_{max})\omega$. This is illustrated in figure 5.5.

The mode shapes of each mode are a direct result of the FE analysis and can be extracted at each frequency.

5.4.1 Dispersion curves for rectangular strips

Using the technique described in the previous section dispersion curves for rectangular strips were obtained. The results for steel ($\rho = 7932kg/m^3$, $E = 216.9GPa$, $\nu = 0.2865$) strip geometries of 1 mm thickness and width 15 and 30 mm will be presented here. A sketch of the finite element model that was defined is shown in figure 5.3. After the finite element program (FINEL 77 [85]) was run the data was

post processed using the codes developed by Wilcox et al. [81]. Figure 5.6 shows the frequency-wavenumber and phase velocity-frequency dispersion curves. The figure looks very busy because many more propagating modes exist at lower frequencies than in the infinite plate case. These extra modes are mainly due to the finite width of the strip.

In figure 5.6 two modes are highlighted. These modes were named A0* and SH*. The A0* mode is very similar to the commonly known A0 mode in an infinite plate. It is a flexural mode with respect to the thickness (x direction), however due to the finite width the mode also has a variation across the width (y direction). In this case the mode is symmetric about the width with maximum displacement at the centre of the rectangular strip. The relationship of the mode to the A0 mode in an infinite plate is underlined by their similarity in phase velocity. Figure 5.7 shows the mode shape of the A0* mode at 2.5 MHz. The main displacement component is in the x direction and displacements are concentrated at the centre of the strip. This is the strip mode that would preferentially be excited to promote mode conversion to a QS-strip mode and carry out fluid property measurements similar to those in chapters 3 and 4.

The SH* mode was identified as the lowest order shear horizontal mode that exists in the rectangular strip. Strictly speaking the term 'shear horizontal' only makes sense if the plate is infinite. Here the width is much larger than the thickness of the plate and therefore 'shear horizontal' mode refers to a mode with similar polarisation to an SH mode in the infinite plate. The same mode could also be described as bending in the width-propagation direction plane. Shearing with respect to the thickness of the strip is bending with respect to the width of the strip. An equivalent to the SH0 mode in an infinite plate does not exist in a strip. The SH* mode has a cut-off that depends on the width of the strip. At frequencies well above the cut-off the mode asymptotes to the shear velocity of the strip. The mode shapes of the SH* mode at different frequencies are shown in figure 5.8. The figure shows that at high frequencies the y displacement component is dominant and concentrated in the centre of the strip. The mode shape is constant across the x direction. Also near

cut-off there are displacements at the edges of the strip. This is better illustrated in figure 5.9 which shows the evolution of the dominant y displacement across the width of the strip over a range of frequencies.

The influence of the shape of the excitation at the end section of the strip was investigated in order to find the best way to excite the SH* mode strongly. A finite element model for a 15mm wide steel strip was prepared in the ABAQUS finite element software. The model was two dimensional with a plane stress condition in the thickness direction of the strip. Due to its special polarisation the SH* mode only contains σ_{zy} stress components, which satisfy the plane stress condition ($\sigma_{xx} = \sigma_{xy} = \sigma_{xz} = 0$). A frequency domain solver was used to solve the problem. At one end of the strip a steady, dynamic force was applied while an absorbing region at the other end of the strip prevented any reflections of the excited waves.

A sketch of the FE model is displayed in figure 5.10. Square quadratic elements of size 0.25mm were used to mesh the strip and the absorbing region. The viscoelastic parameters of the absorbing region were increased in a cubic fashion from the interface with the strip. They were determined as described by Drodz et al. [86]. Different distributions of exciting force over the width of the steel strip ($\rho = 7932$ kg/m^3, $E = 216.9$ GPa, $\nu = 0.2865$) were used to see the influence of the excitation force profile on the excited waves in the strip.

The results of the FE analysis are displayed in figure 5.11. In the figure three different profiles of excitation force across the width are shown as well as the y (width) direction displacement field that they produce. For a uniformly applied force the displacement field (figure 5.11a) in the strip becomes relatively complicated. It can be concluded that many modes are excited and interfere. If the stress profile of the SH* mode (from the FE eigensolver) is applied at the strip end (figure 5.11b), a pure mode can be excited in the strip. Displacements are concentrated at the centre of the strip. For a triangular forcing profile, the SH* mode is also preferentially excited (figure 5.11c). However some other modes are also excited so that the displacement field in the strip is not as uniform as in the case of the exact mode shape

forcing which is visualised in figure 5.12. Figure 5.12 shows that differences between the exact mode shape excitation and the excitation by a triangular force profile are mainly caused at the edges of the strip. It was concluded that any excitation that resembles the mode shape better than a triangular forcing will preferentially excite the SH* mode in the strip.

It was later realised that the SH* mode could also be modelled with the DISPERSE software. DISPERSE usually only traces dispersion curves for infinitely wide plates. The software assumes plane strain conditions to model the infinite width of the plate. Assuming that the direction in which the structure is infinite is the x direction of figure 5.8, this implies

$$\frac{\partial}{\partial x} = 0. \tag{5.5}$$

The x direction is the thickness direction of the plate or strip. If the mode shape across the thickness (x) is constant then the derivative of any variable with respect to the x direction equals zero and the plane strain condition of equation 5.5 is fulfilled. The mode shape of the SH* mode is constant across the thickness of the strip (see figure 5.8) and can therefore be modelled with the DISPERSE software assuming bending of an infinite plate of thickness equal to the width of the strip (as soon as the mode shapes become non-uniform across the thickness of the strip this analysis breaks down which is the case for most of the other strip modes). It was found that the first higher order anti-symmetric plate mode A1 (see figure 2.1) corresponds to the identified SH* mode in the strip. Figure 5.13 shows the phase velocity dispersion curves obtained using Disperse and the FE routine described by Wilcox et al. [81]. The results are in virtually perfect agreement.

It was sought to define the range of operational frequencies in which the SH* mode propagates virtually non-dispersively and can be successfully excited. It was found that the mode had to fulfill two criteria to do this:

1. Since the spatial transducer output is unlikely to change with frequency, the mode shape of the mode should not vary by more than 10% over the range of frequencies

contained within the excitation signal.

2. In order to guarantee very low levels of dispersion the phase velocity of the mode should not vary by more than 2% over the range of frequencies contained within the excitation signal.

By analysing the phase velocity dispersion curves and the mode shape of the SH* mode it was found that these criteria are fulfilled above a frequency-width product of 15MHz mm for a steel strip. To make this condition independent of the material the frequency width was normalised by the shear wavelength of the material. The shear wavelength of a 1 MHz signal in steel is approximately 3mm. The strip has to be 15mm wide at 1MHz to fulfill the above conditions. Therefore the width of a 1 mm thick strip has to be at least 5 bulk shear wavelengths to ensure the possibility of exciting a virtually non dispersive SH* mode. It can be concluded that if a broadband signal is excited the width of the strip has to be larger than 5 bulk shear wavelengths of the lowest frequency component contained within the signal. While this criterion is true for the SH* mode in waveguides of any thickness as long as the mode shape is constant across the thickness, thin waveguides of thicknesses less than a shear bulk wavelength are more flexible, cheaper and more practical.

5.5 Experimental work and preferential excitation of a single mode

Initially experiments on rods and wires were carried out. The traditional route of minimising the frequency-radius product to achieve non-dispersive propagation was employed. This had the advantage of limiting the number of propagating modes in the wire to the fundamental three modes which can easily be excited selectively by choosing appropriate transduction methods. At low frequency-radius products this also makes wave propagation virtually non-dispersive for the $L(0,1)$ mode, the $T(0,1)$ mode being non-dispersive anyway. Since excitation of the $T(0,1)$ mode at high frequencies becomes difficult with standard transducers (due to the short wavelength), experiments were focused on the $L(0,1)$ mode which could be excited

at the cross section of the wire end. The main problems with these traditional methods becomes the transduction of energy into very thin wires, see 5.5.1.

When difficulties with wire experiments arose, attention was turned to experiments with rectangular cross section strips. The move to a strip geometry was also motivated by the better source characteristics of a strip source on a half space compared to a point source, see chapter 6. As was shown above in section 5.4, for a rectangular strip waveguide the traditional method of achieving low dispersion by reducing the frequency thickness product does not apply. On the contrary the SH* mode in a strip becomes less dispersive at higher frequencies (frequency-width products). For the strip mode attention was focused on the transducer loading distribution required to achieve pure mode excitation. Experiments with rectangular strips are described in section 5.5.2.

5.5.1 Rods and Wires

At first two experiments were carried out to highlight the problems of dispersion and multiple mode excitation in larger radius rod waveguides compared to small radius wire waveguides. For this purpose a 160mm long and 5mm diameter stainless steel rod and a 160mm long bundle of 18 steel wires of 1mm diameter were made. A 1MHz standard ultrasonic transducer (Panametrics) was coupled to the waveguide ends using ultrasonic coupling gel. A waveform generator sent a 5 cycle 1 MHz Hanning windowed toneburst. The received echo was recorded on a digital storage oscilloscope (LeCroy 9400) and then transferred to a PC. The received signals showing multiple reflections from the rod end, schematics of the waveguides and a group velocity dispersion curve for steel rods are shown in figure 5.14. The figure illustrates the detrimental effects of the excitation of multiple modes and the spreading out of signals due to dispersion. The 5 mm diameter rod clearly exhibits both signals due to multiple modes and strong dispersion. Multiple mode excitation is prevented in the case of the bundle. However the signal is still slightly distorted due to dispersion. As predicted by the dispersion curves in figure 5.14 the group velocity of the waves in the thicker rod is slower which manifests itself in the later arrival of the main signal packet.

The signal transmission from the transducer into the rod and bundle was very inefficient and the detected signals were very weak. It was also attempted to bond piezo ceramic elements directly to the bundle using adhesive. This was known to work well at low frequency in a solid rod. However due to the relatively large diameter of the piezo ceramic discs, radial resonances in the disc were excited at high frequencies and the discs proved to be useless for $L(0,1)$ excitation in the wire bundle. An attempt was then made to isolate a single wire in order to excite a strong signal in the single wire. Two possible ways of achieving this were:

1. the amplification of the signal of a standard ultrasonic transducer by means of a horn

2. the direct bonding of a piezo electric disc of the diameter of the wire to the end of the wire.

Nicholson and McDicken [87] have reported experimental trials to transmit ultrasonic energy via a horn into wires. They tried several different shapes of horns and did transmit energy through the horn into the wires. However the signal shapes were severely distorted and signs of excitation of multiple modes in the wires were shown. Tang and Lau [88] modelled sound transmission through a non-uniform section, similar to a taper, and also concluded that the transmitted signal is very complicated and hard to predict.

Both the above studies were carried out at frequencies where the wavelength of the wave is considerably smaller than the dimension of the cross section. The author believes that this was the cause of the problem. Many modes can exist across the large diameter of the taper and therefore a distorted and complicated multi mode signal is transmitted into the wire. A possible remedy for this problem was thought to be the use of a hollow tapered section, similar to a funnel, that would connect the transducer to the wire. The wall thickness of the funnel would be chosen to be much smaller than a wavelength. Finite element simulations of propagation from the tapered hollow section to the wire initially showed good results and minimal signal distortion. However the manufacture of a thin hollow tapered section was found to be difficult and since a wire point source on a half space was found to be

undesirable, work on a prototype was abandoned.

For the second approach miniature piezo electric discs had to be manufactured since piezo discs are not readily available in sizes below 1mm radius. Ideally the piezo electric disc had the same diameter as the wire waveguide and a thickness equal to or smaller than the waveguide diameter. This ensured that the resonances of the piezo disc lay above the desired operating frequency. The piezo disc was then attached to the wire with epoxy. Very strong and clean signals could be produced in a 1mm thick wire at up to 1 MHz using this method, see figure 5.15. However to operate at frequencies above 1 MHz it was found that the disc diameter had to be reduced well below 1mm diameter. At those dimensions the manufacture becomes impossible without sophisticated machinery and this becomes an expensive procedure. For this reason and the poor performance of a wire waveguide source on a half space (see section 6) alternative methods enabling the excitation of non-dispersively propagating waves in waveguides were sought.

5.5.2 Rectangular strips

The experimental investigation for wave propagation in rectangular strips was focused on exciting A0* and SH* modes. To achieve this the exciting transducer had to mimic the mode shape as closely as possible. Additionally for broadband signals the mode shape should not change significantly over the range of excited frequencies. For clean excitation of the A0* and SH* modes the simple uniform excitation across the waveguide width that is employed for the fundamental modes is insufficient. However since the mode shapes are uniform across the thickness the transducer output has to be varied across the width of the strip only, see figure 5.7 and figure 5.8. Displacements for both modes are strong at the centre of the strip and decay towards the edges in approximately parabolic fashion. The main difference between the two modes is the polarisation of the A0* mode in the thickness (x) direction and the polarisation of the SH* mode displacements in the width (y) direction.

It was found that good results could be achieved by simply coupling a standard

circular ultrasonic shear transducer (Panametrics) to the end cross section of the strip. The circular shape of the piezo electric element within the transducer was believed to transmit stronger shear stresses at the centre of the strip width than at the outside and thus led to preferential excitation of the SH* or $A0$* mode.

SH* mode

Figure 5.16 shows a 5 cycle 2MHz Hanning windowed toneburst that was sent along a 15mm wide, 1mm thick and 300mm long stainless steel strip and received by the same standard contact shear transducer after reflection from the far end of the strip. The 13mm transducer was clamped to the steel strip by a purpose made clamp using treacle as a shear couplant between the transducer face and the waveguide end section. The transducer was polarised to cause motion in the direction of the width of the strip (y direction). Figure 5.16 shows that a very clean signal without significant dispersion can be excited and received in the strip. The presence of other modes about 30dB weaker than the main signal can also be seen in figure 5.16.

To be absolutely certain that the desired mode was excited in the above experiment an in-plane dual head laser doppler vibrometer (Polytech OFV 512) was used to measure the in-plane surface displacement (y direction) of the strip along the centre line of the strip. The signal was recorded every 0.5mm over a distance of 200mm at a sampling frequency of 10MHz (the laser decoder however has a 1.5MHz low-pass filter built in). This is schematically illustrated in figure 5.17(a). From the measurements a two dimensional Fourier Transform was computed. The 2D-FFT has been described by Alleyne and Cawley [89]. It is a technique to detect and identify multiple modes travelling in a waveguide. The 2D-FFT displays the frequency-wavenumber relation of the signals that have been measured in the waveguide. This plot can directly be compared to analytical frequency-wavenumber predictions. In figure 5.17(b) the 2D-FFT result for a 30mm wide and 1mm thick steel strip is plotted. A line indicating the theoretically predicted SH* mode frequency-wavenumber relation for a 30mm wide and 1mm thick steel strip ($\rho = 7932 kg/m^3$, Cl=6000 m/s, Cs= 3060 m/s) is also displayed. There is very good agreement between the measured data and the predicted values for the SH* mode.

A0* mode

The setup was changed slightly to excite the $A0^*$ mode. A 30 mm wide, 0.2mm thick and 300mm long steel strip was used and the transducer was turned by 90° to excite displacements in the thickness (x) direction. Figure 5.18 shows the 10 cycle 2MHz pulse echo signal received by the transducer. The $A0^*$ mode is very dispersive in this frequency range which explains the very strong distortion of the 10 cycle signal, but the signal seems to be very clean without interference from other modes.

Again to verify the excited modes in the strip the laser vibrometer was scanned along the centre line of the strip and a 2D-FFT was computed. Figure 5.19 shows the result. Out-of-plane (x direction) displacement measurements were carried out over a distance of 200 mm at increments of 0.5 mm with a temporal sampling frequency of 10 MHz (the laser decoder however has a 1.5MHz low-pass filter built in). This resulted in good resolution in the frequency-wavenumber domain. The 2D-FFT shows that the $A0^*$ mode is the dominantly excited mode. Other modes excited are ~ 20 dB less strong than the A0* mode.

Finally one more experiment was carried out to show that a quasi-Scholte strip mode can be excited using a rectangular strip. The same steel strip (0.2 mm thick, 30 mm wide and 300 mm long) was partly immersed in water. This experiment is very similar to the experiments carried out in chapter 4. The A0* mode is sent along the strip until it reaches the point where the strip enters the water, at this location most of the energy converts into the QS* mode (the quasi-Scholte strip mode whose existence is expected) and travels to the end of the strip to be reflected. At the point where the strip enters the water the QS* mode reconverts into the A0* mode of the strip in air. The group velocity of the QS* mode is slower than that of the A0* mode, therefore a delay in the arrival of the back wall reflection is expected, the delay increasing the further the strip is immersed into the fluid.

Figure 5.20 shows signals collected when the strip was immersed 0mm and 70mm into the water. The figure illustrates that the arrival of the $A0^*$ mode that converted into the QS* mode in the water is delayed considerably. The group velocity of the quasi-Scholte strip mode was extracted from the signals in figure 5.20 using equation

4.1. The DISPERSE software was also used to predict the quasi-Scholte mode group velocity for an infinite plate immersed in water. The measurement and prediction are shown in figure 5.21. The result suggest that the rectangular strip A0* mode can be used to excite a quasi-Scholte strip mode when the strip is partly immersed in water. The behaviour also seems to be similar to the infinite plate case.

5.6 Summary

In this chapter wave propagation in waveguides of different geometries was discussed. The work was initially motivated by the search for a suitable A0 like mode in a rectangular strip which could be used to excite a QS strip mode for fluid characterisation. When the modes of a rectangular strip were analysed a marginally dispersive shear horizontal type mode was found. The potential of this mode in applications like ultrasonic buffer waveguides was realised and research was diverted towards the development of an 'acoustic cable' waveguide system that allows the transmission of ultrasonic energy from a transducer in a safe environment to an object that is to be interrogated in a harsh environment or a place where access is limited.

It was found that to date publications report a reasonable amount of work that has been carried out on the subject of non-dispersive waveguides. Most of this work was motivated by the need for high temperature flow measurements. In the published work the major problems of dispersion and presence of multiple modes were overcome by working at low frequency thickness/radius products. The use of the SH* strip mode that is suggested here differs from the traditional methods since it is non-dispersive at high frequency thickness (width) products. The mode can be selectively excited due to its distinct mode shape that is concentrated in the centre of the strip. Some experimental results for the traditional low frequency radius regime excitation of signals in cylindrical structures were presented. The experimental excitation of the SH* mode was also demonstrated. With the current transduction method in the pulse echo mode the SH* mode could be excited and received at least 30dB stronger than other modes of the strip.

5.7 Figures

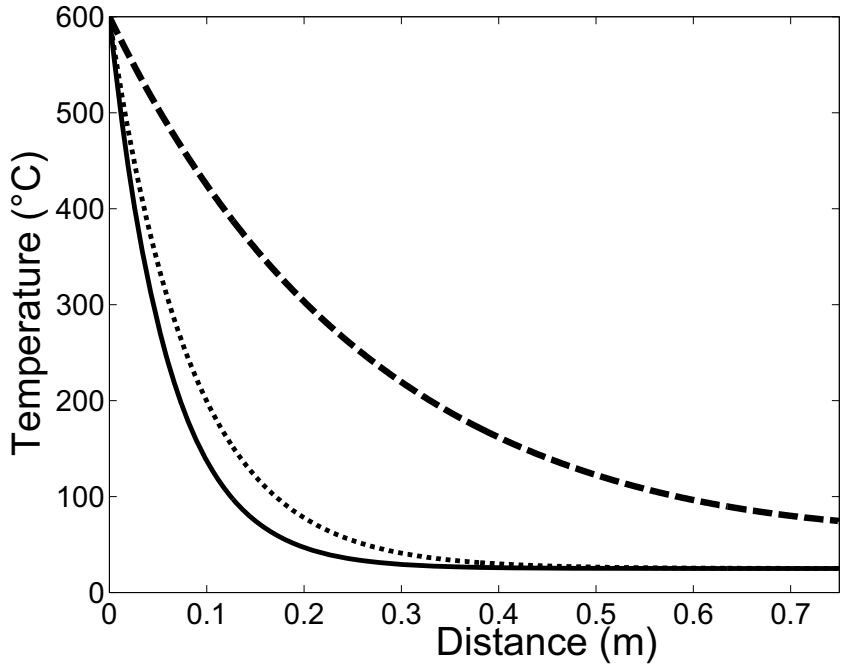

Figure 5.1: Temperature distribution along a (—) steel wire of 0.5mm radius, a (- - -) steel rod of 10mm radius and a ($\cdots$) rectangular steel strip of 15mm and 1mm width and thickness respectively. One end cross section of each is maintained at 600°C while the air surrounding the waveguide is at 25°C. Calculation after Mills [65] with steel conductivity of $k = 15$ W/m/K and heat transfer coefficient of free convective air $hc = 1$ W/m/K.

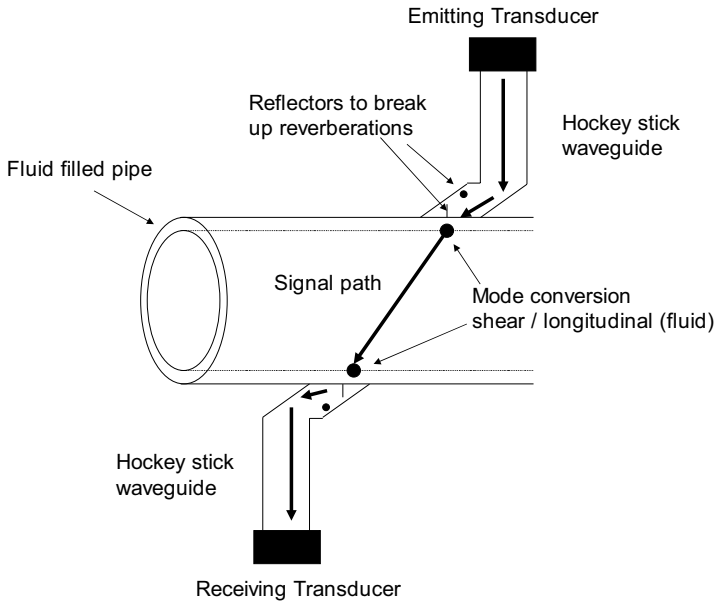

Figure 5.2: Sketch of the "hockey stick" system for fluid flow metering (after Lynnworth [79])

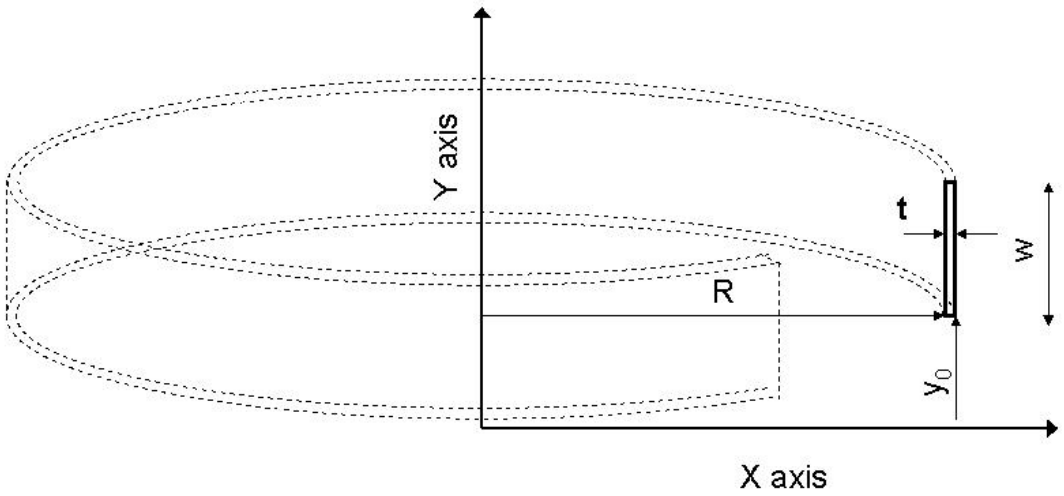

Figure 5.3: Sketch of the geometry of the FE model used to obtain the dispersion curves of a strip of rectangular cross section (see text for dimensions).

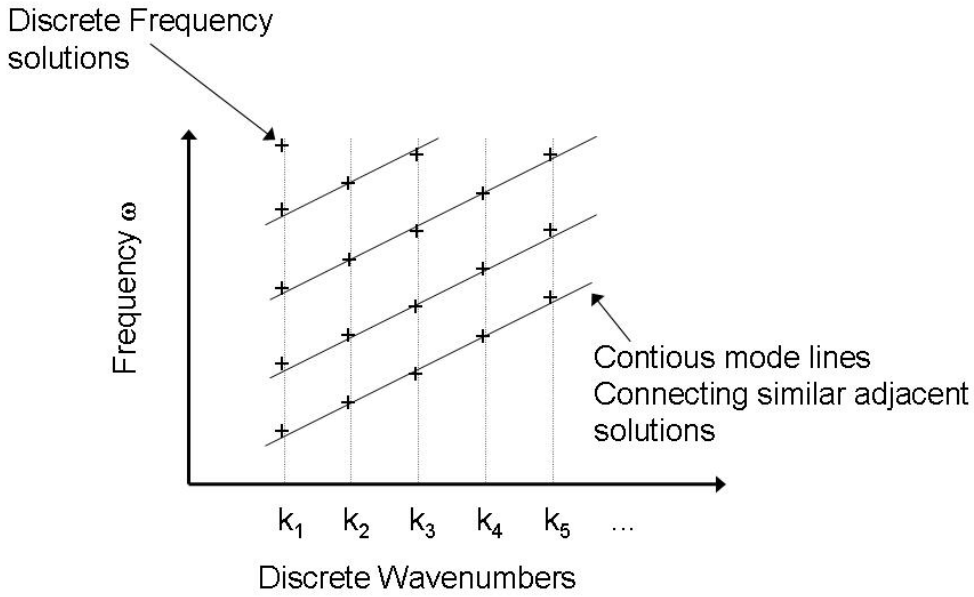

Figure 5.4: Sketch of the frequency-wavenumber results obtained from a FE eigen solver at different cyclic orders.

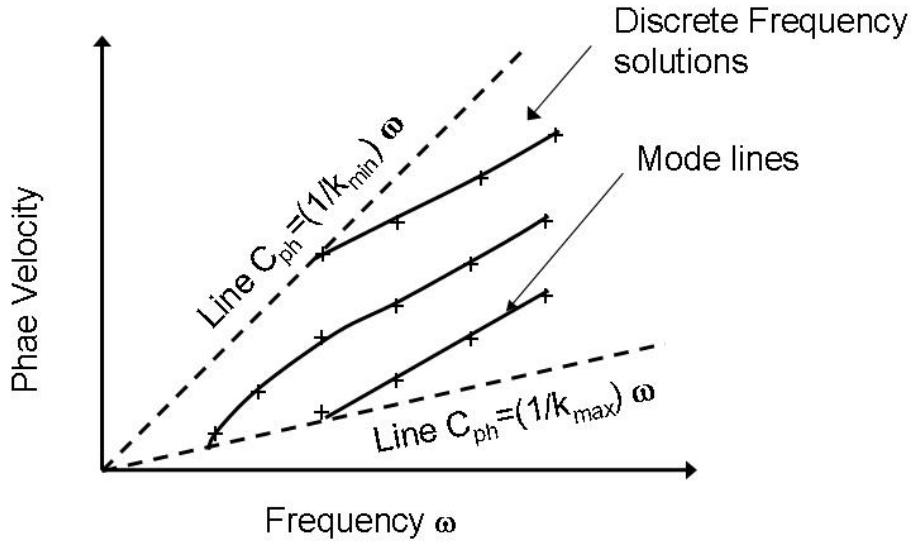

Figure 5.5: Sketch of the frequency-wavenumber results transformed into the phase velocity frequency domain.

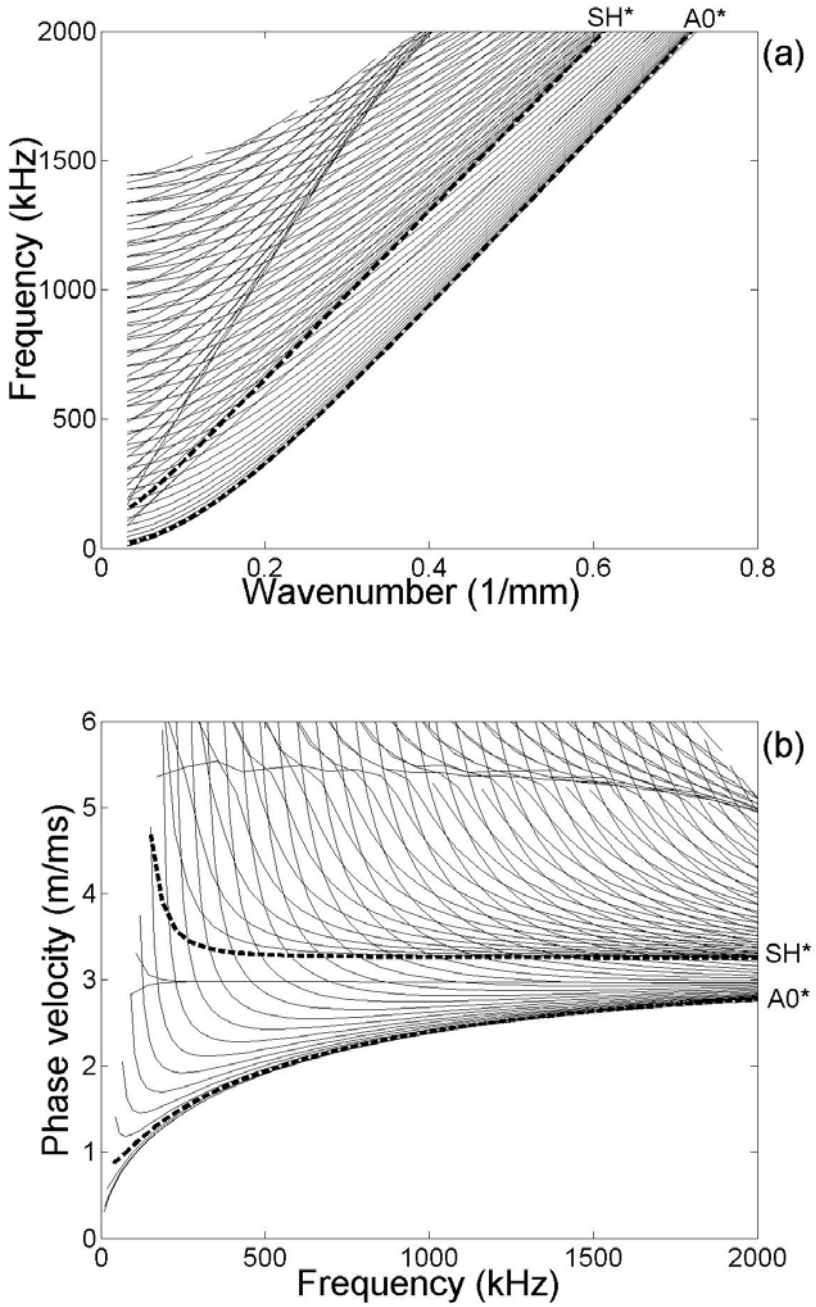

Figure 5.6: Dispersion curves for a 1mm thick and 30mm wide rectangular steel strip determined by FEM a) frequency-wavenumber b) phase velocity frequency. Two interesting modes that correspond to the lowest order shear horizontal mode (SH*) and the lowest order flexural mode (A0*) that is symmetric with respect to its width are highlighted by the bold dashed (- - -) lines.

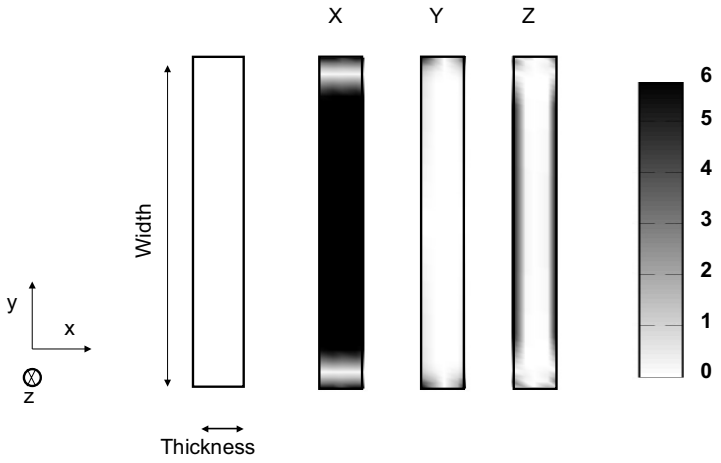

Figure 5.7: Modulus of the displacement mode shape in the x, y and z direction of the A0* mode at 2.5 MHz.

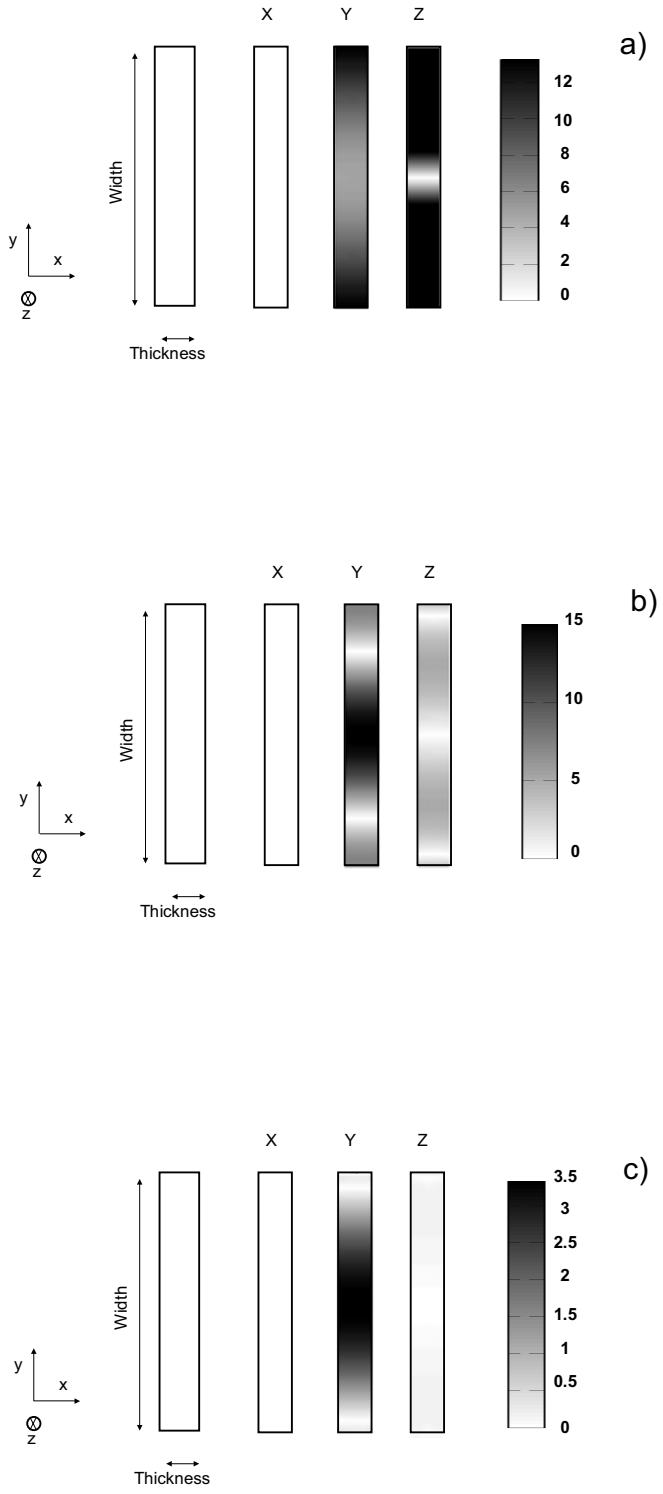

Figure 5.8: Modulus of the displacement mode shapes of the SH* mode in the x, y and z directions at a) 0.14, b) 0.5 and c) 2 MHz of a 15mm wide and 1mm thick rectangular steel strip.

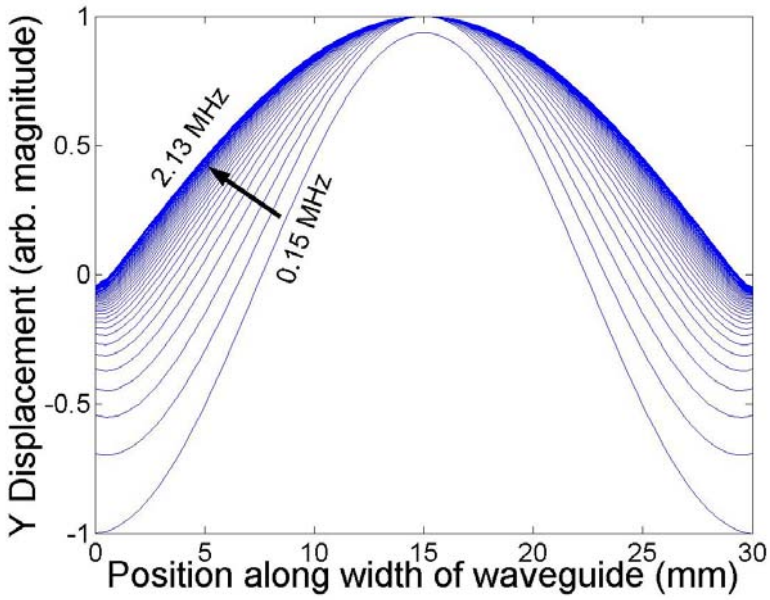

Figure 5.9: Evolution of the SH* mode y displacement mode shape of a 30mm wide and 1mm thick steel strip over a range of frequencies.

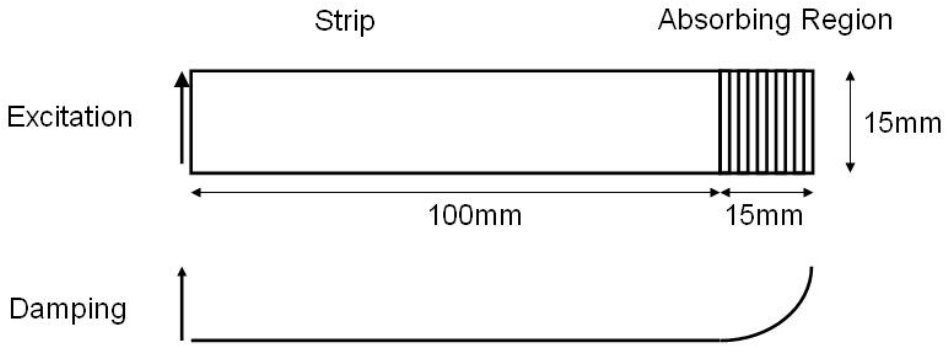

Figure 5.10: Sketch of the 2D plane stress model that was defined in ABAQUS to analyse the effect of different excitation force profiles.

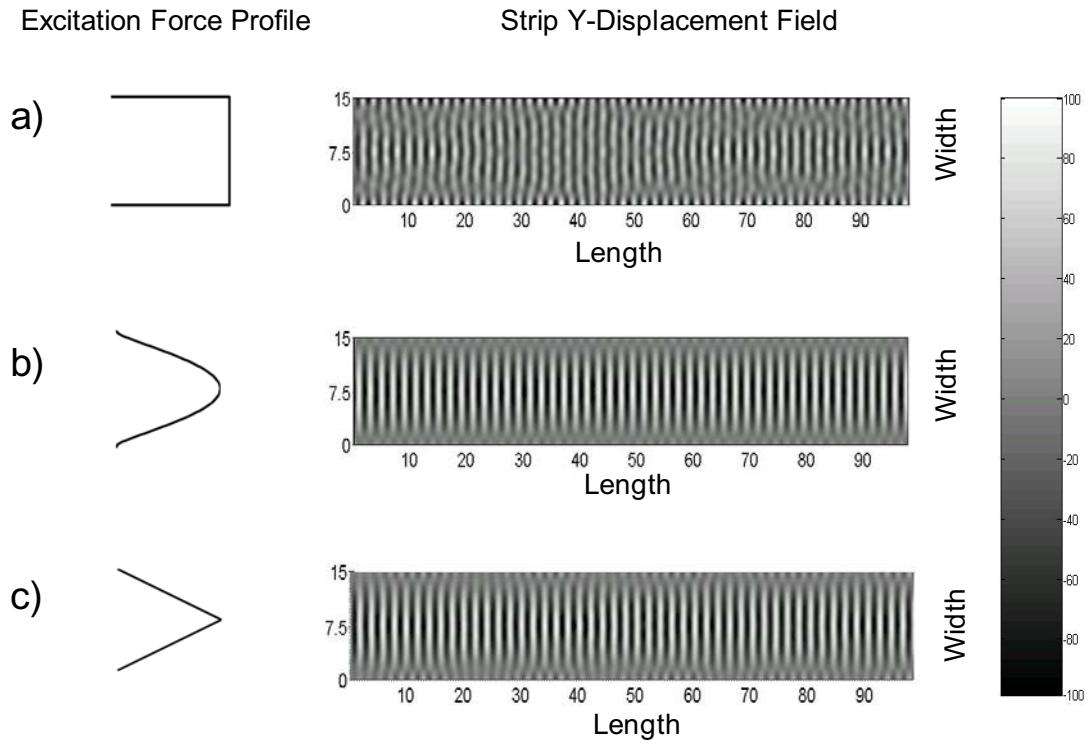

Figure 5.11: Y-direction displacement field output of the plane stress steady state frequency domain finite element model of a steel strip (15mm) under a) rectangular excitation force profile b) exact mode shape excitation force profile c) triangular excitation force profile across the width of the strip. The difference between cases b) and c) is highlighted in figure 5.12.

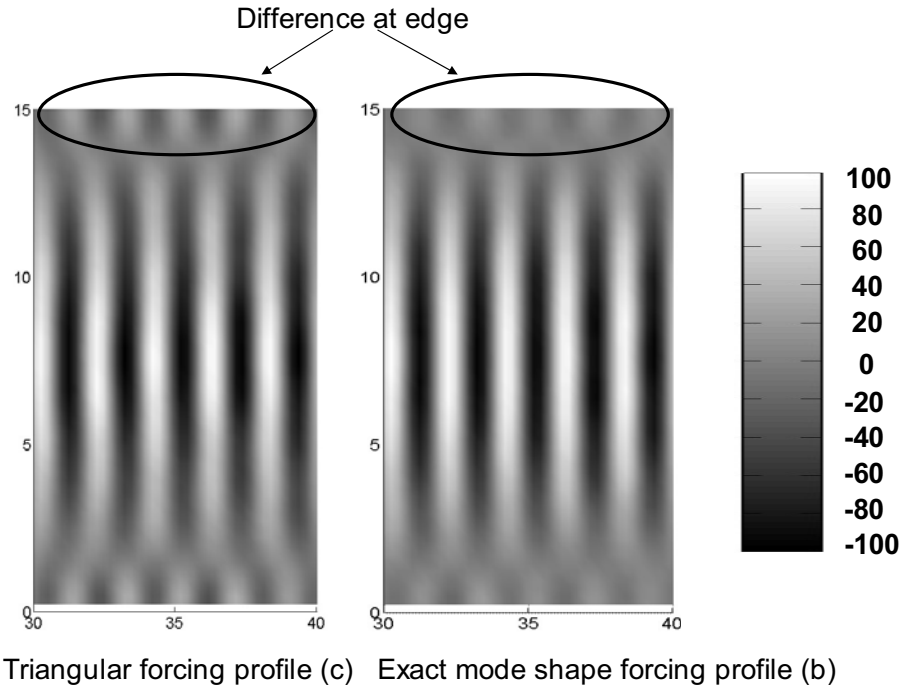

Figure 5.12: Zoom on the Y-direction displacement fields of figure 5.11 b) and c) highlighting the subtle difference between the field excited by a triangular forcing profile and the exact mode shape forcing profile.

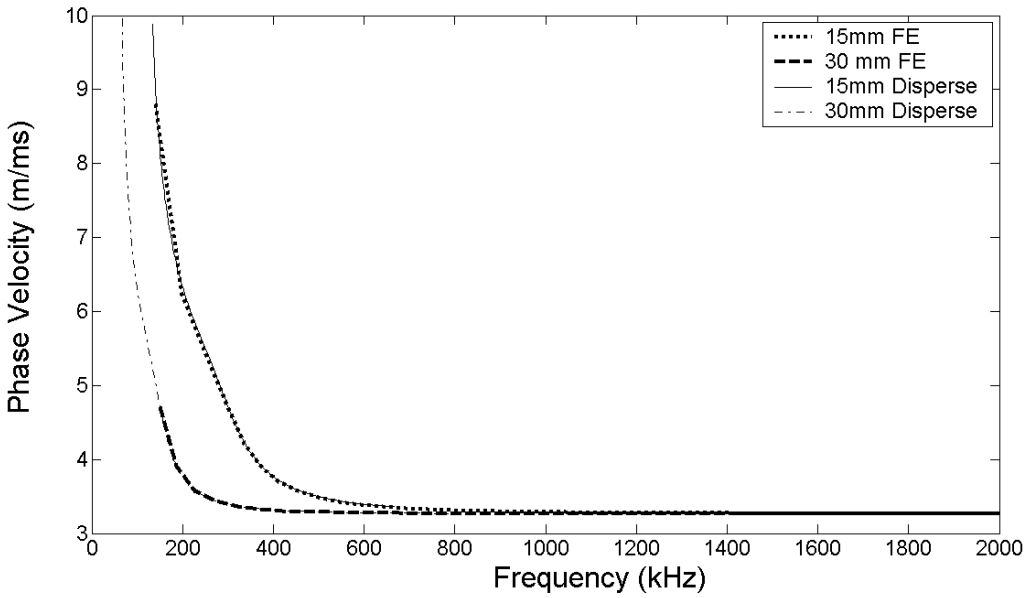

Figure 5.13: Phase velocity curves for the SH* mode of a 1mm thick rectangular steel strip of width indicated in the legend and traced using the FE eigensolver routine written by Wilcox et al. [81] and the DISPERSE software [22] . Note that the cut-off of the modes occurs at the same frequency-width product (i.e. the cut-off of the 30mm wide strip occurs at half the frequency of the cut-off of the 15mm wide strip).

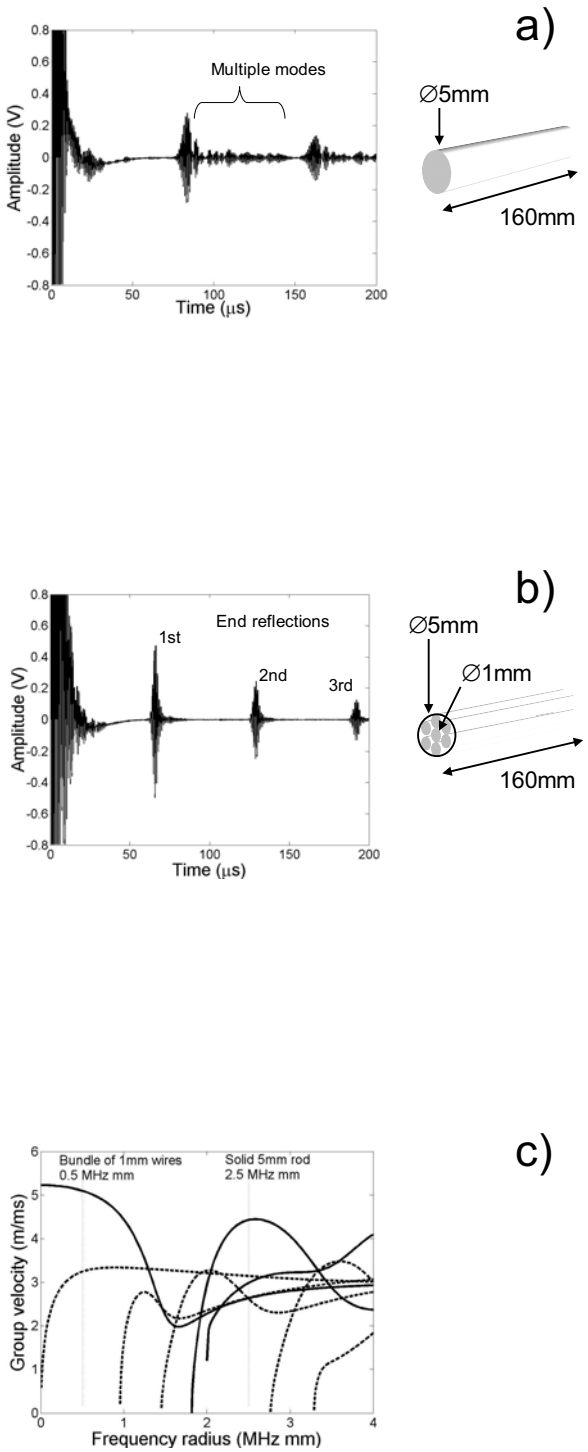

Figure 5.14: Schematics and pulse echo signals received from a) a solid 5mm diameter and 160mm long steel rod b) a bundle of 18 steel wires of diameter 1mm. The group velocity dispersion curve for rod/wire waveguides is also shown in c).

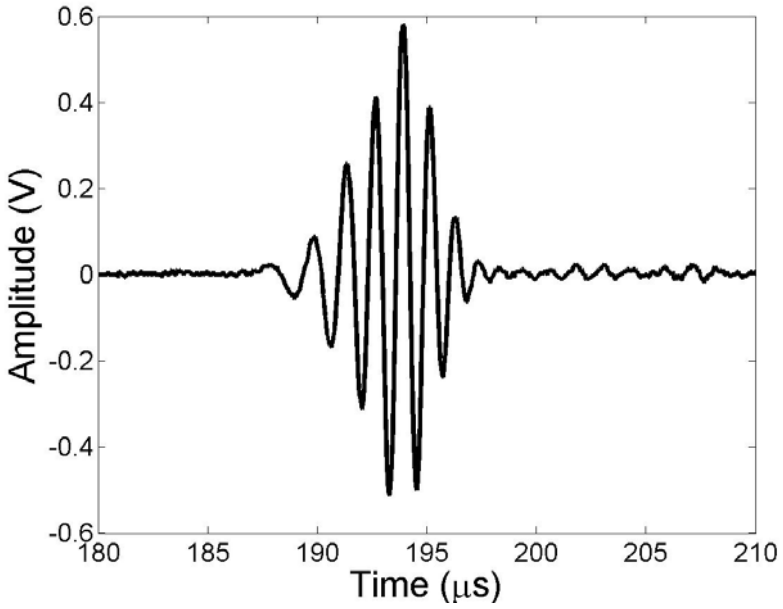

Figure 5.15: Pulse echo signal (0.8 MHz) excited and received by a 1mm diameter and 0.5mm thick piezo disc attached to a 0.5m long steel wire of 1mm diameter.

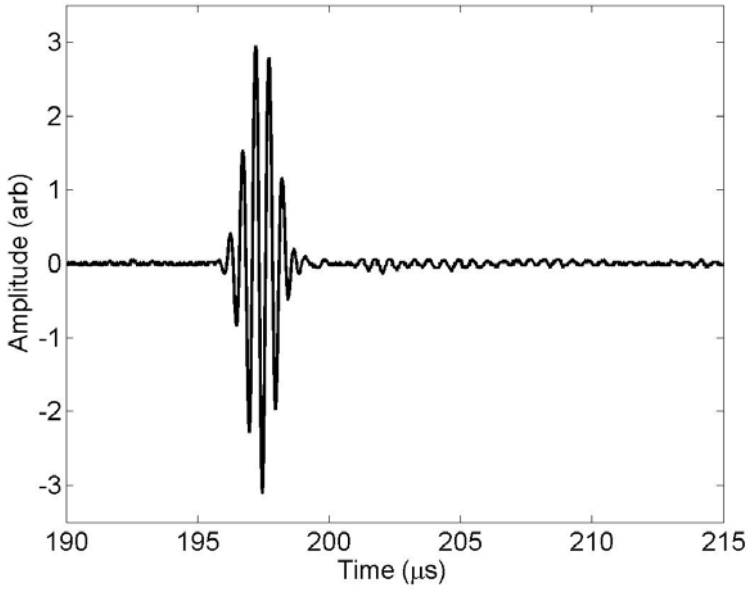

Figure 5.16: 2 MHz centre frequency SH* signal received in pulse echo mode from a standard shear transducer coupled to the end of a 15mm wide and 1mm thick stainless steel strip.

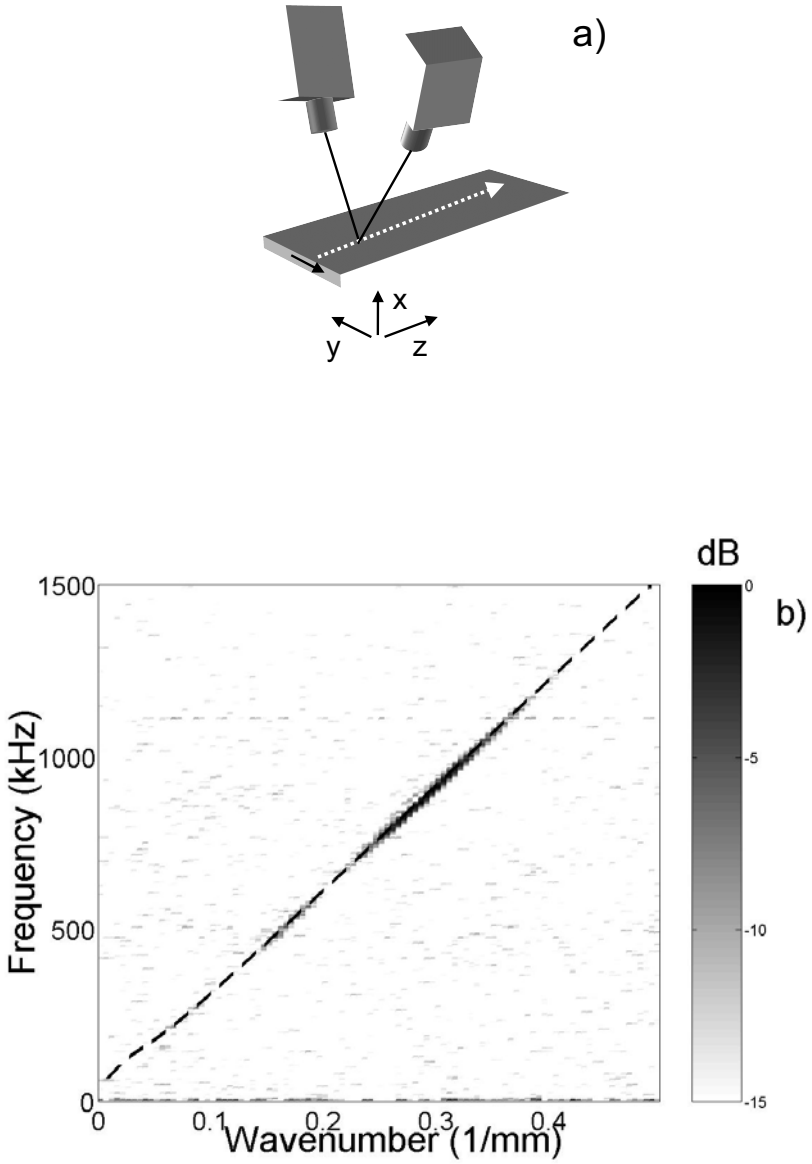

Figure 5.17: a) Sketch of the in-plane laser doppler vibrometer scanning configuration along the strip. b) Two dimensional fourier transform of in plane surface displacements (polarised in the width direction of the strip) along the centre line of 1mm thick and 30mm wide the steel strip. The dashed line (- - -) shows the predicted dispersion relation for the SH* mode of steel ($\rho = 7932kg/m^3$, $Cl = 6000$ m/s, $Cs = 3060$ m/s).

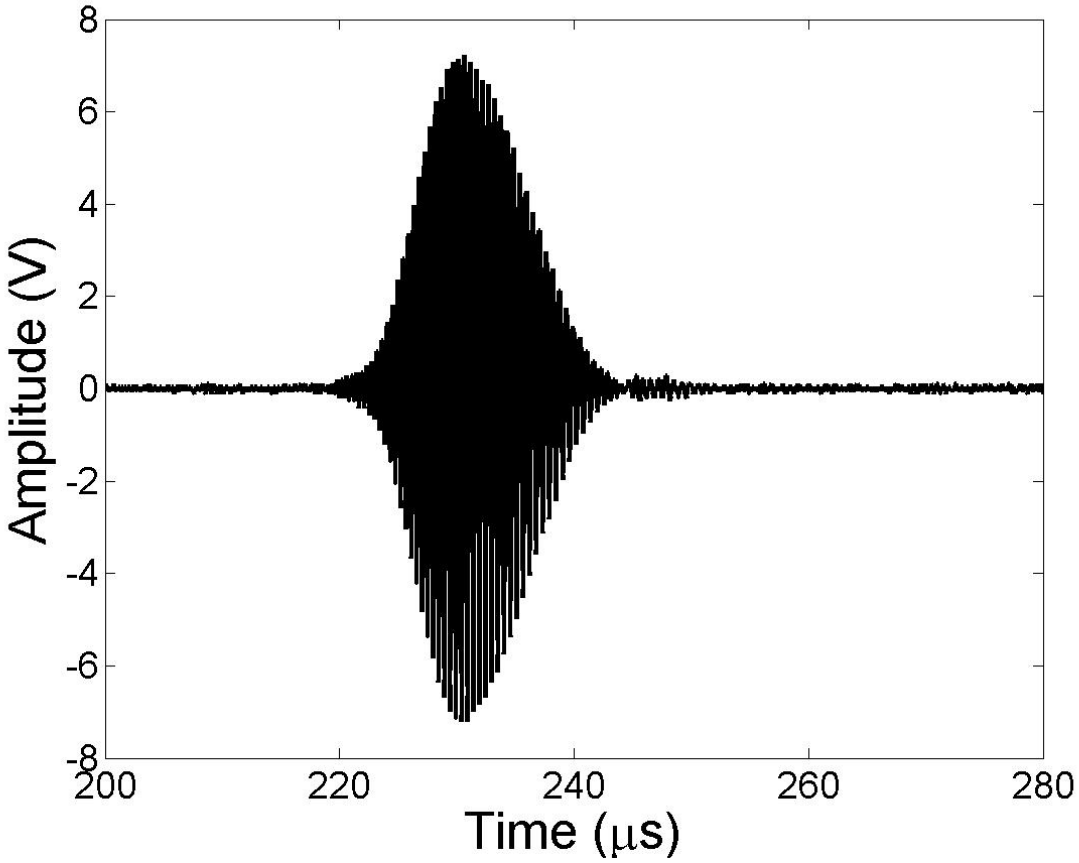

Figure 5.18: 10 cycle 2 MHz centre frequency $A0^*$ signal received in pulse echo mode from a standard shear transducer coupled to the end of a 30mm wide and 0.2mm thick stainless steel strip.

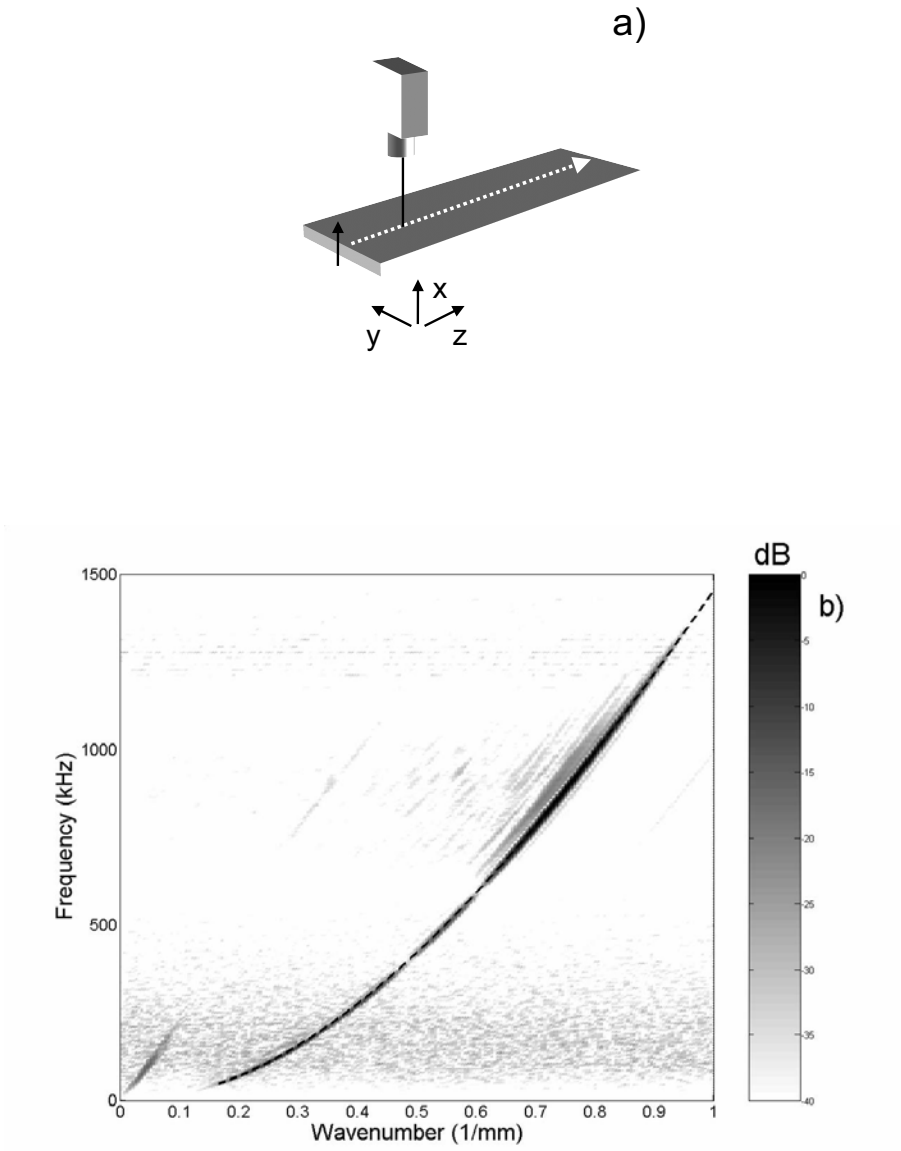

Figure 5.19: a) Sketch of the out-of-plane laser doppler vibrometer measurements on a strip. b) Two dimensional Fourier Transform of the out-of-plane displacements of the centre line of a 0.2mm thick and 30mm wide steel strip along the centre line of the strip. The dashed line (- - -) shows the predicted dispersion relation for the $A0^*$ mode of steel ($\rho = 7932kg/m^3$, $Cl = 6000$ m/s, $Cs = 2840$ m/s).

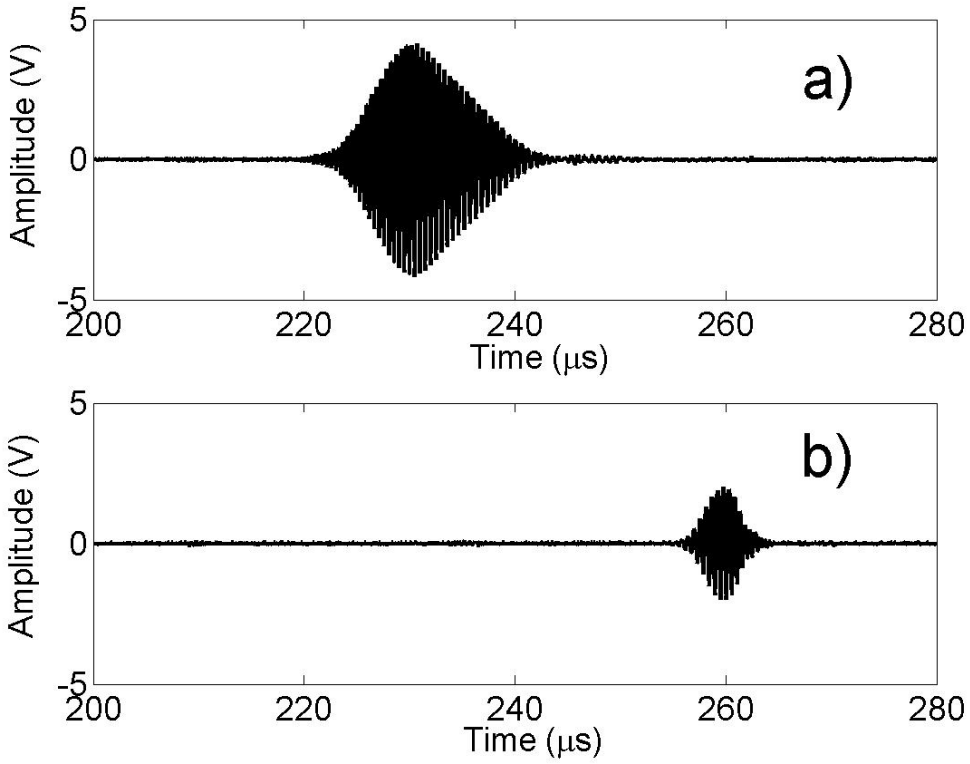

Figure 5.20: 2 MHz centre frequency signal received in pulse echo mode from a standard shear transducer coupled to the end of a 30mm wide and 0.2mm thick stainless steel strip a)just touching a water bath and b) immersed 70mm into a water bath.

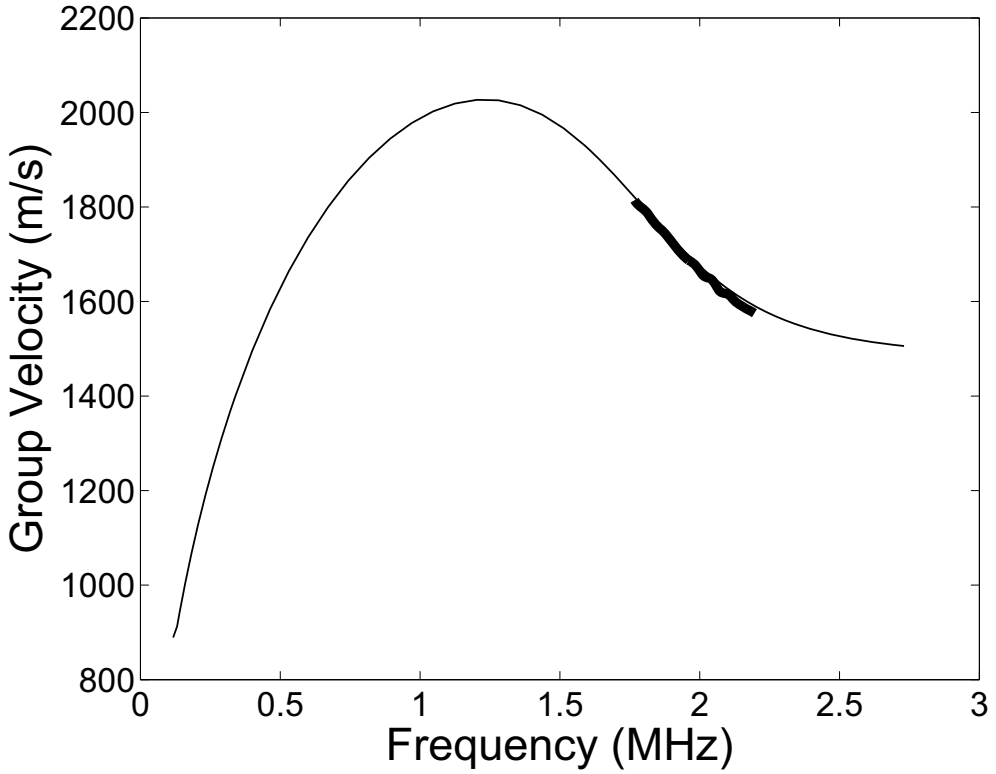

Figure 5.21: Group velocity for the quasi-Scholte mode of an infinite plate in water as predicted by DISPERSE (thin line) and measured group velocity of a thin stainless steel strip (0.2mm thick, 30mm wide and 300mm long) immersed in water (bold line).

Chapter 6

Waveguide sources on half spaces

In the previous chapter wave propagation along thin flexible waveguides was discussed. The objective was to find a waveguide geometry that allowed the transmission of a strong and undistorted signal over relatively long distances. The traditional approach of reducing the frequency thickness product of the waveguide and a new approach using a single shear horizontal mode at higher frequencies were identified as possible techniques.

Once the ultrasonic energy has been excited in the waveguide and a signal has been transmitted non dispersively along the waveguide up to the surface of the object that is to be interrogated, the ultrasonic signal has to enter the object. This is a completely new challenge and the junction of the waveguide and the structure has to be optimised to transmit a maximum of energy in the direction of interest within the structure without distorting the signal. Therefore the characteristics of waveguide sources on the structure has to be studied.

This chapter is dedicated to the investigation of waveguide source characteristics on half spaces of elastic material. Semi-infinite half spaces are used since the waveguide is believed to be thin and flexible, which implies that its thickness is small compared to the structure and even the wavelength of the wave. Once attached to the structure the waveguide will transmit stresses and displacements from its free

end (transducer location) to the surface of the structure. It is assumed that the strip has very low impedance compared to the half space and therefore does not restrain the surface of the half space. This conveniently makes it possible to uncouple the waveguide from the surface and simply consider a surface loaded by a distribution of forces.

Traditionally the solution to surface loading of a half space has attracted a great deal of interest and many publications can be found on this subject. However the subject is complex and many lengthy mathematical elaborations can be found in textbooks. Graff [17] and Achenbach [90] give excellent descriptions of the solution methods for sources on half spaces. A detailed study of the techniques is far beyond the scope of this chapter, therefore only the simplest solution for an anti-plane shear line source will be outlined. For other cases the solutions that were reported in the literature will be quoted and their significance with respect to the waveguide source will be discussed.

6.1 Strip sources on a half space

Figure 6.1 displays schematics of the different loading conditions for strip sources that were considered. The loads are constant across the strip so that in the limit of infinitely small thickness a perfect line source is obtained. The infinite strip source in this case represents a plate mode entering the half space from an infinitely wide plate. The mode amplitude is uniform across the width. Even though in real life the waveguide will be a finite strip and the mode amplitude will not necessarily be uniform across the width of the strip the line source is a good approximation because the aspect ratio of the strip is large and while the thickness will be of the order of a wavelength the strip will be many wavelengths wide. The different fundamental modes in a plate represent the various loading cases. The S0 mode will cause normal loading of the half space, the SH0 mode will cause anti-plane shear loading and the A0 mode will cause tangential shear loading. The S0 and SH0 modes are the most interesting since they can propagate with low dispersion in the waveguide leading to the source point on the half space.

The solution for normal or tangential in-plane loading of a strip source on a half space is much more complicated than anti-plane shear loading. Due to normal and tangential in-plane sources, a shear, a compressional and a Rayleigh surface wave are excited in the half space in order to satisfy the boundary condition imposed by the loads. The problem is also commonly known as 'Lamb's problem' since Lamb [91] was the first to present a solution. Graff [17] gives references to researchers who subsequently contributed to or extended the analysis.

The work by Miller and Pursey [92] is one of the most comprehensive and it is often quoted in the context of waves excited by surface loads. The expressions that they derived for the distribution of shear and compressional waves excited by different surface sources will be recalled. Surface waves will also be excited by the sources. However surface waves do not penetrate into the structure and thus become of limited use for structural investigations. Therefore this study was focused on the shear and compressional waves that spread into the half space. The case of tangential anti-plane shear loading of the half space will be considered first.

6.1.1 Tangential anti-plane loading

The analysis presented here follows that presented by Graff [17] and Achenbach [90] closely. Consider the half space displayed in figure 6.1a. The half space is defined by $y \geq 0$. Waves are generated by a distribution of harmonically oscillating loads represented by

$$\sigma_{yz}(x, 0, z, t) = \tau(x)e^{i\omega t} \tag{6.1}$$

$$\sigma_{yy}(x, 0, z, t) = \sigma_{yx}(x, 0, z, t) = 0. \tag{6.2}$$

The problem is uniform in the z-direction and therefore two dimensional. The shear tractions cause motion in the z direction only ($u_z = u_z(x, y, t)$), and the equations

of motion can be reduced to

$$\frac{\partial^2 u_z}{\partial x^2} + \frac{\partial^2 u_z}{\partial y^2} = \frac{1}{C_T^2}\frac{\partial^2 u_z}{\partial t^2} \tag{6.3}$$

where C_T is the shear wave velocity in the half space. By assuming harmonically oscillating displacements of the form

$$u_z(x, y, t) = u_z(x, y)e^{i\omega t} \tag{6.4}$$

and the identity $k_T = \frac{\omega}{C_T}$ equation 6.3 reduces to

$$\frac{\partial^2 u_z}{\partial x^2} + \frac{\partial^2 u_z}{\partial y^2} + k_T^2 u_z = 0. \tag{6.5}$$

The boundary condition due to the surface load can now also be expressed as

$$\mu\frac{\partial u_z}{\partial y} = \tau(x) \qquad \text{at y=0} \tag{6.6}$$

where μ is the shear modulus of the material. Using Fourier transformation (indicated by adding * to a variable) equation 6.5 can be rewritten in the form of an ordinary partial differential equation

$$\frac{\partial^2 u*_z}{\partial y^2} - (\xi^2 - k_T^2)u*_z = 0. \tag{6.7}$$

with solution

$$u*_z(\xi, y, \omega) = Ae^{-\gamma y} + Be^{\gamma y} \tag{6.8}$$

where

$$\gamma^2 = \xi^2 - k_T^2. \tag{6.9}$$

Using the transformed boundary condition from 6.6

$$\mu \frac{\partial u*_z}{\partial y} = \tau * (\xi) \qquad \text{at y=0.} \tag{6.10}$$

results in the solution in the Fourier domain

$$u *_z (\xi, y) = -\frac{\tau(\xi)}{\mu\gamma} e^{-\gamma y}. \tag{6.11}$$

All that remains is to invert the solution

$$u_z(x, y) = -\frac{1}{\mu 2\pi} \int_{-\infty}^{\infty} \frac{\tau * (\xi)}{\gamma} e^{-\gamma y} e^{-i\xi x} d\xi. \tag{6.12}$$

and insert the specific loading conditions in the integral. For a strip of uniformly applied loads as shown in figure 6.1a this is expressed by

$$\tau(x) = \begin{cases} \tau_0, & \text{for } \mid x \mid < a \\ 0, & \text{for } \mid x \mid > a \end{cases} \tag{6.13}$$

and in Fourier transformed form

$$\tau * (\xi) = \frac{2\tau_0}{2\pi} \frac{sin\xi a}{\xi a}. \tag{6.14}$$

therefore the solution for the anti-plane strip loading becomes

$$u_z(x, y) = -\frac{\tau_0}{\mu\pi} \int_{-\infty}^{\infty} \frac{sin\xi a}{\gamma\xi a} e^{-\gamma y} e^{-i\xi x} d\xi. \tag{6.15}$$

Equation 6.15 is the solution to the problem. However equation 6.15 is in form of an integral. The evaluation of this integral is usually the most challenging part of the analysis. Achenbach [90] shows a lengthy derivation for the special case of a line source, when the strip width '2a' tends to zero. The solution is transformed into polar coordinates and the final result becomes

$$u_z(x, y, \omega) = \frac{Pi}{2\mu} H_0^{(2)}(k_T r) \tag{6.16}$$

where r is the distance from the origin located at $x = y = 0$, P is the loading force, μ the shear modulus of the material and $H_0^2(x)$ is the Hankel function of the second kind.

Equation 6.16 shows that the displacement field is entirely dependent on the distance (radius) of a point in the half space from the source point, the field therefore spreads cylindrically into the half space. Figure 6.2 shows a contour plot of the magnitude of the displacement field computed using equation 6.16 for a SH line source on a half space.

6.1.2 Normal line source loading

Miller and Pursey [92] found an approximation for the displacements in the field far from a very thin strip source of thickness 2a. They separated the displacement fields into displacements due to compressional waves (U_R) and displacements due to shear waves (U_θ)

$$u_R \sim \frac{ae^{i(3/4\pi - R)}}{\mu}\sqrt{\frac{2}{\pi R}}\frac{cos\theta(k^2 - 2sin^2\theta)}{F_0(sin\theta)} \tag{6.17}$$

$$u_\theta \sim \frac{ae^{i(5/4\pi - kR)}}{\mu}\sqrt{\frac{2k^5}{\pi R}}\frac{sin2\theta\sqrt{k^2sin^2\theta - 1}}{F_0(ksin\theta)} \tag{6.18}$$

where

$$F_0(\xi) = (2\xi^2 - k^2)^2 - 4\xi^2(\xi^2 - 1)^{1/2}(\xi^2 - k^2)^{1/2} \tag{6.19}$$

and

$$k^2 = \frac{C_l^2}{C_s^2}. \tag{6.20}$$

In the above equation R is the distance (radius) from the origin (centre of the strip), θ is the angle from the normal (y direction) and μ is the shear modulus of the material. The normalised result of these functions for a steel half space is

plotted in figure 6.3. It can be seen that, as intuitively expected, the compressional waves are directed forwards into the half space. Two shear wave lobes are also sent into the semi infinite solid by the source. In this case the maximum amplitude of the excited shear waves is travelling approximately at 45° to the normal. This angle changes slightly depending on the material properties. Figure 6.3 does not give any indication of the relative amplitude of the shear waves compared to the compressional waves. Therefore in figure 6.4 both fields are shown in the correct amplitude ratio. Figure 6.4 leads to the conclusion that the normal line source excites shear waves more strongly than compressional waves.

6.1.3 Tangential line source loading

Miller and Pursey [92] also treated the case of a tangential line force on a half space. They found the following approximate solutions for the displacement fields

$$u_R \sim \frac{ae^{i(3/4\pi - R)}}{\mu}\sqrt{\frac{2}{\pi R}}\frac{sin2\theta(k^2 - sin^2\theta)}{F_0(sin\theta)} \tag{6.21}$$

$$u_\theta \sim \frac{ae^{i(3/4\pi - kR)}}{\mu}\sqrt{\frac{2k^7}{\pi R}}\frac{cos\theta cos2\theta}{F_0(ksin\theta)} \tag{6.22}$$

where F_0 and other variables are the same as in equations 6.17-6.20.

These functions were also plotted and are displayed in figure 6.5. Figure 6.6 shows the relative amplitudes of both shear and compressional waves. The shape of the lobes of excited waves are considerably different compared to the normal line source. Under tangential surface loading the compressional waves travel at a shallow angle ($\sim 30°$) into the half space, while shear waves penetrate into the half space in a generally normal direction to the surface with a strong peak at about 30° to the normal. The shear wave amplitude is considerably stronger than the compressional wave amplitude as shown in figure 6.6.

6.2 Circular sources on a half space

Line sources do not exist in practice even though they can be approximated reasonably well by a wide and thin strip. However rod waveguides that cause circular sources on a half space are easily available, which makes this geometry very attractive. Miller and Pursey [92] also investigated the source characteristics of small circular sources on a half space. They found the following expressions for the far field displacement characteristics of compressional and shear waves:

$$u_R \sim -\frac{a^2}{2\mu}\frac{e^{-iR}}{R}\frac{cos\theta(k^2 - 2sin^2\theta)}{F_0(sin\theta)} \tag{6.23}$$

$$u_\theta \sim \frac{ia^2k^3}{2\mu}\frac{e^{-ikR}}{R}\frac{sin2\theta(k^2sin^2\theta - 1)}{F_0(ksin\theta)} \tag{6.24}$$

where $0 \leq \theta < pi/2$, and the radius of the circular source is given by a.

Again the results of equations 6.23 and 6.24 were plotted and are displayed in figure 6.7; figure 6.8 displays the relative amplitudes. For a point source normal to the surface the excited shear wave is stronger than the compressional wave. The shear wave lobes enter the half space at a shallower angle than in the normal line source case and the lobes have a rounder shape. The shape of the compressional wave lobe remains almost the same as for the normal line source.

The final case that was considered by Miller and Pursey [92] was a circular torsional radiator on the surface of a half space. Again their analysis yielded an approximate expression for the displacement field excited by the torsional source

$$u_\theta \sim \frac{-ia^4}{8\mu}\frac{e^{-iR}}{R}sin\theta \tag{6.25}$$

For the torsional radiator no compressional waves are excited, which potentially removes some complexity in the excited signals. The excited displacement field is shown in figure 6.9. Shear waves are excited and travel in two lobes outward from the source. No waves are directed normally (along the y axis) into the half space. The shear wave amplitude grows with angle from the normal to reach a maximum

when the waves are travelling parallel to the surface.

In a second paper Miller and Pursey [93] investigated how much of the source energy from a normal point source is converted into each of the different wave types. Woods [94] summarised this information in the sketch shown in figure 6.10. Most of the source energy is transformed into a Rayleigh wave and stays trapped at the surface. Only 26% of the energy converts into shear waves that travel at an angle $\sim 45^\circ$ to the excitation (y) direction. Just 7% of the energy is converted into compressional waves that travel normal to the surface into the material (in the direction of the source and y axis). A normal point source is very efficient at creating surface disturbances but rather bad at exciting waves that penetrate into the material.

Miller and Pursey [93] further investigated the effect of the energy transfer of a combination of sources on the surface. They found that by augmenting the number of sources to three and distributing them in an equilateral triangle the amount of energy that is transferred into compressional waves ($\sim 31\%$) can be increased to come close to that of the shear wave energy ($\sim 43\%$) and even exceed the energy converted into a surface wave ($\sim 26\%$). But such sources become more complicated to create and if each of them were separate waveguides the interpretation of results would be complicated by crosstalk.

6.3 Choice of the most suitable waveguide source on a half space

In chapter 5 it was shown that several strategies can be successfully employed to achieve non-dispersive wave propagation along a waveguide. The geometry of the waveguide dictates which type of wave mode (shear/compressional/flexural) can successfully be excited and propagate non-dispersively in a certain range of frequencies. However the waveguide geometry also determines the source geometry unless the system is even further complicated by creating an adapter section that connects the waveguide to the object surface. The radiation patterns of bulk shear and

compressional waves due to line sources, strip sources and circular point sources show that for cases with normal loading, i.e. compressional waves incident from the waveguide, a dominating surface wave and strong shear waves at about $\sim 45°$ to the normal are excited. The fraction of energy excited as compressional waves is very low, $\sim 7\%$ for a circular point source. The geometry change from a circular point source to a line source does not show a great deal of improvement. Therefore a waveguide that transmits and receives compressional waves is not very efficient for thickness gauging of a structure from a remote location.

Circular torsional radiators on a half space show improvements compared to the normally loading sources since only shear waves are excited in the object. However the polar distribution of the excited shear waves is not ideal. Surface skimming shear waves are excited most strongly, while no waves at all are excited in the direction normal to the surface (y axis). Another problem is the reception quality of such torsional radiators. A shear wave that will be scattered back to the source area (junction of waveguide and object), will not be polarised to excite torsional waves in the waveguide. The polarisation of such waves would be more optimised to excite flexural waves, however these would not be effectively received by a torsional wave transducer at the end of the waveguide.

Line sources that cause normal tangential loading on a half-space show favorable source characteristics compared to normal line sources. Shear waves are excited strongly in a direction parallel to the waveguide axis. However surface waves and compressional waves at non-normal angles are also excited. This method was also ruled out because it would need a strongly dispersive flexural waveguide mode to act as a source. This would complicate the design of the excitation method.

It was found that a line or strip source exciting anti-plane shear motion showed the most desirable source characteristics. An anti-plane shear source solely excites shear horizontal waves in the half space. Surface waves or compressional waves are not excited. Also an ideal line source causes perfectly cylindrical spreading of wavefronts in the half space. This ensures that all areas of the half space are irradiated equally

strongly, preventing the creation of blind spots. In real life however the source will have the form of a strip of finite thickness and width.

A two dimensional Huygens model was used to approximate the field produced by the strip source in a plane of the half space. Huygens' principle states that every point on a wavefront acts as a source, emitting waves at velocity c. Using Huygens' principle the field of a transducer is approximated by superposition of the field of many point sources. The point sources are evenly distributed over the area of the transducer. The amplitude at any point in the field was calculated by:

$$A(x,y) = \sum_{1}^{Tn} \frac{e^{(ikD_{Tn}(x,y))}}{\sqrt{D_{Tn}(x,y)}} \tag{6.26}$$

where A is the field amplitude at point (x,y), k is the wavenumber of the wave, D_{Tn} is the distance to each individual point source on the transducer and Tn is an index for the different point sources that model the transducer. For more information on modelling transducers using Huygens' principle see for example Wilcox et al. [95].

Using the model it was verified that as long as the thickness of the strip was less than a wavelength and the width of the order of several wavelengths the cylindrical radiation pattern would not be significantly altered. The radiation from such a finite strip source rather resembles a barrel shape with cylindrical spreading in the thickness direction of the strip and a relatively clearly defined beam of the width of the strip in the width direction of the strip. Two dimensional radiation patterns in the thickness and width direction predicted by a 2D-Huygens model are shown in figure 6.11. The model assumes a monochromatic wave and excitation of only shear waves in the half space. This assumption is reasonable if edge effects are small and can be ignored. Even though the three dimensional field will be different, the two dimensional simulations are believed to give an idea of the shape of the field that is to be expected.

6.4 Wave reflection at the waveguide half space joint

The ideal configuration of the 'acoustic cable' allows it to be operated in pulse echo mode. Here a signal is sent along the waveguide, transforms into a bulk wave in the structure, interacts with features of the structure, returns to the waveguide/structure junction and is converted into the same waveguide mode to be finally picked up by the transducer again. Therefore it is necessary for the waveguide source to efficiently excite waves in the right direction. It also has to be ensured that most of the energy enters the structure, otherwise a very large entry reflection might mask the more interesting signals that return from the object to be investigated.

A finite element study was carried out to investigate the influence of the strip thickness on the size of the entry reflection. A three dimensional model of thin steel ($\rho = 7932kg/m^3$, $C_l = 6000m/s$ and $C_s = 3260m/s$) strips entering an infinite plate at normal angle was created. The plate was 6mm thick and the infinite direction was modelled by 3mm of real elements connected to infinite elements at the edges in order to extend the boundary to infinity. These infinite elements were also used at the edge of the strip and the block to extend the width of both to infinity. (The reader may rightly wonder why the model was not carried out in two dimensions if the width of the strip was made infinite; however a three dimensional model had to be used because the ABAQUS explicit finite element software does not model shear horizontal waves in two dimensions). A symmetry condition in the centre of the strip was used to reduce the model size. The mesh was made up of cubic elements of sizes between $1/8 - 1/10$ of the shear wavelength of the material at the centre frequency. Sketches of the side view, top view as well as a three dimensional view of the model are shown in figure 6.12. The mesh and the infinite element boundaries that were used for the analysis are also shown in the figure.

The ABAQUS finite element software was used. A time marching explicit solver that automatically determines the time step was chosen and a uniform anti-plane shear load was applied across the strips end section. Temporally a 5 cycle Hanning

windowed toneburst at 2 MHz centre frequency was applied. Signals were monitored at a point in the centre of the strip at the excitation location, see figure 6.12. The analysis resulted in time traces such as the one shown in figure 6.13.

The reflection coefficient was determined from the results for strips of thicknesses $0.25 - 1.5$mm. The incoming signal was isolated and the entry reflection signal was isolated. The Fourier transforms of both signals were obtained and the reflection coefficient was defined as ratio of the amplitude of the signal reflected by the junction and the incoming signal at the centre frequency (2MHz)

$$C_{Entry} = \frac{A_{reflected}}{A_{incoming}}. \tag{6.27}$$

Figure 6.14 shows the reflection coefficients obtained for different thicknesses of strips. The figure clearly shows that the thinner the strip is the more energy is reflected. (This result is in agreement with results reported by Vogt [36] for the entry reflection of the L$(0,1)$ mode of a thin wire embedded in curing adhesives like epoxy.) The thicker the strip becomes the more energy is transferred into the half-space and the more collimated its beam becomes. Once the thickness of the source exceeds a bulk wavelength in the material side lobes will appear in the field excited by the source; this is believed to be undesirable since it limits the field of view. For the current operational frequency of 2 MHz the shear wavelength of steel is approximately 1.5mm. Therefore a waveguide strip of thickness of about 1mm will still show good performance without any local minima (blind spots in the field of view) in the beam pattern .

6.5 Summary

In this chapter the source characteristics of different waveguide sources on a half space were considered. The waveguide was considered to transmit a distribution of loads to the surface of the object, which is modelled as a half space since it is assumed to be much larger than the thin and flexible waveguide. This allowed the analysis of the strip and object to be uncoupled so that the forcing from the strip

was simply modelled as distribution of loads on a half space. The subject has been thoroughly treated in the literature. Work presented in text books such as Graff [17] and excellent papers on different sources on infinite elastic solids by Miller and Pursey [92], [93] was recalled and its consequences for the purpose of remote waveguide excitation and reception were considered.

It was found that a source of anti-plane shear on a half space was most suited to the application. Other sources, especially those with normal loading, have the disadvantage of sending a very strong surface wave, a strong shear wave and a very weak compressional wave at different angles into the structure. For torsional sources the excitation of shear waves alone is possible, however reception would have to occur in the form of flexural modes which are not well suited for transmission along the waveguide. For the same reason tangential shear sources on the half space were ruled out.

The selected anti-plane shear source had the advantage of only exciting shear horizontal waves in the half space. The waves also spread cylindrically into the object under investigation which maximises the field of view. The entry reflection is minimised when the strip thickness is large, however in order to ensure reasonably cylindrical spreading of the wave in the half space the waveguide thickness has to stay below the wavelength of a shear bulk wave.

6.6 Figures

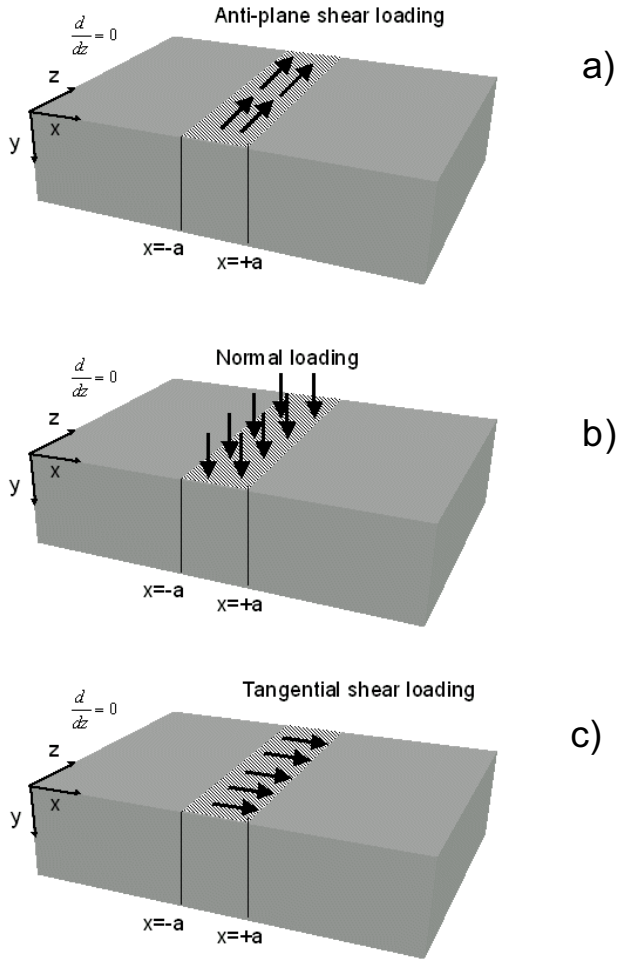

Figure 6.1: Schematics of the different line source (2D) loading conditions that were considered a) anti-plane shear loading b) normal loading c) tangential shear loading. The sources are infinitely long in the z direction and have a finite width in the x direction (from -a to a).

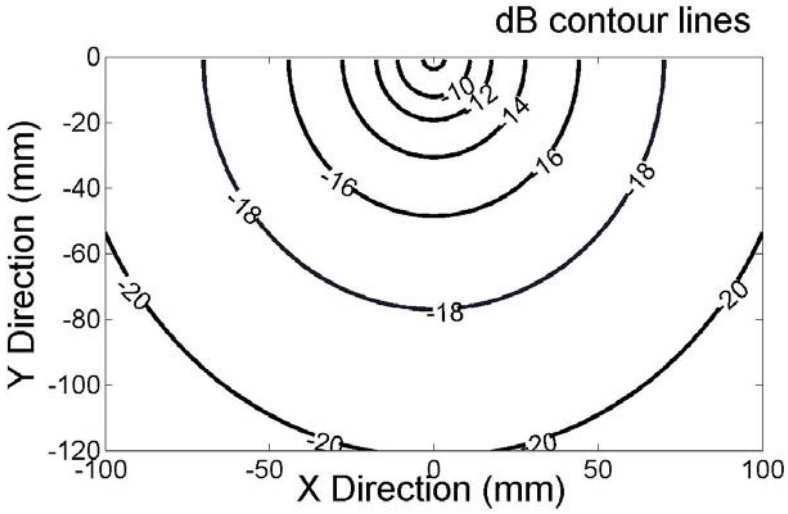

Figure 6.2: Contour plot of the u_z displacement field magnitude for a SH-line source on a half space of steel.

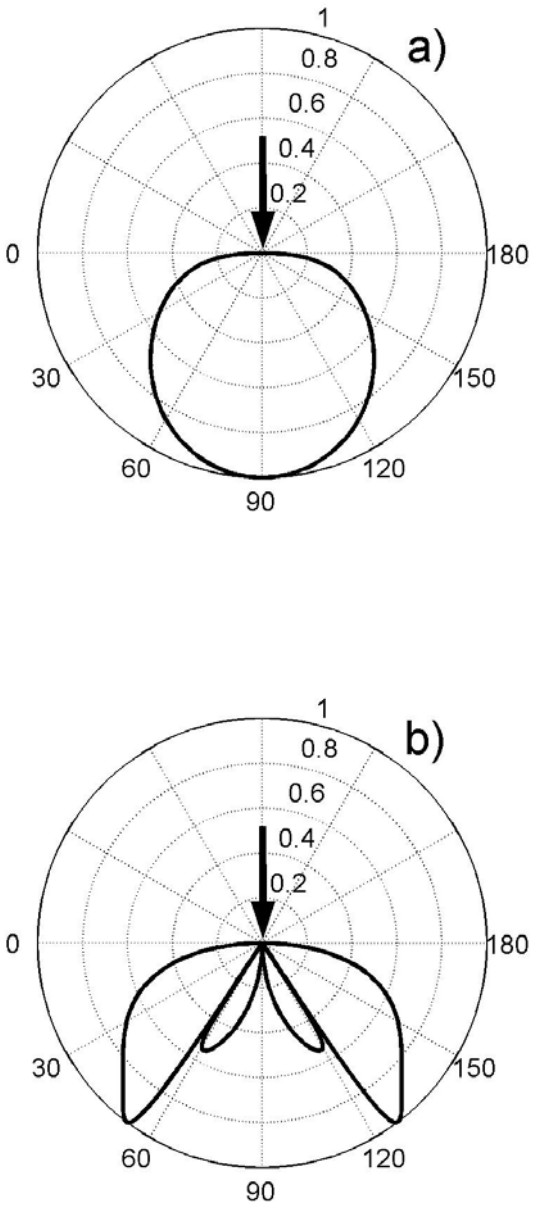

Figure 6.3: Angular distribution of the magnitude of the displacement for a) compressional waves b) shear waves excited by a normal line source on a steel ($C_L = 6000$m/s, $C_s = 3260$m/s) half space.

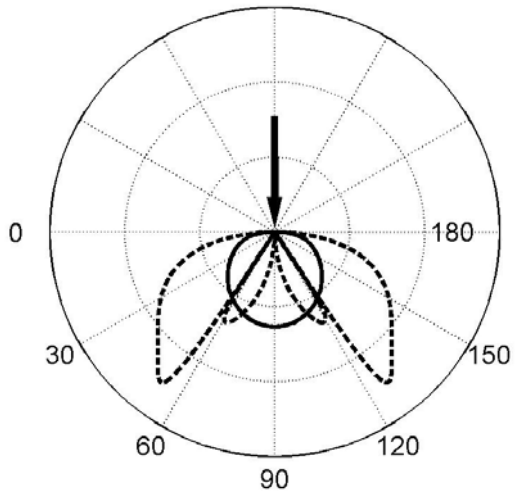

Figure 6.4: Displacement fields for the shear (- - -) and compressional (—) waves excited by a normal line source with correct relative amplitude ratios.

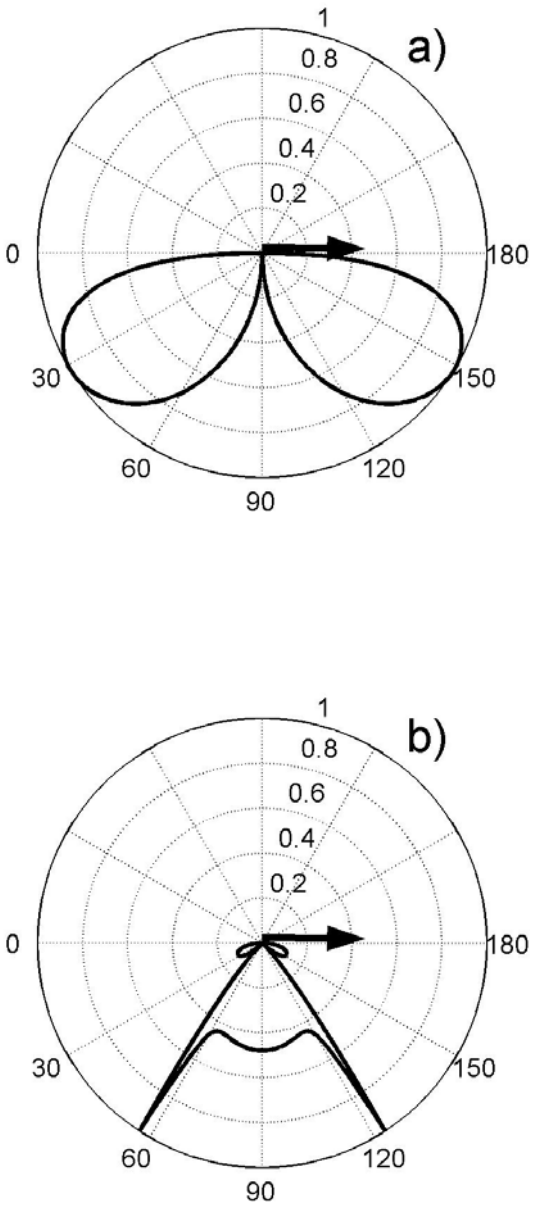

Figure 6.5: Angular distribution of the magnitude of the displacement for a) compressional waves b) shear waves excited by a tangential shear line source on a steel ($C_L = 6000$m/s, $C_s = 3260$m/s) half space.

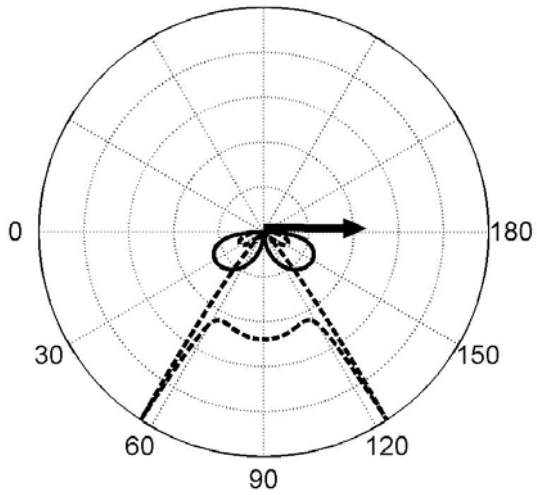

Figure 6.6: Displacement fields for the shear (- - -) and compressional (—) waves excited by a tangential shear line source with correct relative amplitude ratios.

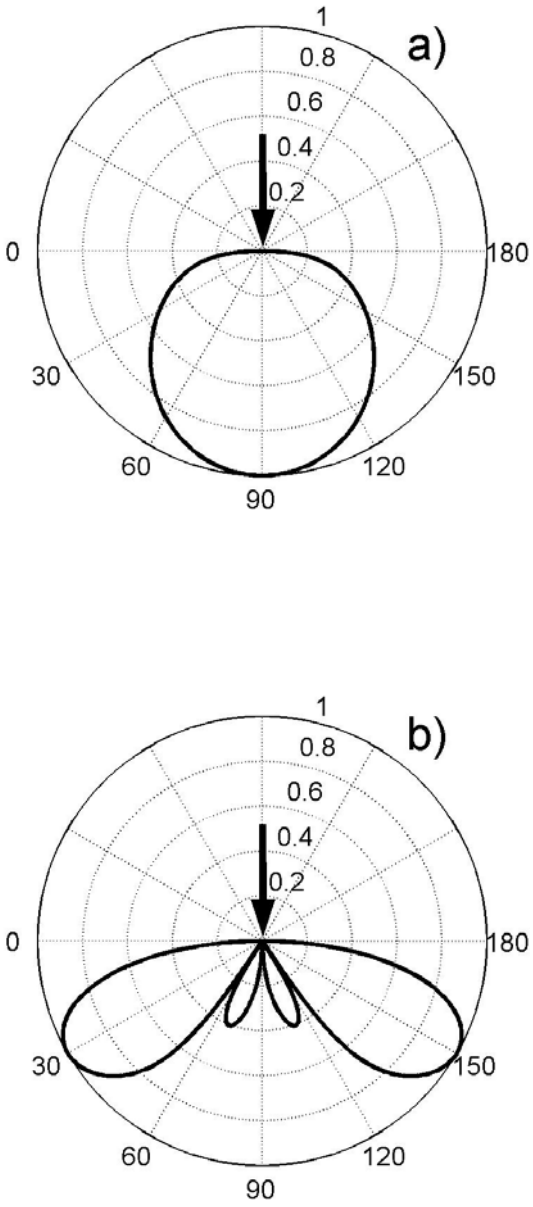

Figure 6.7: Axisymmetric angular distribution of the magnitude of the displacement for a) compressional waves b) shear waves excited by a normal circular point source on a steel ($C_L = 6000$m/s, $C_s = 3260$m/s) half space.

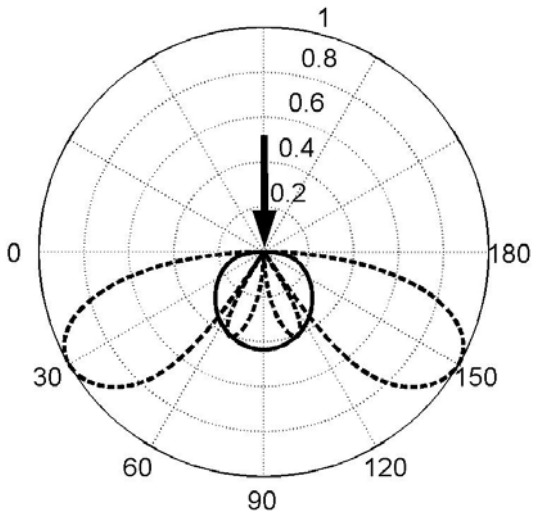

Figure 6.8: Axisymmetric displacement fields for the shear (- - -) and compressional (—) waves excited by a normal point source with correct relative amplitude ratios.

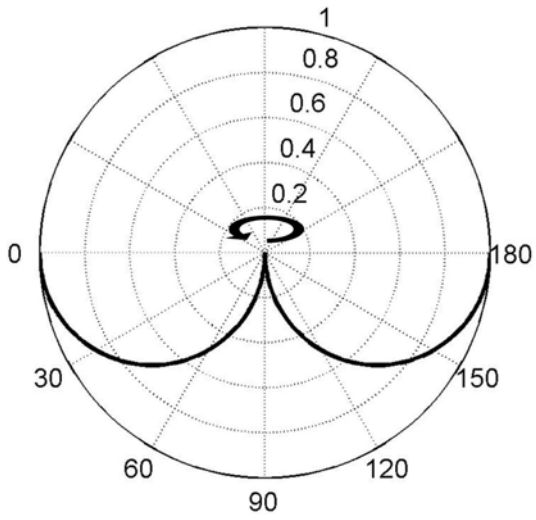

Figure 6.9: Axisymmetric displacement fields for the shear (—) waves excited by a circular torsional source on a steel ($C_L = 6000$m/s, $C_s = 3260$m/s) half space.

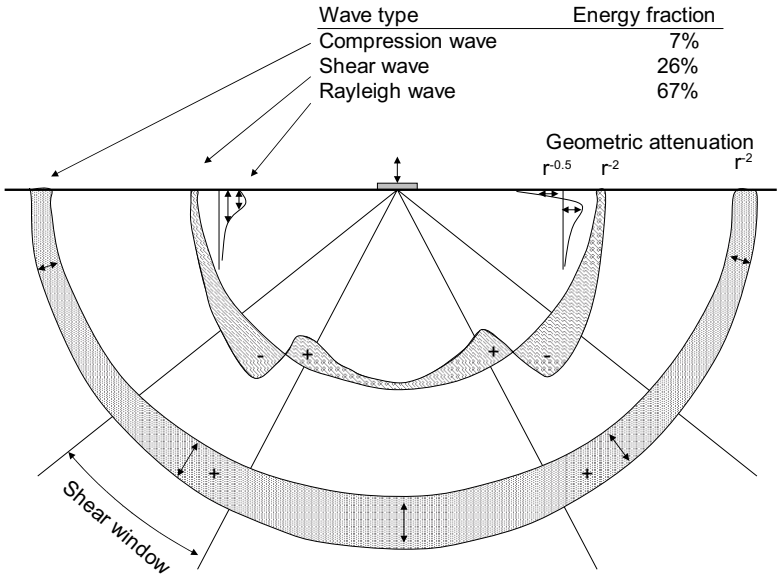

Figure 6.10: Sketch of the different wave types excited by a normal point force on a half space and their share of the total excitation energy. (After Woods [94] , for Poisson's ratio $\sim 1/4$)

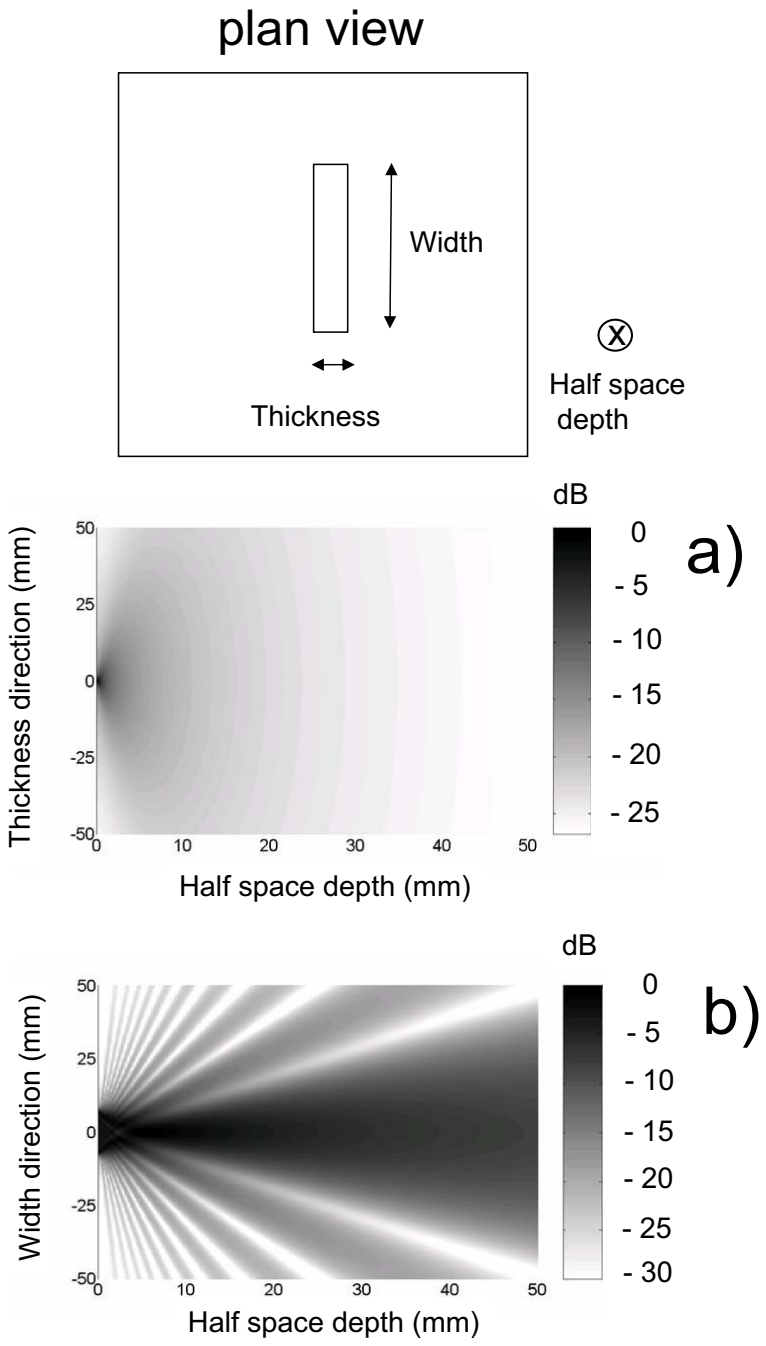

Figure 6.11: Two dimensional Huygens models of a) a 1mm source and b) a 15mm source in a plane. The sources are modelled by 21 point sources distributed evenly along the transducer line. The wavelength is 1.5mm which approximately corresponds to a 2MHz shear wave in steel.

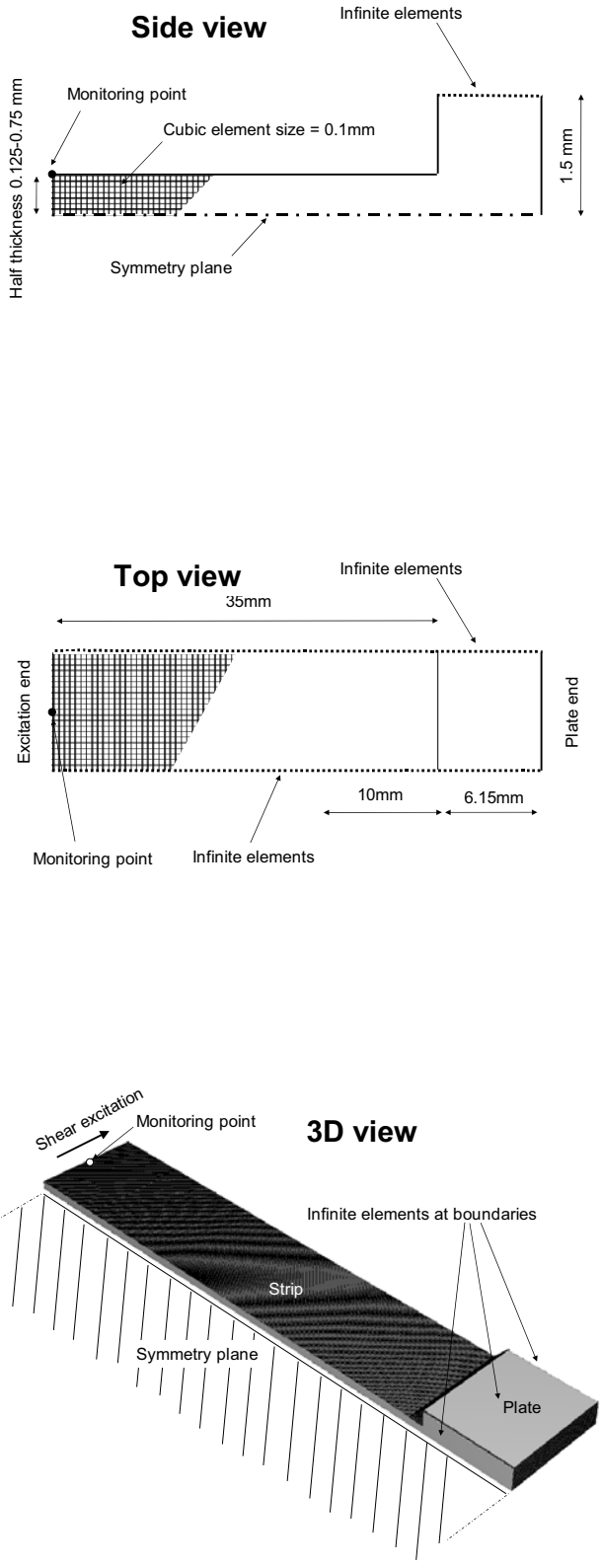

Figure 6.12: Schematic of the finite element mesh used to analyse the reflection coefficient of a shear horizontal wave in a waveguide entering a half space of the same material (steel).

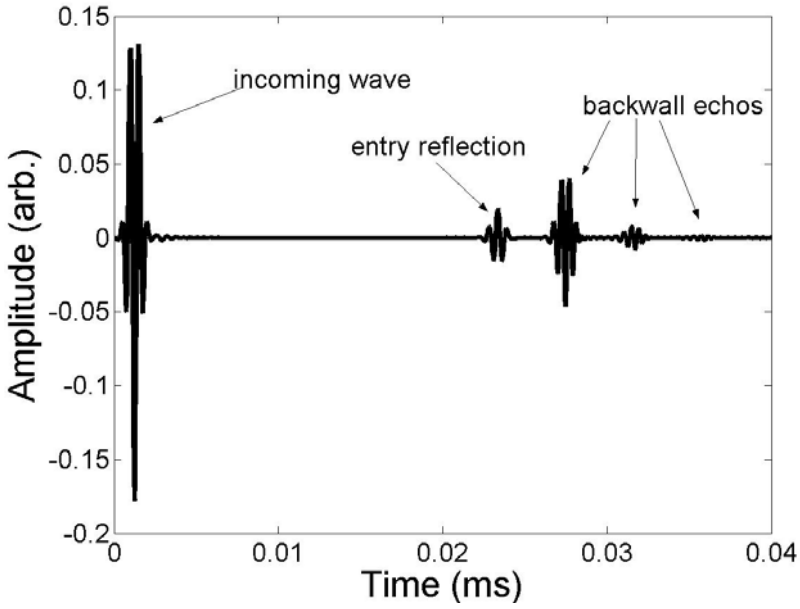

Figure 6.13: Timetrace obtained from the finite element (ABAQUS) analysis of the model in figure 6.12 of a 1mm thick strip in which a 5 cycle 2MHz shear horizontal wave enters a steel half space.

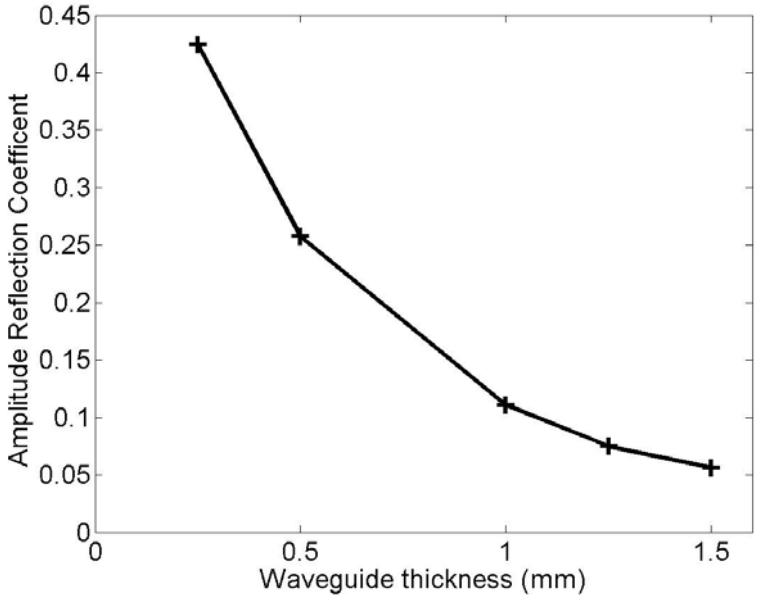

Figure 6.14: SH-wave reflection coefficient for different waveguide thicknesses at the junction to a half space. Results were obtained using the ABAQUS finite element modelling software.

Chapter 7

Remote thickness gauging using a waveguide

7.1 The waveguide-structure joint

The outcome of chapter 6 showed that theoretically a shear horizontal line source is best suited for exciting waves in an object that is to be investigated. Simulations showed that a perfect joint between the waveguide and a plate of the same material ensured that most of the energy was transmitted from the waveguide into the object (see section 6.4).

In practice the position of attachment of the waveguide is rarely known prior to the installation of the structure; the waveguide is added later for monitoring applications. Therefore the waveguide will have to be attached to the structure in some way. Permanent attachment is possible by bonding, welding, brazing, soldering or other methods. Detachable attachment methods like clamping can also be envisaged. The permanent attachment methods are potentially preferable because they optimise ultrasonic coupling between both parts while clamped contact will cause high losses even if a coupling agent is used. However defects in the bonding method and alterations that it causes to the joint geometry might adversely affect the wave propagation through the junction. Also the use of standard coupling agents will not

be possible at elevated temperatures. The different joining techniques were investigated experimentally.

7.2 Experimental setups for thickness gauging

It was decided to set up a thickness gauging experiment to test the different joining methods on specimens of the same thickness. The stainless steel strip geometry (1mm thick, 15mm wide and 300mm long) and thickness of the steel plate specimen (6mm) were kept constant while only the joining method was altered. The experiments were carried out in the pulse echo and pitch catch modes. Measurements in the pulse echo mode would be the preferred embodiment since only one waveguide is needed to send and receive the signal. Figure 7.1 illustrates the different test configurations.

Excitation of the SH* mode in the stainless steel strip was achieved in the same way as in chapter 5. A 5 cycle 2MHz Hanning windowed toneburst was sent and received by a standard ultrasonic shear transducer (Panametrics). The 13mm diameter shear transducer was clamped to the waveguide end with treacle as a shear couplant. It was ensured that the polarisation direction of the transducer was parallel to the width of the strip. The clamp design was optimised to minimise its effect on the mode propagating in the strip. The SH* mode energy is concentrated at the centre of the strip (see section 5.4.1) and it is therefore not strongly influenced by attachments to the edges. This arrangement was used to attach two blocks to either side of the strip. The blocks sandwiched the edges of the strip and bolts were used to tightly push the blocks onto the strip in order to strongly grip onto the edges of the strip. A back plate was then bolted to the four blocks that were just clamped to the strip. In between the back plate and the strip end a transducer was inserted and thus clamped against the end of the strip. Figure 7.2 illustrates the transducer clamp.

7.2.1 Coupling with coupling agent

The pulse echo mode experiment with treacle as coupling agent is the simplest: once the surface of the plate had been evenly covered with treacle the strip was manually pushed onto the surface at right angles. Signals were collected and are displayed in figure 7.3.

Figure 7.3 shows a pulse echo signal when the strip is not in contact with the plate and a signal when strip and plate are in contact. The signal when both pieces are coupled is slightly less strong. However there are no additional echoes from within the plate specimen, which leads to the conclusion that not enough energy is sent and received through the shear-couplant joint to enable inspection of the plate specimen in the pulse echo mode.

After the negative results of the pulse echo mode experiments, experiments in the pitch catch mode (see figure 7.1 II a) were performed. Two strip waveguides were fixed together so that they were roughly parallel and separated by a gap of 1mm at the remote end with respect to the transducer. The assembly was then manually put in contact with the plate specimen. A signal was sent from one waveguide and received on the other strip. Signals were collected and are displayed in figure 7.4.

For the pitch catch mode good results were obtained as shown in figure 7.4. The signals are much weaker ($\sim$ 30dB) than the control signal (unattached pulse echo signal of the sending strip), however the backwall echoes from the plate specimen are clearly visible. The better but weaker signals are achieved because only the signals that were transmitted from the sending waveguide into the plate are picked up by the receiving waveguide. In the pulse echo mode these weaker signals were completely masked by coherent noise from waveguide modes that were either excited by the transducer or caused by mode conversion at the junction of the strip and the plate.

The first arrival in figure 7.4b is a shear horizontal wave that was excited on the surface of the plate and travelled across the 1mm gap directly into the receiving strip. Later arrivals are echoes that have travelled to the backwall, were reflected and then reached the receiving waveguide or completed further reflections between the top and bottom surface of the plate before reaching the strip receiver. Figure 7.5 shows the different paths that the SH wave travels in the plate specimen. The time delay between different echoes can be used to evaluate the thickness of the material if the shear velocity is known (or the shear velocity if the thickness is known).

7.2.2 Welded and soldered strips

Finite element simulations (see section 6.4) predicted good functioning of a T-junction between the waveguide strip and the plate specimen. The most intuitive practical implementation of joining the two parts was by means of welding. Tungsten inert gas (TIG) welding was initially used to attach the strip to the plate. Due to the thinness of the strip and the relatively large plate dimensions the welding is very difficult. Problems that were encountered were burning through the steel strip, material burn off at the edges of the strip and excessive build up of flash along the joint. Despite these difficulties a welded sample was produced.

Silver soldering was identified as another possible joining method. The silver solder has a lower melting point ($\sim$ 1000°C) than the steel and therefore problems like burning off or burning through the steel strip can be avoided. It is also known that the solder material fills gaps very effectively which limits the formation of defects within the joint. Six samples with silver solder joints were also produced.

A pulse echo measurement on a welded sample is shown in figure 7.6. The returning signal amplitude is reduced compared to an unattached strip and many more wave packet arrivals interfere. Noticeably the strongest arrival occurs at the same time as the end reflection in an unattached strip, therefore it is believed to be the reflection from the interface. A signal arrival prior to the interface reflection can also be recog-

nised. This signal is believed to be due to flash and defects on the strip waveguide that are located in front of the junction with respect to the transducer. Another strong arrival occurs about 4μs after the interface reflection and could reasonably be attributed to the backwall of the plate. However the signal contains very strong coherent noise ($\sim$ 6dB below the maximum amplitude) which makes the attribution of features in the signal very difficult and unreliable. The excessive noise level is believed to be caused by defects, geometry changes and imperfection introduced during the welding process.

The silver soldered strips were then investigated. Figure 7.7 displays the time traces collected from the six samples. On examination of figure 7.7 one first notices that all samples show distinctly different signals. By comparison with the control signal from an unattached strip of the same dimensions a strong but very differently shaped entry reflection from the waveguide-plate interface can be identified in each sample. Smaller amplitude signals preceding the entry reflection can also be noticed: after soldering the joint was cleaned by grinding and filing during which the waveguide close to the joint could have become damaged by momentary contact with tools. Strong but very late arrivals at around 215μs are believed to be due to the finite plate dimensions (50 by 50 mm). These signals are very complicated and thus merely indicate that energy transmission from the waveguide into the plate is strong.

Even though the $SS1$ sample showed a reasonable result it was concluded that welding or soldering are unsuitable attachment processes for the waveguide. The large variation in outcome between samples that were prepared in the same fashion is unacceptable for the construction of a reliable NDT device.

7.2.3 Clamped contact

A clamp had to be designed for the attachment of the strip or strips to the plate specimen. Theoretically a clamp similar to the transducer clamp (see figure 7.2) could have been employed for the coupling of a single waveguide in pulse echo

mode. However with the need for pitch catch experiments in mind a new clamp was developed. Two 1mm deep, parallel channels separated by a 1mm gap were cut into two blocks. The strips were slotted into the channels, which allowed the strips to be rigidly locked into position by pulling the two blocks together using bolts. Slots were cut into the bottom of the clamping blocks to allow them to be bolted onto the specimen plate. Figure 7.8 shows a top and front view of the clamping arrangement.

The clamp was attached to the plate specimen and pulse echo and pitch catch time traces were recorded. Figure 7.9 shows the results. It was seen that the pitch catch signal is about 30 dB weaker than the pulse echo signal. In the pulse echo mode, signals that were transmitted into the plate specimen and returned into the waveguide are too weak to surpass the coherent noise levels within the waveguide. However good results were obtained in the pitch catch mode. The results of the clamped waveguides in the pitch catch mode were comparable to those of the manual coupling with shear couplant which were shown in figure 7.4b.

7.3 Room temperature thickness gauging with shear couplant

In the previous section it was shown that pitch catch mode experiments are successful when the waveguides are clamped to the structure or if shear couplant is used at the interface. Here results of thickness measurements on a calibration block using a shear coupling agent are presented. The use of coupling agent rather than clamping was chosen simply for reasons of easy implementation. The calibration block was made of steel. It contained 6 steps in thickness. A sketch of the block is shown in figure 7.10.

Time traces recorded by the SH* mode waveguide system are displayed in figure 7.11. The first arrival stays constant for all block thicknesses while the second and later arrivals are delayed in proportion to the thickness of the block. This is ex-

pected since the first signal corresponds to the signal travelling from the sending waveguide along the surface of the block to the receiving waveguide. Therefore the first signal is independent of the thickness of the block. Later arrivals are echoes from the other side of the block and therefore depend on the block thickness.

From the peak of the envelope of the signal the time difference between the second and third arrival was determined and then used to calculate the thickness of the specimen. The necessary bulk shear velocity was determined by a reference measurement on the largest thickness of the block. Figure 7.12 shows thicknesses evaluated by the SH* mode measurement plotted against the thicknesses determined by means of a caliper. The two measurements agree within 0.1mm (standard error). Differences are mainly believed to be due to different thicknesses of the coupling layer. It is believed that measurements using the clamping configuration are more accurate.

7.4 High temperature measurements

In the previous sections it was shown that the SH* mode waveguide successfully measures thicknesses at room temperature if used in the pitch catch mode. The technique was ready to be tested at high temperatures. Since joining the strip to the specimen by welding did not show good results, a clamping configuration was seen as the only possible method of attachment; standard coupling agent cannot withstand the high temperatures.

Two 1mm thick, 15mm wide and 500mm long stainless steel waveguides were clamped to a 6mm thick stainless steel plate. For temperature measurements a thermocouple was welded onto the steel plate at a location that was unlikely to influence wave propagation. The specimen was then placed in a furnace. A hole at the bottom of the furnace allowed the waveguide strips to reach outside the furnace creating a clearance distance of at least 350mm between the oven and the transducer location.

According to the predictions in figure 5.1 this clearance distance should be ample to allow for the temperature to drop from the furnace temperature at the specimen end of the waveguide to room temperature at the transducer end of the waveguide. When the furnace was heated to $500 - 600°C$ no increase in temperature at the transducer end could be detected.

During heating the temperature and ultrasonic signals were acquired by a PC. The temperature was logged every minute using a thermocouple logger (TC08) and the Picolog software (both from Pico Technologies Ltd.). Ultrasonic signals were acquired using the desktop ultrasonic instrument (DUI) which is a combined arbitrary function generator and oscilloscope system produced by NDT Solutions Ltd. Signals were automatically recorded every 3 minutes during heating and every 5 minutes while cooling.

Figure 7.13 displays signals acquired during a typical heating cycle and a corresponding temperature curve is also shown. The arrival of the group of signals is delayed at higher temperatures due to the reduction of shear velocity in the waveguide at high temperatures. An increase in the separation between backwall echoes can also be identified, however because the propagation path in the plate is very much shorter compared to the path in the waveguide this effect is more subtle. Signal amplitudes seem to remain strong suggesting that there is no drastic change in attenuation at high temperatures.

The experiment was cycled several times and the recorded time traces were then used to evaluate the shear velocity in the plate specimen. The Hilbert envelope was used to evaluate the arrival time of a signal packet. Knowing the thickness of the plate specimen this allowed the shear velocity of the plate to be calculated. A graph that displays the measured shear velocity from two heating and two cooling cycles is shown in figure 7.14. The velocity scale in the figure is very detailed which might misleadingly suggest that the results are very scattered. However the range of the velocity measured during different cycles at the same temperature is about 50m/s which corresponds to $\pm 0.8\%$ of the overall velocity. There is a linear decrease

in velocity from $\sim$ 3100m/s at room temperature to $\sim$ 2750m/s at 600°C, which represents about 10% of the overall velocity.

In the above calculation the thermal expansion of the material in the furnace and the corresponding thickness change has been neglected. For stainless steel Kaye and Laby [62] quote an expansion coefficient of $19.7 * 10^{-6}$/K at a temperature of 500°C. Below this temperature the expansion coefficient is slightly less and above slightly higher. Using a round figure of $20 * 10^{-6}$/K for the whole 600°C the expected thickness change due to heating is about 1.2%. Therefore the path that the ultrasonic wave travels and the evaluated velocity is also expected to change by $\sim$ 1.2%. Compared to the measured 10% decrease in velocity the change in thickness and velocity due to thermal expansion of $\sim$ 1.2% is therefore believed to be negligible.

The furnace was kept running at a temperature of 500°C for a period of four weeks to demonstrate the long-term stability of the monitoring system. The temperature was monitored every hour to ensure continuity, and temperature and ultrasonic sample traces were recorded every 12 hours. The first and the last collected time traces are shown in figure 7.15. Signal amplitudes increased with time and better signals were achieved after long periods at high temperature. This is believed to be due to changes that occur at the waveguide/specimen junction. High clamping pressures and the increased temperature seem to improve ultrasonic shear wave transmission through the joint which leads to the conclusion that long term monitoring at high temperatures is possible.

7.5 Summary

In the previous sections the attachment of a strip waveguide to a plate specimen was investigated in order to find a joining method that allows clean transmission and reception of the SH* mode into and from the plate. Manual coupling with shear coupling agent, permanent attachment methods like welding or soldering and

attachment via a clamp were tested in the pulse echo and pitch catch modes.

The pulse echo mode was found to be unsuitable for manual coupling with shear couplant and the different clamping configurations because not enough energy was transmitted through the imperfect junction of the waveguide and the specimen. For the permanently attached strip waveguides it was observed that enough energy could be transmitted and received through the joint, however the geometrical imperfections and defects introduced by the welding and soldering processes caused severe distortion of the received signal shape. Partial reflections, reverberations and mode conversions in and at the joint made the returning signal uninterpretable. Since these effects would also be encountered in the pitch catch mode a permanent waveguide attachment by welding or soldering was ruled out.

Experiments with clamping and coupling by shear couplant in the pitch catch configuration proved to be successful. It was shown that different thicknesses of specimens could easily be evaluated. Furthermore the waveguide specimen assembly was successfully tested in a furnace at temperatures between $500-600°C$ and could be used to evaluate the thickness of the sample or alternatively monitor its shear velocity. Experiments during different heat cycles showed that the clamping configuration ensured good ultrasonic contact over a wide range of temperatures and for a long time. The longest test time over which the sample stayed at over 500°C continuously was four weeks. Signal clarity and amplitude was noticed to improve over the long test time, this was believed to be due to favorable changes that occur at the interface between waveguide and specimen under the influence of pressure and temperature.

7.6 Figures

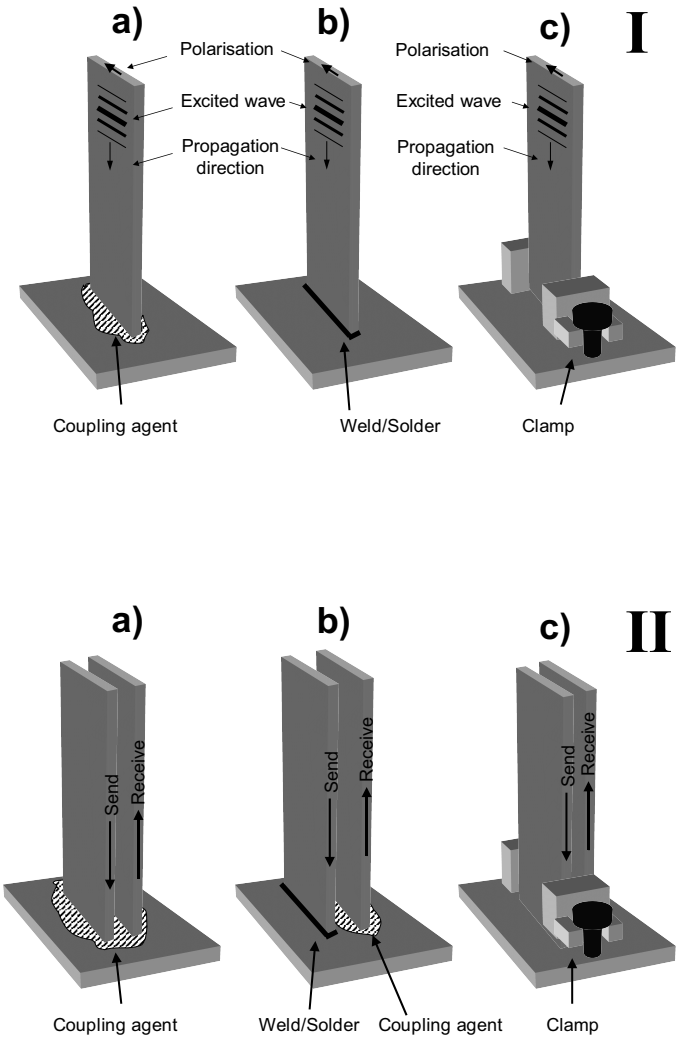

Figure 7.1: Schematics of the thickness gauging test configurations in pulse echo (I) or pitch catch (II) mode for the different joining methods: a) shear coupling by coupling agent b) welding or soldering c) clamping by means of a purpose made clamp.

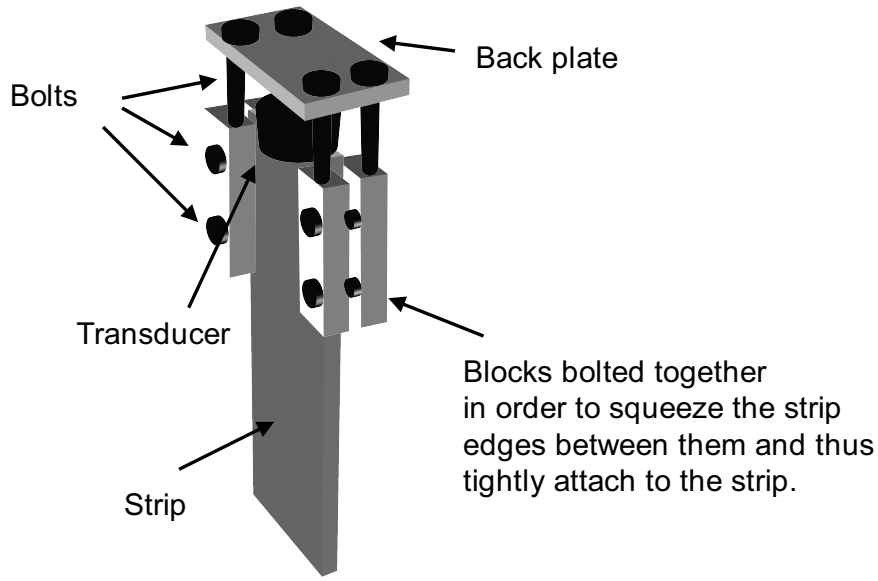

Figure 7.2: Sketch of the attachment configuration of a transducer to a strip.

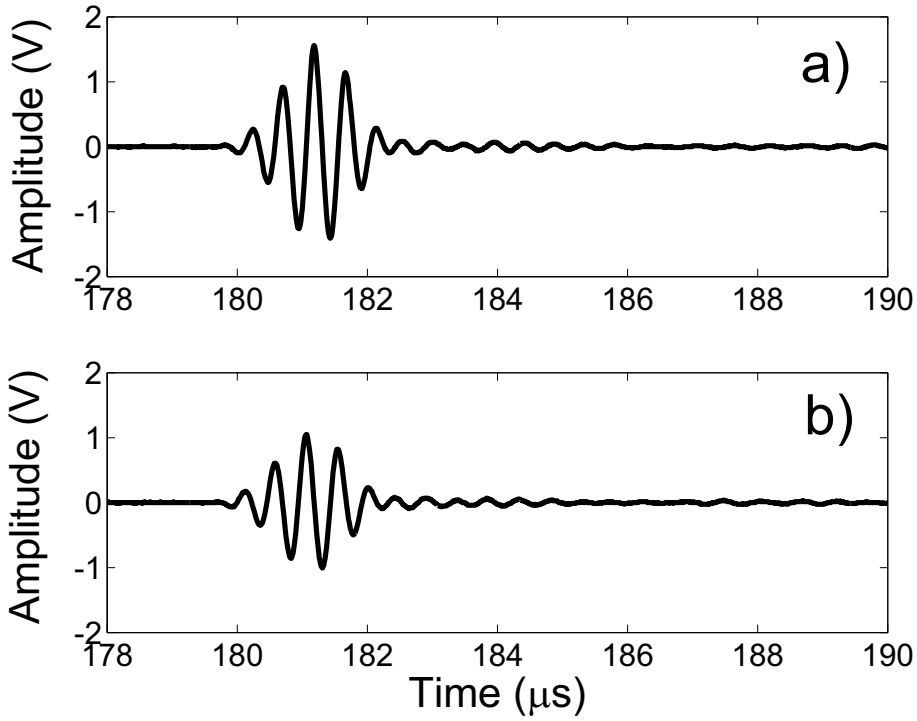

Figure 7.3: SH* mode pulse echo signal received through a 1mm thick and 15mm wide steel strip coupled to a 6mm thick steel plate: a) signal before coupling b) signal when strip is manually pushed onto the treacle covered steel plate surface.

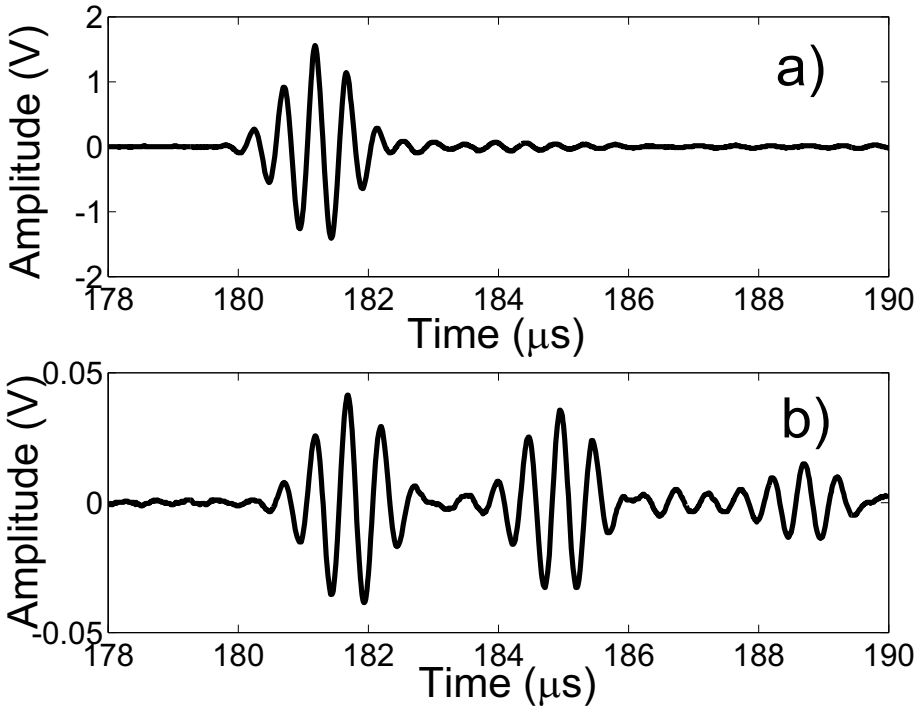

Figure 7.4: SH* mode signal received through a 1mm thick and 15mm wide steel strips coupled to a 6mm thick steel plate: a) signal in pulse echo mode before coupling b) signal when a second strip is manually pushed onto the treacle covered steel plate surface close to the exciting strip.

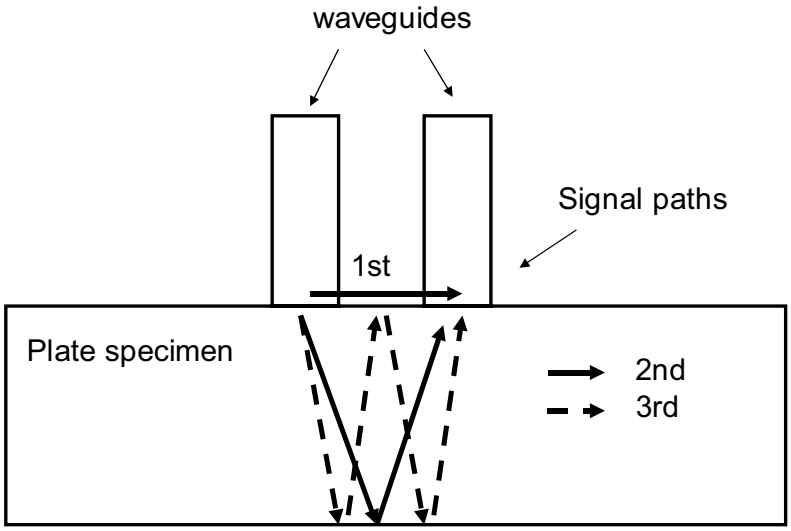

Figure 7.5: Signal paths that the SH waves travel in the plate specimen when the pitch catch mode is employed.

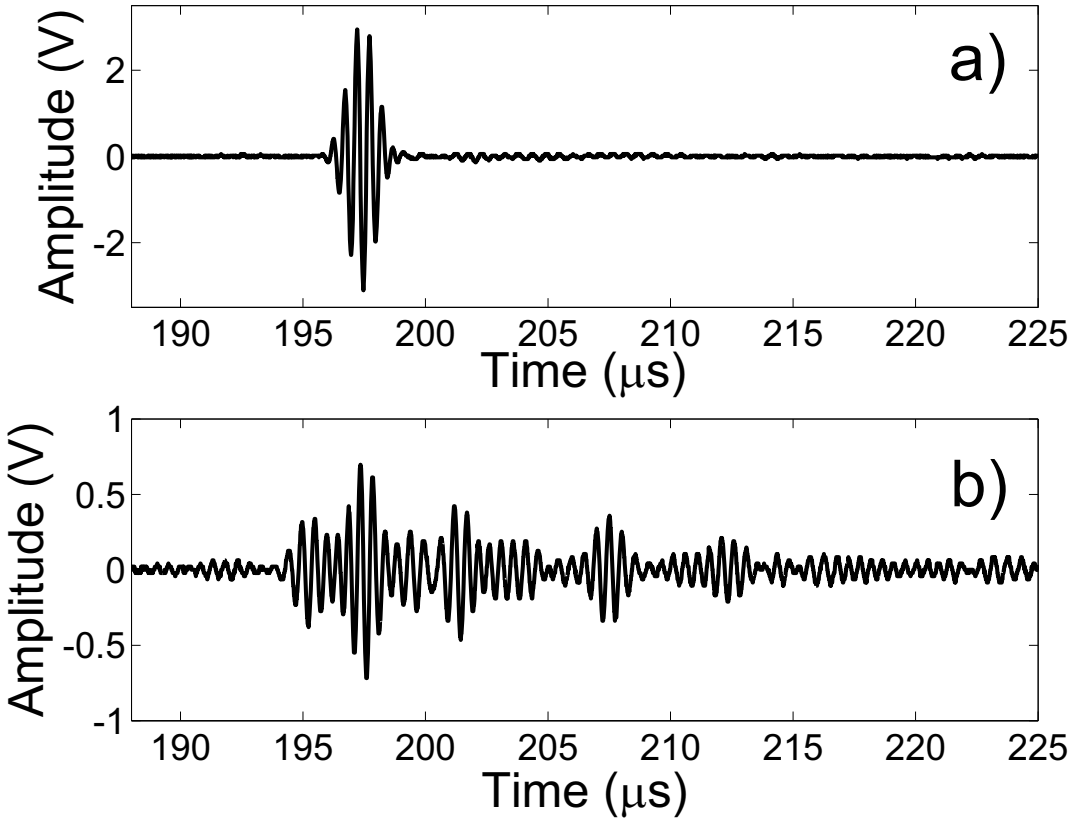

Figure 7.6: SH* mode pulse echo signal received through a 1mm thick and 15mm wide steel strip welded to a 6mm thick steel plate: a) signal before welding b) signal after welding.

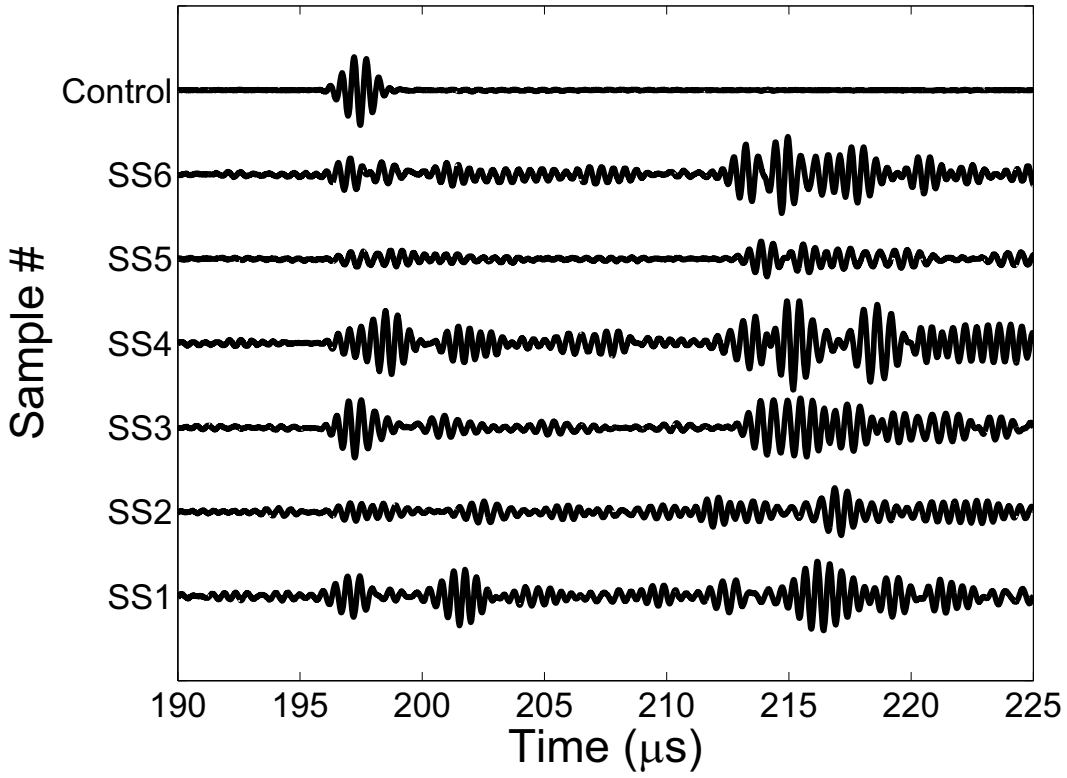

Figure 7.7: SH* mode pulse echo signals received through 1mm thick and 15mm wide steel strips attached to a 6mm thick steel plate by means of silver soldering.

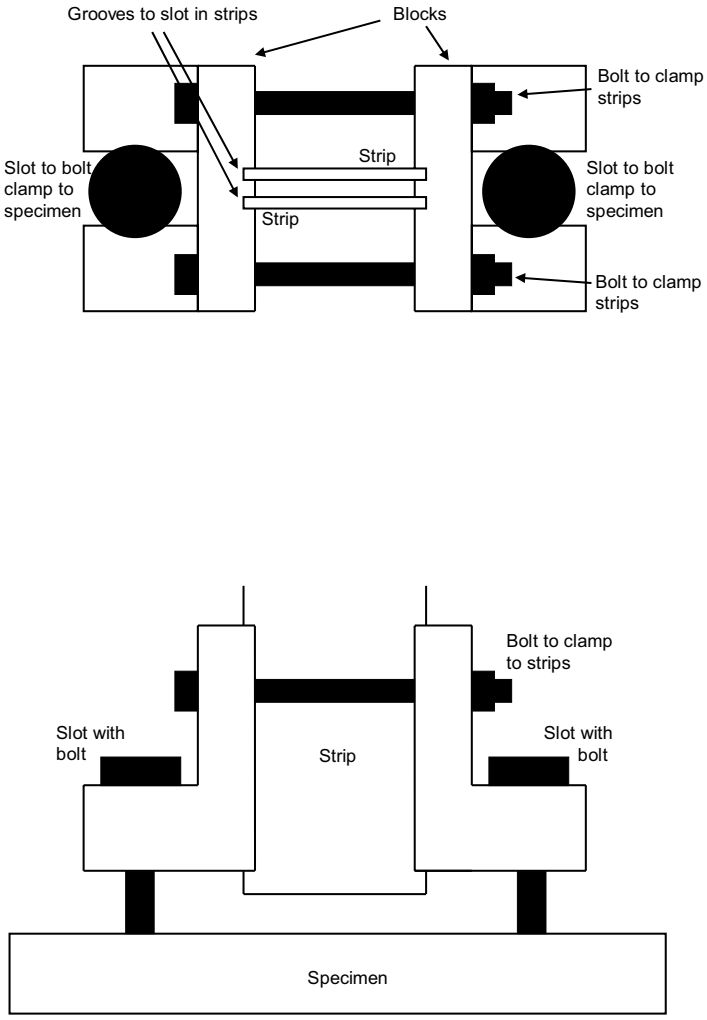

Figure 7.8: Top and front view of the clamp that was used to attach two strip waveguides to the sample plate.

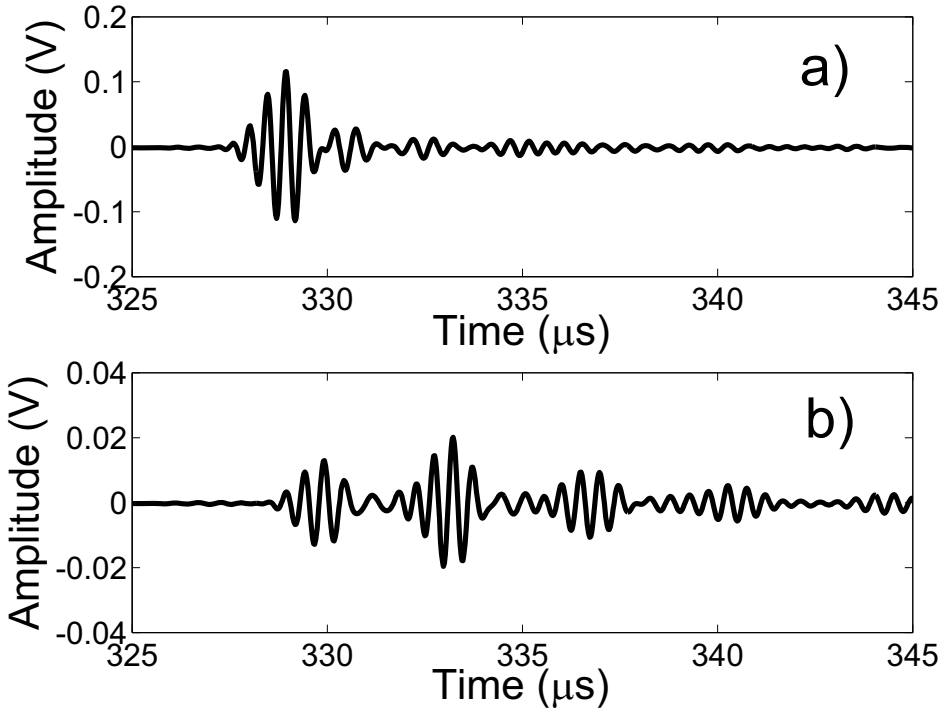

Figure 7.9: SH* mode signals send and received through one or two 1mm thick and 15mm wide steel strips clamped to a 6mm thick steel plate: a) pulse echo signal on sending strip b) pitch catch signal received on second strip (pictured signal already 17dB amplified compared to signal in a)).

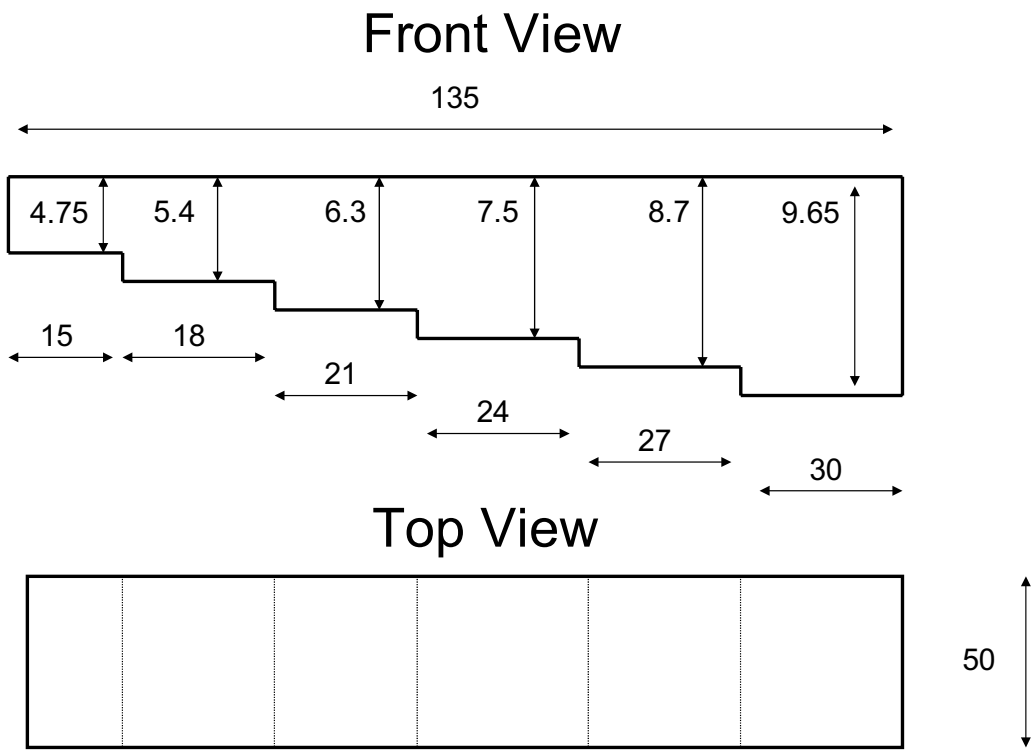

Figure 7.10: Sketch of the calibration block comprising of 6 steps (dimensions in mm).

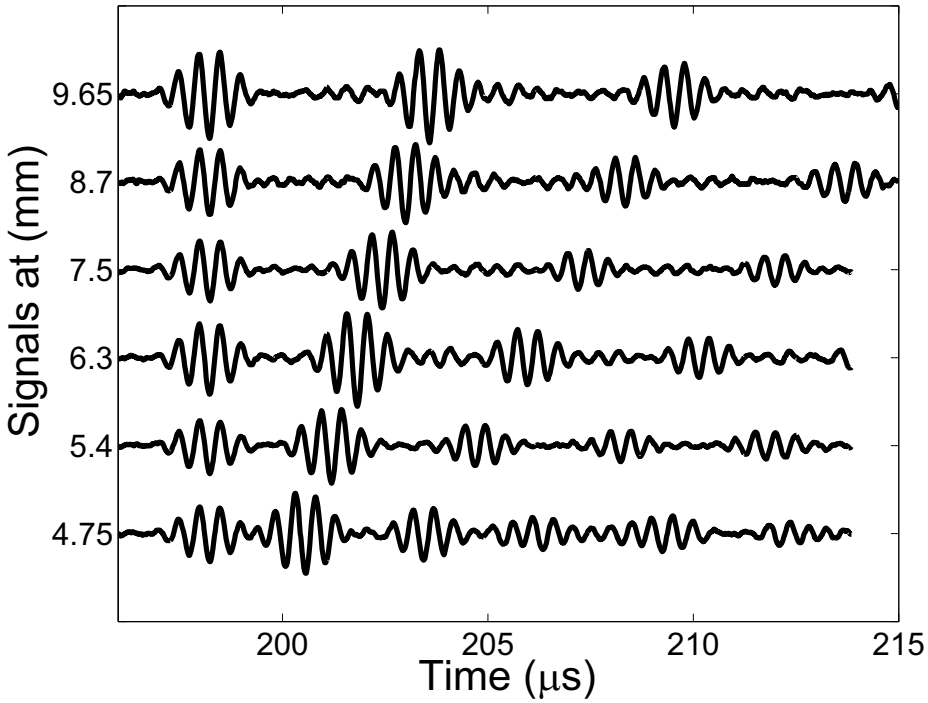

Figure 7.11: 5 cycle 2MHz Hanning windowed tonebursts sent and received by the SH* mode waveguide system coupled to the calibration block of figure 7.10.

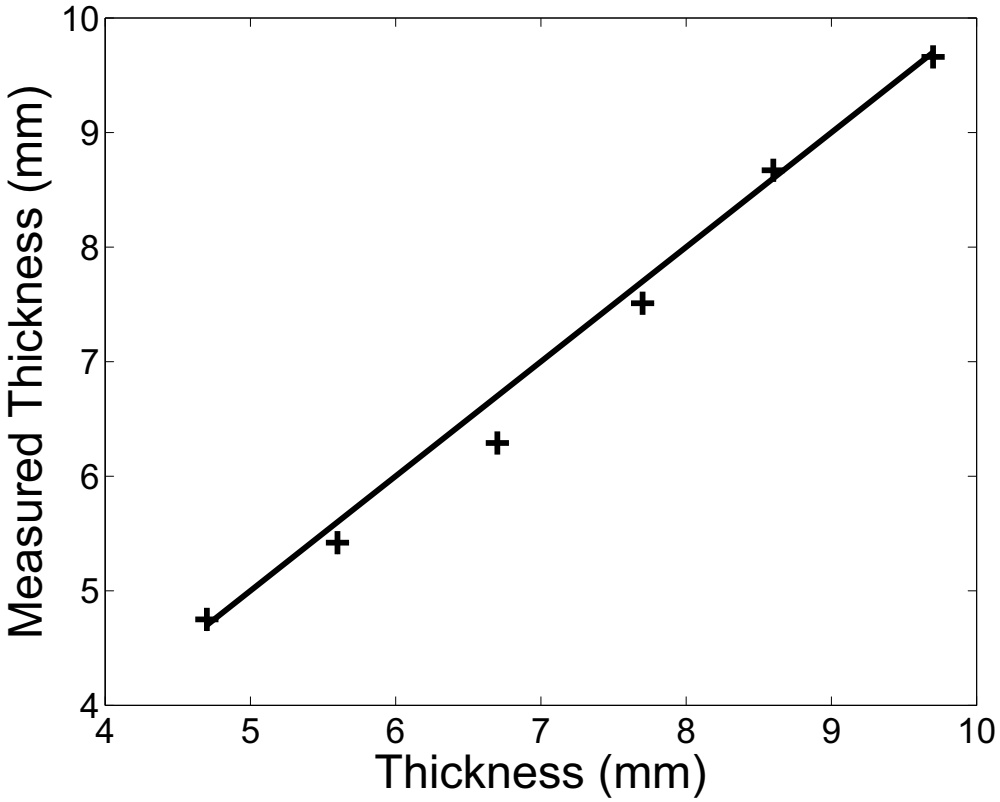

Figure 7.12: Thickness measured using the SH* mode plotted against the thickness measured using a caliper.

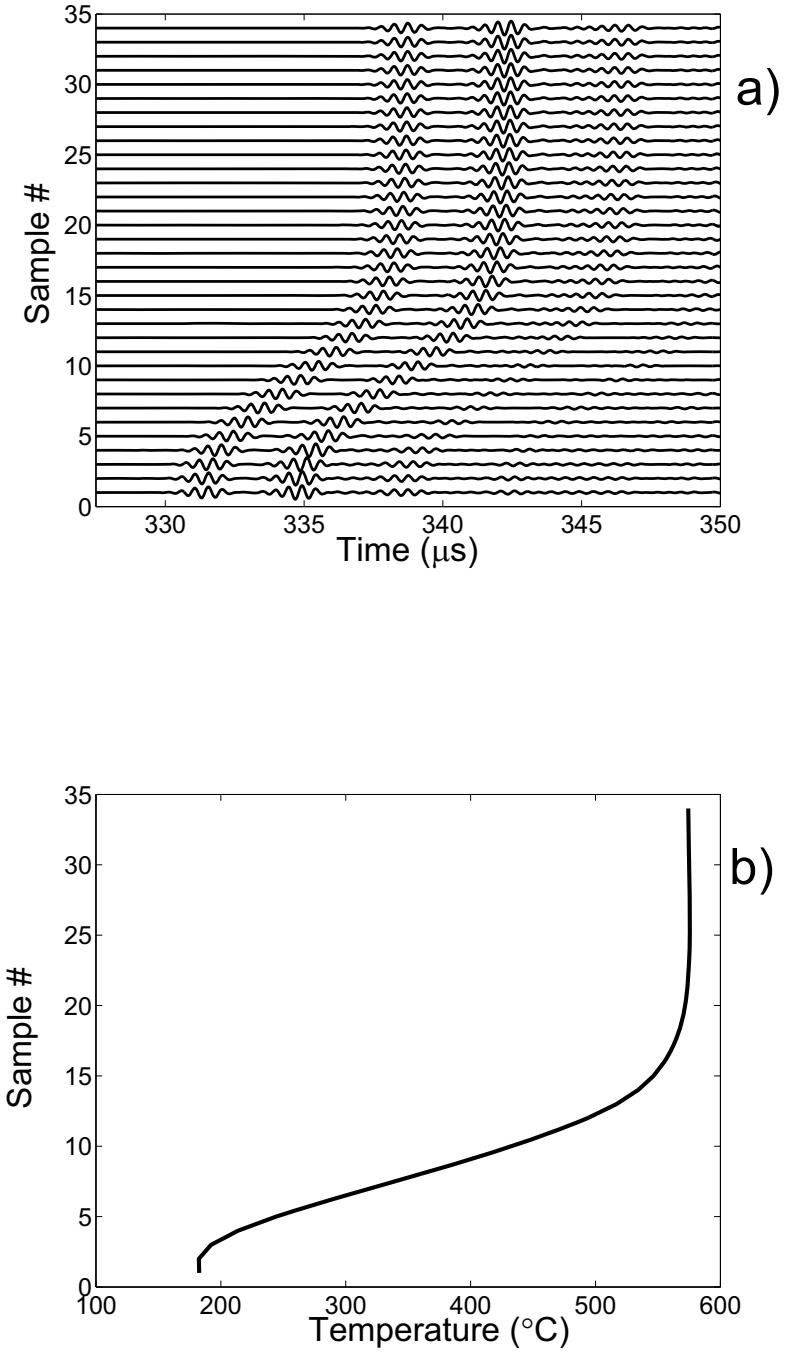

Figure 7.13: a) Signals and b) temperature recorded during a typical heating cycle. (Heating from 20°C to 500 – 600°C usually took about one to one and a half hours.)

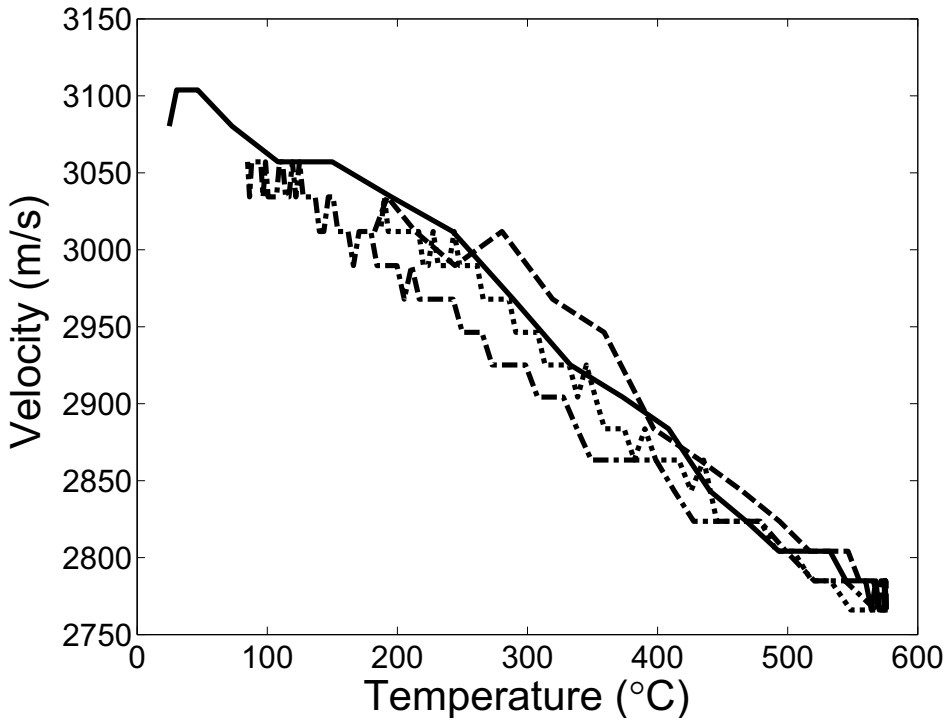

Figure 7.14: Shear velocity of the plate specimen evaluated during different heating and cooling cycles. (—) first heating cycle, (- - -) first cooling cycle, (· · ·) second heating cycle, (· - ·-) second cooling cycle.

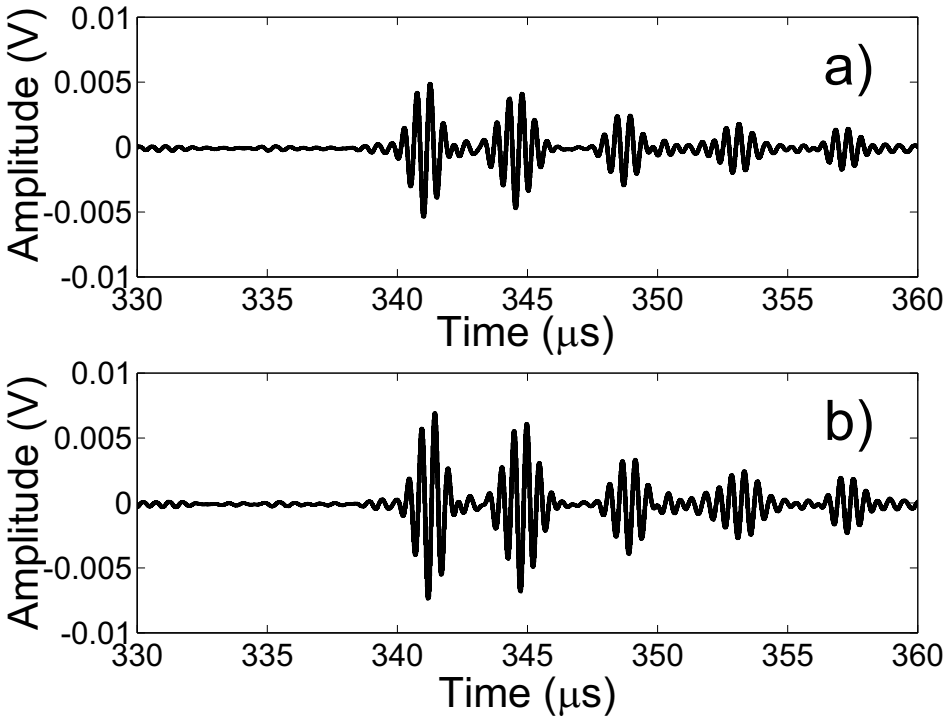

Figure 7.15: Waveguide remote monitoring system signal with sample at 500°C a) at start of experiment and b) after 4 weeks.

Chapter 8

Conclusions

8.1 Thesis Review

In this thesis the use of guided waves for fluid property measurements and remote structural monitoring was investigated. The use of guided ultrasonic waves offers several advantages over conventional techniques: for the application of fluid property measurements the need for a test cell is removed and beam spreading effects are avoided. For remote structural monitoring the waveguide allows the transducer to be situated at a distance from the object that is being monitored. This makes it possible to monitor structures in harsh environments which standard transducers could not withstand.

Existing guided wave techniques for fluid property measurements use the effect of leakage or an entry reflection to evaluate the bulk and shear modulus of an embedding medium. These methods however do not allow the evaluation of attenuation in the surrounding material. Therefore in this thesis an interface wave, called the quasi-Scholte mode, was used for fluid bulk property measurements. The quasi-Scholte mode propagates in both the fluid and the waveguide; however its energy is mainly trapped at the interface between the waveguide and the fluid and decays away with distance from the waveguide surface. The interface wave is sensitive to all of the fluid properties.

In chapter 3 the theory behind the Scholte and quasi-Scholte wave was described. Then in chapter 4 a series of experiments using the quasi-Scholte mode to measure fluid properties was discussed. Some of the outcomes of chapter 4 suggested that it would be beneficial to reduce the width of the plate waveguide as far as possible in order to reduce errors. When the propagating wave modes in a strip were analysed, in addition to an $A0^*$ mode that is suitable for exciting the quasi-Scholte mode, a non-dispersive shear horizontal mode was also found. This mode was termed the SH* mode and it was realised that it could be used for remote inspection of structures in extreme environments.

Chapter 5 concentrated on investigating the characteristics of wave propagation in strips of rectangular cross section. It described the techniques used to obtain dispersion curves for rectangular waveguides and presented results for steel strips.

A challenging problem is the transfer of the wave from the waveguide into the object that is to be investigated. The analysis of the wave propagation in the waveguide and the object was uncoupled by considering the stresses transmitted by the guided wave mode as a surface load on the test piece. A collection of literature results for the radiation characteristics of surface sources on half spaces was therefore considered in chapter 6.

The theoretical findings of chapters 5 and 6 were used to devise an experimental setup to carry out remote thickness gauging using a waveguide. Experiments evaluating different waveguide-structure joints were carried out. Successful thickness gauging experiments on calibration blocks of different thicknesses were also performed to validate the capabilities of the waveguide sensor. Long-term tests at high temperatures (up to 600°C) as well as temperature cycling were also carried out to verify the robustness of the setup and to show that long term monitoring at high temperatures using a waveguide is possible.

8.2 Findings

The work presented in this thesis revealed further insight into the working principles of ultrasonic waveguide sensors and their potential applications. The modelling of the quasi-Scholte wave and the construction of a fluid property sensor lead to a good understanding of the interface wave and its capabilities and limitations when used to extract fluid properties. A general summary of the findings related to the quasi-Scholte mode will be given first before findings from the remote waveguide monitoring system are recalled.

8.2.1 Fluid property measurements using the quasi-Scholte mode

The theoretical investigation into the quasi-Scholte wave showed that the fraction of its energy that travels in the fluid depends on the ratios of the fluid density and bulk velocity to the solid density and bulk velocity. The same is true for the Scholte wave velocity, which is the velocity that the quasi-Scholte mode asymptotes to at high frequency thickness products. Therefore to be sensitive to the fluid the right waveguide material for a certain fluid will have to be chosen. Most fluids are aqueous solutions for which steel is a suitable waveguide material. Over 99% of the Scholte wave energy on a steel/water interface is located in the fluid.

The energy distribution between waveguide material and fluid also depends on the operating frequency-thickness product. At low frequency-thicknesses all the energy is located in the waveguide while at higher frequency-thickness products most of the energy travels in the fluid. Sensitivity to the fluid is generally best at high frequency thickness products with the exception of the quasi-Scholte mode group velocity which is most sensitive to the fluid bulk velocity at frequency thickness products around 350kHz-mm (for steel in aqueous fluids). The group velocity of the quasi-Scholte mode at this frequency-thickness product can be three times more sensitive than a conventional bulk velocity measurement. However the sensitivity

to fluid bulk attenuation is not as high and is expected to perform worse than a measurement in a test cell.

Two attenuation mechanisms of the quasi-Scholte mode were identified. Shear leakage attenuates the interface wave due to in-plane surface displacements of the waveguide that set up energy dissipating bulk shear waves in the fluid. The quasi-Scholte mode is also attenuated by energy scattered or dissipated in the component of the wave that travels in the fluid. This part of the attenuation is related to the fluid bulk attenuation and can be used to evaluate the latter if isolated from the shear leakage.

The excitation method presented excited the quasi-Scholte mode from the plate; it is therefore not very effective at high frequency thickness products. An optimum frequency window in which the quasi-Scholte mode is sensitive to fluid properties and can be excited by a mode conversion from the $A0$ mode in a free waveguide was found to lie around $200 - 500$kHz mm for steel.

The experiments showed that bulk velocity measurements can be performed to within 0.5%. For simple Newtonian fluids the viscosity can also be determined with errors of up to 8%. Bulk attenuation measurements showed poorer performance ($\sim 20\%$ error), which could partly be explained by lower sensitivity, geometrical defects in the setup and the inversion problem being ill-posed. However improvements in performance are possible and it is believed that a successful strategy to achieve this would be the optimisation of the geometry of the measurement apparatus.

Possible applications of a quasi-Scholte mode 'dipstick' could be the monitoring or measurement of fluid bulk velocities in manufacturing processes or the use as rapid testing equipment for bulk materials. Since the transducer is separated from the sensing area, measurements in hot fluids are possible. The quasi-Scholte mode is also well suited for applications such as fluid level sensing. Attenuation measurement based applications like particle sizing are difficult to carry out with the current

quasi-Scholte mode setup due to the poor accuracy and the need for a large frequency bandwidth. However where the differences between viscosity induced attenuation and fluid bulk attenuation have to be detected the sensor is very useful.

8.2.2 Remote monitoring using a flexible waveguide

The investigation into an 'acoustic cable' for remote ultrasonic monitoring of structures in harsh environments was focused on three different issues. The first was the design of a non-dispersive waveguide, secondly the waveguide source characteristics had to be optimised and finally a practical implementation of the best possible system had to be found.

Even though not absolutely necessary the use of non-dispersive wave propagation in the 'acoustic cable' considerably reduces the complexity of the excitation system. The traditional approach of reducing the frequency-thickness product of the waveguide in order to operate in a region where the fundamental compressional wave mode in the waveguide is non-dispersive was overcome by using a shear horizontal (SH*) type mode in a very thin and wide rectangular strip. The strip mode possesses a cut-off at low frequency-width products; however at high frequency-width products, the SH* mode becomes non-dispersive and asymptotes to the shear velocity of the waveguide material. The mode shape of the SH* mode is constant through the thickness of the strip and varies across the width in an approximately parabolic fashion. The displacements are at a maximum in the centre of the strip and very small on the strip edges, so that most of the energy travels along the centre of the strip. Experimentally the SH* mode could reliably and selectively be excited with an amplitude 30 dB above other undesirable modes.

When studying the literature on source characteristics on a half space an anti-plane shear source was identified to have the best radiation characteristics. In the 2D limit of a source of infinite length, which is approximated by the large aspect ratios of the strip, advantages of the SH source are the excitation of only SH waves in the half

space: no compressional or surface waves are excited by an ideal SH line source. The SH source cylindrically spreads in all directions and thus has a wide field of view. When returning to the waveguide, SH waves in the half space excite the SH* mode which propagates the signal back to the transducer. Other waveguide sources such as circular, torsional sources would produce waves that on return to the waveguide excite different modes from those that created them (flexural modes in this case). Normal and tangential loading on the half space produces shear, compressional and surface waves which considerably complicate the analysis. Furthermore the energy content in the surface wave excited by normal or tangential sources is always very large; this makes subsurface inspection very difficult.

An experimental study into the joining method revealed that although they transmit most of the wave energy into the structure, permanent attachment methods are not reliable. Features that are inevitably introduced by the joining process distort the signal shape and cause reflections that greatly complicate the interpretation of results. Other methods could only be successfully employed in the pitch catch mode. While coupling with shear couplant is not possible at high temperatures its use for thickness gauging experiments at room temperature was possible. Clamping with a purpose made clamp showed good results, both at low and high temperatures.

A test system was successfully run at high temperatures for a period of over 4 weeks. Several heating and cooling cycles after the period at constant high temperature also did not deteriorate the strength or shape of signals. The shear velocity drops by about 10% with increase of temperature from room temperature to around 600°C and must be corrected for if measurements are to be taken at different temperatures. Experimentally, no issues with increased shear wave attenuation at high temperatures (up to 600°C) were encountered.

8.3 Future work

In future a detailed study of the quasi-Scholte mode attenuation of a rectangular strip waveguide should be carried out in order to improve the quality of the bulk attenuation measurements that are possible using the QS-mode. The addition of a torsional wave sensor that allows the evaluation of fluid density at the same time as a fluid bulk velocity and attenuation measurement would allow the guided wave sensor to completely characterise the acoustic properties of a fluid. This is not commonly achieved by conventional ultrasonic test cells. The characterisation of hot fluids using the QS mode should also be investigated.

The study of the remote waveguide monitoring sensor has opened many interesting possibilities for further investigations. The effect of uneven or rough reflectors on either side of the structure of the waveguide will have to be researched. This simulates the effects of corrosion or erosion that are most likely encountered in real life situations.

Another field to be explored is the use of the 'acoustic cable' for defect (crack size) monitoring over long periods and at elevated temperatures. For this it might be useful to use the time of flight diffraction technique. Alternatively the construction of arrays of strips and array techniques for monitoring the structure beneath the waveguides could be employed. This would require a detailed study of the three dimensional wave field produced by the SH* strip source.

Appendix A

Global Matrix Solution

In the global matrix method a matrix of the general solutions of wave propagation in the system materials is set up with the appropriate boundary conditions (continuity of stresses and displacements at boundaries). The system of equations results in an eigenvalue/eigenvector problem that can be solved. The matrix equation for a plate immersed in two half spaces of viscous fluid is given below. For more details see also References [53], [23] and [22].

$$\Big[A\Big] \cdot \begin{pmatrix} L_{f-} \\ T_{f-} \\ L_{s+} \\ L_{s-} \\ T_{s+} \\ T_{s-} \\ L_{f+} \\ T_{f+} \end{pmatrix} = 0 \tag{A.1}$$

Where L and T are the amplitudes of the partial longitudinal and transverse waves. The subscripts f and s refer to the fluid and solid respectively and the + and - signs indicate the direction of the partial wave. Terminology here is from Lowe [23]. The matrix A is: $A = [B \vdots C]$, where

$$B = \begin{bmatrix} k & -k_{2Tf} & k & kg_{SL} \\ -k_{2Lf} & -k & k_{2Ls} & -k_{2Ls}g_{SL} \\ i\rho_f B_f & 2i\rho_f\beta_f^2 k k_{2Tf} & i\rho_s B_s & i\rho_s B_s g_{SL} \\ -2i\rho_f\beta_f^2 k k_{2Lf} & i\rho_f B_f & 2i\rho_s\beta_s^2 k k_{2Ls} & -2i\rho_s\beta_s^2 k k_{2Ls} g_{SL} \\ 0 & 0 & kg_{SL} & k \\ 0 & 0 & k_{2Ls}g_{SL} & -k_{2Ls} \\ 0 & 0 & i\rho_s B_s g_{SL} & i\rho_s B_s \\ 0 & 0 & 2i\rho_s\beta_s^2 k k_{2Ls} g_{SL} & -2i\rho_s\beta_s^2 k k_{2Ls} \end{bmatrix} \quad \text{(A.2)}$$

$$C = \begin{bmatrix} k_{2Ts} & -k_{2Ts}g_{ST} & 0 & 0 \\ -k & -kg_{ST} & 0 & 0 \\ -2i\rho_s\beta_s^2 k k_{2Ts} & 2i\rho_s\beta_s^2 k k_{2Ts} g_{ST} & 0 & 0 \\ i\rho_s B_s & i\rho_s B_s g_{ST} & 0 & 0 \\ k_{2Ts}g_{SS} & -k_{2Ts} & k & k_{2Tf} \\ -kg_{ST} & -k & k_{2Lf} & -k \\ -2i\rho_s\beta_s^2 k k_{2Ts} g_{ST} & 2i\rho_s\beta_s^2 k k_{2Ts} & i\rho_f B_f & -2i\rho_f\beta_f^2 k k_{2Tf} \\ i\rho_s B_s g_{ST} & i\rho_s B_s & 2i\rho_f\beta_f^2 k k_{2Lf} & i\rho_f B_f \end{bmatrix} \quad \text{(A.3)}$$

where k is the wavenumber of the guided wave to be solved for, ρ_s is the solid plate material density, ρ_f is the fluid density and the remaining quantities are defined by the following equations:

$$k_{2Lf,s} = \pm\left(\frac{\omega^2}{\alpha_{f,s}^2} - k^2\right)^{1/2} \quad \text{(A.4)}$$

$$k_{2Tf,s} = \pm\left(\frac{\omega^2}{\beta_{f,s}^2} - k^2\right)^{1/2} \quad \text{(A.5)}$$

$$B_{f,s} = \omega^2 - 2\beta_{f,s}^2 k^2 \quad \text{(A.6)}$$

$$G_{SL} = e^{i(k_{2Ls}h)} \quad \text{(A.7)}$$

$$G_{ST} = e^{i(k_{2Ts}h)} \quad \text{(A.8)}$$

where $k_{2Lf,s}$ is the component of the longitudinal bulk wave wavenumber in the direction normal to the plate surface, $k_{2Tf,s}$ is the component of the shear bulk wave wavenumber in the direction normal to the plate surface, $B_{f,s}$, G_{SL} and G_{ST} are multiplication factors, h stands for the plate thickness. α and β are the complex bulk velocities defined by:

$$\alpha_n = \frac{c_l}{1 - i\frac{\kappa_l}{2\pi}} \tag{A.9}$$

$$\beta_n = \frac{c_s}{1 - i\frac{\kappa_s}{2\pi}} \tag{A.10}$$

The media are indicated by the subscripts f and s, which stand for fluid and solid in the subscripts of other quantities.

The equations A.4 and A.5 contain a square root expression; this results in several possible solutions, some of which may be unphysical (e.g. waves with negative attenuation). Therefore care should be taken to chose the right sign of the expression under the square root before entering equations A.4 and A.5 into matrix A.

A solution of equation A.1 exists if matrix A is singular, i.e. when the determinant of the matrix equals zero. There are several wavenumbers that satisfy the equation at each frequency. These are the different propagating modes that may exist. One of these propagating modes is the quasi-Scholte mode. The complex wavenumber gives the phase velocity ($\frac{\omega}{k_{re}}$) and attenuation (k_{im}) of the mode. By specifying one of the partial wave amplitudes and substituting the complex wavenumber into equation A.1 the mode shape can be determined at each frequency. The mode shape is the distribution of displacements, stresses, strains and similar characteristics through the cross section of the plate.

Appendix B

Derivation of an approximate formula for the SH-wave attenuation

The approach here follows closely the derivation of the approximate attenuation of the longitudinal L(0,1) mode in [30]. The system that is described is a plate of thickness h as shown in figure 3.16. The guided wave attenuation for a cross section of a wave guide can be expressed by use of the average power flow:

$$\alpha = \frac{\frac{\partial P}{\partial z}}{2P_{area}} \tag{B.1}$$

Where P_{area} is the average power flow across the cross section of the waveguide, z is the propagation direction. $\frac{\partial P}{\partial z}$ describes the energy leakage across the boundary of the waveguide. We will first evaluate this term.

Assume a Newtonian fluid with appropriate relaxation time. The viscous skin depth is defined as

$$\delta = (2\eta/\rho_f\omega)^{1/2} \tag{B.2}$$

Where η is the liquid viscosity, ρ_f the fluid density and ω the angular frequency. Therefore an expression for the velocity in the liquid adjacent to the waveguide can

be expressed as

$$v = v_0 exp(-y/\delta) \tag{B.3}$$

Where v_0 denotes the surface velocity of the waveguide and y the distance from the surface in the liquid.

The quantity $\frac{\partial P}{\partial z}$, the change in average power flow, is the power leaving the waveguide cross section. Therefore it is the dissipated power over a unit surface area. This quantity is found by integrating the power flow per unit width of the plate across the top and bottom surfaces of the plate

$$\frac{\partial P}{\partial z} = 2 \int_0^1 1/2 \tau_0 v_0 dx \tag{B.4}$$

where

$$\tau_0 = \eta \frac{\partial v}{\partial y} \mid_{y=0} = -\eta v_0/\delta \tag{B.5}$$

and thus

$$\frac{\partial P}{\partial z} = -v_0^2 (\rho_f \omega \eta/2)^{1/2} \tag{B.6}$$

The second quantity that has to be evaluated to find the guided wave attenuation is the term P_{area}, the average power flow across the cross section of the plate. Using the Poynting vector:

$$P_{area} = \int_0^1 \int_0^h -v^* \sigma/2 dy dx \tag{B.7}$$

Where v^* stands for the complex conjugate of the velocity and σ the stress at any point within the cross section. The velocity and stress field variation can be described using the displacement distribution for the SH mode [8]:

$$u_x = Be^{i(kz-\omega t)} \tag{B.8}$$

$$v_x = \frac{du_x}{dt} = -i\omega Be^{i(kz-\omega t)} \tag{B.9}$$

$$\sigma_x = G\frac{du_x}{dz} = ikBGe^{i(kz-\omega t)} \tag{B.10}$$

Hence,

$$P_{area} = \int_0^1 \int_0^h \frac{\omega k B^2 G}{2} dydx \tag{B.11}$$

and using the identities $k = \frac{\omega}{c}$ and $c = \left(\frac{G}{\rho_s}\right)^{1/2}$ yields:

$$P_{area} = -\frac{1}{2}\omega^2 B^2 (G\rho_s)^{1/2} h \tag{B.12}$$

Now substituting the expression $v_0 = -i\omega B$ for the velocity at the interface into the $\frac{\partial P}{\partial z}$ term obtained earlier yields the guided wave attenuation:

$$\alpha = \frac{\frac{\partial P}{\partial z}}{2P_{area}} = \frac{-v_0^2(\frac{\eta\rho_f\omega}{2})^{1/2}}{-\omega^2 B^2 (G\rho_s)^{1/2} h} \tag{B.13}$$

after rearranging and cancellations,

$$\alpha = -\frac{1}{2h}\left(\frac{2\rho_f\omega\eta}{\rho_s G}\right)^{1/2} \tag{B.14}$$

Appendix C

Phase and group velocity

Generally the solution to wave propagation problems results in an expression of the form

$$u(x,t) = Ae^{i(kx-\omega t)} \tag{C.1}$$

where u is the displacement, A is the amplitude, k is the wavenumber of the wave, x the spatial position of the wave along the propagation direction, ω is the angular frequency and t the time. If the wavenumber k is allowed to be complex then

$$k = k_r + ik_i \tag{C.2}$$

with k_r being the real part of the wavenumber and k_i being the imaginary part of the wavenumber. Using C.2 allows us to rewrite equation C.1

$$u(x,t) = Ae^{-k_i x}e^{i(k_r x-\omega t)} = Ae^{-\alpha x}e^{i(k_r x-\omega t)} \tag{C.3}$$

with k_i the imaginary part of the wavenumber being equal to α, the attenuation of the wave.

Equation C.3 now contains two separable terms, the first being $Ae^{-\alpha x}$ that stands for an amplitude that decays with propagation distance due to dissipative mechanisms,

and the second term $e^{i(k_r x - \omega t)}$ that expresses the harmonic oscillations of the wave in time and space. The second term may be used to derive the phase velocity. For propagation at constant phase the term in the brackets of the exponential has to equal zero

$$(k_r x - \omega t) = 0 \tag{C.4}$$

thus

$$\frac{x}{t} = \frac{\omega}{k_r} = c_p \tag{C.5}$$

where c_p is the phase velocity which describes the velocity at which the phase of the wave travels through space.

Cheeke [96] recalls that wave propagation at a single carrier frequency does not contain any information but the frequency of the wave. To transmit information the carrier has to be modulated with another frequency. The combination of several propagating frequencies forms a wave packet. The wave packet also propagates through the medium but at the group velocity, which in general is different from the phase velocity. A simple example for the derivation of group velocity of two frequencies was shown by Stokes [97] and is also given in Rose [8]. Rose also gave the following derivation of group velocity:

Consider the phase change of an individual frequency component at time increment $t = t_0 + dt$,

$$dP_i = (k_i(x_0 + dx) - \omega_i(t_0 + dt)) - (k_i x_0 - \omega_0 t) = k_i dx - \omega_i dt \tag{C.6}$$

now for the wave group to remain unchanged, the phase changes have to be the same for all of its constituent frequency components, therefore

$$dP_i - dP_j = 0 \qquad or \qquad (k_i - k_j)dx - (\omega_i - \omega_j)dt = 0 \tag{C.7}$$

which can be rewritten as

$$\frac{dx}{dt} - \frac{d\omega}{dk} = 0 \tag{C.8}$$

this defines the group velocity as

$$c_g = \frac{d\omega}{dk} \tag{C.9}$$

The group velocity is the velocity at which a wave packet moves through space (strictly speaking the wave packet travels at the energy velocity [98] however if the attenuation is low as in most real life cases the group velocity is a very good approximation). As with the phase velocity, the group velocity can be frequency dependent; actually the group velocity is a derivative of the wavenumber (and thus also the phase velocity). When the velocities are functions of frequency, the wave propagation is said to be dispersive. A wave packet is always made up of several frequencies. In dispersive media each constituent frequency will travel at a specific velocity. Therefore the shape of a wave packet will be distorted with increasing propagation length. This is the most significant feature of dispersion.

Figure C.1 shows a plot of the phase and group velocities of the lowest order anti-symmetric Lamb wave mode $A0$ of a 1mm thick steel plate as a function of frequency. At low frequencies the mode is very dispersive, meaning that there is a relatively steep velocity slope.

Figure C.2 shows simulated excitation signals and signals that have propagated for 100mm as $A0$ mode (the signals were simulated using the DISPERSE software [22]). Their frequency spectra are also shown. It can be seen that the signal in a) is made up of a broad bandwidth of frequencies and therefore is distorted more as the frequency components travel at different velocities and spread out. The signal in b) has a rather narrow frequency bandwidth and disperses less with distance. In Figure C.2 a) it can also be seen that the higher frequency components of the signal arrive earlier than the low frequency components. This can be predicted from the dispersion curve (C.1).

C.1 Retrieving phase and group velocity from measurements

The accurate retrieval of phase velocity and group velocity data from measurements is of utmost importance in non-destructive testing applications. In relatively non-dispersive media such as metals the characteristic velocity of the material is usually obtained on a sample specimen. With the knowledge of the ultrasonic velocity in the material other techniques such as thickness gauging or defect monitoring can be used. In dispersive media, for example suspensions of particles in a liquid or adhesives, the velocity dispersion itself contains information about the material and can therefore be used for material characterization. An example of this is the measurement of particle size distribution in suspensions [3]; other examples of fluid characterization are well summarized in Povey's book [1].

The measurement of phase velocity is usually based on the comparison of the phase information of two signal pulses that have travelled over two different lengths in the material. A standard procedure for this type of measurements is the phase spectrum method [99]. Another similar method that does not rely on the temporal separation of the two signals to be analyzed is the amplitude spectrum method [60]. In the following section the theoretical background behind these two standard methods will be recalled.

Consider a harmonic wave propagating in an unbound medium. The displacements in the positive propagation directions can be expressed as follows

$$u(x,t) = Ae^{i(\omega t - kx - \phi)}e^{-\alpha x} \tag{C.10}$$

where, u is the displacement, t is the time, x is the propagation distance, ω is the frequency, α the attenuation and ϕ an arbitrary phase angle. Using Fourier transformation and some algebra [60] this can be rewritten in the form

$$F(u(x,t)) = F(u(0,t))e^{i(-kx)}e^{-\alpha x} \tag{C.11}$$

where F indicates a Fourier transformed entity. In this case the wavenumber k and the attenuation α are real. The factor $e^{-\alpha x}$ will therefore not influence the phase

of the signal but only its amplitude. The signal amplitude can be calculated at two different positions as

$$F(u(x_1,t)) = F(u(0,t))e^{i(-kx_1)}e^{-\alpha x_1} \tag{C.12}$$

$$F(u(x_2,t)) = F(u(0,t))e^{i(-kx_2)}e^{-\alpha x_2} \tag{C.13}$$

which when rewritten in the form of a magnitude and phase yields the following:

$$F(u(x_1,t)) = A_1e^{i(-kx_1+\phi_{01})} = A_1e^{i(\phi_1)} \tag{C.14}$$

$$F(u(x_2,t)) = A_2e^{i(-kx_2+\phi_{02})} = A_2e^{i(\phi_2)} \tag{C.15}$$

Now the difference in phase of the two signals at their respective positions allows the phase velocity to be extracted.

$$d\phi = \phi_2 - \phi_1 = -k(x_2 - x_1) \tag{C.16}$$

but $k = \frac{\omega}{c_p}$, therefore

$$d\phi = -\frac{\omega}{c_p}(x_2 - x_1) \qquad and \qquad c_p = \frac{\omega(x_2 - x_1)}{-d\phi} \tag{C.17}$$

Equation C.17 gives a simple expression to evaluate the phase velocity from signals collected at two position along a signal path. However there is a caveat. For the simple expression to work accurately and reliably, the absolute phase difference at each frequency has to be determined. From the signals the phase information will be extracted in a wrapped form, this means that the phase will be limited to values in the range of -π to π. The absolute phase however has to be in an unwrapped form. The unwrapping of the signal causes a problem and is only possible in frequency regions where a strong signal is present. Also unwrapping algorithms are not perfect and an error of 2π can easily be introduced to the unwrapped phase. In cases where the frequency spectrum does not contain any signal at low frequencies, the phase information at low frequencies will be entirely made up of noise. This will make it impossible to unwrap the phase and find the absolute unwrapped phase of the signal.

C.2 Retrieving phase velocity by cosine interpolation

One of the main problems of methods using the phase spectrum method is the phase uncertainty due to the wrapping from $-\pi$ to $+\pi$. Further errors are also introduced by errors in the distance measurement between two transducer locations. If several transducers can be used to collect signals over a short distance (usually less than a wavelength), or one transducer can be scanned over the surface, a cosine interpolation can be used to accurately determine phase velocity. Here the approach as used by Simonetti [100] is recalled. Consider the Fourier transform of a signal that has been received at a reference position:

$$S(\omega)_{ref} = A(\omega)e^{i(-k_r(\omega)x_{ref})}e^{-\alpha(\omega)x_{ref}} \tag{C.18}$$

where S is the received signal, A is the complex amplitude of the travelling wave, k_r is the real wavenumber of the wave, α is the attenuation of the wave and x_{ref} the position at which the signal is received. Note here that all quantities except the distance are frequency dependent. The signal at any other position (x_1) along the travelling path of the wave can be expressed as:

$$S(\omega)_1 = A(\omega)e^{i(-k_r(\omega)x_1)}e^{-\alpha(\omega)x_1} \tag{C.19}$$

Now we can divide the first expression by the second to eliminate the effects of the signal amplitude.

$$\frac{S(\omega)_{ref}}{S(\omega)_1} = \frac{e^{i(-k_r(\omega)x_{ref})}}{e^{i(-k_r(\omega)x_1)}}\frac{e^{-\alpha(\omega)x_{ref}}}{e^{-\alpha(\omega)x_1}} = e^{i(k_r(\omega)(x_1-x_{ref})}e^{-(\alpha(\omega)(x_1-x_{ref})}$$

$$= Fe^{i(k_r(\omega)(x_1-x_{ref})} \tag{C.20}$$

$$= F(cos(k_r(\omega)(x_1 - x_{ref})) - isin(k_r(\omega)(x_1 - x_{ref})))$$

where F is a real factor depending on the wave attenuation. Thus it can be concluded that the real part of the signal ratio is related to the cosine of the wavenumber-

distance product. By evaluating the real part of the signal ratio at different distances from the reference signal the phase velocity can be found using a cosine interpolation.

$$R(\frac{S(\omega)_{ref}}{S(\omega)_1}) = F(cos(k_r(\omega)(x_1 - x_{ref})) = F(cos(\frac{\omega}{C_{ph}(\omega)}(x_1 - x_{ref})) \qquad \text{(C.21)}$$

Figure C.3 shows signals that have been created using the dispersion characteristics of an $A0$ mode, determined using the DISPERSE software. The signals are 5 cycle Hanning windowed tonebursts with a centre frequency of 500 kHz that have been propagated over distances ranging from 100 to 105.5 mm from the source. The signals were processed as described by the above procedure and a cosine interpolation was carried out at the centre frequency. Figure C.4 shows the real part of the ratio of the spectra of the different signals and the reference signal as well as the best result of the cosine interpolation at the signal centre frequency of 500 kHz.

This method works very well and is very accurate provided the distance data is available at a good enough accuracy. However a major drawback is the need of a relatively large set of data to calculate the phase velocity, on average about 8 signals at different distances are needed. The method also only works well if the interval between the scanning points of the signals is much less than a wavelength; this avoids aliasing.

C.3 Group velocity measurement using the zero phase slope

The author learned about the method of zero phase slope in private discussion with Prof. Peter Nagy [101] who developed and used the method previously. The fundamental idea behind the determination of group velocity using the zero phase slope method is the evaluation of the Fourier transform of the signal within a window that is swept over the time domain signal. When the window is aligned with the group arrival time of a frequency component within the signal the phase slope of the frequency component will tend to zero. Thus the group arrival time is evaluated by sweeping a window over the time domain signal and evaluating the phase slope for each frequency. At the zero phase slope point the window centre coincides with

the frequency group arrival. This can be shown using the shift property of Fourier transforms:

$$\begin{gathered} F(f(t)) = \int_{-T}^{+T} f(t)e^{-i\omega t}dt = F(\omega) \\ F(f(t-t_{shift})) = \int_{-T}^{+T} f(t-t_{shift})e^{-i\omega t}dt = \\ \int_{-T}^{+T} f(t-t_{shift})e^{-i\omega(t-t_{shift})}e^{-i\omega t_{shift}}d(t-t_{shift}) \\ = e^{-i\omega t_{shift}}F(\omega) \end{gathered} \tag{C.22}$$

Consider now the Fourier transform of the displacement signal of a travelling wave

$$F(u(x,t)) = F(\omega)e^{-i(kx)}e^{-i\phi_0} \tag{C.23}$$

when the time origin of the signal is shifted to the right by a delay t_{shift} the shift property of the transform leads to the following expression

$$F(u(x,t))_{t_{shift}} = F(\omega)e^{-i(kx)}e^{-i\phi_0}e^{-i\omega t_{shift}} \tag{C.24}$$

Rewriting the expression yields

$$F(u(x,t))_{t_{shift}} = F_1 e^{-i\phi_e} \tag{C.25}$$

where F_1 is a constant and ϕ_e is the overall phase angle. The overall phase ϕ_e has several components:

$$\phi_e = -i(kx + \phi_0 + \omega t_{shift}) \tag{C.26}$$

thus the phase slope can also be found to be

$$\frac{d\phi_e}{d\omega} = -\frac{dk}{d\omega}x - t_{shift} \tag{C.27}$$

but $c_g = \frac{d\omega}{dk}$, therefore

$$\frac{d\phi_e}{d\omega} = -\frac{x}{c_g} - t_{shift} \tag{C.28}$$

if $x \neq 0$ the only condition that fulfils equation C.28 at zero phase slope is

$$\frac{d\phi_e}{d\omega} = 0 = -\frac{x}{c_g} - t_{shift} = -T_g - t_{shift} \tag{C.29}$$

and thus

$$T_g = -t_{shift} \tag{C.30}$$

Where $T_g = x/c_g$ is the group arrival time of the signal. However if the window position, i.e. the time frame, stays the same then the group velocity of the signal can be found by the following expression.

$$\begin{aligned} \frac{d\phi_{e1}}{d\omega} - \frac{d\phi_{e2}}{d\omega} &= -\frac{x_1}{c_g} - t_{shift} - (-\frac{x_2}{c_g} - t_{shift}) \\ &= \frac{x_2 - x_1}{c_g} \end{aligned} \tag{C.31}$$

and thus

$$c_g = \frac{x_2 - x_1}{\frac{d\phi_{e1}}{d\omega} - \frac{d\phi_{e2}}{d\omega}} \tag{C.32}$$

Equation C.32 was used to retrieve the group velocity from two 1 cycle broadband signals with centre frequency 500 kHz. The signals have again propagated as the $A0$ mode on a 1mm thick steel plate for 100 and 200mm respectively and are depicted in figure C.5.

Both signals were Hanning windowed and then a fast Fourier transform algorithm was used to calculated their spectra. The phase was unwrapped and the phase slope

was calculated. It should be mentioned here that unwrapping the phase to calculate the phase slope does not cause similar problems as encountered in the determination of the absolute phase of the signal (as in section C.1) since the phase slope does not depend on the absolute value of the phase but only on its local variation. The method therefore is insensitive to noise in the measured phase at low frequencies, which makes the determination of the absolute phase very difficult if not impossible. The phase slope of both signals is shown in figure C.6.

The calculated group velocity is shown in figure C.7. The performance of the method is very good if a clear signal is available. Figure C.8 shows the error in computed group velocity. The error is in the region of 0.05% for the higher frequency content of the signal. At lower frequencies higher errors are encountered. This is due to distortion of the signal caused by windowing with the Hanning window. Lower frequency components are longer in the time domain and therefore are more distorted by the window and hence larger errors are encountered.

C.4 Velocity measurement using the amplitude spectrum method

The amplitude spectrum method is a versatile technique to retrieve the wave velocity from a signal that contains two distance separated signals (here a front reflection and a back wall reflection from a plate-like specimen of uniform thickness). The technique was first described by Pialucha [60], whose description will be followed here. The simplest case of a signal consisting of a front face and backwall reflection will be treated. The analysis starts with an identity that Sachse and Pao [99] derived for the Fourier transform of an arbitrary signal:

$$F(u(x,t)) = F(u(0,t))e^{-ikx}e^{-\alpha x} \tag{C.33}$$

where $u(x,t)$ is the displacement function of a signal in space and time, F() denotes Fourier transformation, k is the wavenumber of the wave, α is the wave attenuation

and x is a spatial coordinate.

The above identity shows that the Fourier transform of a signal at a position x can be expressed as a function of the Fourier transform at a reference position $x = 0$ and the wave propagation characteristics. This can be used to write an expression for the Fourier transform of a signal containing a front face and back wall reflection from a plate. The first arrival is taken as a reference signal at position $x = 0$ and the second arrival is assumed to be a distance $x = 2T$ (T for thickness) separated from the first echo. Therefore the total recorded signal is the sum of the reference signal and the signal at distance x:

$$S = F(u(0,t)) - F(u(2T,t)) = F(u(0,t))[1 - e^{-ik2T}e^{-\alpha 2T}] \tag{C.34}$$

The attenuation term $e^{-\alpha 2T}$ can be replaced by a positive constant say Q.

$$S = F(u(0,t))[1 - Qe^{-ik2T}] \tag{C.35}$$

F(u(0,t)) is assumed to be a slowly varying function. The term in brackets becomes an oscillatory term that causes the total signal amplitude spectrum to have a series of minima and maxima. The location of the minima occur when

$$e^{-ik2T} = 1. \tag{C.36}$$

This in turn occurs when

$$\frac{2T\omega}{c_p} = 2\pi m. \tag{C.37}$$

Where c_p is the phase velocity of the material, T the thickness of the plate like specimen and m the index of the minimum in the spectrum. Therefore the phase velocity of the material can be evaluated if the index m of the minimum is known:

$$c_p = \frac{2Tf}{m} \tag{C.38}$$

where $\omega = 2\pi f$. Examples of the use of equation C.38 to determine the phase velocity computed from a signal and its first backwall reflection are extensively described by Pialucha et al. [60]. Here an example of a slight variant of the Amplitude Spectrum method which the author has used will be described. In this case the group velocity rather than the phase velocity of the signal will be determined (a strict proof which shows that the variant allows group velocity determination has not been carried out but from experience it is known that the method yields reasonable results):

$$c_g = \frac{2T\Delta F}{\Delta M} \tag{C.39}$$

where ΔF is the frequency difference between two minima and ΔM the difference in index number M. Equation C.39 can be simply derived from equation C.36 by replacing k with ∂k and using the identity $c_g = \partial k/\partial\omega$ for the group velocity.

The DISPERSE software was used to simulate two $A0$ mode signals that have propagated 100 and 120mm from the source. The signals are shown in figure C.9. As predicted by theory the Fourier transform of the sum of both signals in figure C.9 a) and b) contains a series of minima and maxima. An image of the spectra of the sum of signals a) and b) is shown in figure C.10. The index number of each minimum as well as the frequency difference (ΔF) between minima is shown.

Using equation C.39 the group velocity of the signals was then computed. Figure C.11 shows the group velocity that was computed using the Amplitude Spectrum method as well as the correct group velocity from the DISPERSE software. The relative error between the velocity evaluated by the amplitude spectrum method and the original group velocity from the DISPERSE software was also computed and is shown in figure C.12.

Figure C.12 shows that the performance of the method is very good and the error in computed group velocity is small. As in the zero phase slope method the error is in the region of 0.05% for the higher frequency content of the signal. At lower frequencies higher errors are encountered and again this is believed to be due to

distortion of the signal caused by windowing with the Hanning window before the Fourier transform is evaluated. Lower frequency components are longer in the time domain and therefore are more distorted by the window which results in larger errors.

C.5 Preferred method for velocity evaluation

Before choosing any of the above methods for a velocity measurement it has to be stressed that the above analysis assumed that signals are due to a single propagating mode only. The above examples also have not taken any noise into account and can therefore give no indication of the methods robustness with respect to noise levels.

The velocity measurement method that is sought here is for the quasi-Scholte mode; therefore apart from good accuracy there are a couple of other desirable features that the measurement method should possess. For reasons of practicality, ideally only two signals at each of the two immersion states will be needed to evaluate the velocity. Due to the dispersiveness of the signals the velocity measurement method should also be able to detect the velocity variations with frequency. For the quasi-Scholte mode the measurement of group velocity is preferred.

The method of cosine interpolation requires measurements at more than 5 distances along the propagation path of the wave which is impractical. It also evaluates the phase velocity while the group velocity is more desirable for quasi-Scholte mode applications. It was therefore not chosen.

The Amplitude Spectrum method and the method of zero phase-slope are very similar and also perform equally well. However the method of zero phase-slope is the preferred measurement method. Its main advantage are the determination of group velocity at each point within the frequency spectrum, while the amplitude spectrum method only allows the evaluation at discreet frequencies where minima occur within the signal of the combined spectra. The Amplitude Spectrum method also runs

into resolution problems when the term ΔF becomes small and of a comparable magnitude to the frequency resolution of the spectrum (see section 4.7).

C.6 Figures

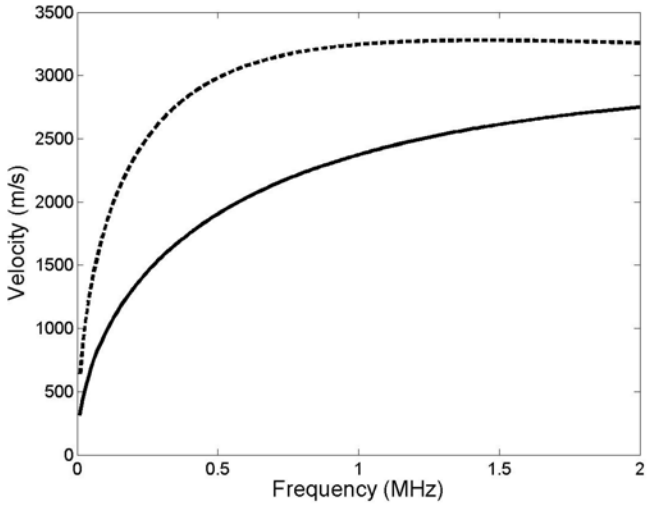

Figure C.1: Phase(—) and group velocity (- - -) dispersion curve of the A0 mode of a 1mm thick steel plate ($\rho_{steel} = 7932kg/m^3$,$C_l = 5959.5m/s$, $C_s = 3260m/s$).

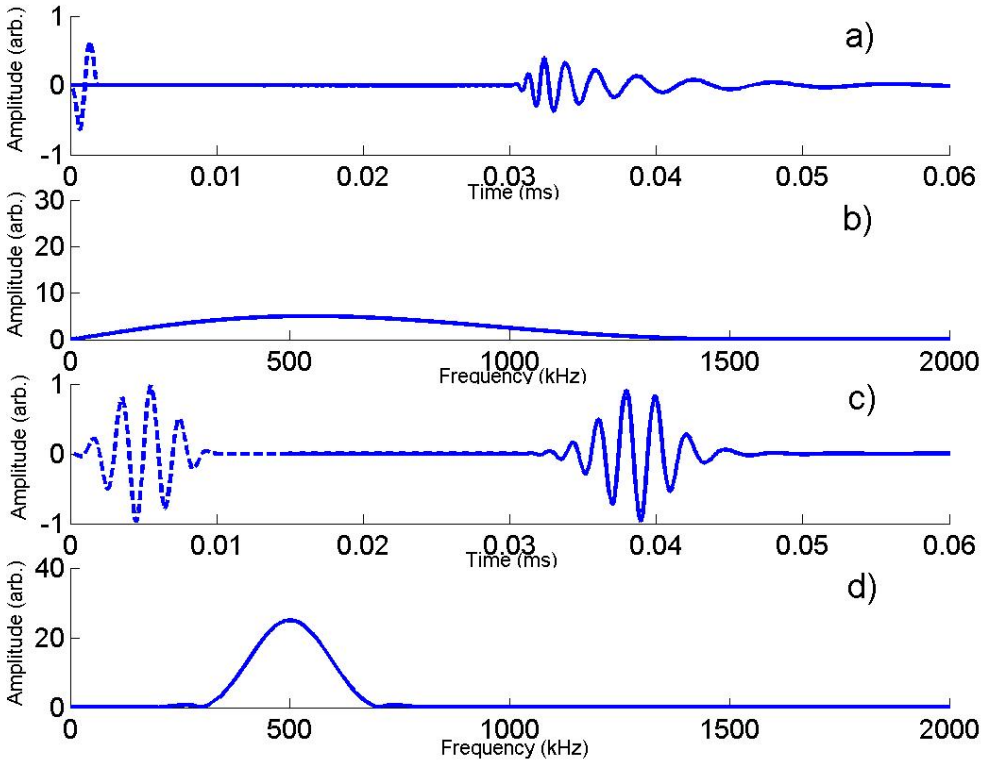

Figure C.2: Simulated excitation signals (- - -) and signals after 100 mm propagation (—) as $A0$ on a 1mm thick steel plate ($\rho_{steel} = 7932kg/m^3$,$C_l = 5959.5m/s$, $C_s = 3260m/s$). a) for a 1 cycle Hanning windowed toneburst with centre frequency 500 kHz b) frequency spectrum of a) c)for a 5 cycle Hanning windowed toneburst with centre frequency 500 kHz d) frequency spectrum of c)

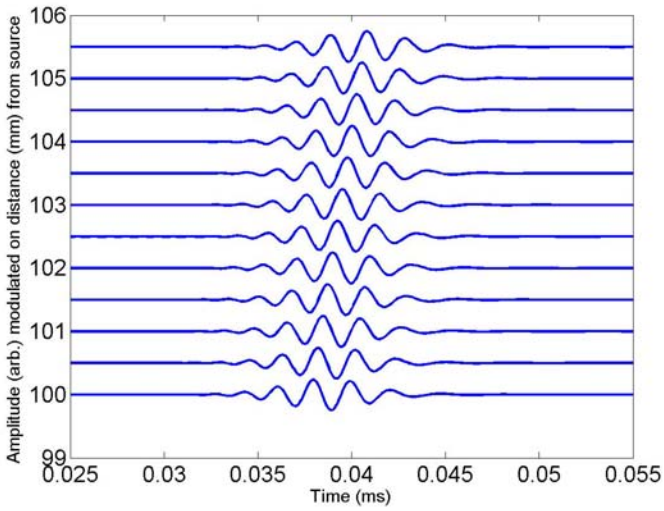

Figure C.3: Signals of the $A0$ mode propagated over distance from 100 to 105.5 mm from the source.

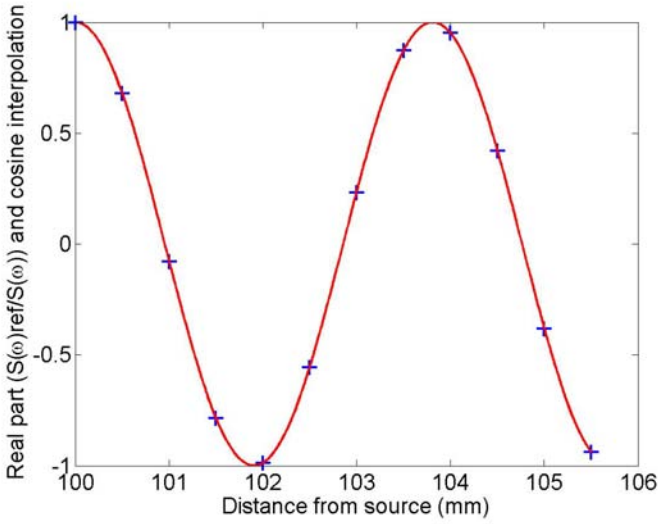

Figure C.4: Real part of the quantity $(\frac{S(\omega)_{ref}}{S(\omega)_x})$ [+] and the best result of the cosine interpolation $cos(\frac{\omega}{C_{ph}(\omega)}(x_1 - x_{ref}))$ [—] for a phase velocity of 1905 m/s at 500 kHz.

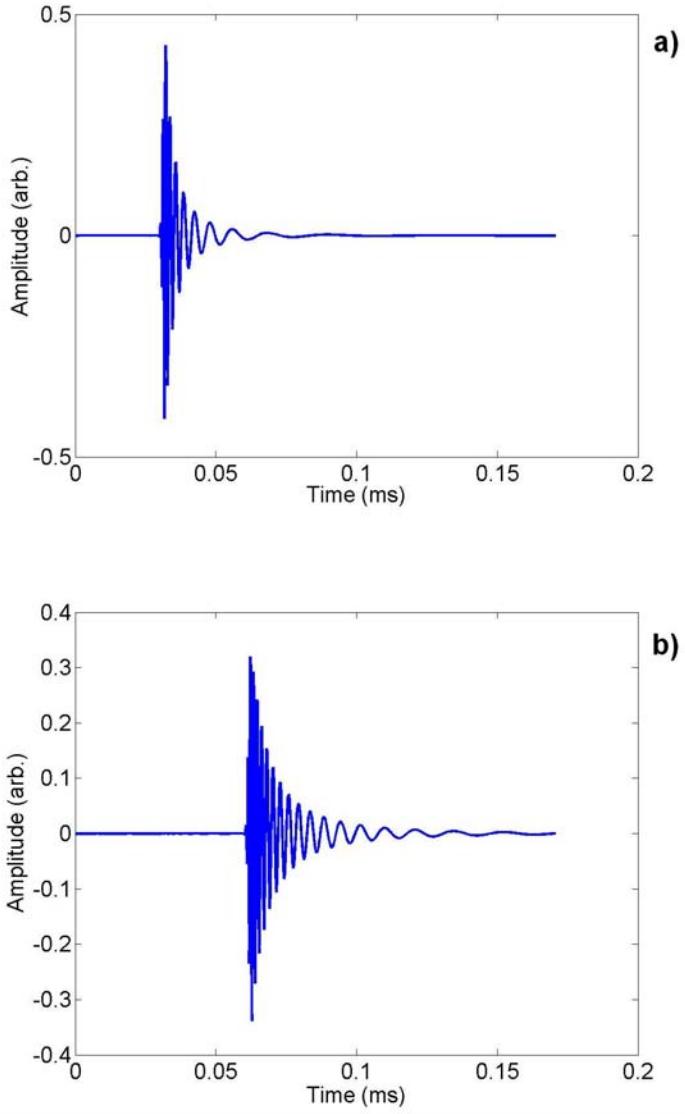

Figure C.5: $A0$ mode signals that were used to test the zero phase slope method for group velocity measurement. Signal in a) has travelled for 100mm and signal in b) for 200mm as $A0$ mode in a 1mm thick steel plate.

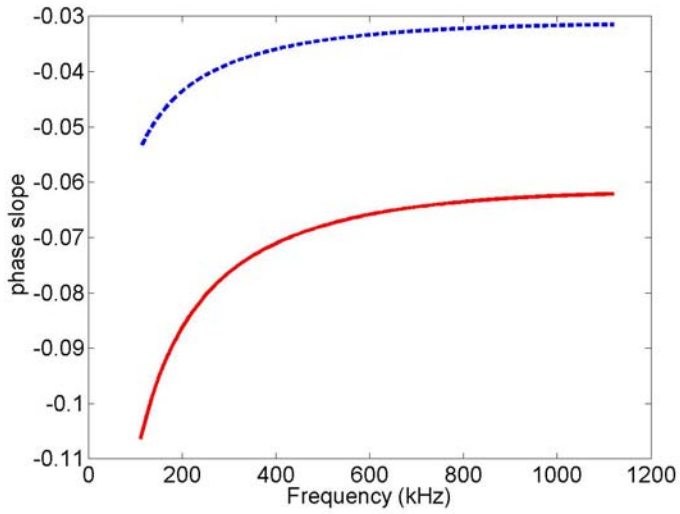

Figure C.6: Phase slope of both signals in figure C.5. [(- - -) signal a), (—) signal b)]

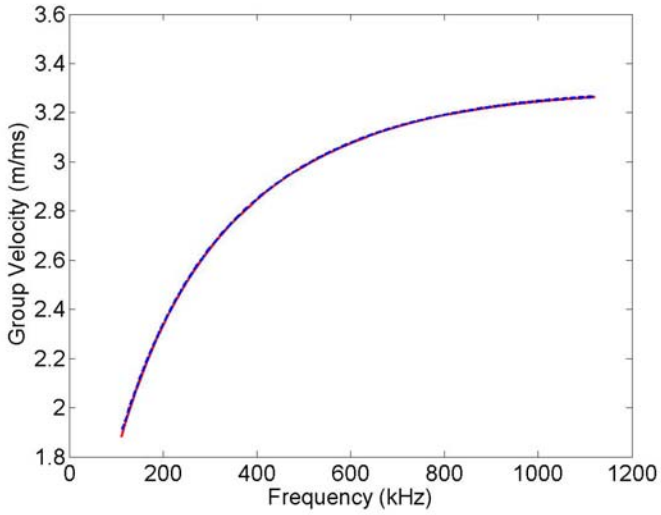

Figure C.7: Group velocity obtained using the zero phase slope method (- - -) and the group velocity curve that was used to simulated the signals(—)

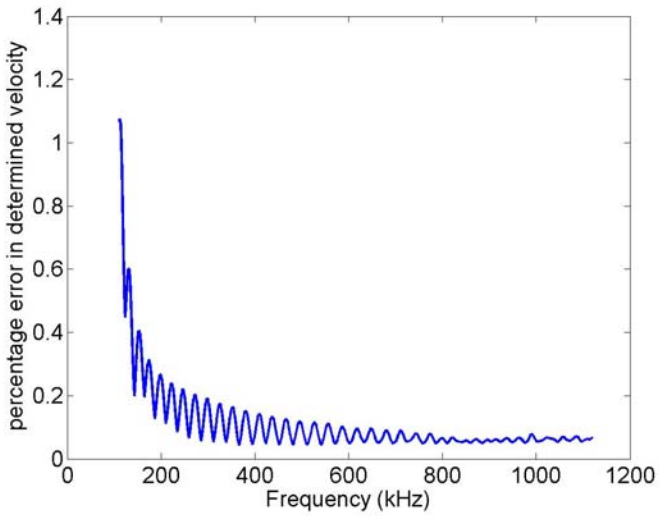

Figure C.8: Group velocity error calculated from the results in figure C.7.

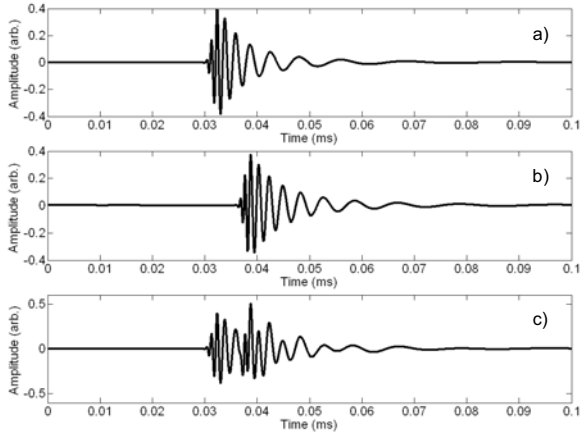

Figure C.9: DISPERSE simulations of $A0$ mode signals on a $1mm$ thick steel plate that have propagated a) 100mm from the source, b) 120mm from the source and c) the sum of both signals in a) and b).

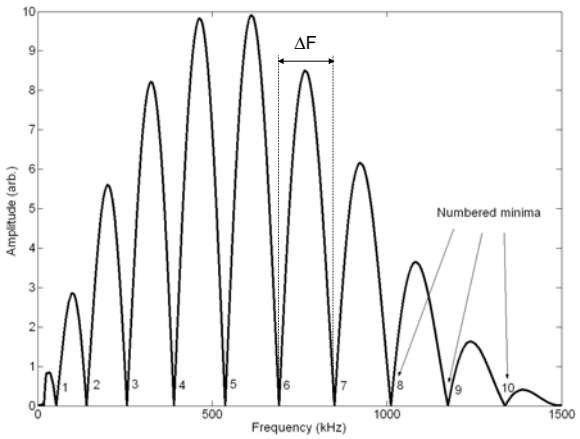

Figure C.10: Fourier transform of the signal c) in figure C.9 displaying a series of minima and maxima.

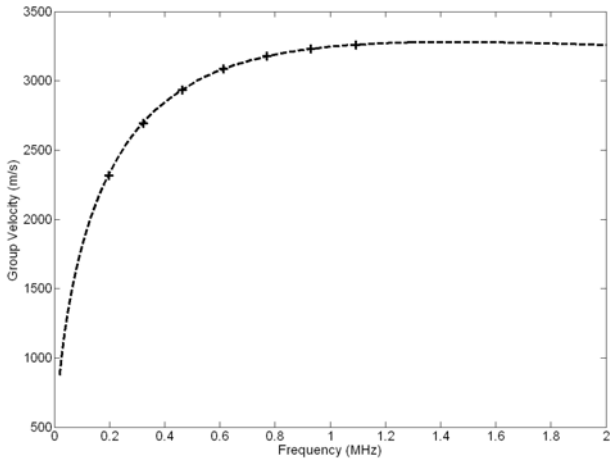

Figure C.11: Group velocity computed at each minimum using the amplitude spectrum (+) and the DISPERSE software reference group velocity (- - -) from which the signals in C.9 were computed.

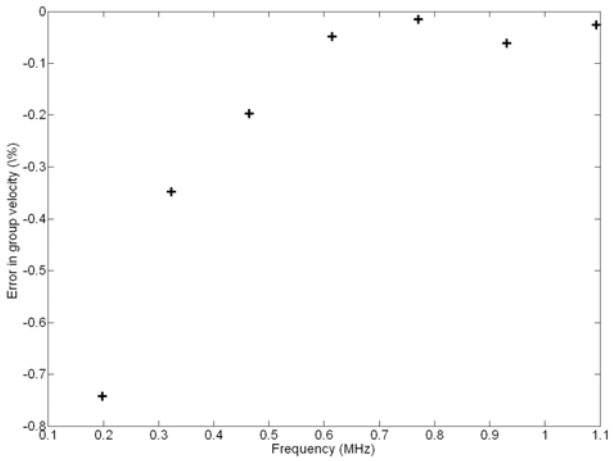

Figure C.12: Percentage group velocity error of the group velocity computed with the Amplitude spectrum method compared to the original DISPERSE data that signals were produced from.

References

[1] M. J. W. Povey. *Ultrasonic techniques for fluids characterization.* Academic Press, 1997.

[2] D.J. McClements. Advances in the application of ultrasound in food analysis and processing. *Trends in Food Sciences and Technology*, 6, 1995.

[3] R. E. Challis, J. S. Tebbutt, and A. K. Holmes. Equivalence between three scattering formulations for ultrasonic wave propagation in particluate mixtures. *Journal of Physics D*, 31:3481–3497, 1998.

[4] A. McNab, K.J. Kirk, and A. Cochran. Ultrasonic transducers for high temperature applications. *Science Measurement and Technology, IEE Proceedings*, 145:229–236, 1998.

[5] N. Schmarje, J.F. Saillant, K.J. Kirk, and S. Cochran. Imaging with lithium niobate/epoxy composites. *Ultrasonics*, 42:439–444, 2004.

[6] B. A. Auld. *Acoustic fields and waves in solids I.* Krieger Publishing Company, 1990.

[7] L.M. Brekhovskikh and V. Goncharov. *Mechanics of continua and wave dynamics.* Springer-Verlag, 1985.

[8] J. L. Rose. *Ultrasonic Waves in Solid Media.* Cambridge University Press, 1999.

[9] H. Kolsky. *Stress waves in solids.* Dover Publications, 1963.

[10] P. M. Morse and H. Feshbach. *Methods of Theoretical Physics.* McGraw-Hill Book Company, 1953.

[11] V.G. Mozhaev and M. Weihnacht. Subsonic leaky rayleigh waves at liquid-solid interfaces. *Ultrasonics*, 40:927–933, 2002.

[12] N. Favretto-Anres. Theoretical study of the stoneley-scholte wave at the interface between an ideal fluid and a viscoelastic solid. *Acustica*, 82:829 – 838, 1996.

[13] W. Fluegge. *Viscoelasticity*. Springer-Verlag, second edition, 1975.

[14] R.M. Christensen. *Theory of Viscoelasticity*. Academic Press, second edition, 1982.

[15] Y. M. Haddad. *Viscoelasticity of engineering materials*. Chapman and Hall, 1995.

[16] Lord Rayleigh. On waves propagating along the plane of an elastic solid. *Proceedings of the London Mathematical Society*, 17:4–11, 1885.

[17] K. F. Graff. *Wave Motion in Elastic Solids*. Dover Publications, 1973.

[18] L.M. Brekhovskikh. *Waves in layered media*. Academic Press, 1980.

[19] H. Lamb. On waves in an elastic plate. In *Conference of the Royal Society*, pages 114–128, London, 1917.

[20] D. Alleyne and P. Cawley. The long range detection of corrosion in pipes using lamb waves. In D.O. Thompson and D.E. Chimenti, editors, *Review of Progress in Quantitative NDE*, volume 14. Plenum Press, 1994.

[21] P. Wilcox, M. Lowe, and P. Cawley. Long range lamb wave inspection: The effect of dispersion and modal selectivity. In D.O. Thompson and D.E. Chimenti, editors, *Review of Progress in Quantitative NDE*, volume 18. Plenum Press, 1999.

[22] M.J.S. Lowe and B.N. Pavlakovic. Disperse user manual, version 2.0.11d. Technical report, Imperial College of Science, Technology and Medicine, London, UK; www.ndt.imperial.ac.uk, 2001.

[23] M. Lowe. Matrix techniques for modelling ultrasonic waves in multilayered media. *IEEE Transactions on Ultrasonics, Ferroelectrics and Frequency control*, 42:525–542, 1995.

[24] B. Pavlakovic, M. Lowe, D. Alleyne, and P. Cawley. Disperse: a general purpose program for creating dispersion curves. In D.O. Thompson and D.E. Chimenti, editors, *Review of Progress in Quantitative NDE*, volume 16A. Plenum Press, 1997.

[25] L. Knopoff. A matrix method for elastic wave problems. *Bulletin of the Seismological Society of America*, 54:431–438, 1964.

[26] P.D. Wilcox. *Lamb wave inspection of large structures using permanently attached transducers.* PhD thesis, Imperial College London, 1998.

[27] P. D. Wilcox, M. J. S. Lowe, and P. Cawley. A signal processing technique to remove the effect of dispersion from guided wave signals. In D. O. Thompson and D. E. Chimenti, editors, *Review of Progress in Quantitative NDE*, volume 20. Plenum Press, 2001.

[28] P. Roux, B. Roman, and M. Fink. Time-reversal in an ultrasonic waveguide. *Applied Physics Letters*, 70:1811–1813, 1997.

[29] M.G. Silk and K.F. Bainton. The propagation in metal tubing of ultrasonic wave modes equivalent to lamb waves. *Ultrasonics*, 17:11–19, 1979.

[30] P. B. Nagy and R. M. Kent. Ultrasonic assessment of poisson's ratio in thin rods. *Journal of the Acoustical Society of America*, 98:269–2701, 1995.

[31] P.B. Nagy and A.H. Nayfeh. Viscosity-induced attenuation of longitudinal guided waves in fluid-loaded rods. *Journal of the Acoustical Society of America*, 100:1501–1508, 1996.

[32] J. O. Kim and H. H. Bau. Online, real-time densimeter - theory and optimsation. *Journal of the Acoustical Society of America*, 85:432 – 439, 1989.

[33] C. L. Shepard and Friesel M. A. et al. Measurement of density and viscostiy of one- and two-phase fluids with torsional waveguides. *IEEE Transactions on Ultrasonics, Ferroelectrics and Frequency control*, 46:536–548, 1999.

[34] T. Vogt, M. Lowe, and P. Cawley. Cure monitoring using ultrasonic guided waves in wires. *Journal of the Acoustical Society of America*, 114:1303–1313, 2003.

[35] T.K. Vogt, J.S. Lowe, and P Cawley. Measurement of the material properties of viscous liquids using ultrasonic guided waves. *Ultrasonics, Ferroelectrics and Frequency Control, IEEE Transactions on*, 51:737–747, 2004.

[36] T. Vogt. *Determination of Material Properties Using Guided Waves*. PhD thesis, Imperial College London, 2002.

[37] D.J. McClements. Principles of ultrasonic droplet size determination in emulsions. *Langmuir*, 12:3454–3461, 1996.

[38] A.K. Holmes and R.E. Challis. The applicability of acoustic wave propagation models to silica sols and gels. *Journal of Colloid and Interface Science*, 216:50–58, 1999.

[39] P.S. Epstein and R.R. Carhart. The absorption of sound in suspensions and emulsions. i. water fog in air. *Journal of the Acoustical Society of America*, 25:553–565, 1953.

[40] J.R. Allegra and S.A. Hawley. Attenuation of sound in suspensions and emulsions: Theory and experiment. *Journal of the Acoustical Society of America*, 51:1545–1564, 1972.

[41] A.H. Harker and J.A. Temple. Velocity and attenuation of ultrasound in suspensions of particles in fluids. *Journal of Physics D*, 21:1576–1588, 1988.

[42] A.N. Kalashnikov and R.E. Challis. Errors in the measurement of ultrasonic absorption for materials evaluation. In D.O. Thompson and D.E. Chimenti, editors, *Review of Progress in Quantitative NDE*, volume 21B, pages 1997–2004. Plenum Press, 2002.

[43] P.C. Waterman and R.J. Truell. Multiple scattering of waves. *Journal of Mathematical Physics*, 2:512–537, 1961.

[44] C. Glorieux, K. V. Rostyne, K. Nelson, W. Gao, W. Lauriks, and J. Thoen. On the character of acoustic waves at the interface between hard and soft solids and liquids. *Journal of the Acoustical Society of America*, 110:1299 – 1306, 2001.

[45] J. G. Scholte. On the stoneley wave equation. In *Geophysics*, volume 45, pages 20–25. North Holland publishing, 1941.

[46] W.L. Pilant. Complex roots of the stonely wave equation. *Bulletin of the Seismological Society of America*, 62:285–299, 1972.

[47] M. M. Vol'kenshtein and V. M. Levin. Structure of a stoneley wave at an interface between a viscosus fluid and a solid. *Soviet Physics - Acoustics*, 34:351 – 355, 1987.

[48] F. Padilla, M. De Billy, and G. Quentin. Theoretical and experimental studies of surface waves on solid-fluid interfaces when the value of the fluid sound velocity is located between the shear and the longitudinal ones in the solid. *Journal of the Acoustical Society of America*, 106:666 – 673, 1999.

[49] G. D. Meegan, M. F. Hamilton, Y. A. Il'nskii, and E. A. Zabolotskaya. Nonlinear stoneley and scholte waves. *Journal of the Acoustical Society of America*, 106:1712 – 1723, 1999.

[50] N. Favretto-Anres and G. Rabau. Excitation of the stoneley-scholte wave at the boundary between an ideal fluid and a viscoelastic solid. *Journal of Sound and Vibration*, 203:193 – 208, 1997.

[51] M. J. S. Lowe. *Plate waves for the NDT of diffusion bonded titanium.* PhD thesis, Imperial College, 1992.

[52] T. Vogt, M. J. S. Lowe, and P. Cawley. Ultrasonic waveguide techniques for the measurement of material properties. In D. O. Thompson and D. E. Chimenti, editors, *Review of Progress in Quantitative NDE*, volume 21, pages 1 – 8. Plenum Press, 2002.

[53] F.B. Cegla, P. Cawley, and M.J.S. Lowe. Material property measurements using the quasi-scholte mode - a waveguide sensor. *Journal of the Acoustical Society of America*, 117:1098–1108, 2005.

[54] S. Nasr, J. Duclos, and M. Leduc. Pvdf transducers generating scholte waves. *Electronic Letters*, 24:309 – 311, 1988.

[55] J. McLean and F.L. Degertekin. Directional scholte wave generation and detection using interdigital capacitive micomachined ultrasonic transducers. *IEEE Transactions on Ultrasonics, Ferroelectrics and Frequency control*, 51:756–64, 2004.

[56] C. Desmet, V. Gusev, W. Lauriks, C. Glorieux, and J. Thoen. Laser-induced thermoelastic excitation of scholte wave. *Applied Physics Letters*, 68:2939 – 2941, 1996.

[57] M. De Billy and G. Quentin. Experimental study of the scholte wave propagation on a plane surface partially immersed in a liquid. *Journal of Applied Physics*, 54:4314–4322, 1983.

[58] T.J. Matula and P.L. Marston. Energy branching of a subsonic flexural wave on a plate at an air-water interface. observation of the wave field near the interface and near the plate. *Journal of the Acoustical Society of America*, 97:1389–1398, 1995.

[59] J. Dickey, G. Maidanik, and H. Ueberall. The splitting of dispersion curves for the fluid-loaded plate. *Journal of the Acoustical Society of America*, 98:2365–2367, 1995.

[60] T. Pialucha, C. C. H. Guyott, and P. Cawley. Amplitude spectrum method for the measurement of phase velocity. *Ultrasonics*, 27:270–279, 1989.

[61] R. E. Challis, J. A. Harrison, A. K. Holmes, and R. P. Cocker. A wide bandwidth spectrometer for rapid ultrasonic absorption measurements in liquids. *Journal of the Acoustical Society of America*, 90:730–740, 1991.

[62] G.W.C. Kaye and T.H. Laby. *Tables of physical and chemical constants*. Longman, Harlow, 16 edition, 1995.

[63] A. Kulmyrzaev and D.J. McClements. High frequency dynamic shear rheology of honey. *Journal of Food Engineering*, 45:219–224, 2000.

[64] R. S. C. Monkhouse, P. D. Wilcox, and P. Cawley. Flexible interdigital pvdf transducers for the generation of lamb waves in structures. *Ultrasonics*, 35:489–498, 1997.

[65] A. M. Mills. *Heat Transfer*. Prentice-Hall, 1999.

[66] E. Papadakis, L.C. Lynnworth, K. A. Fowler, and E.H. Carnevale. Ultrasonic attenuation and velocity in hot specimens by the momentary contact method with pressure coupling, and some results on steel to 1200c. *Journal of the Acoustical Society of America*, 52:850–857, 1972.

[67] W.N. Reynolds and R.L. Smith. Ultrasonic wave attenuation spectra in steels. *Journal of Applied Physics*, 17:109–116, 1984.

[68] L.C. Lynnworth. Marginally dispersive ultrasonic waveguides, us patent 5,159,838, 1992.

[69] L.C. Lynnworth. Ultrasonic path bundle and systems, us patent 5,962,790, 1999.

[70] L.C. Lynnworth, L. Yi, and J.A. Umina. Extensional bundle waveguide techniques for measuring flow of hot fluids. *IEEE Transactions on Ultrasonics, Ferroelectrics and Frequency control*, 52:538–544, 2005.

[71] T.R. Winston and J.A. Brunk. Method and apparatus for ultrasonic inspection of inaccessible areas, us patent 6,230,568, 2001.

[72] A.M. Heijnsdijk and J.M. van Klooster. Ultrasonic waveguide, us patent 6,400,648, 2002.

[73] C.K. Jen and J. G. Legoux. Clad ultrasonic waveguides with reduced trailing echoes, us patent 5,828,274, 1998.

[74] C. K. Jen, J. W. Liaw, T. F. Chen, A. Moreau, J. P. Monchalin, and C. C. Yang. Ultrasonic evaluation of semi-solid metals during processing. *Measurement Science & Technology*, 11:1570–1575, 2000.

[75] A. U. Rehman, C. K. Jen, and I. Ihara. Ultrasonic probes for high temperature immersion measurements. *Measurement Science & Technology*, 12:306–312, 2001.

[76] Y. Ono, Y. B. Zhang, C. K. Jen, J. F. Moisan, and C. Y. Su. Aluminum buffer rods for ultrasonic monitoring at elevated temperatures. *IEEE Transactions on Ultrasonics Ferroelectrics and Frequency Control*, 52:1042–1047, 2005.

[77] H. Araki and Y. Matsunaga. Ultrasonic flow meter, us patent 4,014,211, 1977.

[78] A. Sather. Ultasonic buffer-rod technique for the high temperature measurement of the elastic moduli of short specimens. *Journal of the Acoustical Society of America*, 43:1291–1294, 1968.

[79] L.C. Lynnworth. Ultrasonic buffer/waveguide, us patent 6,047,602, 2000.

[80] R.D. Mindlin and E.A. Fox. Vibrations and waves in elastic bars of rectangular cross section. *Journal of Applied Mechanics*, 27:152–158, 1960.

[81] P. Wilcox, M. Evans, O. Diligent, M. Lowe, and P. Cawley. Dispersion and excitability of guided acoustic waves in isotropic beams with arbitrary cross section. In D. O. Thompson and D. E. Chimenti, editors, *Review of Progress in Quantitative NDE*, volume 20. Plenum Press, 2002.

[82] O. M. Mukdadi, Y. M. Desai, S. Datta, A. H. Shah, and A. J. Niklasson. Elastic guided waves in a layered plate with rectangular cross section. *Journal of the Acoustical Society of America*, 112:1766 – 1779, 2002.

[83] T. Hayashi, W. Song, and J.L. Rose. Guided wave dispersion curves for a bar with an arbitrary cross-section, a rod and rail example. *Ultrasonics*, 41:175 – 183, 2003.

[84] L. Gavric. Computation of propagative waves in free rail using a finite element technique. *Journal of Sound and Vibration*, 185:531–543, 1995.

[85] D. Hitchings. Fe77 user manual. Technical report, Imperial College of Science, Technology and Medicine, London, UK, 1994.

[86] M. Drodz, L. Moreau, Castaings M., M.J.S. Lowe, and P. Cawley. Efficient finite element modelling of absorbing regions for boundaries of guided wave problems. In D. O. Thompson and D. E. Chimenti, editors, *Review of Progress in Quantitative NDE*, 2005.

[87] N.C. Nicholson and W.N. McDicken. A comparison of coupling horns for waveguides used in medical ultrasonics. *Ultrasonics*, 34:747–755, 1996.

[88] S.K. Tang and C.K. Lau. Sound transmission across a smooth nonuniform section in an infinitely long duct. *Journal of the Acoustical Society of America*, 112:2602–2611, 2002.

[89] D. Alleyne and P. Cawley. A two-dimensional fourier transform method for the measurement of propagating multimode signals. *Journal of the Acoustical Society of America*, 89:1159–1168, 1991.

[90] J.D. Achenbach. *Wave propagation in elastic solids*. North-Holland Publishing Company, 1975.

[91] H. Lamb. On the propagation of tremors over the surface of an elastic solid. *Philosophical Transactions of the Royal Society of London. Series A*, 203:1–42, 1904.

[92] G. F. Miller and H. Pursey. The field and radiation impedance of mechanical radiators on the free surface of a semi-infinite isotropic solid. *Proceedings of the Royal Society*, 223:521–541, 1954.

[93] G. F. Miller and H. Pursey. On the Partition of Energy between Elastic Waves in a Semi-Infinite Solid. *Royal Society of London Proceedings Series A*, 233:55–69, December 1955.

[94] R.D. Woods. Screening of surface waves in soils. *J. Soil Mech. Founds Div. Am. Soc. civ. Engrs.*, July 94:951–79, 1968.

[95] P. Wilcox, R. Monkhouse, M. Lowe, and P. Cawley. The use of huygens' principle to model the acoustic field from interdigital lamb wave transducers. In D. O. Thompson and D. E. Chimenti, editors, *Review of progress in quantitative NDE*, 1998.

[96] J. D. N. Cheeke. *Fundamentals and Applications of Ultrasonic waves*. CRC Press LLC, 2002.

[97] G. G. Stokes. Smith's prize examination 1876. *Mathematics and Physics Papers (reprint), Cambridge University Press*, 5:362, 1905.

[98] A. Bernard, M. J. S. Lowe, and M. Deschamps. Guided waves energy velocity in absorbing and non-absorbing plates. *Journal of the Acoustical Society of America*, 110:186 – 196, 2001.

[99] W. Sachse and Y-H. Pao. On the determination of phase and group velocities of dispersive waves in solids. *Journal of Applied Physics*, 49:4320–4327, 1978.

[100] F. Simonetti and Cawley P. A guided wave technique for the characterization of highly attenuative viscoelastic materials. *Journal of the Acoustical Society of America*, 114:158–165, 2003.

[101] P. B. Nagy. Personal communication: group velocity measurement using the zero phase slope method, Nondestructive Evaluation Laboratory, Department of Aerospace Engineering, University of Cincinnati, USA, 2005.

Publications

Some of the material presented in this thesis has been published. The publication details are listed below.

F.B. Cegla, P. Cawley, M.J.S. Lowe. Fluid characterisation using the Quasi-Scholte mode. In D.O. Thompson and D.E. Chimenti, editors, *Review of Progress in Quantitative NDE*, Vol.24, pages 1584 – 1591, 2005

F.B. Cegla, P. Cawley, M.J.S. Lowe. Material property measurement using the quasi-Scholte mode - A waveguide sensor. *Journal of the Acoustical Society of America*, Vol.117, Issue 3, pages 1098 – 1107, March 2005

F.B. Cegla, P. Cawley, M.J.S. Lowe. Measurement of bulk velocity and attenuation in fluids and particle suspensions using the Quassi-Scholte mode. In D.O. Thompson and D.E. Chimenti, editors, *Review of Progress in Quantitative NDE*, In press 2006

F.B. Cegla, P. Cawley, M.J.S. Lowe. Fluid bulk velocity and attenuation measurements in non-Newtonian liquids using a dipstick sensor. *Measurement Science and Technology*, Vol.17, Number 2, pages 264 – 274, February 2006